Universal Behavior of Driven Diffusive Lattice Gases

Inaugural-Dissertation

zur

Erlangung des Doktorgrades

der Mathematisch-Naturwissenschaftlichen Fakultät

der Universität zu Köln

vorgelegt von

Johannes Schmidt

aus Saran

Köln 2016

Berichterstatter: Prof. Dr. Andreas Schadschneider
Prof. Dr. Joachim Krug
Prof. Dr. Dr. h.c Herbert Spohn
(Techische Universität München)

Tag der mündlichen Prüfung: 5. Dezember 2016

Abstract

This cumulative dissertation is dedicated to the study of universal behavior in one-dimensional driven diffusive systems far from equilibrium. To capture essential aspects of such systems we will make use of modified versions of the paradigmatic totally asymmetric simple exclusion process (TASEP).

Universality is a well-established central concept of equilibrium physics. Over the last years indications for its relevance in nonequilibrium systems were found, while a deeper understanding of mechanisms leading to universality is still lacking. Besides, only a few classes of universal behavior have been identified so far. The two most prominent examples are the diffusive class with dynamical exponent $z = 2$ and the superdiffusive Kardar-Parisi-Zhang (KPZ) class with $z = 3/2$. Very recently for systems exhibiting several conservation laws, e.g., anharmonic chains, a new class with exponent $z = 5/3$ appeared. Using Nonlinear Fluctuating Hydrodynamics and Mode Coupling Theory, we show that these nonequilibrium universality classes are only part of an infinite discrete family. Remarkably, their exponents z_α are given by quotients of neighboring Fibonacci numbers, starting with either $z_1 = 2$ (if a diffusion mode exists) or $z_1 = 3/2$ (if a KPZ mode is present and no diffusion mode exists). If neither a diffusion nor a KPZ mode are present, all modes have the golden mean $\varphi = (1 + \sqrt{5})$ as their dynamical exponent $z_\alpha = \varphi$. The universal scaling functions of these Fibonacci modes are asymmetric Lévy distributions, while the dynamical exponents and scaling functions are completely fixed by the macroscopic stationary current-density relation and the compressibility matrix. Using dynamical Monte Carlo simulations we establish these exponents for a multi-species TASEP, consisting of coupled single-lane TASEPs. In particular, we show the appearance of superdiffusive modes with exponents $z_\alpha = 3/2$ (but different from the KPZ class), $z_\alpha = 5/3$, $z_\alpha = 8/5$ and $z_\alpha = (1 + \sqrt{5})/2$. This phenomenon is believed to be generic for short-ranged driven diffusive systems with more than one conserved density.

Furthermore, we reconsider the long-standing question of the critical defect hopping rate r_c in the TASEP with a slow bond (defect). For $r < r_c$ the system reacts globally and a defect-induced phase transition is observed due to queuing at the defect site. On the other hand, the defect for $r \geq r_c$ has only local effects on the stationary state. Mean-field theory predicts a global influence already for arbitrarily small defect strength, $r_c = 1$. Up to now it was not possible to verify this prediction using computer simulations. Indeed, a recent numerical study indicated that a small defect strength would not have a global influence and further $r_c = 0.80(2)$ was suggested. Studying density profiles of parallel evolving systems we improve the numerics to show that $r_c > 0.99$ and give strong evidence for $r_c = 1$ as predicted by the mean-field theory and anticipated by recent theoretical findings.

Kurzzusammenfassung

Diese kumulative Dissertation befasst sich mit der Untersuchung von universellem Verhalten in eindimensionalen getriebenen diffusiven Systemen fern vom Gleichgewicht. Um wesentliche Aspekte solcher Systeme zu untersuchen, werden wir modifizierte Versionen des paradigmatischen "totally asymmetric simple exclusion process" (TASEP) nutzen.

Universalität ist ein etabliertes, zentrales Konzept für die Beschreibung von physikalischen Systemen im Gleichgewicht. In den letzten Jahren wurden Anzeichen ihrer Relevanz auch für Systeme fern vom Gleichgewicht gefunden. Jedoch fehlt es immer noch an einem tieferen Verständnis von Mechanismen, die zu Universalität in Nichtgleichgewichtssystemen führen. Außerdem sind bisher nur wenige Universalitätsklassen identifiziert worden. Die zwei bekanntesten Beispiele sind die diffusive Klasse mit dynamischen Exponenten $z = 2$ und die superdiffusive Kardar-Parisi-Zhang (KPZ) Klasse mit $z = 3/2$. Kürzlich ist außerdem eine neue Klasse mit dem Exponenten $z = 5/3$ für Systeme mit mehreren Erhaltungsgrößen, wie z.B. anharmonische Ketten, entdeckt worden. Mit Hilfe der nichtlinearen Fluktiations-Hydrodynamik und der Mode-Coupling Theorie zeigen wir, dass diese Universalitätsklassen von Nichtgleichgewichtssystemen Teil einer unendlich diskreten Familie sind. Bemerkenswerterweise können die Exponenten z_α durch Quotienten benachbarter Fibonacci Zahlen dargestellt werden, welche entweder mit $z_1 = 2$ (falls eine Diffusions-Mode existiert) oder mit $z_1 = 3/2$ (falls eine KPZ-Mode, aber keine Diffusions-Mode existiert) starten. Ist weder eine Diffusions- noch eine KPZ-Mode vorhanden, so haben alle Moden den goldenen Schnitt $\varphi = (1 + \sqrt{5})/2$ als dynamischen Exponenten $z_\alpha = \varphi$. Die universellen Skalenfunktionen dieser Fibonacci-Moden sind asymmetrische Lévy-Verteilungen, wobei die dynamischen Exponenten und Skalenfunktionen vollständig durch die makroskopische stationäre Strom-Dichte Beziehung und die Kompressibilitätsmatrix fixiert sind. Mit Hilfe von dynamischen Monte Carlo-Simulationen weisen wir diese Konzepte für einen Mehrspur-TASEP nach, der aus gekoppelten einspurigen TASEPs besteht. Insbesondere werden wir das Auftreten von superdiffusiven Moden mit Exponenten $z_\alpha = 3/2$ (verschieden von der KPZ Klasse), $z_\alpha = 5/3$, $z_\alpha = 8/5$ und $z_\alpha = (1 + \sqrt{5})/2$ zeigen. Es ist anzunehmen, dass dieses Verhalten generisch für getrieben diffusive Systeme mit mehr als einer erhaltenen Dichte gilt.

Darüber hinaus untersuchen wir die kritische Defekt-Sprungrate r_c in einem TASEP mit einem gestörten Gitterplatz (Defekt). Für $r < r_c$ reagiert das System global und man kann aufgrund einer Anstauung an der Defektstelle einen defekt-induzierten Phasenübergang feststellen. Auf der anderen Seite, für $r \geq r_c$ hat der Defekt nur einen lokalen Effekt auf den stationären Zustand. Die Meanfield-Theorie sagt einen globalen Einfluss des Defekts schon für beliebig kleine Defektstärken voraus. Bislang war es nicht möglich, diese Vorhersage mit Computersimulationen zu überprüfen. Allerdings weist eine aktuelle, numerische Studie darauf hin, dass eine kleine Defektstärke keinen globalen Einfluss hätte und schlägt $r_c = 0,80(2)$ vor. Durch die Untersuchung der Dichteprofile von zwei sich parallel entwickelnder Systeme verbessern wir die Numerik um schließlich zu zeigen, dass $r_c > 0,99$ gilt und liefern starke Argumente für $r_c = 1$ wie es von der Meanfield-Theorie und aktuellen theoretischen Arbeiten vorhergesagt wird.

Inhaltsverzeichnis

Part I.

Introduction and Outline

1. Introduction

The precise description of numerous complex systems appearing in nature[1] involves so many degrees of freedom that it is impossible to consider all of them. In addition, many of them behave on a phenomenological level in somehow random manner. Concentrating only on a few variables and regarding the rest as noise with certain presumed distributions, statistical approaches become a powerful toolbox for qualitative and quantitative studies of such systems. Moreover, universality has become a central concept of statistical mechanics. Universality, which was established by the study of specific systems and simple models, asserts that the system's properties do not depend on its details such as the precise form of interactions[2]. Therefore, universality permits the identification of appropriate variables and simpler underlying mechanisms that are considered to be essential for the understanding of observations in real systems.

One typically classifies systems in statistical mechanics in two groups: (1) systems in or near equilibrium, and (2) systems far from equilibrium. There are general frameworks for the statistical description of systems in or near equilibrium. For the thermodynamic equilibrium, once the microscopic Hamiltonian $\mathcal{H}$ of the system is specified, a state configuration $\mathcal{C}$ at the absolute temperature T occurs with the probability given by the Gibbsian form $P(\mathcal{C}) \propto \exp\left(-\mathcal{H}_{\mathcal{C}}/\mathrm{k_B}T\right)$, where $\mathcal{H}_{\mathcal{C}}$ is the energy corresponding to the configuration $\mathcal{C}$ and $\mathrm{k_B}$ is the Boltzmann constant.

Further, the regression of spontaneous microscopic fluctuations in equilibrium systems is well understood in terms of linear response theory [76]. Using Onsager's regression hypothesis, which states that the relaxation of systems near equilibrium is governed by the same laws as the relaxation of fluctuations in equilibrium systems [10], systems near equilibrium become well understood by the study of equilibrium systems.

While equilibrium systems are limiting cases and rather exceptional in nature, nonequilibrium systems form the majority of statistical systems. Far from equilibrium the dynamics is governed by the reaction of the system to the non-zero flux and therefore linear response theory does not apply anymore. Consequently, nonequilibrium systems are characterized by a non-zero flux and show in general time dependent distributions $P(\mathcal{C}, t)$. For the description of nonequilibrium systems many theories[3] and methods[4] have been developed during the last century. In addition, some structure has emerged in the concept of universality even for nonequilibrium systems [12, 37, 43, 46, 72, 56, 88, 93]. For all that, a deeper understanding of underlying principles is still lacking and our knowledge of nonequilibrium phenomena is far from complete. Thus, the current state of statistical description of nonequilibrium systems may be seen as a treasury of accumulated knowledge and toolboxes, but without a profound common foundation yet.

In fact, nonequilibrium systems contain a large class of systems defined by transition rates between different configurations for which neither the Hamiltonian nor the Gibbsian equilibrium exists. This subclass of systems may attain a nonequilibrium steady state, more precisely a state with nonzero flux and time independent observables. As nonequilibrium steady states are easier to handle and still cover anomalous transport properties, one promising inroad for the identification of underlying mechanisms characterizing nonequilibrium phenomena in general is the study of universal behavior in nonequilibrium steady states.

[1] e.g., biological systems [62, 64, 94, 95], chemical reactions [51], traffic flow [79, 92], surface growth [3, 45, 57], economics [41, 54], networks [21, 33, 60]

[2] This holds especially near critical phase transitions [35, 37, 50, 58]

[3] e.g., stochastic processes [79], kinetic theories [76, 86, 49], entropy production [42]

[4] e.g., quantum formalism of the master equation [19, 20, 27, 36, 85], Bethe ansatz [2, 6, 85], matrix product ansatz [7, 48], density matrix renormalization group methods [11, 31, 63, 82], mean-field and cluster approximations (structure theory) [1, 8, 14, 28, 83], computer simulations [26, 49, 61], etc.

One-dimensional systems of interacting driven particles are typically far from thermal equilibrium and show complex behavior with interesting collective properties.

Thus, simple models belonging to the family of truly nonequilibrium driven diffusive systems [79, 80, 81, 85] such as the totally asymmetric simple exclusion process (TASEP)[5] widely serve as paradigmatic models for the detailed study of nonequilibrium phenomena like superdiffusive dynamical structure functions [69, 70, 71, 74], current fluctuations [73], boundary or defect-induced phase transitions [4, 44, 47], spontaneous jam formation [59], symmetry breaking and hysteresis [68, 77], etc. The investigation of these nonequilibrium phenomena are also relevant for many applications, especially for interdisciplinary problems like traffic flow on various scales, ranging from intracellular transport by molecular motors to vehicular traffic. Due to its simplicity, the richness of supported nonequilibrium phenomena and its relevance for all other traffic models, the TASEP becomes known as the '*Mother of all traffic models*'[79].

This cumulative dissertation is dedicated to the study of universal behavior in one-dimensional driven diffusive systems far from equilibrium. The contributed papers can be arranged in two different groups. Part II of this thesis will study the dynamical phase diagram of multi-species systems with conserved density fluctuations using analytic mode coupling techniques and comparing results to numerical simulations of multi-species TASEPs. Part III will readdress the long-standing question of a critical defect strength of a single defect site leading to a phase transition. By using advanced Monte Carlo techniques we will dissolve the contradiction of recent anticipated theoretical findings and numerical investigations.

In the subsequent sections a brief summary of the most important basic knowledge is provided, followed by an outline chapter placing the contributed papers into a concept.

[5] The TASEP was initially introduced by MacDonald *et al* for the kinetic study of multiple ribosomes translating the same mRNA [53].

1.1. Totally Asymmetric Simple Exclusion Process (TASEP)

This section briefly introduces the TASEP, relevant modifications and its technical aspects without celebrating the beauty and richness of this model. For a very detailed discussion of the TASEP and related results we refer to [79].

The bulk of a TASEP is given by a one-dimensional lattice where particles move to their empty right neighbor sites with rate p (see Fig. 1.1). There are various ways to modify the update rules and boundary conditions. In this thesis we will restrict the update rule to the random-sequential update (RSU). The RSU aims to efficiently approximate continuous time dynamics in computer simulations. In continuous time models jump attempts are encoded in rates. These rates could be assigned to sites or even to particles while for our purposes rates will be assigned to sites. A single RSU is then given by a site k drawn from equidistribution which is updated with the probability $r_k/R_{\max}$, where $R_{\max}$ is the maximal rate appearing in the system. To point out the macroscopic time scale, $\Delta t = 1$ corresponds to $R_{\max}L$ RSUs where L is the number of sites which have to be considered for an update of the model. Therefore, on average each particle attempts to jump at least once within $\Delta t = 1$ and larger systems allow for a finer time resolution.

A TASEP configuration at time t is typically described in terms of occupation numbers $\{n_k(t)\}$, telling if site k at time t is occupied, $n_k(t) = 1$, or empty, $n_k(t) = 0$.

Our major interest is the nonequilibrium steady state for various systems. Stationary states are characterized by a time independent probability distribution $P(\mathcal{C})$ to observe a certain configuration $\mathcal{C}$ in the allowed configuration space Σ. Therefore, one gets a time independent expectation value $\langle\, f(\{n_k(t)\})\,\rangle$ in the steady state ensemble average for any arbitrary function f. Using the continuity equation one deduces that the system will have a constant particle current j for all sites, i.e.,

$$j \equiv \langle\, j_k(t)\,\rangle = \text{const.}\ \forall\ k, t \tag{1.1}$$

with the current measure at site k and time t

$$j_k(t) = r_k(t) n_k(t)(1 - n_{k+1}(t)) \tag{1.2}$$

where $r_k(t)$ is the jump rate, $n_k(t)$ checks for a particle which might jump and $(1 - n_{k+1}(t))$ checks the exclusion principle.

For our studies nonequilibrium systems with factorized stationary distributions play an important role. At this point we will be more precise with the terminology factorized stationary distribution. A factorized steady state distribution means that each site is occupied, independently on other sites, with probability ρ, where $\rho \in [0, 1]$ is the particle density. Or in other words, correlation functions vanish and mean-field theory becomes exact. Due to our main interest in infinite systems we use this terminology simultaneously for finite systems with periodic boundaries. We have a fixed number of particles for periodic finite systems and the steady state distribution factorizes only for the grand-canonical ensemble. For a finite system this distribution is uniform and all allowed configurations are equally likely. Calculating correlation functions involving multiple sites one has to be aware of finite size effects of order L^{-1}. To demonstrate the appearance of finite size effects, we calculate the space correlation $\langle\, n_0 n_k\,\rangle - \rho^2$ for a periodic TASEP of length L and density ρ. The uniform stationary distribution tells us that if we measure

Figure 1.1.: Dynamics of the TASEP: Particles jump unidirectionally to their empty right neighbor sites with rate p. The exclusion principle forbids to occupy a site with more than one particle.

a particle at site 0 there will be $\rho L - 1$ particles left for $L - 1$ sites. Thus, we get for the space correlation

$$\langle\, n_0 n_k \,\rangle - \rho^2 \quad = \quad \rho(1-\rho)\left(\delta_{k,0} - \frac{1-\delta_{k,0}}{L-1}\right) \tag{1.3}$$

where $\delta_{k,0}$ is a Kronecker delta. However, when calculating quantities like currents we will assume an infinite system and neglect finite-size corrections.

In the published contributions of Part II we study the statistics of steady state density fluctuations for multi-species settings aiming to observe universal behavior[6]. For this purpose, we use a multi-species TASEP, consisting of N transversally coupled single-lane TASEPs with periodic boundary conditions. The coupling is designed such that the hopping rates depend on the occupation of neighboring sites on adjacent lanes, while lane interchanges are forbidden. Being more precise, the hopping rate $r_k^{(\lambda)}$ from site k to $k+1$ on lane λ is given by

$$r_k^{\lambda} = b_\lambda + \frac{1}{2} \sum_{\{\mu:\mu\neq\lambda\}} \gamma_{\lambda\mu} \left(n_k^{(\mu)} + n_{k+1}^{(\mu)} \right) \tag{1.4}$$

where $n_k^{(\mu)}$ measures the number of particles on lane μ and site k, b_λ is a species dependent drift parameter and $\gamma_{\lambda\mu} = \gamma_{\mu\lambda}$ are symmetric interaction constants. Hopping attempts onto occupied sites are forbidden by construction. For a two-species setting this will exemplarily look like:

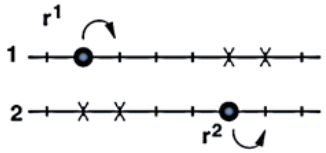

Using that the stationary distribution factorizes for this model [67] we calculate the steady state current as

$$j_\lambda \quad = \quad \rho_\lambda(1-\rho_\lambda)\left(b_\lambda + \sum_{\mu:\mu\neq\lambda} \gamma_{\lambda\mu}\rho_\mu \right). \tag{1.5}$$

Here we want to stress that the choice of this model is motivated by two simple reasons. Firstly, the factorizing stationary distribution allows for exact calculations of indispensable quantities such as current-density relation $j_\lambda(\rho_1, \ldots, \rho_N)$. Secondly, the nonlinearities of the current-density relation are of minimal order $\rho_\lambda^2 \rho_\mu$ providing a minimum setting which might support new universality.

In Section 1.2 we provide an introduction of universal behavior in driven diffusive systems of single and multi-component systems. In Subsection 1.3.2 we introduce our used Monte Carlo techniques and point out crucial optimizations.

In Part III we investigate a TASEP with open boundaries. In particular, we readdress numerically the critical strength of a single defect site leading to a global effect on the density profile and a reduction of the current. An open system is realized by adding an entry and exit reservoir to the ends of the system of size L. Particles may enter (exit) the system at the first (last) site with rate α (β) (see. Fig. 1.2). Except for the defect site we choose the bulk hopping rate to be $p = 1$. To perform a RSU in an open system we have to consider additionally the update of an

[6] A detailed introduction to universal behavior for single and multi-species driven diffusive systems is provided in Section 1.2.

'entry site'. Therefore, a RSU selects uniformly randomly one site out of $L+1$ sites. In contrast to bulk sites the entry site is always occupied and does not depend on the bulk dynamics. Note that performing the limit $\alpha \to \infty$ ($\beta \to \infty$) would correspond to a replacing of the first (last) site by a reservoir with rate $\alpha = 1$ ($\beta = 1$). Therefore, it is sufficient to study the phase diagram for $p = 1$ and $\alpha, \beta \leq 1$. Depending on the boundary rates the TASEP steady state might show three different phases (see. Fig. 1.2) which we will discuss in more detail. The open setting is the firstly in 1968 introduced TASEP setting [53] aiming to study kinetics of ribosomes on mRNA. Using mean-field theory the authors were able to predict boundary controlled low- and high-density (LD and HD) phases and additionally for $\alpha, \beta \leq 1/2$ a bulk controlled maximum current (MC) phase. Anyway, these results were achieved within the mean-field approximation and a detailed understanding of supported phases was incomplete. Although the TASEP was introduced two years later to the probabilistic literature by Spitzer [87], it became known to the statistical physics community only in 1991 by Krug [44], who pointed out that the TASEP shows a second order boundary induced phase transition from the low-density to the maximum current phase. Since then the TASEP became a widely studied model in statistical physics. Two years later in 1993 exact steady state solutions for the open boundary TASEP appeared in [17, 84] using different approaches. One year before, Derrida *et al* managed to solve the exact steady state density profile and current for the maximum current system with $\alpha = \beta = 1$ [16]. This solution shows two interesting characteristics. Firstly, the density profile decays monotonically decays as $\langle\, n_k - 1/2 \,\rangle \propto k^{-1/2}$ at the left end and as $\langle\, n_{L+1-k} - 1/2 \,\rangle \propto -k^{-1/2}$ at the right end. Secondly, the maximal supported finite-size current was determined as

$$j_{\alpha=\beta=1,L} = \frac{1}{4}\left(1 + \frac{3}{1+4L}\right). \tag{1.6}$$

In contrast to that, the steady state for a MC system with $\alpha = \beta = 1/2$ factorizes and one finds a flat density profile $\rho = 1/2$ and the current $j_{\alpha=\beta=1/2,L} = 1/4$ for all system lengths. Therefore, one finds upper and lower bounds for the steady state current within the MC phase ($1/2 \leq \alpha, \beta \leq 1$)

$$\frac{1}{4} \leq j_{\alpha,\beta} \leq \frac{1}{4}\left(1 + \frac{3}{1+4L}\right). \tag{1.7}$$

For an infinite system the current is given by $j_\infty = 1/4$ within the whole maximum current phase. Motivated by the gap for currents within the MC phase, the question arose if an introduced defect site (slow bond) in the middle of an open system with $\alpha = \beta = 1$ (Fig. 1.3) would have global or local effects on the system. This is motivated by the fact that a slow bond with hopping rate $r \in [r_{c,L}, 1]$ supports a steady state current $j_{\alpha=\beta=1,L<\infty}(r) \geq 1/4$ which 'indicates' a MC phase [38] although a defect is present. Taking the limit $L \to \infty$ it is unclear if one gets $r_c = 1$ or $r_c < 1$. Mean-field theory predicts a global influence already for an arbitrarily small defect strength, i.e., $r_c = 1$, while its predictions for the defect current $j(r)$ poorly fit simulation results. Although the phase-diagram became well understood two years after its proposal, the verification of r_c and the identification of the defect current $j_\infty(r)$ is a challenging problem for the statistical physics and mathematical community since 1993. In Chapter 7 we provide an introductory article to the defect setting and its relevance for interdisciplinary applications. In Subsection 1.3.3 we discuss crucial insights for Monte Carlo simulations which are needed to detect effects of minuscule defects.

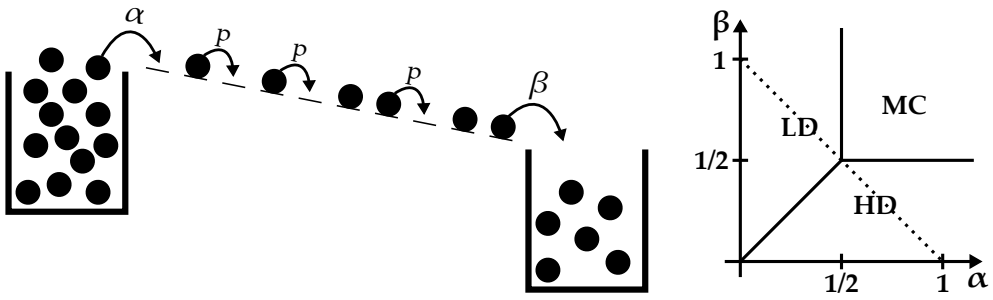

Figure 1.2.: **Left:** TASEP with open boundaries. Particle enter (exit) the system on the left (right) with rate α (β). Bulk dynamics is unchanged. **Right:** Exact phase diagram for open boundary TASEP with $p = 1$ and RSU. The low-density (LD) phase is controlled by an inefficient ($\alpha < 1/2$) entry rate and an efficient ($\beta > \alpha$) exit rate. In contrast to that, the high density (HD) phase is controlled by an inefficient ($\beta < 1/2$) exit- and efficient ($\alpha > \beta$) entry-rate. For an efficient out- and input rate $\alpha, \beta \geq 1/2$ the system is controlled by its bulk dynamics which shows a saturated maximum current (MC). The dotted line $\beta = 1-\alpha$ indicates systems with factorized steady states.

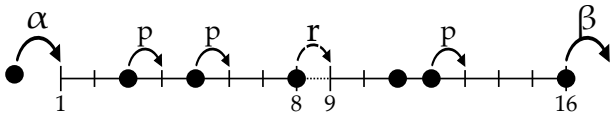

Figure 1.3.: Open boundary TASEP with $L = 16$ sites and a slow bond ($r < 1$) in the middle.

1.2. Classification of dynamics in stationary states

This section aims to explain where one can find universal behavior and how to classify dynamics. Universality groups different kinds of systems into one universality class which show the same statistical properties for appropriate variables. Dynamical universality classes are typically identified by some exponents, distributions and scaling functions characterizing fluctuations of these variables.

To introduce dynamical universality classes we will first study the time evolution of locally conserved density fluctuations for two paradigmatic one-dimensional lattice gas models in a periodic system of length L with random-sequential update. These models are the above introduced TASEP and the simple diffusion model where particles jumps with rate q (p) to the left (right). Comparing the steady state current-density relations $j(\rho)$, one should note that due to the absence of interactions the diffusion model has a simple linear current-density relation $j(\rho) = (p - q)\rho$ in contrast to the TASEP showing a quadratic relation $j(\rho) = \rho(1 - \rho)$.

To study density fluctuations it is convenient to use the steady state dynamical structure function[7]

$$\bar{S}_k(t) = \langle\, n_k(t) n_0(0) \,\rangle - \rho^2 \tag{1.8}$$

where $n_k(t)$ measures the number of particles on lattice site k at time t and $\rho = \langle\, n_k \,\rangle$ is the uniform steady state density. $\langle \cdot \rangle$ denotes the expectation value for a steady state ensemble average. One intuitive picture to understand the dynamical structure function $S_k(t)$ is its interpretation as a probability distribution for finding a particle at position k and time t under the condition that there was a particle at position $k = 0$ and time $t = 0$. Evolving this distribution in time one naturally discovers a decay and growth of its amplitude and variance, respectively, caused by the randomness, while the distribution will drift with constant velocity $v = j'(\rho)$. In the asymptotic limit ($t \to \infty$) this distribution shows a universal self-similar form $f(x)$ and its amplitude decays

[7] also known as the two-point correlation function

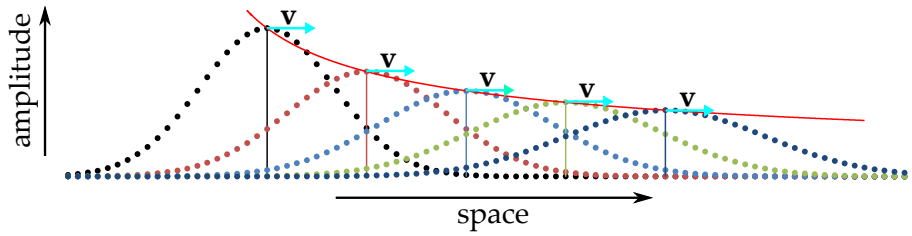

Figure 1.4.: Exemplary space-time propagation of the asymptotic dynamical structure function with equally spaced time points encoded in the color. The time evolution of the dynamical structure function shows a self-similar form $f(x)$ with constant drift velocity v. Due to the process's randomness the amplitude (red) decays like $\max_k(S_k(t)) \sim t^{-1/z}$ with dynamical exponent z.

with a universal dynamical exponent z as $\max_k S_k(t) \sim t^{-1/z}$. Figure 1.4 shows an exemplary space-time evolution. Accordingly, the asymptotic structure function can be expressed as

$$\bar{S}_k(t) \simeq K(Et)^{-1/z} f\left((Et)^{-1/z}(k - vt)\right) \tag{1.9}$$

with nonuniversal scale parameter E, drift velocity v and conserved compressibility factor K

$$K = \frac{1}{L}\left\langle \left(\rho L - \sum_{k=1}^{L} n_k\right)^2 \right\rangle \tag{1.10}$$

where K contains information about space correlations and is the nonequilibrium analogue of the thermodynamic compressibility which measures the response to pressure.

In case of the simple diffusion model, where no interaction between particles is present, one finds the well known Gaussian scaling function $f(x) = \exp(-x^2)/\sqrt{\pi}$ and dynamical exponent $z = 2$. In contrast to the diffusion model a TASEP includes interaction between particles via the exclusion principle. Therefore, the TASEP turns out to belong to the universality class of the Kardar-Parisi-Zhang (KPZ) equation [39] suggested in 1986 to describe the growth of interfaces. Different to diffusion, the KPZ universality class shows a superdiffusive ($z < 2$) dynamical structure function with dynamical exponent $z = 3/2$. Its nontrivial symmetric scaling function f_{PS} was calculated, up to numerical precision of 100 digits, by M. Prähofer and H. Spohn studying the TASEP [74, 75] which came as a major breakthrough. Using the KPZ scaling function provided in [75] the nonuniversal scale factor is given by

$$E = \sqrt{2K}\,\left|j''(\rho)\right|. \tag{1.11}$$

Indeed, simulation results of the TASEP confirm perfectly within error bars the dynamical exponent $z = 3/2$ and a self-similar form satisfying the Prähofer-Spohn scaling function f_{PS} already for early and therefore numerically accessible times, see Fig. 1.5.

To understand the universality in more detail, we will investigate the large scale dynamics by making use of Nonlinear Fluctuating Hydrodynamics (NLFH) theory [89], which describes the time evolution of density fluctuations in terms of stochastic partial differential equations. To do so, we switch from a discrete to a hydrodynamic description, where the dynamics is investigated in terms of the coarse-grained local density field $\rho(x,t)$ and associated current $j(x,t)$. Our starting point is the continuity equation $\partial_t\rho(x,t) + \partial_x j(x,t) = 0$ expressing mass conservation [40]. Given the stationary current as a function of local density $j(\rho(x,t))$ this equation can be rewritten as follows

$$\frac{\partial}{\partial t}\rho(x,t) + A\frac{\partial}{\partial x}\rho(x,t) = 0 \tag{1.12}$$

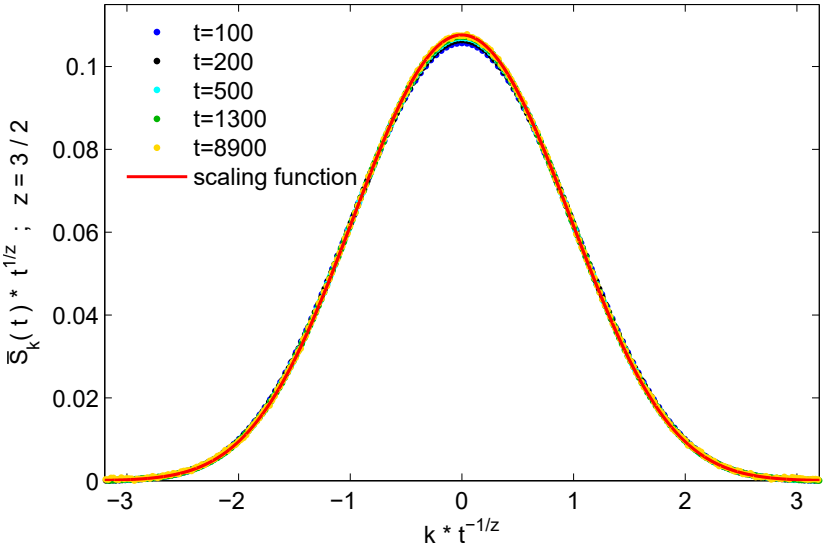

Figure 1.5.: Scaling plot of the measured TASEP structure function with dynamical exponent $z = 3/2$. The data approaches nicely the asymptotic solution Eq. (1.9) with dynamical exponent $z = 3/2$ and Prähofer-Spohn KPZ scaling function. Fitting the dynamical exponent within the time window $t \in [100, 1300]$ we find $z_{\text{early time}} = 1.505 \pm 0.005$ (0.33%) while for $t \geq 1300$ no difference to the asymptotic solution could be observed within error bounds. The structure function is recorded in a periodic system with random-sequential-update, density $\rho = \frac{1}{2}$ and length $L = 10^6$. The statistical error $\epsilon_{99\%}$ with 99% confidence bound is for every data point $S_k(t)$ smaller than $3.4 \cdot 10^{-6}$. The plotted scaling function is obtained without fitting and is described by Eq. (1.9) with scale factor $E = \sqrt{2}$, drift velocity $v = 0$ and compressibility factor $K = \rho(1-\rho) = 1/4$. Simulation details are discussed in Sec. 1.3.2.

where A is the current Jacobian $A = \partial j/\partial\rho$. Up to now Eq. (1.12), describes the deterministic time evolution of the density $\rho(x,t)$ under Eulerian scaling [40]. The effects of randomness occurring on finer time scales are captured by adding phenomenological diffusion $\partial_x^2 D\rho(x,t)$ and conservative white noise[8] $\partial_x B\xi$, while the fluctuation dissipation theorem $KD+DK = B$ connects compressibility, diffusion- and noise-strength. In this framework one expands the local density $\rho(x,t) = \rho + u(x,t)$ around its stationary value ρ. Using the steady state current-density relation $j(\rho) = (p-q)\rho$ for the diffusion model we arrive at

$$\partial_t u(x,t) = -\partial_x \Big(\ (p-q)u(x,t) - \partial_x D u(x,t) + B\xi(x,t) \ \Big) \tag{1.13}$$

which is the partial differential equation for diffusion with conservative white noise known to show a Gaussian scaling function with variance growing linearly in time ($z = 2$). Doing the same for the TASEP we first recognize the quadratic current-density relation $j(\rho) = \rho(1-\rho)$ resulting in

$$\partial_t u(x,t) = -\partial_x \Big(\ (1-2\rho)u(x,t) - \partial_x D u(x,t) - (u(x,t))^2 + B\xi(x,t) \ \Big) . \tag{1.14}$$

This stochastic partial differential equation belongs to the family of the noisy Burgers' equation [9]. Comparing Eqs. (1.13) and (1.14), one notices that the difference causing different universality is the nonlinear term appearing for the TASEP model.

So far, we have derived the fluctuating hydrodynamic description just for two specific models. Therefore, we will now assume some more general model with local interactions ($z > 1$), locally conserved density fields and infinitely differentiable steady state current-density relation $j(\rho)$. NLFH assumes that in order to capture universal behavior correctly it suffices to expand the

[8] Gaussian distributed random variable satisfying $\langle\, \xi(x,t) \,\rangle = 0$, $\langle\, \xi(x,t)\xi(x',t') \,\rangle = \delta(x-x')\delta(t-t')$

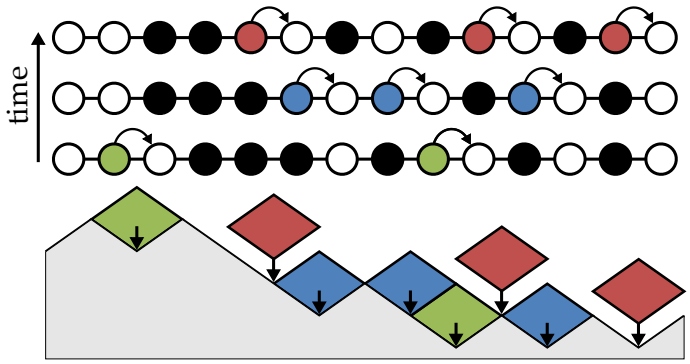

Figure 1.6.: Mapping of TASEP dynamics to a surface growth. The figure shows a TASEP configuration evolving in time, while the color-coded particle will jump within the next time step. Mapping a particle to a down-slope ($\bullet \rightarrow \diagdown$) and a hole to a up-slope ($\circ \rightarrow \diagup$) a state configuration corresponds to some height profile. If a particle jumps a diamond is added to the surface between the initial and final position. This mapping can be generalized easily to the asymmetric simple exclusion process (ASEP) where a jump to the left will correspond to a diamond removal.

current-density relation up to second order [89]. Possible logarithmic corrections arrising from higher orders [5, 15] are neglected. Consequently, given the current-density relation $j(\rho)$ we obtain the NLFH equation as

$$\partial_t u(x,t) = -\partial_x \left(\; j'(\rho)u(x,t) - \partial_x D u(x,t) + \frac{1}{2} j''(\rho)(u(x,t))^2 + B\xi(x,t) \; \right). \tag{1.15}$$

Going back, we mentioned that the KPZ universality belongs to the KPZ equation, initially suggested to describe surface growth. Performing the Galilei transformation $x \rightarrow x - j'(\rho) \cdot t$ to get rid of the drift term and then using $\partial_x h(x,t) = -u(x,t)$, Eq. (1.15) can be transformed into the KPZ-equation

$$\partial_t h(x,t) = \nu \nabla^2 h + \frac{\lambda}{2}(\nabla h)^2 + \eta(x,t) \tag{1.16}$$

with $\nu = D$, $\lambda = j''(\rho)$ and $\eta(x,t) = B\xi(x,t)$. Indeed, one can map the TASEP to a surface growth process [3, 32, 43, 45, 65] that became known as the single step model (see Fig. 1.6). This mapping motivates the used substitution $\partial_x h(x,t) = -u(x,t)$. Considering that the critical nonlinear term leading to KPZ universality is $\lambda_c = 0$ [39], we can summarize:

> The universality class is encoded in the nonlinear part of the fluctuating hydrodynamic equation. Therefore, a model with just one locally conserved field belongs either to the diffusion class ($j''(\rho) = 0$) or to the KPZ class ($j''(\rho) \neq 0$).
>
> To allow for a richer dynamical phase diagram showing other dynamical exponents and scaling functions the system should have more than one locally conserved density field.

Assuming a local interacting system with N locally conserved density fields, the NLFH equations are derived analogously starting with the system of conservation laws $\partial_t \rho_\lambda(x,t) + \partial_x j_\lambda(x,t) = 0$. The key steps are again expanding the local density $\rho_\lambda(x,t) = \rho_\lambda + u_\lambda(x,t)$ and expressing the associated current $j_\lambda(\rho_1, \ldots, \rho_n)$ as a function of densities. Finally, one arrives at

$$\partial_t \vec{u} = -\partial_x \left(J\vec{u} + \frac{1}{2} \sum_\lambda \vec{u}^T H^\lambda \vec{u} + \partial_x D\vec{u} + B\vec{\xi} \right) \tag{1.17}$$

where J is the Jacobian and H^λ are the Hessians of the current with matrix elements $J_{\lambda\mu} = \partial j_\lambda/\partial\rho_\mu$ and $(H^\lambda)_{\mu\nu} = \partial^2 j_\lambda/(\partial\rho_\mu\partial\rho_\nu)$. Additionally, a phenomenological diffusion matrix D and normalized white noise ξ_λ with strength matrix B have been added. Transforming the fluctuation fields $\vec{u}$ into eigenmodes $\vec{\phi} = R\vec{u}$ with $RJR^{-1} = \mathrm{diag}(v_\alpha)$, the time-evolution of $\phi_\alpha \coloneqq (\vec{\phi})_\alpha$ is governed by

$$\partial_t\phi_\alpha = -\partial_x\left(v_\alpha\phi_\alpha + \vec{\phi}^T G^\alpha\vec{\phi} + \partial_x(\tilde{D}\vec{\phi})_\alpha + (\tilde{B}\vec{\xi})_\alpha\right) \tag{1.18}$$

with $\tilde{D} = RDR^{-1}$, $\tilde{B} = RB$ and mode coupling matrices

$$G^\alpha = \frac{1}{2}\sum_\lambda R_{\alpha\lambda}(R^{-1})^T H^\lambda R^{-1}. \tag{1.19}$$

To elaborate universal behavior in density fluctuations for multiple conserved quantities we start with the structure function in density representation

$$\bar{S}_{\lambda\mu}(x,t) = \langle\, u_\lambda(x,t)u_\mu(0,0)\,\rangle. \tag{1.20}$$

Since the conserved densities interact in general, a perturbation in one component will cause a nontrivial relaxation of other components. Eq. (1.18) implies that the eigenmode ϕ_α will move with velocity v_α through the system. Therefore, a perturbation may split into different peaks moving with distinct velocities. It is a lot easier to investigate the structure function in eigenmode representation

$$S_{\alpha\beta}(x,t) = [R\bar{S}(x,t)R^T]_{\alpha\beta} = \langle\, \phi_\alpha(x,t)\phi_\beta(0,0)\,\rangle. \tag{1.21}$$

Distinct velocities now tell that off-diagonal terms are expected to decay quickly. For long times and large distances between the peaks one is left with the diagonal elements which we denote by

$$S_\alpha(x,t) \coloneqq S_{\alpha\alpha}(x,t). \tag{1.22}$$

Analogously to the one-component case, the asymptotic behavior of the diagonal elements is expected to show a scaling form

$$S_\alpha(x,t) \simeq (E_\alpha t)^{-1/z_\alpha} f_\alpha((E_\alpha t)^{-1/z_\alpha}(x - v_\alpha t)) \tag{1.23}$$

with a dynamical exponent z_α and scaling function f_α that might be different for the N modes, especially they might differ from the diffusion and KPZ class.

Nonlinear stochastic conservation laws Eqs. (1.15) and (1.18) are difficult, in particular for multi-component systems. Nevertheless, using mode coupling theory to calculate the asymptotic dynamical structure function provides an inroad for the evaluation of dynamical exponents and scaling functions. The basic idea is to capture the combined effects of nonlinearity and noise by a memory kernel. While it is not clear how to formulate the memory kernel in general, the one-loop kernel provides a good approximation and might even reveal exact results. Thus, our starting point for the computation of $S_\alpha(x,t)$ is the mode coupling one-loop approximation in a strictly hyperbolic ($v_\alpha \neq v_\beta$) setting

$$\partial_t S_\alpha(x,t) = (-v_\alpha\partial_x + \tilde{D}_{\alpha\alpha}\partial_x^2)S_\alpha(x,t) + \int_0^t \mathrm{d}s \int_{\mathbb{R}} \mathrm{d}y S_\alpha(x-y,t-s)\partial_y^2 M_{\alpha\alpha}(y,s) \tag{1.24}$$

with the memory kernel

$$M_{\alpha\alpha}(y,s) = 2\sum_{\beta,\gamma}(G^\alpha_{\beta\gamma})^2 S_\beta(y,s)S_\gamma(y,s). \tag{1.25}$$

Limiting our interest to the asymptotic solution, the analysis reveals[9] for hyperbolic settings that only the diagonal terms of $\{G^\alpha\}$ will contribute the dynamical exponent z_α and its associated scaling function f_α. Thus, we may further simplify the memory kernel to

$$M_{\alpha\alpha}(y,s) = 2\sum_\beta (G^\alpha_{\beta\beta} S_\beta(y,s))^2 \tag{1.26}$$

which clarifies that the dynamical exponents $\{z_\alpha\}$ and scaling functions $\{f_\alpha\}$ are encoded in the roots of the diagonal elements of $\{G^\alpha\}$. For this purpose, we define the set

$$\mathbb{I}_\alpha \coloneqq \{\beta \ : \ G^\alpha_{\beta\beta} \neq 0\} \tag{1.27}$$

and summarize the results:

> Universality is encoded in the roots of the diagonal elements of the matrices G^α. Very similar to the one-component case one finds the diffusion ($z_\alpha = 2$) universality class for $\mathbb{I}_\alpha = \emptyset$ and the KPZ ($z_\alpha = 3/2$) universality class for $\alpha \in \mathbb{I}_\alpha$.
>
> A new universality class will emerge for mode α if the self-coupling term vanishes ($\alpha \notin \mathbb{I}_\alpha$) and a nonlinear coupling to some other mode β is still present ($\beta \in \mathbb{I}_\alpha$). The dynamical exponent is then given by
>
> $$z_\alpha = \min_{\beta\in\mathbb{I}_\alpha} \left[\left(1 + \frac{1}{z_\beta}\right)\right] \tag{1.28}$$
>
> and its associated scaling function is a z_α-stable distribution with analytic representation
>
> $$\hat{S}_\alpha(p,t) = \frac{1}{\sqrt{2\pi}} \exp\left\{-iv_\alpha pt - E_\alpha t|p|^{z_\alpha}\left[1 - iA_\alpha \mathrm{sgn}(p)\tan(\frac{\pi z_\alpha}{2})\right]\right\} \tag{1.29}$$
>
> in the Fourier-space $\hat{S}(p,t) = (2\pi)^{-1/2}\int_{-\infty}^{\infty} S(x,t)\exp(-ikx)\mathrm{d}x$ with nonuniversal scale factor E_α and asymmetry $A_\alpha \in [-1,1]$. Notably, for the fastest left/right-moving peak mode coupling theory predicts maximum asymmetry $A = \pm 1$. This is the classical analogue to the Lieb-Robinson bound which is a theoretical upper limit at which information can propagate in nonrelativistic quantum systems [52]. Starting with either $z = 2$ or $z = 3/2$ the evaluation of Eq. (1.28) yields that all feasible exponents are ratios of neighboring Fibonacci numbers
>
> $$z_\alpha \in \left\{\frac{F_{n+3}}{F_{n+2}} \ : \ n \leq N\right\} \tag{1.30}$$
>
> where F_n are Fibonacci numbers defined by $F_{n+2} = F_{n+1} + F_n$ starting with $F_1 = F_2 = 1$. If neither a diffusion nor a KPZ mode are present then the unique solution to the recursion in Eq. (1.28) is the golden mean $z_\alpha = \varphi = (\sqrt{5}+1)/2$ for all modes. Figure 5.1 in Chapter 5 shows some representative examples of the scaling functions which are quite different in shape.

[9] For more details see Sec 6.2.2.

1.3. Monte Carlo simulations

Monte Carlo simulations are, broadly speaking, a huge set of random experiments aiming to estimate quantities of interest based on the law of large numbers. Highly accurate Monte Carlo data is essential for the measurement of sensitive quantities such as dynamical exponents or critical defect strength causing phase transitions. Naïve Monte Carlo approaches often fail to reach the aspired accuracy which requires the use of advanced Monte Carlo techniques. There is a broad spectrum of well established and recently developed sampling techniques improving the accuracy [24, 25, 26, 30, 34, 61]. However, in many fields there is no clear guideline for the most efficient techniques. Due to the richness of nonequilibrium phenomena each pair of system and measure comes along with its own strengths, weaknesses and computation bottlenecks one has to overcome. Therefore, this section briefly discusses the concept of Monte Carlo simulations, quantifies the uncertainty of its results and gives insights into crucial optimizations we have used in simulations.

1.3.1. Concept of Monte Carlo simulations for expectation values

Throughout this thesis Monte Carlo simulations are used to calculate expectation values in nonequilibrium stochastic processes. In this context, a nonequilibrium stochastic system should be interpreted as a time-dependent probability-weighted path in the system's configuration space Σ containing all possible configurations.

Let us assume we are interested in the expectation value of a function f in a system far from equilibrium. To calculate the expectation value, we need to specify the phase space $\Omega_t \subseteq \Sigma$. This phase space is for nonequilibrium systems in general time-dependent and takes the evolution of the conditioned configuration space under the system's dynamics into account. E.g., Ω_t covers the states arising from the time evolution of some initial state $\mathcal{C} \in \Omega_{t=0}$ while the time evolution of Ω_t depends on system specific transition probabilities $W(\tilde{\mathcal{C}} \to \mathcal{C})$ between configuration $\tilde{\mathcal{C}}$ and $\mathcal{C}$. That means

$$\langle f \rangle(t) = \sum_{\mathcal{C} \in \Omega_t} P(\mathcal{C}, t) f(\mathcal{C}) \tag{1.31}$$

where $P(\mathcal{C}, t)$ is the probability to observe configuration $\mathcal{C}$ at time t and encodes the time evolution of the system.

Calculating such quantities in nonequilibrium systems numerically has two major problems. Firstly, often the sum cannot be reduced to a compact analytical form which is easy to compute. Also numerically, it is in general a hopeless task since the phase space Ω_t is enormous. The second major problem is the typically unknown probability distribution $P(\mathcal{C}, t)$.

Nevertheless, Monte Carlo simulations allow the calculation of such expectation values with, in principle, arbitrary precision and become powerful tools in many fields since the quality does not depend on the dimensionality of the problem. The common idea of all Monte Carlo estimators is to limit the sum to a random sample $\mathcal{S}_t \subseteq \Omega_t$ where $Q(\mathcal{C}, t)$ denotes the probability to create state $\mathcal{C} \in \Omega_t$ at time t. The unbiased Monte Carlo estimator for $\langle f \rangle$ is given by

$$Y_{\mathcal{S}_t} = \frac{\sum_{\mathcal{C} \in \mathcal{S}_t} \frac{P(\mathcal{C},t)}{Q(\mathcal{C},t)} f(\mathcal{C})}{\sum_{\mathcal{C} \in \mathcal{S}_t} \frac{P(\mathcal{C},t)}{Q(\mathcal{C},t)}} \tag{1.32}$$

and the law of large numbers guarantees

$$\lim_{|\mathcal{S}_t| \to \infty} Y_{\mathcal{S}_t} = \langle f \rangle(t). \tag{1.33}$$

Knowing the distribution $P(\mathcal{C}, t)$ a suitable choice of $Q(\mathcal{C}, t)$ might reduce the variance $\mathrm{var}(Y_{\mathcal{S}_t})$ and therefore allow for better results with less samples. The choice of the most favorable $Q(\mathcal{C}, t)$

depends on $f(\mathcal{C})$ and $P(\mathcal{C},t)$. Anyway, this will not be the case for our purpose, since we do not know $P(\mathcal{C},t)$ in general. To get rid of the unknown distribution $P(\mathcal{C},t)$ we have to ensure $Q(\mathcal{C},t) \propto P(\mathcal{C},t)$.

This characteristic can be achieved in the context of **Markov Chain Monte Carlo** (MCMC). Without going into much detail we define a Markov chain ζ as a time series of configurations $\zeta = (\mathcal{C}_t)$ consisting of configurations $\mathcal{C}_t \in \Sigma$ of the systems configuration space Σ. Or, in other words, a Markov chain describes a possible evolution of the system. To apply MCMC the phase space Ω, the function of interest f and the set of independent Monte Carlo samples $\mathcal{S}$ should be redefined. Therefore, the phase space Ω is now a set of all possible Markov chains starting at $t = 0$ in Ω_0 and ending at some maximum time which is required by the argument of f. Note that if f is a time-independent function the Markov chain reduces to length one and we get $\Omega = \Omega_0$. The sought expectation value of f is calculated as

$$\langle f \rangle = \sum_{\zeta \in \Omega} P(\zeta) f(\zeta) \tag{1.34}$$

where $P(\zeta)$ is the probability to observe ζ. To apply the MCMC approach we define a set $\mathcal{S}$ of independent random samples as a set of Markov chains independently generated from the distribution $Q(\zeta)$. Similar to Eq. (1.32) the unbiased MCMC estimator is given by

$$Y_{\mathcal{S}} = \frac{\sum_{\zeta \in \mathcal{S}} \frac{P(\zeta)}{Q(\zeta)} f(\zeta)}{\sum_{\zeta \in \mathcal{S}} \frac{P(\zeta)}{Q(\zeta)}}. \tag{1.35}$$

To generate a random Markov chain ζ from a distribution $Q(\zeta) \propto P(\zeta)$ we will choose a random initial configuration $\mathcal{C}_0 \in \Omega_0$ from the distribution $P(\mathcal{C}_0, t = 0)$ and generate a Markov chain by propagating the system under its defined transition probabilities $W(\tilde{\mathcal{C}} \to \mathcal{C})$. If $P(\mathcal{C}_0, t = 0)$ is unknown one can alternatively relax[10] the system into its desired random initial condition. Finally, the Monte Carlo estimator for $\langle f \rangle$ is given by

$$Y_{\mathcal{S}} = \frac{1}{|\mathcal{S}|} \sum_{\zeta \in \mathcal{S}} f(\zeta). \tag{1.36}$$

Assuming a sufficiently large sample $\mathcal{S}$ and using the central limit theorem the uncertainty of the Monte Carlo estimator is quantified as

$$\epsilon_{1-\alpha}(\mathcal{S}) \coloneqq c_\alpha \sqrt{\frac{\mathrm{var}(f)}{|\mathcal{S}|}} \tag{1.37}$$

with variance $\mathrm{var}(f) = \langle f^2 \rangle - \langle f \rangle^2$ and significance parameter c_α ensuring a $1 - \alpha$ confidence level, i.e.,

$$P\left(|\langle f \rangle - Y_{\mathcal{S}}| \leq c_\alpha \sqrt{\frac{\mathrm{var}(f)}{|\mathcal{S}|}} \right) = 1 - \alpha. \tag{1.38}$$

Further, $|\langle f \rangle - Y_{\mathcal{S}}|$ is expected to be normal distributed with zero mean and standard deviation $\sqrt{\mathrm{var}(f)/|\mathcal{S}|}$. Thus the significance parameter c_α is determined by

$$1 - \alpha = \frac{1}{\sqrt{2\pi}} \int_{-c_\alpha}^{c_\alpha} \exp\left(-\frac{x^2}{2}\right) \mathrm{d}x \tag{1.39}$$

[10] A relaxation corresponds to a sufficiently long propagation in time until the steady state is reached.

$$= \operatorname{erf}\left(\frac{c_\alpha}{\sqrt{2}}\right) \tag{1.40}$$

$$\Leftrightarrow c_\alpha = \sqrt{2}\operatorname{erf}^{-1}(1-\alpha) \tag{1.41}$$

with erf denoting the error function. Throughout this thesis we typically use a confidence level of at least 99% given by

$$\epsilon_{99\%}(\mathcal{S}) = 2.5758 \cdot \sqrt{\frac{\operatorname{var}(f)}{|\mathcal{S}|}} \tag{1.42}$$

and estimate the variance $\operatorname{var}(f)$ from the sample

$$\operatorname{var}(f) \approx \frac{1}{|\mathcal{S}|-1} \sum_{\zeta \in \mathcal{S}} \left(f(\zeta) - Y_{\mathcal{S}}\right)^2 . \tag{1.43}$$

Note that the derived error estimation holds as long as the measures f are generated independently from the same distribution. If one is interested in very accurate data, it is advisable to construct measures f which support a lower variance. For example, in a steady state one can perform ergodic measurements[11] using a steady state Markov chain instead of single states. Furthermore, to reduce the variance it might be useful to evaluate the Monte Carlo estimator on a set $\{\zeta_1, \ldots, \zeta_n\}$ of n correlated Markov chains, i.e., $f(\{\zeta_1, \ldots, \zeta_n\})$. To ensure that the uncertainty statements derived above hold, one should redefine the set of independent measures such that $\mathcal{S}$ becomes a set of sets which are independently generated from the same distribution, i.e., $\{\zeta_1, \ldots, \zeta_n\} \in \mathcal{S}$.

Finally, we stress that the Monte Carlo theory holds only for random events without correlations. To produce randomness in computer simulations we are limited to pseudo random number generators (pRNG) producing a series of deterministic **quasi**-random numbers. These **quasi**-random numbers are supposed to behave randomly but might introduce correlations[12]. A careful choice of the pRNG is essential to produce trustworthy results. To verify the quality of random number generators many tests have been developed and applied to standard pRNGs [22]. All Monte Carlo data presented in this thesis are generated by a C++ code and the Mersenne Twister MT19937 pRNG. Every RNG initialization had a different seed value taken from a static list, once produced by measuring temperature fluctuations of the CPU. For simulations where analytic results are available we could not notice significant deviations within the simulation accuracy. For all other cases we could not find untypical behavior indicating pRNG influences. Therefore, the presented data are assumed to be significant within their errors.

1.3.2. Monte Carlo simulations of density fluctuations

In the published contributions of Part II we study the statistics of steady state density fluctuations for a multi-species setting aiming to observe universal behavior. Here we will introduce two different Monte Carlo approaches we have used for the measurement of density fluctuations and discuss their advantages and disadvantages. To simplify the discussion, we investigate a simple periodic TASEP with random-sequential update, density $\rho = 1/2$ and factorizing steady state. When needed we will point out important details for multi-species systems.

The configuration space Σ_N^L for a periodic TASEP with L sites and $N = \rho \cdot L$ particles is given by the set of all possible configurations $\mathcal{C}$ containing N particles and $L-N$ holes. The stationary

[11] An ergodic measurement provides an improved estimating function $\tilde{f}$ by performing a time average of f along the steady state Markov chain.

[12] e.g., in Fig. 8.5 we compare the results of the measured current using different pRNGs.

distribution is uniform and therefore all states are equally likely. Further, using the binomial theorem one can deduce $|\Sigma_N^L| = \binom{L}{N}$.

The most naïve strategy for a Monte Carlo study of steady state density fluctuations starts with a uniformly randomly chosen steady state $\mathcal{C} \in \Sigma_{L/2}^L$ where one adds a particle if possible at position $k = 0$ at time $t = 0$. We denote the arising set of all possible initial configurations $\mathcal{C}_0$ by Ω_0 which is of size $|\Omega_0| = |\Sigma_{L/2}^L|$. Note that by adding a particle whenever it is possible we have enlarged the possible steady state configuration space to $\Sigma = \Sigma_{L/2}^L \cup \Sigma_{L/2+1}^L$ and therefore one observes a relaxation until the steady state is reached. For the periodic TASEP this means all states $\mathcal{C} \in \Sigma$ become equally likely so observe.

Computing the density profile for $t = 0$ one gets

$$\langle\, n_k(t=0) \,\rangle = \frac{1}{2} + \frac{1}{2}\delta_{0k} \tag{1.44}$$

where $n_k(t)$ measures for a particle at site k and time t and δ_{0k} is a Kronecker delta. Evolving the configuration $\mathcal{C} \in \Omega_0$ in time under TASEP update rules, the measure of the time-dependent density profile will uncover the statistics of steady state density fluctuations which are expected to have the form

$$\langle\, n_k(t) \,\rangle \simeq \frac{1}{2} + \frac{1}{2}(\sqrt{2}t)^{-2/3} f_{\mathrm{PS}}\left((\sqrt{2}t)^{-2/3}k\right). \tag{1.45}$$

Recalling that the asymptotic solution is satisfactory already for quite early times (see Fig. 1.5), this is a good starting point to discuss the statistics of Monte Carlo simulations.

In computer simulations we use a system of size L, which results in $|\Omega| = L!/((L/2)!)^2$ possible initial states. For a system of size $L = 300$ this means $\approx 9.4 \cdot 10^{88}$ initial configurations. Additionally, we have to deal with the unknown and complicated time-evolution of the phase space Ω_t and its associated probability $P(\mathcal{C}, t)$ to observe a certain configuration $\mathcal{C} \in \Omega_t \subseteq \Sigma$ during the relaxation process. Already, this setting illustrates why exact solutions are extremely rare for nonequilibrium systems.

However, Markov chain Monte Carlo simulations will allow to obtain results with satisfactory precision. First of all, we have to define an independent set $\mathcal{S}$ of Monte Carlo samples allowing the use of the central limit theorem. Since all states in Ω_0 are equally likely, each Markov chain starts at $t = 0$ with some configuration $\mathcal{C} \in \Omega_0$ drawn from equidistribution. Additionally, we assign to each Markov chain an independent set of random numbers needed for its time evolution. Note that we use just one process realization per sample. In the context of variance reduction, one could produce a set of independent initial configurations and a set of independent pseudo random number sequences separately. By averaging over all pairs the variance of the estimator is reduced. However, our Monte Carlo estimator is given by

$$Y_k(t) = \frac{1}{|\mathcal{S}|} \sum_{\zeta \in \mathcal{S}} n_k(t)|_\zeta \,. \tag{1.46}$$

The next step is to analytically quantify the uncertainty of our Monte Carlo estimator. The placed particle will exhibit a lower variance for the estimator inside its peak region than outside where no signal is present. Thus, we get an upper error bound by computing the uncertainty outside the peak region

$$\mathrm{var}(n_k(t)) \leq \left\langle\, (n_k - \rho)^2 \,\right\rangle = \langle\, n_k \,\rangle - \rho^2 = \rho(1-\rho) = 1/4. \tag{1.47}$$

Using Eq. (1.42) the Monte Carlo error within confidence level 99% is given by

$$|\langle\, n_k(t) \,\rangle - Y_k(t)| \leq \frac{2.5758}{\sqrt{4|\mathcal{S}|}}. \tag{1.48}$$

From Eq. (1.45) and using $\max_x f_{\mathrm{PS}}(x) = 0.54246$ we can deduce that the amplitude of $\langle\, n_k(t)\,\rangle - 1/2$ will be of order $0.21528 \cdot t^{-2/3}$. Assuming we need data with at least 1% of the amplitude accuracy for further analysis, the minimum sample size with 99% confidence level is then

$$|\mathcal{S}| \gtrsim 3.58 \cdot 10^5 \cdot t^{4/3} \tag{1.49}$$

or $4.19 \cdot 10^8$ samples for $t_{\max} = 200$. Note that each sample requires an independent propagation of the system up to $t_{\max}$. Additionally, to guarantee that the peak will not fill the system one should increase the system size as $L \propto t_{\max}^{1/z}$. It is even worse for a multi-species system, since due to the periodic boundary condition peaks with different velocities overlap again after a certain time. To exclude this event the minimum system size should scale as $L \propto t_{\max}$. Large systems and the huge amount of required samples make this procedure unsuitable for greater times where a better agreement with the asymptotic solution is expected.

There is still potential to significantly reduce the variance. For example, as mentioned above, one can assign multiple initial configurations to the same set of random numbers and propagate them in parallel. Additionally, one should simulate the system with and without the added particle in parallel and keep track of their difference. These differences could be detected very efficiently and especially allow for a very high resolution in the tail regions of the peak. A similar method and potential improvements are described in the subsequent section about defect effects. In case one is interested in very precise early time data this is the most promising technique.

Nevertheless, the major problem not reaching the asymptotic limit within computation time will persist. This is caused by the fact that each simulation run carries the information of only one placed particle for which we have to simulate a complete system. Furthermore, the computation time needed for the state propagation will limit us to small systems and in addition we have to expect finite size effects. Anyway, this procedure inhibits high potentials to generate high quality early time data.

Next, we discuss a different approach which allows us to reach further into the asymptotic regime. Especially, this technique allows for precise data in the peak region which is strongly required for a precise fit of z. The two most costly parts are propagating the system and recording the observable. To overcome the weaknesses of this technique we investigate the structure function Eq. (1.8) instead. The structure function tells us basically the same information, but the observable is translation invariant and the system stays in its steady state and thus time-invariant phase space Ω_0. Thus, we can apply an average over the whole system size and perform ergodic measures to reduce the cost of propagation which is crucial to get far inside the asymptotic regime. Again, we start with the definition of an independent Monte Carlo sampling set $\mathcal{S}$ of Markov chains. Each Markov chain starts at $t = 0$ with some randomly chosen steady state configuration $\mathcal{C} \in \Omega_0$ and got its own set of independent random numbers needed for the propagation in time. Since $Q(\mathcal{C})$ and $P(\mathcal{C})$ are both uniform distributions our initial state is drawn from the correct distribution. Therefore, the unbiased Monte Carlo estimator for the structure function is given by

$$S_k^{MC}(t) = \frac{1}{|\mathcal{S}|} \sum_{\zeta \in \mathcal{S}} \sigma_k(t)|_\zeta \,. \tag{1.50}$$

with an estimating function designed as

$$\sigma_k(t; L, T, \tau) = \frac{1}{T} \sum_{j=0}^{T-1} \frac{1}{L} \sum_{l=0}^{L-1} n_{l+k}(t + j\tau) n_l(j\tau) - \rho^2 \tag{1.51}$$

where we made use of translational invariance and included ergodic measures such that intermediate propagation results are reused. More precisely, choosing $T > 1$ will allow for a variance

reduction which scales as $\mathrm{var}(\sigma_k(t;L,T,\tau)) \sim T^{-1/2}$. This is accomplished by introducing additional measurements for which we *only* have to propagate the system with time τ instead of $t_{\max} \gg \tau$. Limiting the support points for k to a fixed number (typically $300-500$) equally placed within the peak, an increase of system size brings us in a win-win situation, since increasing the system size improves statistics $\mathrm{var}(\sigma_k(t;L,T,\tau)) \sim L^{-1/2}$ and suppresses finite-size effects. The achieved optimization turns out to be enormous and crucial to efficiently produce accurate data far inside the asymptotic regime. However, we have to pay the price for the storage of all intermediate states and restrict the observable time to $t \in \tau \cdot \mathbb{N}_0$. Therefore, one has to find for each model a good trade-off for $t_{\max}$, L, τ and T. Although we have achieved massive improvements, the recording is still expensive and it is advisable to limit the observation times and grid points to a required minimum. In case one is interested in measuring dynamical exponents we recommend to increase the observation times exponentially.

Either way, to quantify the uncertainty of this approach we use a 99% confidence level

$$\left|S_k^{MC}(t) - S_k(t)\right| \quad \leq \quad 2.5758\sqrt{\frac{\mathrm{var}(\sigma_k(t;L,T,\tau))}{|\mathcal{S}|}}. \tag{1.52}$$

To demonstrate the potential we compare results of this approach to the naïve version of the first introduced approach.

In Fig. 1.5 we have already shown simulation data recorded with the Monte Carlo method described above using the parameters

$$|\mathcal{S}| = 120;\ L = 10^6;\ T = 3000;\ \tau = 100. \tag{1.53}$$

The statistical error is less than $3.4 \cdot 10^{-6}$ for all data points. Using the first technique would require at least $|\mathcal{S}^1| = 1.4 \cdot 10^{11}$ samples to reach the same accuracy, while the system size should be at least $L^1 = 5000$ guaranteeing that the peak will not fill the whole system. To compare both methods we calculate an equivalent quantity for the time needed to perform the propagation of all states. These are $E^1 = |\mathcal{S}^1| \cdot L^1 \cdot t_{\max}$ for the first technique and $E^2 = |\mathcal{S}| \cdot L \cdot (t_{\max} + (T-1)\tau)$ for the new technique using translational invariance and ergodic measures. Setting $t_{\max} = 8900$ as in Fig. 1.5 we get $E^1 = 6.2 \cdot 10^{18}$ or $E^2 = 3.7 \cdot 10^{13}$. The first and second approach shows already a very huge difference $E^1/E^2 = 1.7 \cdot 10^5$. In case we would have two peaks this would be even bigger since we should have taken a larger system. This stresses the improvement and indicates why the use of the first technique is limited to early times.

In case one needs data only for a small amount of time points ($n \leq 10$) growing exponentially, one can avoid memory problems by implementing the next generation of computer code as follows: Instead of storing all intermediate states one should store only the states for times of interest and its full random-number generator initialization. This largely reduces the required memory but comes with the cost of computing the time evolution of n stored frames instead of just decompressing them from storage. The additional cost for propagation could be compensated or even reduced by using a smaller τ. The computation time equivalent quantity defined above would be $E_{next} = |\mathcal{S}| \cdot L \cdot (t_{\max} + (T-1)n\tau)$. Using this kind of code would allow to get further into the asymptotic regime and simulations of even bigger systems. Especially for the calculation of dynamical correlation functions in 2D systems this would be of great interest. It will allow to run simulations in parallel with sufficiently large systems and without filling the whole memory space. Further improvements can be achieved by evaluating the estimator function for multiple correlated Markov chains with different initial conditions but generated with the same random numbers. Extra costs will be negligible since producing high quality random numbers is the most costly part of propagation.

1.3.3. Monte Carlo simulations of defect systems

In this section we will explain how to efficiently detect effects of inhomogeneities and defects in steady states. The system without the defect will be called pure system. We shall define the steady state phase space Ω_p (Ω_d) and its associated probability distribution P_p (P_d) for the pure (defect) system. The major interest for a defect system is often the difference of some observable f to the pure system, i.e.,

$$\langle \delta f \rangle_{d,p} \coloneqq \langle f \rangle_d - \langle f \rangle_p. \tag{1.54}$$

The most naïve and simplest Monte Carlo strategy to calculate $\langle \delta f \rangle_{d,p}$ is running independent simulations for $\langle f \rangle_d$ and $\langle f \rangle_p$. Having said that, it is also the inefficient strategy one can use if one needs accurate data. In general Ω_d and P_d are unknown which means we have to create a state $\mathcal{C}$ with the probability $Q_d(\mathcal{C}) \propto P_d(\mathcal{C})$. This is usually achieved by starting with some configuration $\mathcal{C}_\star$ from the distribution $Q_\star(\mathcal{C}_\star)$ and propagating the defect system into its steady state. To improve the statistics our idea is to start with some configuration $\mathcal{C}_\star$ generated with the probability $Q_\star(\mathcal{C}_\star) \propto P_p(\mathcal{C}_\star)$. The crucial step is to take a copy of $\mathcal{C}_\star$ and propagating one configuration with the defect and the other with the pure update rules in parallel using the same random numbers until we reach the steady state $\mathcal{C}_{d,0}$ of the defect system. The obtained configuration $\mathcal{C}_{d,0}$ is produced with a probability $Q_d(\mathcal{C}_{d,0}) \propto P_d(\mathcal{C}_{d,0})$. Thereby, the propagated pure state $\mathcal{C}_{p,0}$ stays by construction a steady state generated with a probability $Q_p(\mathcal{C}_{p,0}) \propto P_p(\mathcal{C}_{p,0})$. In case $P_p(\mathcal{C})$ is an unknown distribution as well one could start with an initial state from the distribution $Q_\star$, but then one has to ensure that both states are relaxed. Relaxations in computer simulations are often insufficient and one has to be aware of its finite-time effects. It might be useful to look for relaxation strategies reducing the finite-time effects. In computer simulations the cost for the propagation of the second state is negligible since the pRNG is the propagation bottleneck and expensive random numbers are reused. Taking into account that both systems are in steady states it is advisable to perform ergodic measurements.

In particular for the defect TASEP with open boundary conditions (Fig. 1.3), we update each site at exactly the same time and with exactly the same random number needed for the jump event decision. Although $P_p(C)$ is exactly known for the open boundary TASEP we cannot produce states according to $Q_\star(\mathcal{C}_\star) \propto P_p(\mathcal{C}_\star)$. Our main interest is to discover a phase transition for small defect strength inside the maximum current phase. Therefore, to exclude errors arising from relaxation effects we start with a product state where each site is occupied with probability 1/2. This initial state $\mathcal{C}_\star$ corresponds to the factorizing maximum current steady state for a system with entry and exit rates $\alpha = \beta = \frac{1}{2}$. To ensure that our measured defect phenomena are not dominated by relaxation effects we introduce a two level relaxation. Firstly, we drive the pure system into its steady state while our initial condition guarantees the system to stay inside the maximum current phase. For the second relaxation we take a copy of the relaxed pure state and propagate the defect and pure system in parallel until we reach the steady state of the defect system.

Following this strategy, we ensure that the measured effects are induced by the system's defect. The parallel evolution of both system in the second relaxation level secures a covariance between the systems which is needed for efficient Monte Carlo sampling. In contrast, when performing independent simulations with independent Markov chains we have to average over many samples until we see significant differences. These differences might additionally contain some systematic errors caused by the relaxation process.

The procedure described above can be interpreted as the second level of a Multi-Level Monte Carlo simulation [24]. Indeed, this idea turned out to be very powerful and we want to discuss

the achieved improvements. Therefore, the coherently[13] generated initial configurations propagated into coherent Markov Chains are denoted as ζ_d (ζ_p) for the defect (pure) system and the set of Monte Carlo samples is given by a set of pairs $\{\zeta_d, \zeta_p\} \in \mathcal{S}$. The set of only pure/defect states in the sample set $\mathcal{S}$ are denoted by $\mathcal{S}_{d/p}$. The new function of interest is

$$\Delta f(\{\zeta_d, \zeta_p\}) \coloneqq f(\zeta_d) - f(\zeta_p) \tag{1.55}$$

and the Monte Carlo estimator is given by

$$Y_{\mathcal{S}} = \frac{1}{|\mathcal{S}|} \sum_{\{\zeta_d, \zeta_p\} \in \mathcal{S}} \Delta f(\{\zeta_d, \zeta_p\}). \tag{1.56}$$

Although Ω_d and Ω_p might be of different size the linearity of Eq. (1.55) guarantees an unbiased sample

$$\lim_{|\mathcal{S}| \to \infty} Y_{\mathcal{S}} \quad = \quad \langle\, \delta f \,\rangle_{d,p}. \tag{1.57}$$

To quantify the uncertainty we need to know the variance of $\Delta f(\{\zeta_d, \zeta_p\})$ which can be rewritten as

$$\mathrm{var}_{d,p}(\Delta f) \quad = \quad \mathrm{var}_d(f) + \mathrm{var}_p(f) - 2\mathrm{cov}_{d,p}(f, f) \tag{1.58}$$

with the covariance

$$\mathrm{cov}_{d,p}(f, f) \quad = \quad \lim_{|\mathcal{S}| \to \infty} \frac{1}{|\mathcal{S}|} \sum_{\{\zeta_d, \zeta_p\} \in \mathcal{S}} f(\zeta_d) f(\zeta_p) - \langle\, f \,\rangle_d \langle\, f \,\rangle_p. \tag{1.59}$$

In fact, we cannot calculate the covariance analytically, but one should note that for the trivial case of identical systems the variance Eq. (1.58) vanishes.

Nevertheless, we will demonstrate the potential of this method by discussing the results for differences in density profiles in the open boundary TASEP defect system. Subtracting the defect state from the pure state in parallel evolving systems, differences are encoded in ± 1. These differences can be mapped to two types of second-class particles, which we will call up and down 'second-class' particle. 'First-class' particles correspond to sites which are occupied in both system's (Top of Fig. 1.7). Instead of evolving both systems in parallel, it is equivalent to simulate the system with two classes of particles (Bottom of Fig. 1.7). These particles follow the same TASEP rules but might interact with each other. A first-class particle will not care about second-class particles and push them back. Therefore, the dynamics of the first-class particles remains unchanged. In case a first-class particle cannot cross the defect site it separates into a up-down pair of second-class particles. When a up and down particle meet each other at any site they recombine to a 'first-class' particle. At the entry reservoir we feed in first-class particles which might remove second-class particles from the system. The exit reservoir does not distinguish between particle classes and all particles are removed with the same rate. The second-class particles allow to keep track of defect effects without biasing the dynamics of the pure and defect systems. This idea is different to the work by Derrida *et al* [18], where one type of conserved second-class particles was introduced to measure the shock position.

A weak defect rate $r \lesssim 1$, which is the most interesting case for us, corresponds to a small birth rate of second-class particles. Since these second-class particles may recover to a first-class

[13] Coherent is used in the sense that a covariance between states is present.

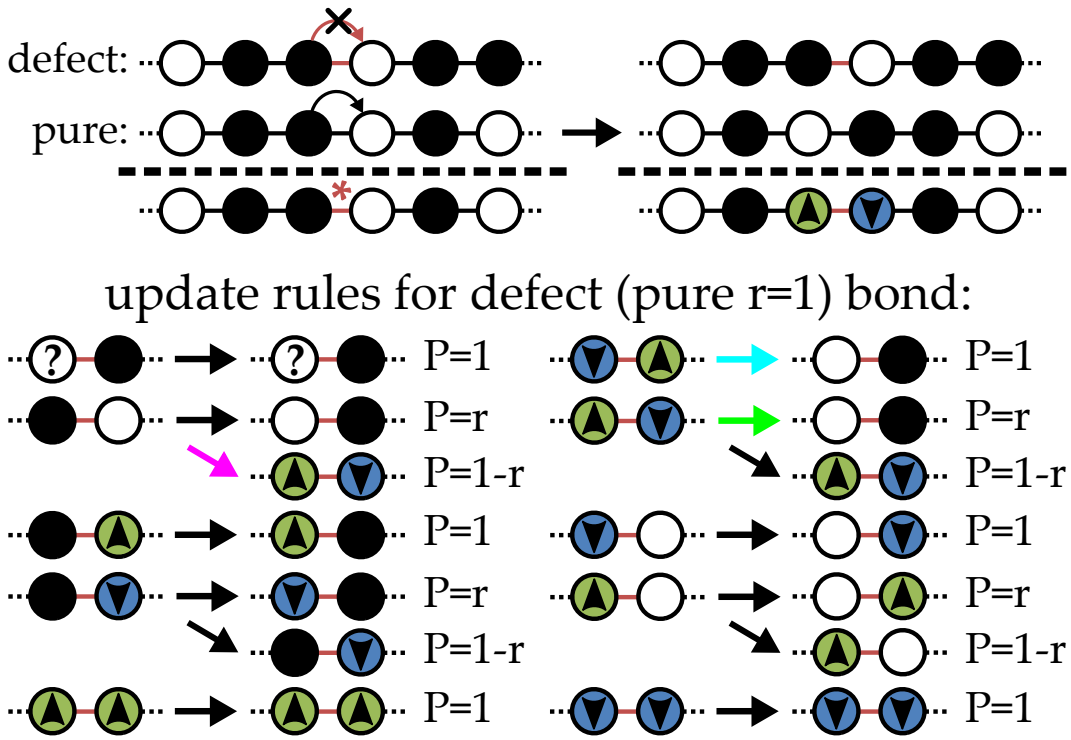

Figure 1.7.: **Top:** Mapping of parallel evolving systems (defect and pure) to a two types second-class particles system. Here a pair of second-class particle is created at the defect site (red bond). Differences between the defect and pure system are encoded in up/down particles. Black and up (down) particles correspond to particles in the defect (pure) system. **Bottom:** Site update rules for the two type second-class particle system. r is the defect strength at the slow bond. Update rules for a pure bond are obtained for $r = 1$. P denotes the probability for the indicated event. Question marks are placeholders to show the exclusion with respect to 'first-class' particles. The magenta arrow indicates the separation process from a "first-class" particle into a pair of "second-class" particles (only at defect site!) while cyan and green indicate the possible recoveries to a 'first-class' particle (all sites!).

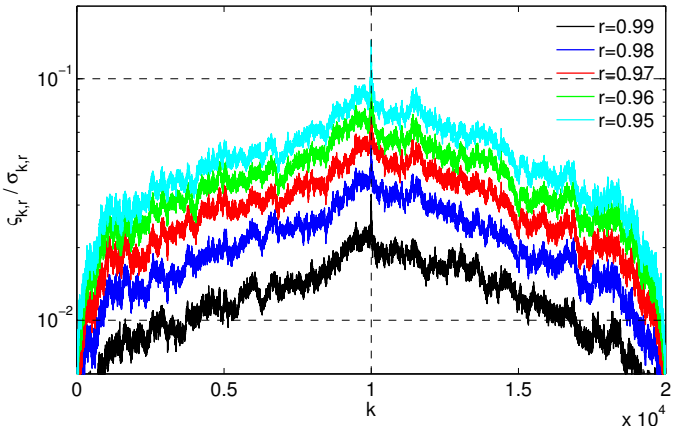

Figure 1.8.: Semilog plot for the quotient of the estimator's standard deviations versus system site k and different defect hopping rates. We find a lower improvement in the region of the defect site since the defect reduces the covariance between the parallel evolving systems while in the vicinity of the boundaries the covariance is reestablished due to the coherent feeding in process. For a decreasing hopping rate the improvement vanishes within the bulk but persists next to the boundaries.

particle or may exit the system at its boundaries, we will find only a few of them in a steady state. Decoding the second-class particle picture into separately evolving systems, their configurations will show a significant covariance. Therefore, we expect a significant improvement especially for a small defect strength. The densities are recorded by using ergodic measurements

$$f_{k,r} = \frac{1}{M} \sum_{m=0}^{M-1} n_k(t + m\Delta t) \tag{1.60}$$

where r denotes the defect hopping rate, $n_k(t)$ measures for a particle at site k and time t, M number of ergodic measures, Δt is the time between to measures while $\Delta t = 1$ corresponds to $L + 1$ random-sequential time updates. To compare the naïve and parallel evolving approach we compute their standard deviations for different system sites and defect hopping rates, i.e.,

$$\varsigma_{k,r} = \sqrt{\mathrm{var}(f_{k,r}) + \mathrm{var}(f_{k,1})} \tag{1.61}$$

$$\sigma_{k,r} = \sqrt{\mathrm{var}(f_{k,r}) + \mathrm{var}(f_{k,1}) - 2\mathrm{cov}(f_{k,r}, f_{k,1})}. \tag{1.62}$$

The quotient $\varsigma_{k,r}/\sigma_{k,r}$ is equivalent to the quotient of achieved accuracy within the same computation time. For a *weak* defect ($r = 0.99$) the data near the boundary are at least 100 times more accurate (Fig. 1.8). This means we have to run the naïve approach 10^4 times longer to achieve the same accuracy. The produced accuracy is indeed needed to detect significant defect effects in the vicinity of the boundaries. However, we generated the data for $r = 0.99$ on our department's desktop cluster within 20 hours using 100 CPUs. To produce data with the same accuracy using the naïve approach would have taken 23 years.

Up to now, we have only discussed the interest in differences of some observable f. Finally, we will point out another prime example to apply this idea to a bit more general setting. Therefore, we are interested in $\langle f_1 \rangle_s$ for some system s. The naïve way to estimate $\langle f_1 \rangle_s$ would be

$$Y = \frac{1}{|\mathcal{S}_s|} \sum_{\zeta_s \in \mathcal{S}_s} f_1(\zeta_s). \tag{1.63}$$

But in case one knows $\langle f_2 \rangle_{s'}$ and is able to introduce correlations between the functions f_1, f_2 or the systems s, s' one should make use of the linearity of the expectation value and simulate

$$\bar{Y} = \frac{1}{|\mathcal{S}|} \sum_{\{\zeta_s, \zeta_{s'}\} \in \mathcal{S}} (f_1(\zeta_s) - \lambda f_2(\zeta_{s'})) + \lambda \langle f_2 \rangle_{s'} \tag{1.64}$$

where we have added a control variate λ. Both Monte Carlo estimators are unbiased and will converge to the sought expectation value $\langle f_1 \rangle_s$, but comparing their variances one finds

$$\begin{aligned} \mathrm{var}(Y) &= \frac{\mathrm{var}(f_1)}{|\mathcal{S}_s|} & (1.65) \\ \mathrm{var}(\bar{Y}) &= \frac{1}{|\mathcal{S}|} \left(\mathrm{var}(f_1) + \lambda^2 \mathrm{var}(f_2) - 2\lambda \mathrm{cov}(f_1, f_2) \right) & (1.66) \end{aligned}$$

and therefore the choice of λ allows to reduce the variance. The optimal value for λ is given by

$$\lambda_o = \frac{\mathrm{cov}(f_1, f_2)}{\mathrm{var}(f_2)} \tag{1.67}$$

where one should note the two limiting cases $\lambda = 0$ for vanishing and $|\lambda| = 1$ and strong covariance which tells us basically when to use this technique. Using λ_o the minimum variance becomes

$$\mathrm{var}(\bar{Y}) = \frac{1}{|\mathcal{S}|} \left(\mathrm{var}(f_1) - \frac{(\mathrm{cov}(f_1, f_2))^2}{\mathrm{var}(f_2)} \right). \tag{1.68}$$

One could extend these ideas to multiple levels [24, 25] which might allow for further improvements. These ideas apply especially to parameter studies, where one could reduce the simulation cost by generating only for relatively few simulations accurate data and estimating the other expectation values using multi-level Monte Carlo. For multi-dimensional parameter studies these ideas have recently been extended to multi-index Monte Carlo methods [30]. In summary, we have shown the potential of advanced Monte Carlo techniques and conclude that it is worth investing some time to get familiar with the broad spectrum of Monte Carlo variance reduction techniques and create ideas how to introduce correlations in a clever way without biasing the sample but allowing for better results.

2. Outline

2.1. Outline of Part II - Dynamical Universality Classes

Part II contains published articles addressing universal behavior of one-dimensional short-ranged driven diffusive lattice gases with locally conserved density fields. Dynamical universality classes characterize transport properties of nonequilibrium systems, such as the steady state fluctuations and how these decay in time. Until recently the only two known dynamical universality classes were the diffusive class with dynamical exponent $z = 2$ along with the superdiffusive KPZ class with dynamical exponent $z = 3/2$.

Some years ago the dynamical exponent $z = 5/3$ was discovered in the context of anharmonic chains [55] and very general short-ranged one-dimensional Hamiltonian systems [5]. These systems contain three conservation laws and by symmetry the dynamical exponent $z = 5/3$ appears for this so-called heat-mode with collective velocity $v = 0$. Other sound-modes belong to the KPZ class ($z = 3/2$) and move with velocity $v = \pm c$. This raises the question if superdiffusive modes with dynamical exponent $z = 5/3$ may exist for driven diffusive systems and if they can be realized in a minimal required setting with two conservation laws.

As a part of my master's project, supervised by Vladislav Popkov, Andreas Schadschneider, and in collaboration with Gunter Schütz, we started to investigate a two-species TASEP which provides a minimal setting for the support of a $z = 5/3$ mode.

In Chapter 3[1], we demonstrate the appearance of a superdiffusive mode with dynamical exponent $z = 5/3$ by using mode coupling theory and dynamical Monte Carlo simulations of a two-species TASEP. When the dynamics is symmetric under the interchange of the lanes we find for our model a diffusive mode with $z = 2$ besides a modified KPZ[2] mode with exponent $z = 3/2$.

A crucial hint by Herbert Spohn pointing out the possibility for the golden-mean $\varphi = (1+\sqrt{5})/2$ universality class with dynamical exponent $z = \varphi$ prior to publication of [90] motivated us to systematically explore the mode coupling equations and its relevance for driven diffusive systems. This work, which was supervised by Andreas Schadschneider, Gunter Schütz, and Vladislav Popkov, was pursued within my PhD project.

In Chapter 4[3], we extend our results from the previous article and show that all universality classes predicted by mode coupling theory, for systems with two conservation laws, occur in two-component driven diffusive systems. The macroscopic current-density relation and the compressibility matrix determine completely all permissible universality classes through the mode coupling matrices. Using dynamical Monte Carlo simulations we present numerical evidence for the golden mean universality class ($z = \varphi$) and the 3/2-Fibonacci class showing the dynamical exponent $z = 3/2$ (but different from the KPZ universality class). Both universality classes have maximally asymmetric z-stable Lévy scaling functions and have not been reported before in the literature on driven diffusive systems.

Going beyond, we generalize in Chapter 5[4] our results to an arbitrary number of conservation laws and find that all feasible dynamical exponents z_α are ratios of neighboring Fibonacci numbers, starting with either $z_1 = 3/2$ (if a KPZ mode exists) or $z_1 = 2$ (if a diffusive mode is present). If neither a diffusive nor a KPZ mode are present, all dynamical exponents correspond to the

[1] Chapter 3 contains an article published with V. Popkov and G. Schütz.
[2] A modified KPZ class consists of a KPZ mode which couples nonlinear to a diffusion mode ($z = 2$).
[3] Chapter 4 contains an article published with V. Popkov and G. Schütz.
[4] Chapter 5 contains an article published with V. Popkov, A. Schadschneider, and G. Schütz.

golden mean $z_\alpha = (1+\sqrt{5})/2$. The universal scaling functions of these Fibonacci modes are asymmetric Lévy distributions, while the dynamical exponents and scaling functions are completely fixed by the macroscopic stationary current-density relation and the compressibility matrix. Due to the fact that these Fibonacci modes already occur in systems with nonlinearities of the minimal order $\rho_\lambda^2 \rho_\mu$ in the associated currents we argue that the universality classes predicted by the mode coupling theory are generic for multi-species driven diffusive systems.

In Chapter 6[5], we provide a detailed derivation for the dynamical exponents and its associated scaling functions of the Fibonacci modes by exactly solving the one-loop mode coupling equations for the strictly hyperbolic setting.

2.2. Outline of Part III - Defect-Induced Phase Transitions

Local reductions of capacity are one of the most important scenarios for traffic systems. Similar to boundaries, a local defect can have global influences on the system. Much less is known for weak inhomogeneities, like sites with reduced hopping rates in a TASEP. One of the most natural question is "When does a local inhomogeneity lead to global effects in the system?". The minimal setting addressing this problem is the study of an open boundary TASEP in the maximum current phase where a single defect hopping rate r (slow bond) is placed in the middle. Intuition and mean-field calculation reveal that an arbitrarily small defect, i.e., $r_c = 1$, would have a global effect in the system. Up to now it was not possible to verify this prediction using computer simulations since subtle defect phenomena are easily lost in fluctuations. Indeed a recent numerical study indicated that a small defect strength would not have a global influence and further $r_c = 0.80(2)$ was suggested. As discussed in Section 1.3.3 we improved the Monte Carlo estimator such that we may distinguish defect-induced phenomena from fluctuations. This new technique allows us to show $r_c > 0.99$ and gives strong evidence that it is indeed $r_c = 1$ as predicted by the mean-field theory and supported by series expansion results [13, 38].

Part III contains two published articles which are a joint work with Andreas Schadschneider and Vladislav Popkov. The article in Chapter 7 originates from a conference contribution based on our results in Chapter 8. Chapter 7 aims to introduce the generic nature of defect phenomena and give implications for the analysis of empirical and numerical data. Chapter 8 is more technical and addresses r_c for the TASEP.

[5] Chapter 3 contains an article published with V. Popkov, A. Schadschneider, and G. Schütz.

Part II.

Published Contributions: Dynamical Universality Classes In Driven Diffusive Systems

3. Non-KPZ modes in two-species driven diffusive systems

Vladislav Popkov[1,2], **Johannes Schmidt**[1]
and Gunter M. Schütz[3,4]

[1] *Institut für Theoretische Physik, Universität zu Köln,*
Zülpicher Str. 77, 50937 Cologne, Germany
[2] *CSDC Università di Firenze, via G.Sansone 1, 50019 Sesto Fiorentino, Italy*
[3] *Institute of Complex Systems II, Theoretical Soft Matter and Biophysics,*
Forschungszentrum Jülich, 52425 Jülich, Germany
[4] *Interdisziplinäres Zentrum für Komplexe Systeme,*
Universität Bonn, Brühler Str. 7, 53119 Bonn, Germany

PACS numbers: 05.60.Cd, 05.20.Jj, 05.70.Ln, 47.10.-g

Published in: Physical Review Letters (PRL)
May 2014, vol. 112, iss. 20, p. 200602
doi: 10.1103/PhysRevLett.112.200602

Abstract: Using mode coupling theory and dynamical Monte-Carlo simulations we investigate the scaling behaviour of the dynamical structure function of a two-species asymmetric simple exclusion process, consisting of two coupled single-lane asymmetric simple exclusion processes. We demonstrate the appearence of a superdiffusive mode with dynamical exponent $z = 5/3$ in the density fluctuations, along with a KPZ mode with $z = 3/2$ and argue that this phenomenon is generic for short-ranged driven diffusive systems with more than one conserved density. When the dynamics is symmetric under the interchange of the two lanes a diffusive mode with $z = 2$ appears instead of the non-KPZ superdiffusive mode.

Transport in one dimension has been known for a long time to be usually anomalous [1, 2]. Signatures of this behaviour are a superdiffusive dynamical structure function and a power law divergence of transport coefficients with system size, characterized by universal critical exponents. Unfortunately, however, despite a vast body of work, analytical results for model systems have remained scarce and numerical results are often inconclusive. Therefore the exact calculation [3] of the dynamic structure function for the universality class of the Kardar-Parisi-Zhang-equation [4] with dynamical exponent $z = 3/2$ some ten years ago came as a major breakthrough. This function was obtained for a specific driven diffusive system, the asymmetric simple exclusion process, which has a single conserved density and hence a single mode, the KPZ-mode. By virtue of universality then also systems such as growth models [5, 6] or one-dimensional driven fluids [7] can be described in terms of the KPZ universality class.

More recently it was established in the context of anharmonic chains [8] and very general short-ranged one-dimensional Hamiltonian systems [9] that in the presence of more than one conserved quantity the dynamics is richer and other modes have to be expected. In particular, in systems with three conservation laws a heat mode with $z = 5/3$ may be present besides two KPZ modes. The main assumption underlying these conclusions is that the relevant slow variables are the long wave length Fourier components of the conserved quantities and products of these [2, 9].

Going back to driven diffusive systems we note that somewhat surprisingly there is little information about the dynamical structure functions in driven diffusive systems with more than one conservation law. In one dimension these systems are known to exhibit extremely rich stationary and dynamical behaviour and they serve widely as paradigmatic models for the detailed study of non-equilibrium fluctuation phenomena such as shocks [11, 12, 13], spontaneous symmetry breaking and hysteresis [14, 15], phase separation and coarsening [16, 17, 18], or dynamical phase transitions [19]. In view of this it is of interest to explore the transport properties of such systems, in particular which modes govern the fluctuations of the locally conserved slow modes and how these decay in time.

In this spirit Ferrari et al. [20] studied very recently a two-species exclusion process, using mode-coupling theory and Monte-Carlo simulations, and found two very clean KPZ-modes, but no other modes. For a similar model, exact finite size scaling analysis of the spectrum indicates a dynamical exponent $z = 3/2$ [21]. In older work on other lattice gas models with two conservation laws the presence of a KPZ mode and a diffusive mode was observed [22, 12]. So far there has been no indication of the existence of a heat-like mode with $z = 5/3$. In the light of the work [9, 8] on short-ranged Hamiltonian systems this is intriguing and raises the question whether a heat-like mode can exist in driven diffusive systems, and, if yes, how many conservation laws are required to generate it. In this letter we answer these questions by using the mode coupling theory developed in [8, 20] for non-linear fluctuating hydrodynamics and by confirming the analytical findings with Monte-Carlo simulations of a two-species asymmetric simple exclusion process. It will transpire that a superdiffusive $z = 5/3$ mode along with a KPZ mode exists and that two conservation laws are sufficient to generate the phenomenon. Also a KPZ mode along with a diffusive mode can occur on a line of higher symmetry, a phenomenon which cannot appear in Hamiltonian systems [10].

We consider the following stochastic lattice gas model. Particles hop randomly on two parallel chains with N sites each, without exchanging the lane, unidirectionally and with a hard core exclusion and periodic boundary conditions. We denote the particle occupation number on site k in lane i by $n_k^{(i)}$. A hopping event from site k to site $k+1$ on the same lane may happen if site k is occupied and site $k+1$ is empty. The rate of hopping r_i in lane i depends on the sum

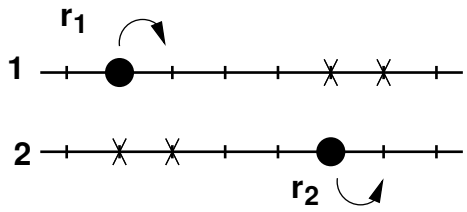

Figure 3.1.: Schematic representation of the two-lane totally asymmetric simple exclusion process. A particle on lane i hops to the neighbouring site (provided this target site is empty) on the same lane with rate r_i that depends on the number of particles on the adjacent sites of the other lane (marked by a cross).

of particle numbers at sites $k, k+1$ on the adjacent lane as follows (Fig. 3.1): Let us denote the sum of particles on the sites $k, k+1$ of lane i as $n^{(i)} := n_k^{(i)} + n_{k+1}^{(i)}$. Then the rates r_i of hopping from site k to site $k+1$ on lane i are given by

$$r_1 = 1 + \frac{\gamma n^{(2)}}{2}, \quad r_2 = b + \frac{\gamma n^{(1)}}{2} \tag{3.1}$$

where $\gamma \geq -\min(1, b)$ is a coupling parameter. For $b = 1$ we recover the two-lane model of [25]. Since there is only hopping within lanes, the total number of particles M_i in each lane is conserved.

The model in a more general multilane geometry was introduced in [23]. It was shown that the choice of rates (3.1) results in a stationary distribution which is a product measure, both between lanes and between the sites. For the two-lane system that we study here this leads to stationary currents

$$\begin{aligned} j_1(\rho_1, \rho_2) &= \rho_1(1-\rho_1)(1+\gamma\rho_2) \\ j_2(\rho_1, \rho_2) &= \rho_2(1-\rho_2)(b+\gamma\rho_1) \end{aligned} \tag{3.2}$$

where $\rho_{1,2} = M_{1,2}/N$ are the densities of particles in the first and second lane respectively. Notice that a product measure corresponds to a grandcanonical ensemble with a fluctuating particle number. These fluctuations are described by the symmetric compressibility matrix C with matrix elements

$$C_{ij} = \frac{1}{N} < (M_i - \rho_i N)(M_j - \rho_j N) >= \rho_i(1-\rho_i)\delta_{i,j}. \tag{3.3}$$

The starting point for investigating the large-scale dynamics of this microscopic model is the system of conservation laws $\partial_t \rho_i(x,t) + \partial_x j_i(x,t) = 0$ [24] where $\rho_i(x,t)$ is the coarse-grained local density field of component i and $j_i(x,t)$ is the associated current, given as a function of the local densities by (3.2). With the vector $\vec{\rho}$ of densities $\rho_i(x,t)$ these equations can be written

$$\frac{\partial}{\partial t}\vec{\rho} + A\frac{\partial}{\partial x}\vec{\rho} = 0 \tag{3.4}$$

where A is the Jacobian with matrix elements $A_{ij} = \partial j_i / \partial \rho_j$. Its eigenvalues c_i are the characteristic velocities which on microscopic scale are the speeds of local perturbations [25]. As a function of the ρ_i the matrix AC is symmetric [26] which guarantees that the system (3.4) is hyperbolic [27].

The hydrodynamic equations (3.4) describe the deterministic time evolution of the density $\rho_i(x,t)$ under Eulerian scaling [24]. The effect of fluctuations, which occur on finer space-time

scales, can be captured by adding phenomenological white noise terms ξ_i and taking the nonlinear fluctuating hydrodynamics approach together with a mode-coupling analysis of the nonlinear equation [20]. In this framework one expands the local densities around their stationary values $\rho_i(x,t) = \rho_i + u_i(x,t)$ and transforms to normal modes $\vec{\phi} = R\vec{u}$ where A is diagonal. The transformation matrix R uniquely defined by $RAR^{-1} = \mathrm{diag}(c_i)$ and the normalization condition $RCR^T = 1$. Keeping terms to first non-linear order yields

$$\partial_t \phi_i = -\partial_x \left(c_i \phi_i + \frac{1}{2} \langle \vec{\phi}, G^{(i)} \vec{\phi} \rangle - \partial_x (D\vec{\phi})_i + (B\vec{\xi})_i \right). \tag{3.5}$$

Here the angular brackets denote the inner product in component space and

$$G^{(i)} = \frac{1}{2} \sum_j R_{ij} (R^{-1})^T H^{(j)} R^{-1}. \tag{3.6}$$

are the mode coupling matrices obtained from the Hessian $H^{(i)}$ with matrix elements $\partial^2 j_i / (\partial \rho_j \partial \rho_k)$. The matrices D (transformed diffusion matrix) and B (transformed noise strength) do not appear explicitly below.

For strictly hyperbolic systems the normal modes have different speeds and hence their interaction becomes very weak for long times. Thus, by identifying ϕ_i with the gradient of a height variable one has to leading order generically two decoupled KPZ-equations with nonlinearity coefficients $G^{(i)}_{ii}$. The other diagonal elements $G^{(i)}_{jj}$ provide the leading corrections to the KPZ modes, the offdiagonal elements result in subleading corrections. We point out the scenarios relevant to our model, as predicted by mode-coupling theory. (i) If both $G^{(1)}_{11}$ and $G^{(2)}_{22}$ are non-zero we expect two KPZ modes with $z = 3/2$. (ii) On the other hand, if e.g. $G^{(1)}_{11} = 0$, but $G^{(1)}_{22} \neq 0$ and $G^{(2)}_{22} \neq 0$, then mode coupling theory predicts mode 1 to be a superdiffusive mode with $z = 5/3$ and mode 2 to be KPZ. (iii) Finally, if both $G^{(1)}_{11} = G^{(1)}_{22} = 0$ but $G^{(2)}_{22} \neq 0$ then mode 2 remains KPZ while mode 1 becomes diffusive, up to possible logarithmic corrections which may arise from cubic couplings to triplets of modes [9, 28].

For our system, the explicit forms of A and $H^{(i)}$ are

$$A = \begin{pmatrix} (1+\gamma\rho_2)(1-2\rho_1) & \gamma\rho_1(1-\rho_1) \\ \gamma\rho_2(1-\rho_2) & (b+\gamma\rho_1)(1-2\rho_2) \end{pmatrix} \tag{3.7}$$

$$H^{(1)} = \begin{pmatrix} -2(1+\gamma\rho_2) & \gamma(1-2\rho_1) \\ \gamma(1-2\rho_1) & 0 \end{pmatrix} \tag{3.8}$$

$$H^{(2)} = \begin{pmatrix} 0 & \gamma(1-2\rho_2) \\ \gamma(1-2\rho_2) & -2(b+\gamma\rho_1) \end{pmatrix} \tag{3.9}$$

To prove that all three scenarios (i) - (iii) can be realized, we choose $\rho_1 = \rho_2 =: \rho$ and for convenience we set $\gamma = 1$.

Consider first $b = 2$. Then

$$R = R_0 \begin{pmatrix} 1-\rho & -\rho \\ \rho & 1-\rho \end{pmatrix} \tag{3.10}$$

where $R_0^{-1} = \sqrt{\rho(1-\rho)(\rho^2 + (1-\rho)^2)}$. The characteristic velocities are

$$c_1 = 1 - \rho - 3\rho^2, \quad c_2 = 2 - 3\rho - \rho^2 \tag{3.11}$$

The matrices $G^{(1)}, G^{(2)}$ are symmetric and have matrix elements $G^{(1)}_{11} = -2g_0(6\rho^4 - 8\rho^3 + 5\rho^2 + \rho - 1)$, $G^{(1)}_{12} = G^{(1)}_{21} = g_0(4\rho^3 - 10\rho^2 + 8\rho - 1)$, $G^{(1)}_{22} = -2g_0\rho(1-\rho)(2\rho^2 - 6\rho + 3)$ and $G^{(2)}_{11} = 4g_0\rho(1-\rho)$, $G^{(2)}_{12} = G^{(2)}_{21} = -g_0(1-2\rho^2)^2$, $G^{(2)}_{22} = 4g_0(1 - 3\rho(1-\rho))$ with $g_0 = -1/2\left[\rho(1-\rho)/(1-2\rho(1-\rho))^3\right]^{1/2}$. Therefore, generically condition (i) for the presence of two KPZ modes is satisfied. However, while $G^{(2)}_{11} \neq 0$ and $G^{(2)}_{22} \neq 0\ \forall \rho \in (0,1)$, the self coupling coefficient $G^{(1)}_{11}$ changes sign at $\rho^* = 0.45721\ldots$. Since $G^{(1)}_{22}(\rho^*) \neq 0$, the condition for case (ii), KPZ mode plus superdiffusive non-KPZ mode, is thus satisfied at density $\rho = \rho^*$. In fact, diagonalizing A for arbitrary densities ρ_1, ρ_2 one can show that for $b \neq 1$ there is a curve in the space of densities where condition (ii) is satisfied. On the other hand, there is no density where condition (iii), $G^{(1)}_{11} = G^{(1)}_{22} = 0$, is satisfied. Indeed, numerical inspection of the mode coupling matrices for several other parameter choices of γ and b suggests that condition (iii) cannot be satisfied when $b \neq 1$.

Next we study $b = 1$. In this case the system is symmetric under interchange of the two lanes, which is reflected in the relation $j_2(\rho_1, \rho_2) = j_1(\rho_2, \rho_1)$ for the currents (3.2). Calculating the mode coupling matrices for $\rho_1 = \rho_2 =: \rho$ and $\gamma = 1$ yields

$$G^{(1)} = \tilde{g}_0(1+\rho)\begin{pmatrix} 0 & 1 \\ 1 & 0 \end{pmatrix}, G^{(2)} = \tilde{g}_0\begin{pmatrix} 2-\rho & 0 \\ 0 & 3\rho \end{pmatrix} \tag{3.12}$$

with $\tilde{g}_0 = -\sqrt{2\rho(1-\rho)}$. Interestingly, in this case condition (iii) is satisfied for all ρ, i.e., mode 1 is expected to be diffusive and mode 2 is KPZ. The occurrence of a diffusive mode is somewhat counter-intuitive as both particle species interact and hop in a totally asymmetric fashion which in the case of the AHR-model prevents the existence of a diffusive mode [20].

In order to check the predictions of mode coupling theory we performed dynamical Monte-Carlo simulations, using a random sequential update where in each step a random site is chosen uniformly and jumps are performed, provided the target site is empty, with probabilities obtained from normalizing the jump rates (3.1) by the largest jump rate. A full Monte Carlo time step then corresponds to $2N$ such update steps. The initial distribution is sampled from the uniform distribution, except for the occupation number at site $N/2$ which is determined so that the normal modes can be studied separately [25]. Averages are performed over up to 10^8 realizations of the process and $N = 300\ldots600$. In order to measure the dynamical exponent, we compute the first and second moment of the dynamical structure function, from which we obtain the variance $\sigma(t) \propto t^{2/z}$ of the density distribution as a function of time for times where $\sigma(t)$ is small enough to avoid finite-size effects.

In order to test the existence of a superdiffusive non-KPZ mode we have chosen $\gamma = -0.52588$ and $b = 1.3$. This yields $G^{(2)}_{22} = 0$ at $\rho^*_1 = \rho^*_2 = 0.5500003 \approx 55/100$. The matrices $G^{(1)}, G^{(2)}$ become

$$G^{(1)} = \begin{pmatrix} 0.2950 & 0.0717 \\ 0.0717 & 0.3157 \end{pmatrix}, \quad G^{(2)} = \begin{pmatrix} 0.0706 & 0.2972 \\ 0.2972 & 0 \end{pmatrix}$$

which means that mode 2 is expected to be a non-KPZ mode and mode 1 is KPZ. The corresponding characteristic velocities are $c_1(\rho^*) = -0.2171$, $c_2(\rho^*) = 0.0449$. and the eigenvectors are $(-0.7465, 0.6654)^T$ for c_2 (non-KPZ mode) and $(0.6654, 0.7465)^T$ for c_1 (KPZ mode).

The simulations confirm the predictions, see Figs. 3.2 and 3.3. For both modes the measured velocity differs from the theoretical prediction by less than 0.003. A linear least-square fit on log-log scale of the simulation results for the variance of the non-KPZ mode 2 yields $2/z_2^{MC} = 1.19 \pm 0.02$, very close to the mode-coupling value $2/z_2 = 6/5 = 1.2$. For the amplitude $\propto t^{-1/z}$

at the maximum as a function of time we find $1/z_2^{MC} = 0.58$, also in good agreement with $1/z_2 = 0.6$. The fitted exponent $2/z_1^{MC} = 1.302$ of the KPZ mode 1 deviates slightly from 4/3, which is consistent with the strong coupling to the non-KPZ mode: The matrix element $G_{22}^{(1)} \approx 0.3157$ is larger than the KPZ self-coupling constant $G_{11}^{(1)} \approx 0.2950$.

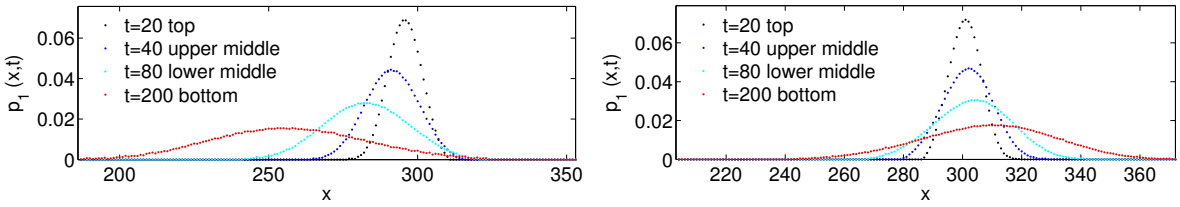

Figure 3.2.: (Colour online) Case (ii): Case (ii): Dynamical structure functions for particles on chain 1, for the KPZ mode (top) and the non-KPZ mode (bottom) at different times from Monte Carlo simulations, averaged over $2.7 \cdot 10^7 (5 \cdot 10^7)$ histories for the KPZ (non-KPZ) mode for $N = 600$. Statistical errors are smaller than symbol size.

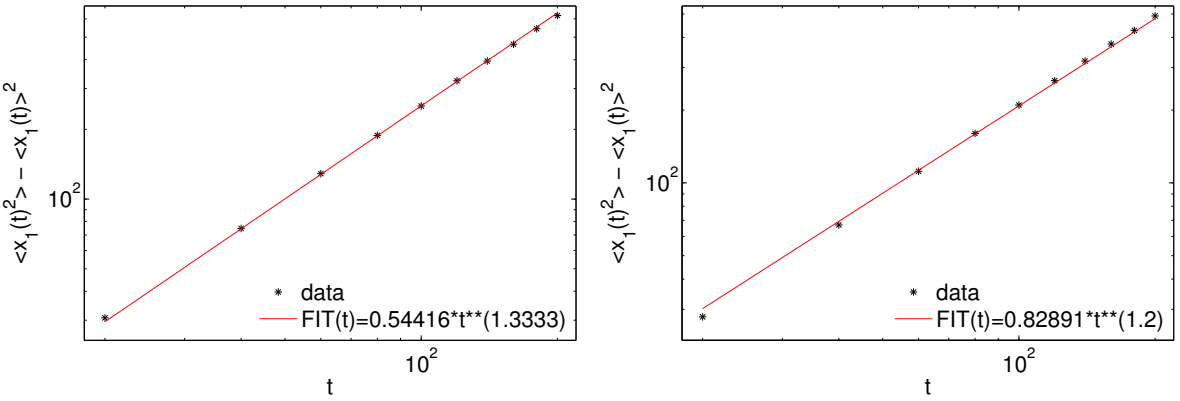

Figure 3.3.: (Colour online) Case (ii). Variance of the dynamical structure function shown in Fig. 2. as function of time. The lines with the predicted universal slopes $2/z = 4/3$ for KPZ mode (top) and $2/z = 6/5$ for the non-KPZ mode (bottom) are guides to the eye. Error bars (not shown) are approximately symbol size.

In order to test case (iii) (KPZ and diffusive mode), we choose $\gamma = -0.8, b = 1, \rho_1 = \rho_2 = 0.5$. The characteristic velocities are $c_1 = -0.2$ (eigenvector $(1,1)^T/\sqrt{(2)}$) and $c_1 = 0.2$ (eigenvector $(1,-1)^T/\sqrt{(2)}$). The mode coupling matrices are given by

$$G^1 = 0.2121 \begin{pmatrix} 1 & 0 \\ 0 & 1 \end{pmatrix}, \quad G^2 = 0.2121 \begin{pmatrix} 0 & 1 \\ 1 & 0 \end{pmatrix}$$

corresponding to a KPZ mode 1 and diffusive mode 2, see Figs. 4 and 5. The characteristic velocities agree with the theoretical prediction with an accuracy of better than 1% and also the measured scaling exponents $2/z_1^{MC} = 1.343$, $2/z_2^{MC} = 1.030$ are in good agreement with the theoretical prediction $2/z_1 = 4/3$ and $2/z_2 = 1$. We have also verified numerically the occurrence of two KPZ modes for generic values of the densities. This behaviour is expected and data are not shown here.

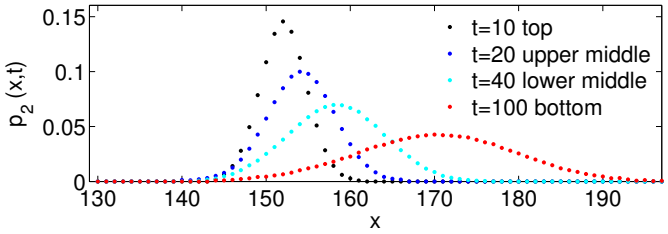

Figure 3.4.: (Colour online) Case (iii): Dynamical structure function of the diffusive mode for particles on chain 2 with $N = 300$, with $c_2 = 0.2$ (bottom) at different times t, from Monte Carlo simulations, averaged over 10^7 histories. Statistical errors are smaller than symbol size.

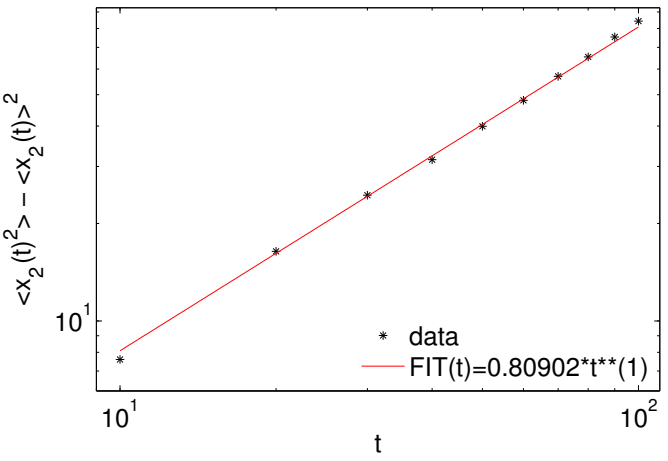

Figure 3.5.: (Colour online) Case (iii). Variance of the dynamical structure function shown in Fig. 4. as function of time. The line with the predicted universal slope $2/z = 1$ for the diffusive mode (bottom) are guides to the eye. Error bars (not shown) are approximately symbol size.

In summary, we have shown that the two-lane asymmetric simple exclusion process with two conservation laws exhibits anomalous transport and has a superdiffusive non-KPZ mode with dynamical exponent $z = 5/3$ on a line in the space of conserved densities (ρ_1, ρ_2). The heat mode in Hamiltonian systems [9] is associated with a symmetry for the velocities of the sound modes, in contrast to our two-component scenario where there is no such symmetry. In the case of higher internal symmetry, where our model is invariant under lane change, a diffusive mode can occur instead of the non-KPZ mode. This is surprising as the hopping of both particle species is totally asymmetric. We did not find any point in parameter space where the KPZ mode would be completely absent. We argue that the existence of a superdiffusive non-KPZ mode is generic for driven diffusive systems with more than one conservation law and will generally occur at some specific manifold in the space of conserved densities ρ_i. This new universality class for anomalous transport in driven diffusive systems is expected to result in a novel exponent for the stationary density profile in open systems [29]. An interesting open problem that is raised by our findings is the role of symmetries for the suppression of the non-KPZ mode and the occurence of a diffusive mode.

Acknowledgments

V.P. acknowledges financial support by DFG. G.M.S. thanks H. Spohn and H. van Beijeren for most illuminating discussions at TU Munich and at the Oberwolfach workshop Large Scale Stochastic Dynamics. We also thank them and C. Mendl for useful comments on the manuscript.

Bibliography

[1] B.J. Alder and T.E. Wainwright, Phys. Rev. Lett. **18**, 988 (1967).

[2] M.H. Ernst, E.H. Hauge, and J.M.J. van Leeuwen, J. Stat. Phys. **15**, 7 (1976).

[3] M. Prähofer and H. Spohn, in: *In and Out of Equilibrium*, edited by V. Sidoravicius, Vol. 51 of Progress in Probability (Birkhauser, Boston, 2002).

[4] M. Kardar, G. Parisi, and Y.-C. Zhang, Phys. Rev. Lett. **56**, 889 (1986).

[5] M. Prähofer and H. Spohn, J. Stat. Phys. **115**, 255 (2004).

[6] K.A. Takeuchi and M. Sano, Phys. Rev. Lett. **104**, 230601 (2010).

[7] A. Nagar, M. Barma, and S. N. Majumdar, Phys. Rev. Lett. **94**, 240601 (2005).

[8] C.B. Mendl and H. Spohn, Phys. Rev. Lett. **111**, 230601 (2013).

[9] H. van Beijeren, Phys. Rev. Lett. **108**, 180601 (2012).

[10] In Hamiltonian systems a coupling of a heat mode to both sound modes is always present. As a consequence, an additional diffusive mode cannot arise. We are indebted to a referee for pointing this out.

[11] B. Derrida, J. L. Lebowitz, and E. Speer, J. Stat. Phys. **89**, 135 (1997).

[12] A. Rákos and G. M. Schütz, J. Stat. Phys. **117**, 55 (2004).

[13] V. Popkov and G. M. Schütz, Phys. Rev. E **86**, 031139 (2012).

[14] M. R. Evans, D. P. Foster, C. Godrèche, and D. Mukamel, Phys. Rev. Lett. **74**, 208 (1995).

[15] V. Popkov, M. R. Evans, D. Mukamel, J. Phys. A **41**, 432002 (2008).

[16] M. R. Evans, Y. Kafri, H. M. Koduvely, and D. Mukamel, Phys. Rev. Lett. **80**, 425 (1998).

[17] R. Lahiri, M. Barma, and S. Ramaswamy, Phys. Rev. E **61**, 1648 (2000).

[18] J.T. Mettetal, B. Schmittmann, and R.K.P. Zia Europhys. Lett. **58**, 653 (2002).

[19] T. Bodineau, B. Derrida, V. Lecomte, and F. van Wijland, J. Stat. Phys. **133**, 1013 (2008).

[20] P.L. Ferrari, T. Sasamoto, and H. Spohn, J. Stat. Phys. **153**, 377 (2013).

[21] C. Arita, A. Kuniba, K. Sakai, and T. Sawabe, J. Phys. A: Math. Theor. **42** 345002 (2009).

[22] D. Das, A. Basu, M. Barma, and S. Ramaswamy, Phys. Rev. E **64**, 021402 (2001).

[23] V. Popkov and M. Salerno, Phys. Rev. E **69**, 046103 (2004).

[24] C. Kipnis and C. Landim, *Scaling limits of interacting particle systems* (Springer, Berlin, 1999).

[25] V. Popkov and G.M. Schütz, J. Stat. Phys. **112**, 523 (2003).

[26] R. Grisi and G.M. Schütz, J. Stat. Phys. **145**, 1499 (2011).

[27] B. Tóth and B. Valkó, J. Stat. Phys. **112**, 497 (2003).

[28] L. Delfini, S. Lepri, R. Livi, and A. Politi, J. Stat. Mech. P02007 (2007).

[29] J. Krug, Phys. Rev. Lett. **67** 1882 (1991).

4. Universality classes in two-component driven diffusive systems

Vladislav Popkov[1,2], **Johannes Schmidt**[1]
and Gunter M. Schütz[3,4]

[1] *Institut für Theoretische Physik, Universität zu Köln,*
Zülpicher Str. 77, 50937 Cologne, Germany
[2] *CSDC Università di Firenze, via G.Sansone 1, 50019 Sesto Fiorentino, Italy*
[3] *Institute of Complex Systems II, Theoretical Soft Matter and Biophysics,*
Forschungszentrum Jülich, 52425 Jülich, Germany
[4] *Interdisziplinäres Zentrum für Komplexe Systeme,*
Universität Bonn, Brühler Str. 7, 53119 Bonn, Germany

Published in: Journal of Statistical Physics (J Stat Phys)
Aug. 2015, vol. 160, iss. 4, pp. 835-860
doi: 10.1007/s10955-015-1241-x

Abstract: We study time-dependent density fluctuations in the stationary state of driven diffusive systems with two conserved densities ρ_λ. Using Monte-Carlo simulations of two coupled single-lane asymmetric simple exclusion processes we present numerical evidence for universality classes with dynamical exponents $z = (1+\sqrt{5})/2$ and $z = 3/2$ (but different from the Kardar-Parisi-Zhang (KPZ) universality class), which have not been reported yet for driven diffusive systems. The numerical asymmetry of the dynamical structure functions converges slowly for some of the non-KPZ superdiffusive modes for which mode coupling theory predicts maximally asymmetric z-stable Lévy scaling functions. We show that all universality classes predicted by mode coupling theory for two conservation laws are generic: They occur in two-component systems with nonlinearities in the associated currents already of the minimal order $\rho_\lambda^2\rho_\mu$. The macroscopic stationary current-density relation and the compressibility matrix determine completely all permissible universality classes through the mode coupling coefficients which we compute explicitly for general two-component systems.

Keywords: Driven diffusive systems | Dynamical critical phenomena | Kardar-Parisi-Zhang equation | Nonlinear fluctuating hydrodynamics | Mode coupling theory

4.1. Introduction

Anomalous transport is the hallmark of many one-dimensional non-equilibrium systems even when interactions are short-ranged [1]. A common way of characterizing 1-d systems that exhibit anomalous transport is through the dynamical structure function which describes the time-dependent fluctuations of the long-lived modes in the stationary state. In systems with short-range interactions and one global conservation law (giving rise to one long-lived mode) only two universality classes are known to exist, the Gaussian universality class with dynamical exponent $z = 2$ (also describing diffusive fluctuations in equilibrium stationary states), and the superdiffusive Kardar-Parisi-Zhang (KPZ) universality class with dynamical exponent $z = 3/2$ [2] for systems driven out of equilibrium. The exact scaling form of the KPZ structure function was found some 10 years ago by Prähofer and Spohn for the polynuclear growth model [3] and for a driven diffusive system, viz. the asymmetric simple exclusion process [4]. Since then the scaling function, which is expected to be universal, has also been observed in various experiments [5, 6].

Superdiffusive fluctuations in systems with more than one conservation law are less well-studied. Stochastic dynamics have been considered for driven diffusive systems with two conservation laws. Naively one might expect both modes to be in the KPZ universality class. This guess is indeed confirmed for the Arndt-Heinzel-Rittenberg model [7] by using exact results for the steady state combined by fluctuating hydrodynamics and mode coupling theory [8] and also for a general class of multi-component exclusion processes [9]. It was also known for some time that one mode can be KPZ, while the other is diffusive, see [10] where exact microscopic and hydrodynamic limit arguments are used, and numerical work [11, 12] for related results.

Recently van Beijeren [13] studied a system with Hamiltonian dynamics with three conservation laws. He predicted KPZ-universality for the two sound modes of the system and a novel superdiffusive universality class with dynamical exponent $z = 5/3$ for the heat mode. The occurrence of a 5/3 mode was subsequently demonstrated for FPU-chains [14, 15] with three conservation laws and generally for anharmonic chains [16] and a family of exclusion process with two conservation laws [17]. Also recent mathematically rigorous work indicates non-trivial anomalous behaviour fluctuations in systems with two conservation laws [18].

Stochastic interacting particle systems with two conservation laws exhibit extremely rich behaviour in one dimension, including spontaneous symmetry breaking [7, 19, 20, 21, 22, 23] or phase separation [7, 20, 24, 25, 26, 27] in nonequilibrium stationary states, see [28] for a review. Studying the coarse-grained time evolution of two-component systems with an umbilic point one finds shocks with unusual properties [29, 30]. It is the purpose of this paper to go beyond stationary and time-dependent mean properties and consider time-dependent fluctuations. Specifically, we show that the complete list of dynamical universality classes that, according to mode coupling theory, can appear in the presence of two conservation laws can be realized in driven diffusive systems with two conserved densities. To this end we compute the exact mode coupling matrices for general strictly hyperbolic two-component systems with the stationary current-density relation and stationary compressibility matrix as the only input. With these input data the scaling form of the dynamical structure function is completely determined, except in the presence of a diffusive mode where the phenomenological diffusion coefficient enters the scale factors in the scaling functions. With these results we use mode coupling theory for computing explicitly the scaling form of the dynamical structure function for two superdiffusive modes which have been not reported yet in the literature on driven diffusive systems. We also present simulation data for a family of exclusion processes which confirm the theoretical predictions.

This paper is organized in the following way. We first introduce the lattice model that we are going to study numerically (Section 4.2). This is an extended version of the two-lane exclusion process presented in our earlier work [17] that allows us to relax constraints on the physically accessible parameter manifold. In Section 4.3 we first present some predictions of mode coupling

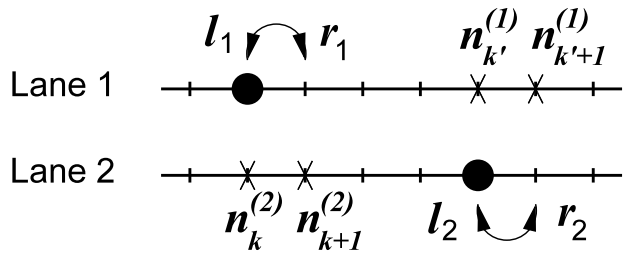

Figure 4.1.: Schematic representation of the two-lane partially asymmetric simple exclusion process. A particle on lane 1 (2) hops to the neighbouring site (provided this target site is empty) with to the right or left with rates (4.1) that depend on the particle configuration on the adjacent sites of the other lane that are marked by a cross.

theory and then use the theory to make predictions for our model. The numerical tests of these predictions and some mode coupling computations are presented in Section 4.4. We finish with some conclusions in Section 4.5. In the appendix we perform the full computation of the mode coupling matrices for arbitrary strictly hyperbolic two-component systems.

4.2. Two-lane asymmetric simple exclusion process

We consider a two-lane asymmetric simple exclusion process where particles hop randomly on two parallel chains with L sites each and periodic boundary conditions. Particles do not change lanes and they obey the hard core exclusion principle which forbids occupancy of a site by more than one particle. We denote the particle occupation number on site k in the first (upper) lane by $n_k^{(1)} \in \{0,1\}$, and on the second (lower) lane by $n_k^{(2)} \in \{0,1\}$. The total particle number is conserved in each lane and denoted N_λ.

A hopping event from site k to site $k+1$ on the same lane may happen if site k is occupied and site $k+1$ on the same lane is empty. The rate of hopping depends on the particle configuration on the adjacent lane as follows: Particles on lane λ hop from site k to site $k+1$ with rate $r_\lambda(k,k+1)$ and from site $k+1$ to site k with rate $\ell_\lambda(k+1,k)$ (Figure 4.1). The rates are given by

$$\begin{aligned} r_1(k,k+1) &= p_1 + b_1 n_k^{(2)} + c_1 n_{k+1}^{(2)} + d_1 n_k^{(2)} n_{k+1}^{(2)} \\ \ell_1(k+1,k) &= q_1 + e_1 n_k^{(2)} + f_1 n_{k+1}^{(2)} + g_1 n_k^{(2)} n_{k+1}^{(2)} \\ r_2(k,k+1) &= p_2 + b_2 n_k^{(1)} + c_2 n_{k+1}^{(1)} + d_2 n_k^{(1)} n_{k+1}^{(1)} \\ \ell_2(k+1,k) &= q_2 + e_2 n_k^{(1)} + f_2 n_{k+1}^{(1)} + g_2 n_k^{(1)} n_{k+1}^{(1)}. \end{aligned} \tag{4.1}$$

The hopping attempts of particles from site k on lane λ to neighbouring sites occur independently of each other, after an exponentially distributed random time with mean $\tau_\lambda(k) = [r_\lambda(k,k+1) + \ell_\lambda(k,k-1)]^{-1}$ for a jump from site k on lane λ. Hopping attempts on an already occupied site are rejected.

Using pairwise balance [31] it is easy to verify that for any pair of total particle numbers N_λ the stationary distribution for this model is the uniform distribution, provided that the symmetry constraints $b_1 - e_1 = c_2 - f_2$, $b_2 - e_2 = c_1 - f_1$, $d_1 = g_1$ and $d_2 = g_2$ are met for the interaction constants between the two lanes. The "bare" hopping rates p_1, p_2, q_1, q_2 are arbitrary. From the canonical uniform measures one constructs stationary grandcanonical product measures where each site of lane λ is occupied independently of the other sites with probability $\rho_\lambda \in [0,1] = N_\lambda/L$. Hence the ρ_λ are the conserved densities of the grandcanonical stationary distribution, which, by construction, is the convex combination of all uniform measures with weight $[\rho_1/(1-\rho_1)]^{N_1}[\rho_2/(1-\rho_2)]^{N_2}$ and $0 \le N_\lambda \le L$.

From the hopping rates (4.1) and the product form of the grandcanonical distribution one reads off the corresponding stationary current vector $\vec{j}$ with components

$$\begin{aligned} j_1(\rho_1,\rho_2) &= \rho_1(1-\rho_1)(a+\gamma\rho_2), \\ j_2(\rho_1,\rho_2) &= \rho_2(1-\rho_2)(b+\gamma\rho_1). \end{aligned} \tag{4.2}$$

with

$$a = p_1 - q_1,\ b = p_2 - q_2,\ \gamma = b_1 + c_1 - e_1 - f_1. \tag{4.3}$$

Notice that this current-density relation depends on the microscopic details of the model only through the parameter combinations a, b, γ which can take arbitrary real values. For $b = 1$ we recover the totally asymmetric two-lane model of [32] which is a special case of the multi-lane model of [33]. Throughout this work we set $a = 1$, $\gamma \neq 0$.

The product measure corresponds to a grandcanonical ensemble with a fluctuating particle number. These fluctuations are described by the symmetric compressibility matrix K with matrix elements

$$K_{\lambda\mu} := \frac{1}{L}\left\langle (N_\lambda - \rho_\lambda L)(N_\mu - \rho_\mu L)\right\rangle = \rho_\lambda(1-\rho_\lambda)\delta_{\lambda,\mu}. \tag{4.4}$$

where $\lambda, \mu \in \{1, 2\}$. In the notation defined in the appendix this corresponds to

$$\kappa_\lambda := K_{\lambda\lambda} = \rho_\lambda(1-\rho_\lambda), \quad \bar{\kappa} := K_{12} = 0. \tag{4.5}$$

As discussed below the current density relation $\vec{j}$ given in (4.2) and the compressibility matrix K given (4.4) are the input data which completely determine the scaling functions describing the large scale behaviour of the particle system, up to a scale factor if a diffusive mode is relevant.

For the Monte-Carlo simulations presented in this paper we consider the totally asymmetric version of the model [17] where $p_1 = 1$, $p_2 = b$, $q_\lambda = e_\lambda = f_\lambda = g_\lambda = d_\lambda = 0$ and $b_\lambda = c_\lambda = \gamma/2 \neq 0$ with $\gamma > -\min(1, b)$. Initially we put N_λ particles randomly drawn from the stationary distribution, i.e., they are placed uniformly on lane λ. For the dynamics we perform random sequential updates where a site k_λ is chosen uniformly and a particle, if present and allowed to jump, jumps with a normalized probability given by (4.1). One Monte-Carlo time unit then corresponds to $2L$ consecutive update attempts. We compute the empirical dynamical structure function defined by $\bar{S}_k^{\lambda\mu}(t) = 1/n \sum_{j=1}^{n} 1/L \sum_{l=1}^{L} n_{l+k}^{(\lambda)}(j\tau + t) n_l^{(\mu)}(j\tau) - \rho_\lambda\rho_\mu$ where for numerical efficiency we exploit translation variance and take a sum over n multiples of τ and over m Monte-Carlo histories. Time t and system size L are chosen such that finite-size corrections to the stationary current (which are of order $1/L$) and to the structure function (at most of order $1/L^{1+\alpha}$ with $\alpha > 1$ as discussed below) are small in absolute terms and negligible compared to statistical errors.

4.3. Dynamical universality classes

4.3.1. Fluctuating hydrodynamics and mode coupling theory

Following the ideas set out in [34, 35] the starting point for investigating the large-scale dynamics of a microscopic lattice model is the system of conservation laws

$$\frac{\partial}{\partial t}\vec{\rho}(x,t) + \frac{\partial}{\partial x}\vec{j}(x,t) = 0 \tag{4.6}$$

where component $\rho_\lambda(x,t)$ of the density vector $\vec{\rho}(x,t)$ is the coarse-grained local density of the component λ of the system, and the component $j_\lambda(x,t)$ of the current vector $\vec{j}(x,t)$ is the associated current. The current is a function of x and t only through its dependence on the local conserved densities. Hence these equations can be rewritten as

$$\frac{\partial}{\partial t}\vec{\rho}(x,t) + J\frac{\partial}{\partial x}\vec{\rho}(x,t) = 0 \tag{4.7}$$

where J is the current Jacobian with matrix elements $J_{\lambda\mu} = \partial j_\lambda / \partial \rho_\mu$. The product JK of the Jacobian with the compressibility matrix (4.4) is symmetric [36] which guarantees that the system (4.7) is hyperbolic [37]. The eigenvalues v_α of J are the characteristic velocities of the system. If $v_1 \neq v_2$ the system is called strictly hyperbolic. Notice that in our convention $\vec{\rho}$ and $\vec{j}$ are regarded as column vectors. Transposition is denoted by a superscript T.

Eq. (4.7) describes the deterministic time evolution of the density under Eulerian scaling where the lattice spacing a is taken to zero such that $x = ka$ remains finite and at the same time the microscopic time τ is taken to infinity such that the macroscopic time $t = \tau a$ is finite. The effect of fluctuations, which occur on finer space-time scales where $t = \tau a^z$ with dynamical exponent $z > 1$, can be captured by adding phenomenological white noise terms ξ_i and taking the non-linear fluctuating hydrodynamics approach together with a mode-coupling analysis of the non-linear equation. Following [16] we summarize here the main ingredients of this well-established description.

One expands the local densities $\rho_\lambda(x,t) = \rho_\lambda + u_\lambda(x,t)$ around their long-time stationary values ρ_λ and keeps terms to first non-linear order in the fluctuation fields $u_\lambda(x,t)$. For quadratic nonlinearities (4.7) then yields

$$\partial_t \vec{u} = -\partial_x \left(J\vec{u} + \frac{1}{2}\vec{u}^T \vec{H} \vec{u} - D\partial_x \vec{u} + B\vec{\xi} \right) \tag{4.8}$$

where $\vec{H}$ is a column vector whose entries $(\vec{H})_\lambda = H^\lambda$ are the Hessians with matrix elements $H^\lambda_{\mu\nu} = \partial^2 j_\lambda / (\partial\rho_\mu \partial\rho_\nu)$. The term $\vec{u}^T H^\lambda \vec{u}$ denotes the inner product in component space. The diffusion matrix D is a phenomenological quantity. The noise strength B does not appear explicitly below, but plays an indirect role in the mode-coupling analysis. One recognizes in (4.8) a system of coupled noisy Burgers equations. If the quadratic non-linearity is absent one has diffusive behaviour, up to possible logarithmic corrections that may arise from cubic non-linearities [38].

In order to analyze this nonlinear equation we transform to normal modes $\vec{\phi} = R\vec{u}$ where $RJR^{-1} = \mathrm{diag}(v_\alpha)$ and the transformation matrix R is normalized such that $RKR^T = \mathbb{1}$, see the appendix. From (4.8) one thus arrives at

$$\partial_t \phi_\alpha = -\partial_x \left(v_\alpha \phi_\alpha + \vec{\phi}^T G^\alpha \vec{\phi} - \partial_x (\tilde{D}\vec{\phi})_\alpha + (\tilde{B}\vec{\xi})_\alpha \right) \tag{4.9}$$

with $\tilde{D} = RDR^{-1}$, $\tilde{B} = RB$ and

$$G^\alpha = \frac{1}{2} \sum_\lambda R_{\alpha\lambda} (R^{-1})^T H^\lambda R^{-1} \tag{4.10}$$

are the mode coupling matrices.

To make contact of this macroscopic description with the microscopic model we first note that the current-density relation given by the components of the current vector $\vec{j}$ arises from the microscopic model by computing the stationary current-density relations $j_\lambda(\rho_1, \rho_2)$ and then substituting the stationary conserved densities by the coarse-grained local densities $\rho_\lambda(x,t)$ which are regarded as slow variables. Similarly, the compressibility matrix K is computed from the stationary distribution. Hence the mode coupling matrices (and with them the dynamical universality classes as shown below) are completely determined by these two macroscopic stationary properties of the system. We stress that the *exact* stationary current-density relations and the *exact* stationary compressibilities are required. Approximations obtained e.g. from stationary mean field theory will, in general, only accidentally provide the information necessary for determining the dynamical universality classes of the system. In the appendix we compute the mode

coupling matrices of a general two-component system with the current vector and compressibility matrix as input parameters.

Second, consider the dynamical structure matrix $\bar{S}_k(t)$ of the microscopic model defined on the lattice.[1] Its matrix elements are the dynamical structure functions

$$\bar{S}_k^{\lambda\mu}(t) := \langle\, (n_k^{(\lambda)}(t) - \rho_\lambda)(n_0^{(\mu)}(t) - \rho_\mu)\,\rangle \tag{4.11}$$

which measure density fluctuations in the stationary state. This quantity has two different physical interpretations. On the one hand, one can regard the random variable $f_k^\lambda(t) := n_k^{(\lambda)}(t) - \rho_\lambda$ as a stochastic process and then the dynamical structure function describes the stationary two-time correlations of this process. The long-time behaviour of the dynamical structure function can thus be determined from the fluctuation fields $u_\lambda(x,t)$ appearing in the non-linear fluctuating hydrodynamics approach (4.8), i.e., $\bar{S}_k^{\lambda\mu}(t) \overset{k,t\to\infty}{\to} \langle\, u_\lambda(x,t)u_\mu(0,0)\,\rangle$. In a different interpretation the dynamical structure function measures the time evolution of the expectation of $f_k^\lambda(t)$ at time t, i.e., the unnormalized density profiles $\bar{\rho}_k^\lambda(t) := \langle\, n_k^{(\lambda)}(t) - \rho_\lambda\,\rangle$ that at time $t = 0$ have a delta-peak at site 0. Since the two conserved quantities interact, an initial perturbation even of only one component will cause a non-trivial relaxation of *both* density profiles. In each component the initial peak will evolve into two separate peaks, which move and spread with time. The characteristic velocities v_α are the collective velocities, i.e., the center-of-mass velocities of the two local perturbations [32]. The variance of the evolving density profiles determines the collective diffusion coefficient. This second interpretation of the dynamical structure matrix as describing a relaxation process, completely equivalent to the first fluctuation interpretation, is quite natural from the viewpoint of regarding (4.8) as a more detailed description of (4.6) in the sense of describing fluctuation effects on finer space-time scales due to the randomness of the stochastic process from which (4.6) arises under Eulerian scaling.

Analogously one can regard the transformed modes of the lattice model $\vec{\phi}_k(t) = R\vec{f}_k(t)$ in the fluctuation interpretation as stationary processes and the transformed dynamical structure functions

$$S_k^{\alpha\beta}(t) = [R\bar{S}_k(t)R^T]_{\alpha\beta} = \langle\, \phi_k^\alpha(t)\phi_0^\beta(0)\,\rangle \tag{4.12}$$

as the stationary space-time fluctuations. The transformation of the dynamical structure functions to the normal modes $\vec{\phi}_k(t)$ on the lattice, which is important for the numerical simulation of lattice models, is discussed in more detail in Appendix 4.A. The large-scale behaviour of $S_k^{\alpha\beta}(t)$ is given in terms of the normal modes $\phi_\alpha(x,t)$ appearing in (4.9) by $S_{\alpha\beta}(x,t) = \langle\, \phi_\alpha(x,t)\phi_\beta(0,0)\,\rangle$. In the second relaxation interpretation the normal modes are seen as local perturbations of a stationary distribution with a specific choice of initial amplitudes in each component.

Since for strictly hyperbolic systems the two characteristic velocities are different, one expects that the off-diagonal elements of S decay quickly. For long times and large distances one is thus left with the diagonal elements which we denote by

$$S_\alpha(x,t) := S^{\alpha\alpha}(x,t) \tag{4.13}$$

with initial value $S_\alpha(x,0) = \delta(x)$. The large scale behaviour of the diagonal elements is expected to have the scaling form

$$S_\alpha(x,t) \sim t^{-1/z_\alpha} f_\alpha((x - v_\alpha t)^{z_\alpha}/t) \tag{4.14}$$

with a dynamical exponent z_α that may be different for the two modes. The exponent in the power law prefactor follows from mass conservation. In momentum space one has

$$\hat{S}_\alpha(p,t) \sim \mathrm{e}^{-iv_\alpha pt}\hat{f}_\alpha(p^{z_\alpha}t) \tag{4.15}$$

[1] We choose the same notation as for the empirical structure function obtained from Monte-Carlo simulations presented below.

for the Fourier transform

$$\hat{S}_\alpha(p,t) := \frac{1}{\sqrt{2\pi}} \int_{-\infty}^{\infty} \mathrm{d}x\, \mathrm{e}^{-ipx} S_\alpha(x,t). \tag{4.16}$$

Whether the difference of the characteristic speeds vanishes or not plays an important role. For the case where $v_1 = v_2$, i.e., when the system (4.7) has an umbilic point, it was found numerically in the framework of dynamic roughening of directed lines that the dynamical exponent is $z = 3/2$, but the scaling functions are not KPZ [40]. On the other hand, for strictly hyperbolic systems the normal modes have different speeds and hence their interaction becomes very weak for long times. By identifying ϕ_α with the gradient of a height variable (4.9) then turns generically into two decoupled KPZ-equations with coefficients $G^\alpha_{\alpha\alpha}$ determining the strength of the nonlinearity.

In order to analyze the system of nonlinear stochastic PDE's in more detail we employ mode coupling theory [16]. The basic idea is to capture the combined effect of non-linearity and noise by a memory kernel. Thus the starting point for computing the $S_\alpha(x,t)$ are the mode coupling equations

$$\partial_t S_\alpha(x,t) = (-v_\alpha \partial_x + D_\alpha \partial_x^2) S_\alpha(x,t) + \int_0^t \mathrm{d}s \int_{-\infty}^{\infty} \mathrm{d}y\, S_\alpha(x-y, t-s) \partial_y^2 M_{\alpha\alpha}(y,s) \tag{4.17}$$

with the diagonal element $D_\alpha := \tilde{D}_{\alpha\alpha}$ of the phenomenological diffusion matrix and the memory kernel

$$M_{\alpha\alpha}(y,s) = 2 \sum_{\beta,\gamma} (G^\alpha_{\beta\gamma})^2 S_\beta(y,s) S_\gamma(y,s). \tag{4.18}$$

The strategy is to plug into this equation, or into its Fourier representation, the scaling ansatz (4.14) (or (4.15)). One gets equations for the dynamical exponents arising from requiring non-trivial scaling solutions and using the known results $z = 3/2$ for KPZ and $z = 2$ for diffusion. In a next step one can then solve for the actual scaling functions, see below. Since for $v_1 \neq v_2$ one has $S_\beta(y,s) S_\gamma(y,s) \approx 0$ for $\beta \neq \gamma$ it is clear that the scaling behaviour of the solutions of (4.17) will be determined largely by the diagonal terms $G^\alpha_{\beta\beta}$ of the mode coupling matrices G^α. If a leading self-coupling term $G^\alpha_{\alpha\alpha}$ vanishes, one finds non-KPZ behaviour for mode α. In particular, if all diagonal terms are zero, the mode is diffusive. A coupling of a diffusive mode to a KPZ-mode leads to a modified KPZ-mode [39]. Thus the crucial property of the mode coupling matrices is whether a diagonal element is zero or not.

Some algebra along the lines of [16] involving power counting then yields the complete list of possible universal classes of strictly hyperbolic two-component systems from the structure of the mode coupling matrices G^α as shown in Table 4.1, see also [39] where a similar table was derived independently. The shorthand KPZ represents the KPZ scaling function, while KPZ' refers to modified KPZ, both with dynamical exponent $z = 3/2$. D represents a Gaussian scaling function f_α with dynamical exponent $z_\alpha = 2$, z_αL represents a z_α-stable Lévy distribution as scaling function f_α with dynamical exponent z_α, GM (for golden mean) represents φL with $\varphi = (1+\sqrt{5})/2$. In what follows we apply these general results to the two-lane model defined above. It will transpire that all theoretically possible scenarios can actually be realized in this family of models.

4.3.2. Mode-coupling matrix for the two-lane model

The input data are the current-density relation (4.2) and the compressibility matrix (4.4). From the current-density relation one computes the current Jacobian and the Hessian, which are used together with the compressibility matrix to compute the basis for normal modes and finally the mode coupling matrices, as shown in detail in the appendix in the general case.

G^2 \ G^1	$\begin{pmatrix} \star & \\ & \bullet \end{pmatrix}$	$\begin{pmatrix} \star & \\ & 0 \end{pmatrix}$	$\begin{pmatrix} \mathbf{0} & \\ & \bullet \end{pmatrix}$	$\begin{pmatrix} \mathbf{0} & \\ & 0 \end{pmatrix}$
$\begin{pmatrix} \bullet & \\ & \star \end{pmatrix}$	(KPZ,KPZ)	(KPZ,KPZ)	($\frac{5}{3}$L,KPZ)	(D,KPZ')
$\begin{pmatrix} 0 & \\ & \star \end{pmatrix}$	(KPZ,KPZ)	(KPZ,KPZ)	($\frac{5}{3}$L,KPZ)	(D,KPZ)
$\begin{pmatrix} \bullet & \\ & \mathbf{0} \end{pmatrix}$	(KPZ,$\frac{5}{3}$L)	(KPZ,$\frac{5}{3}$L)	(GM,GM)	(D,$\frac{3}{2}$L)
$\begin{pmatrix} 0 & \\ & \mathbf{0} \end{pmatrix}$	(KPZ',D)	(KPZ,D)	($\frac{3}{2}$L,D)	(D,D)

Table 4.1.: Classification of universal behaviour of the two modes by the structure of the mode coupling matrices G^α. The acronyms denote: KPZ: KPZ universality class (superdiffusive), KPZ': modified KPZ universality class (superdiffusive), D = Gaussian universality class (normal diffusion), z_αL: superdiffusive universality class with z_α-stable Lévy scaling function and GM = φL with the golden mean $\varphi = (1+\sqrt{5})/2$. An bullet or star in the G^α denotes a non-zero entry, no entry represents an arbitrary value (zero or non-zero). The selfcoupling terms $G^\alpha_{\alpha\alpha}$ are marked as star or boldface 0, resp.

For the present model we remark first that the currents (4.2) are at most quadratic in each density. Hence no logarithmic corrections to diffusive behaviour are expected in the two-lane model defined above. Second, as discussed in the appendix, in any coupled two-component system a vanishing cross compressibility $\bar{\kappa} = 0$ (where $\lambda \neq \mu$) implies that the cross derivatives $\partial j_\lambda / \partial \rho_\mu$ of the currents have to be non-zero except when one of the two components is frozen, i.e., fully occupied or fully empty.

For our system the explicit form of J is

$$J = \begin{pmatrix} (1+\gamma\rho_2)(1-2\rho_1) & \gamma\rho_1(1-\rho_1) \\ \gamma\rho_2(1-\rho_2) & (b+\gamma\rho_1)(1-2\rho_2) \end{pmatrix}. \tag{4.19}$$

and the Hessians H^λ are

$$H^1 = \begin{pmatrix} -2(1+\gamma\rho_2) & \gamma(1-2\rho_1) \\ \gamma(1-2\rho_1) & 0 \end{pmatrix}, \quad H^2 = \begin{pmatrix} 0 & \gamma(1-2\rho_2) \\ \gamma(1-2\rho_2) & -2(b+\gamma\rho_1) \end{pmatrix}. \tag{4.20}$$

The parameters convenient for theoretical analysis are not the matrix elements of the current Jacobian and the Hessians, but the parameters u, $\omega = \tan\vartheta$ (4.70) and the transformed Hessian parameters (4.92), (4.93) defined in the appendix to which we refer for the derivation of the following results. Here we point out only the relevant features of the quantities resulting from these lengthy but simple computations.

The collective velocities $v_{1,2}$ are given in (4.54). Notice that $J_{12}J_{21} = \gamma^2\rho_1(1-\rho_1)\rho_2(1-\rho_2) \geq 0$ in the whole physical parameter regime of the model. In fact, unless one of the lanes is frozen we have the strict inequality $J_{12}J_{21} > 0$. The frozen case is of no interest since then the dynamics in the non-frozen lane reduce to the dynamics of a single exclusion process. Hence we shall assume $J_{12}J_{21} > 0$ throughout this paper. Therefore the discriminant of the characteristic polynomial of J (4.53) is non-zero which implies that the model is strictly hyperbolic in the parameter domain of interest.

The transformation matrix R involves normalization factors $z_\pm$ (4.69) and the parameters u and $\omega = \tan\vartheta$ defined in (4.70). From (4.19) we find

$$\omega = \frac{1-b-(2+b\gamma)\rho_1+(\gamma+2b)\rho_2}{2\gamma\sqrt{\rho_1(1-\rho_1)\rho_2(1-\rho_2)}}\left(1+\sqrt{1+\frac{4\gamma^2(\rho_1(1-\rho_1)\rho_2(1-\rho_2))}{(1-b-(2+b\gamma)\rho_1+(\gamma+2b)\rho_2)^2}}\right) \tag{4.21}$$

and

$$u = \sqrt{\frac{\rho_1(1-\rho_1)}{\rho_2(1-\rho_2)}}. \tag{4.22}$$

For $J_{11} = J_{22}$ one has $\omega = 1$.

From the Hessians (4.20) one obtains the mode coupling parameters (4.92), (4.93)

$$g_1^1 = -2(1+\gamma\rho_2), \quad g_2^1 = 0, \quad \bar{g}^1 = \gamma\sqrt{\frac{\rho_2(1-\rho_2)}{\rho_1(1-\rho_1)}}(1-2\rho_1), \tag{4.23}$$

and

$$g_1^2 = 0, \quad g_2^2 = -2\sqrt{\frac{\rho_2(1-\rho_2)}{\rho_1(1-\rho_1)}}(b+\gamma\rho_1), \quad \bar{g}^2 = \gamma(1-2\rho_2). \tag{4.24}$$

The compressibility matrix enters the mode coupling coefficients only through the normalization factors $z_\pm$ for which we obtain from (4.75)

$$z_\pm = 1/\sqrt{\kappa_1} \notin \{0, \pm\infty\}. \tag{4.25}$$

This yields the desired diagonal elements of the mode coupling matrices

$$G^\alpha_{\beta\beta}(\omega) = A_0 D^\alpha_\beta(\omega) \tag{4.26}$$

with

$$\begin{aligned}
D_1^1(\omega) &= g_1^1 - 2\bar{g}^1\omega + 2\bar{g}^2\omega^2 - g_2^2\omega^3 && (4.27)\\
D_2^1(\omega) &= \left(2\bar{g}^1 - g_2^2\right)\omega + \left(g_1^1 - 2\bar{g}^2\right)\omega^2 && (4.28)\\
D_1^2(\omega) &= \left(g_1^1 - 2\bar{g}^2\right)\omega + \left(g_2^2 - 2\bar{g}^1\right)\omega^2 && (4.29)\\
D_2^2(\omega) &= g_2^2 + 2\bar{g}^2\omega + 2\bar{g}^1\omega^2 + g_1^1\omega^3. && (4.30)
\end{aligned}$$

and

$$A_0 = \frac{1}{2}\sqrt{\kappa_1}\cos^3(\vartheta) \neq 0. \tag{4.31}$$

As discussed in the appendix the vanishing cross-compressibility $\bar{\kappa} = 0$ of our model guarantees that $A_0 \neq 0$. Therefore a diagonal element $G^\alpha_{\beta\beta}$ of a mode coupling matrix vanishes if and only if the polynomial D^α_β defined in (4.27) - (4.30) vanishes. In order to see whether all scenarios listed in Table 4.1 can be realized by making the appropriate diagonal matrix elements zero we study all these cases. The relation between vanishing diagonal elements and the universality class as well as the values of the dynamical exponents follows from straightforward power counting in the mode coupling equations derived in [16], see below for the two special cases we focus on in this work.

Purely diffusive case (D,D):

First consider the purely diffusive case (D,D) for which mode coupling theory requires $D_1^1 = D_2^1 = D_1^2 = D_2^2 = 0$. Demanding that $D_2^1 = D_1^2 = 0$ leads to the constraints $g_1^1 = 2\bar{g}^2$ and

$g_2^2 = 2\bar{g}^1$. In terms of the parameters b, γ, ρ_λ this reads $-\gamma = 1/(1-\rho_2) = b/(1-\rho_1)$. This is outside the physical parameter range $\gamma > -\min(1, b)$ of the totally asymmetric model of [17], but can be realized in the general two-lane model defined in Section 4.2. Plugging this condition into $D_1^1 = D_2^2 = 0$ yields the further conditions that $g_1^1 = g_2^2 = 0$, i.e., both Hessians must vanish. This requires

$$\rho_1 = \rho_2 = 1/2, \quad b = 1, \quad \gamma = -2. \tag{4.32}$$

The characteristic velocities are then $v_{1,2} = \mp 1$. It is somewhat counterintuitive that for these values one has $j_1 = j_2 = 0$, i.e., the system appears to be macroscopically in equilibrium, but the Gaussian mass fluctuations travel with non-zero velocities. A simple parameter choice for this scenario is $p_1 = p_2 = 1$, $q_1 = d_1 = g_1 = q_2 = d_2 = g_2 = 0$, $b_1 = c_1 = b_2 = c_2 = -1/2$, $e_1 = f_1 = e_2 = f_2 = 1/2$.

Superdiffusive mixed cases (D,KPZ'), (D,KPZ), (D,$\frac{3}{2}$L), (KPZ,$\frac{5}{3}$L):

Consider $b = 1$ where the hopping rates are completely symmetric with respect to the lane interchange and take $\rho_1 = \rho_2 =: \rho$. Then $g_1^1 = g_2^2 = -2(1+\gamma\rho)$, $g_2^1 = g_1^2 = 0$, $\bar{g}^1 = \bar{g}^1 = \gamma(1-2\rho)$ and $u = 1$, $\omega = 1$. This yields $D_1^1 = D_2^1 = 0$ and $D_2^2 = 2A_0(g_1^1 + 2\bar{g}^1)$, $D_1^2 = 2A_0(g_1^1 - 2\bar{g}^1)$ with $A_0 = \sqrt{\rho(1-\rho)/32}$. Computing the off-diagonal elements from (4.88), (4.91) we find the full mode coupling matrices

$$G^1 = -4A_0(1+\gamma\rho)\begin{pmatrix} 0 & 1 \\ 1 & 0 \end{pmatrix}, \quad G^2 = -4A_0\begin{pmatrix} 1+\gamma(1-\rho) & 0 \\ 0 & 1-\gamma(1-3\rho) \end{pmatrix} \tag{4.33}$$

Thus generically this line is in the (D,KPZ') universality class (Figure 4.2).

Notice that at $\gamma = -1/(1-\rho)$ one has $D_1^2 = 0$, corresponding to the (D,KPZ) universality class which can be realized in the generalized two-lane model defined above and that occurs also in the single-lane multi-component asymmetric simple exclusion process with stationary product measure [9]. For $\gamma = 1/(1-3\rho)$ one has $D_2^2 = 0$, corresponding to the (D,$\frac{3}{2}$L) scenario, see next section. If one moves away from the line $\rho_1 = \rho_2$, but stays on the curves indicated in Figure 4.2 for special values of γ the self-coupling coefficient G_{11}^1 is non-zero, but $G_{22}^2 = 0$. This can be straightforwardly verified by calculating the linear response of the diagonal elements of G^1, G^2 to small deviations $\delta\rho_1, \delta\rho_2$ from the line $\rho_1 = \rho_2$. Hence one has the (KPZ,$\frac{5}{3}$L) scenario. The three cases (D,KPZ'), (D,$\frac{3}{2}$L) and (KPZ,$\frac{5}{3}$L) can be realized in the totally asymmetric two-lane model.

Golden mean universality class (GM,GM):

Next consider $b \neq 1$. The formulas for the mode coupling matrices become cumbersome and we do not present them here in explicit form in full generality. It turns out that one can have that both self-coupling coefficients $G_{\alpha\alpha}^\alpha$ vanish and both subleading diagonal elements $G_{\beta\beta}^\alpha$ with $\beta \neq \alpha$ are non-zero, corresponding to the (φL,φL) scenario where both dynamical exponents are the golden mean $\varphi = (1+\sqrt{5})/2$, see Figure 4.3. This can be realized by choosing unequal densities such that

$$(1+\gamma\rho_2)(1-2\rho_1) = (b+\gamma\rho_1)(1-2\rho_2) \tag{4.34}$$

which corresponds to $J_{11} = J_{22}$ and hence $\omega = 1$. Then the requirement $D_1^1 = D_2^2 = 0$ yields

$$\rho_1 = \frac{1-b}{3\gamma}, \quad \rho_2 = \frac{\gamma-1}{3\gamma} \tag{4.35}$$

which implies $\gamma \in (-\infty, -1/2] \cup [1, \infty)$ and b is in the range between γ and -2γ. For general values of ω the analytical formulas for the lines $G_{11}^1 = G_{22}^2 = 0$ in the $\rho_1 - \rho_2$ plane are complicated. In

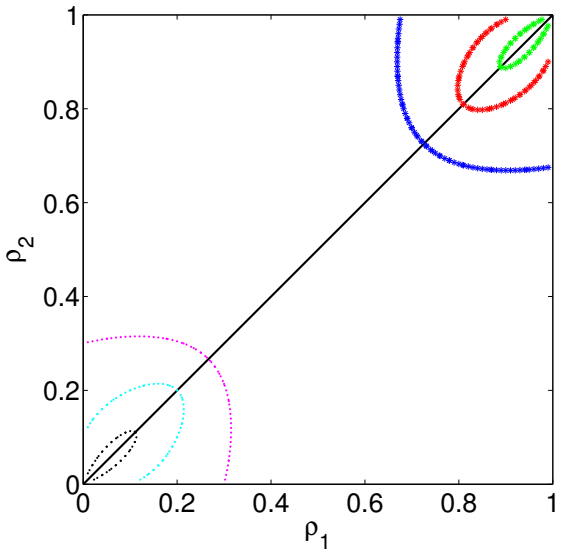

Figure 4.2.: Location of points where $G^2_{22} = 0$, $G^2_{11} \neq 0$ for $b = 1$ and different values of γ. In the upper right (lower left) corner the points grouped along curves of increasing length correspond to $\gamma = 1.5, 2.5, 5$ ($\gamma = -0.6, -0.7, -0.85$). On these curves one generically has the ($\frac{5}{3}$L,KPZ) universality class. On the diagonal line $\rho_1 = \rho_2$ one has $G^1_{11} = G^1_{22} = 0$, generically corresponding to the (D,KPZ') universality class. On the intersection of this line with a curve parametrized by γ one has the (D,$\frac{3}{2}$L) universality class.

order to demonstrate the existence of solutions we show numerical plots for fixed $\gamma = -3/4$ and various values b in Figure 4.3. Notice also that there are parameter ranges of b without solutions in the physical range of densities $(\rho_1, \rho_2) \in [0, 1] \times [0, 1]$.

In what follows we investigate in more detail the two novel universality classes (D,$\frac{3}{2}$L) and (GM,GM) which have not been reported yet in the literature on driven diffusive systems. We also comment on the shape of the structure function for the $\frac{5}{3}$-mode discussed in [17].

4.4. Superdiffusive non-KPZ universality classes

4.4.1. Diffusive mode and 3/2 - Lévy mode

We consider the case where mode 1 is Gaussian, and mode 2 has non-vanishing cross-coupling,

$$G^1_{11} = G^1_{22} = G^2_{22} = 0, \quad G^2_{11} \neq 0 \tag{4.36}$$

The mode coupling equation (4.17) for mode 2 reads in Fourier space

$$\begin{aligned} \partial_t \hat{S}_2(p,t) &= -ipv_2 \hat{S}_2(p,t) - p^2 D_2 \hat{S}_2 \\ &\quad -2(G^2_{11})^2 p^2 \int_0^t ds \hat{S}_2(p, t-s) \int_{-\infty}^{\infty} dq \hat{S}_1((p-q,s)\hat{S}_1((q,s). \end{aligned} \tag{4.37}$$

with $D_2 = \tilde{D}_{22}$. For the Gaussian mode 1 the mode coupling equation is obtained by the exchange $1 \leftrightarrow 2$ in (4.37) and dropping the term containing the integral. Note that we are interested in the large x behaviour of the scaling function, meaning $p \to 0$ in Fourier space.

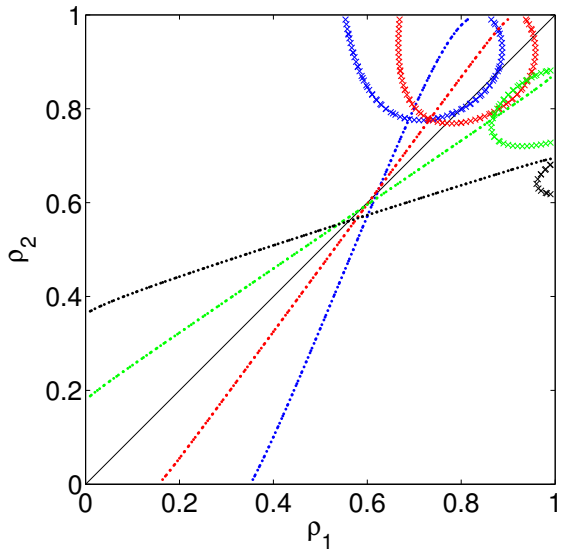

Figure 4.3.: Location of points where $G^1_{11} = 0$ $G^1_{22} \neq 0$ (crosses in the upper right corner) or $G^2_{22} = 0$ and $G^2_{11} \neq 0$ (thin bullets), for fixed $\gamma = -3/4$ and $b = 1.5$ (black), $b = 1.2$ green), $b = 0.9$ (red), $b = 0.8$ (blue), corresponding to the order from left to right in the lower half of the figure and opposite order in the upper part of the figure. Along the curves indicated by the dots (crosses) one has generically the ($\frac{5}{3}$L,KPZ) or (KPZ,$\frac{5}{3}$L) universality class. At the intersections of curves with the same colour one has the golden mean universality class (φL,φL).

We start with the observation that the Gaussian mode has the usual scaling form

$$S_1(x,t) = \frac{1}{\sqrt{4\pi D_1 t}} \mathrm{e}^{-\frac{(x-v_1 t)^2}{4D_1 t}} \tag{4.38}$$

with Fourier transform $\hat{S}_1(p,t) = 1/\sqrt{2\pi}\exp\left(-iv_1 pt - D_1 p^2 t\right)$. Inserting this into (4.37) and performing the integration over q, we obtain

$$\partial_t \hat{S}_2(p,t) = -(ipv_2 + p^2 D_2)\hat{S}_2(p,t) - p^2\left(G^2_{11}\right)^2 \int_0^t ds \hat{S}_2(p,t-s)\frac{\mathrm{e}^{-iv_1 ps - D_2 p^2 s/2}}{\sqrt{2\pi D_2 s}}. \tag{4.39}$$

This equation can be solved in terms of the Laplace transform $\tilde{S}_2(p,\omega) := \int_0^\infty \mathrm{d}t \mathrm{e}^{-\omega t}\hat{S}_2(p,t)$ which yields

$$\tilde{S}_2(p,\omega) = \frac{\hat{S}_2(p,0)}{\omega + ipv_2 + p^2\left(D_2 + \left(G^2_{11}\right)^2\left(\sqrt{2D_2(\omega + ipv_1 + D_2 p^2/2)}\right)^{-1}\right)}. \tag{4.40}$$

For large times we assume the real-space scaling form $S_2(x,t) = t^{-1/z}h\left(\frac{(x-v_2 t)^z}{t}\right)$ with dynamical exponent $z > 1$. This is equivalent to the scaling forms

$$\hat{S}_2(p,t) = \mathrm{e}^{-iv_2 pt} f(|p|^z t), \quad \tilde{S}_2(p,\omega) = |p|^{-z} g\left(\frac{\omega + ipv_2}{|p|^z}\right) \tag{4.41}$$

for the Fourier- and Laplace transforms respectively. By introducing the shifted Laplace parameter $\tilde{\omega} := \omega + ipv_2$ one finds that the leading small-p behaviour of the Laplace transform (4.40)

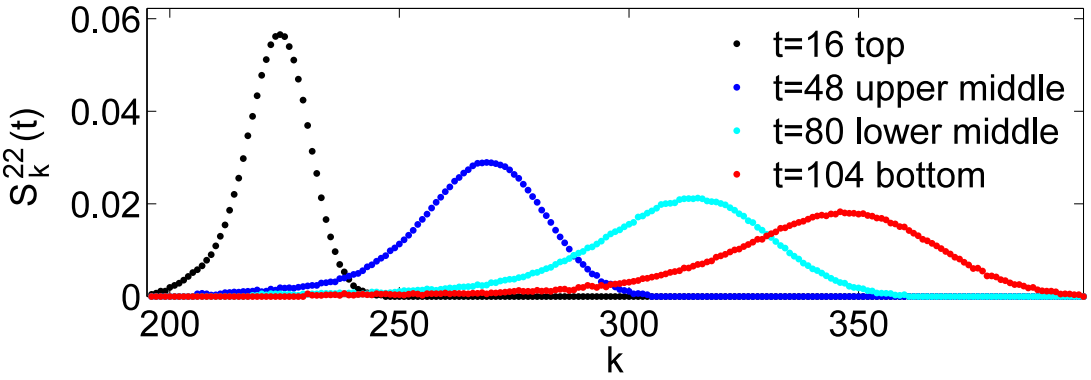

Figure 4.4.: Dynamical structure function $S_k^{22}(t)$ for 3/2-Lévy mode with $v_2 = 1.3$ measured by Monte Carlo simulation at different times, averaged over $18{\cdot}10^7$ histories. Parameters: $L = 600$, $\gamma = 2.5$, $b = 1$, $\rho_1 = 0.2$, $\rho_2 = 0.2$. Statistical errors are smaller than symbol size.

comes from the term proportional to $v_1 - v_2$ under the square root. This yields $z = 3/2$ and we obtain in the limit $\tilde{\omega} \to 0$ (with scaling variable $\tilde{\omega}/|p|^z$ kept fixed) after performing the inverse Laplace transformation

$$\hat{S}_2(p,t) = \frac{1}{\sqrt{2\pi}} \exp\left(-iv_2pt - C_0|p|^{3/2}t\,[1 - i\,\mathrm{sgn}(p(v_1 - v_2))]\right) \tag{4.42}$$

with

$$C_0 = \frac{\left(G_{11}^2\right)^2}{2\sqrt{D_1|v_2 - v_1|}}. \tag{4.43}$$

We recognize here the characteristic function of an α-stable Lévy distribution

$$\hat{\phi}(p;\mu,c,\alpha,\beta) := \exp\left(ip\mu - |cp|^\alpha(1 - i\beta\tan\left(\frac{\pi\alpha}{2}\right)\mathrm{sgn}(p))\right) \tag{4.44}$$

with $\mu = -v_2t$, $\alpha = 3/2$, $c = (C_0t)^{2/3}$ and maximal asymmetry $\beta = \mathrm{sgn}(v_1 - v_2) = \pm 1$.

We remark that in real space the asymmetric Lévy scaling function has only one heavy tail decaying as $1/x^{1+\alpha}$ which in a finite system leads to finite size corrections of order $1/L^{1+\alpha}$ for times $t \ll L^\alpha$. The other tail, that extends away from the position of the other mode, decays exponentially. This effect, which defines a kind of light cone, is a classical analogue of the Lieb-Robinson-bound for the spreading of perturbations in quantum systems [41]. The scaling function (4.42) is similar to the one found to describe the hydrodynamics of the anharmonic chain in the case of an "even potential", see [16].

Monte-Carlo simulation data for the 3/2-Lévy mode are shown in Figure 4.4 for small times up to $t \approx 100$. The mode moves with a velocity that, numerically, cannot be distinguished from the theoretical prediction $v_2 = 1.3$. Indeed, one expects the error in the velocity, if at all, to be small, since the velocity comes from mass conservation and is an exact constant for all times even on the lattice [32].

The scaling exponent and asymmetry predicted by mode coupling theory are in a good agreement with the Monte Carlo simulations, see Figs. 4.5, 4.6. In Figure 4.5 we show the growth of the variance $V_2(t)$ of the measured 3/2-Lévy mode. This quantity is not infinite for finite times, since the (single) heavy tail of the asymptotic asymmetric Lévy scaling function (4.42) is cut off at finite times by the coupling to the other mode at a distance of the order $(v_2 - v_1)t$. Thus one

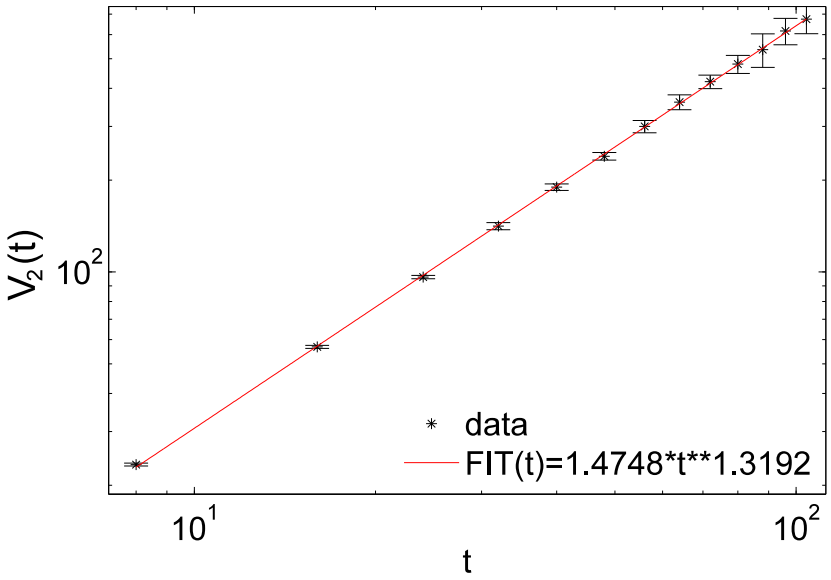

Figure 4.5.: (Color online) Variance $V_2(t)$ of the measured dynamical structure function shown in Fig. 4.4 versus time.

expects the empirical variance $V_2(t)$ to be finite but growing in time. Mass conservation together with dynamical scaling predicts a growth $V_2(t) \propto t^\nu$ with $\nu = 2/z$ [17]. The measured exponent $\nu_{exp} \approx 1.32$ is very close to the theoretical value $\nu = 4/3$ even for the early time regime shown in the figures.

The only parameter that has slow convergence to the asymptotic value is the asymmetry of the scaling function. A similar phenomenon is discussed in [16] in terms of corrections to scaling of the memory kernel for the 5/3-Lévy mode. They are shown to vanish slowly with a power law decay in time. Here we measure the deviation of the asymmetry from its asymptotic value. The measured quantity $1 + \beta_{exp}$ decreases monotonically with time. The decay is approximately algebraic with exponent $\approx 1/6$, see Fig. 4.7.

4.4.2. Two golden mean modes

We consider now the case where both self-coupling coefficients $G^\alpha_{\alpha\alpha}$ of the mode coupling matrix vanish and *both* subleading coefficients $G^\alpha_{\beta\beta}$ are non-zero and in general unequal. In this case one cannot use the Gaussian or the KPZ scaling function as an input into the mode coupling equations. However, the equations give a self-consistency relation which allows one to compute the scaling function for the two modes, see [39] for the symmetric case where $G^1_{22} = G^2_{11}$. For the generic non-symmetric case $G^1_{22} \neq G^2_{11}$ the calculation of [39] is not directly applicable. However, one can adopt a similar philosophy with two scaling functions

$$\hat{S}_1(p,t) = \mathrm{e}^{-iv_1pt} g(b|p|t^\beta), \quad \hat{S}_2(p,t) = \mathrm{e}^{-iv_2pt} h(c|p|^\gamma t) \tag{4.45}$$

as input, which, in addition to the *a priori* unknown dynamical exponents γ and $1/\beta$, have different scale factors b, c as free variables. With this ansatz one obtains by power counting the consistency conditions $\gamma = 1 + \beta$ and $\gamma = 1/\beta$ for the dynamical exponent. From the mode coupling equations we have computed also the scale factors. These computations are lengthy, but

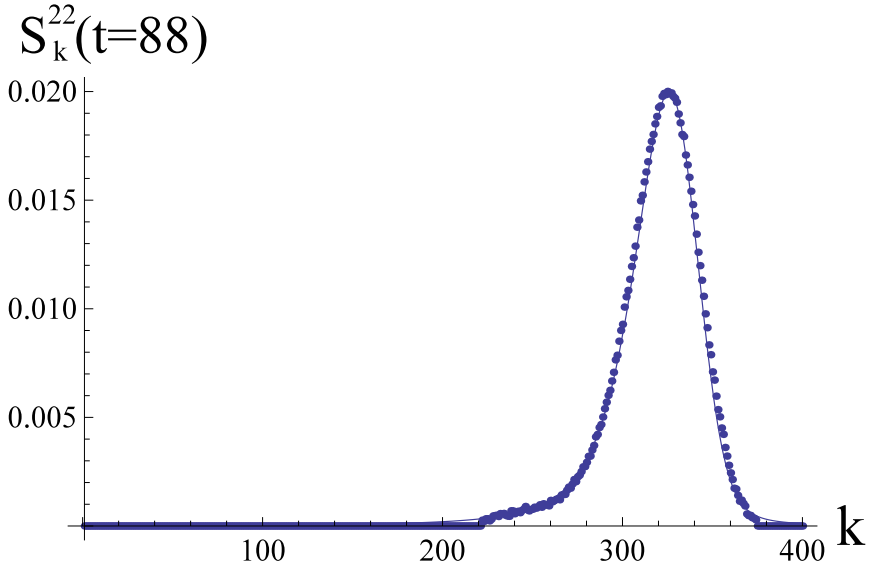

Figure 4.6.: Fit of the dynamical structure function $S_k^{22}(t)$ for time $t = 88$ with a 3/2-stable Lévy distribution with asymmetry $\beta = -0.692$. For parameters see Fig. 4.4.

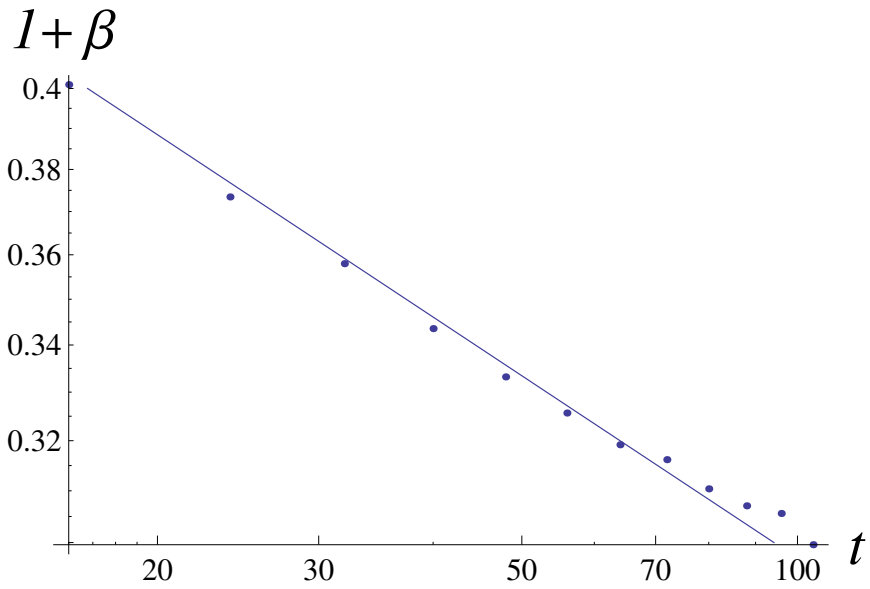

Figure 4.7.: Asymmetry $1+\beta$ versus time, obtained by fitting the numerically obtained dynamical structure function with the PDF of 3/2 Lévy stable law. The line with the power law $\propto t^{-1/6}$ is a guide to the eye. For parameters see Figure 4.4.

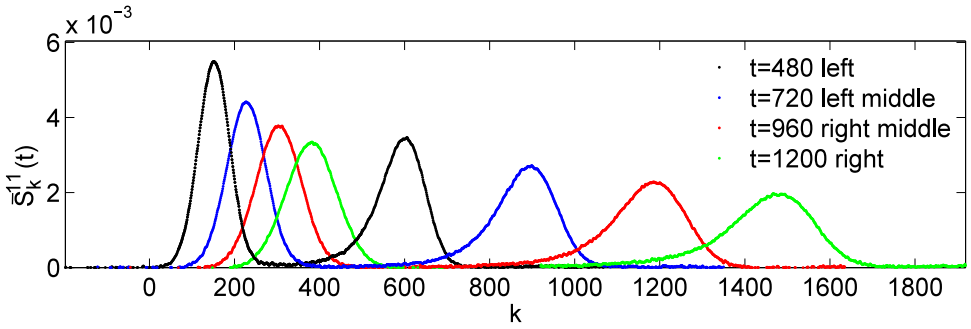

Figure 4.8.: Dynamical structure function showing both modes for particles on chain 1, for the golden mean mode with $v_2 = 1.183$ at different times. Parameters: $L = 10^6, \gamma = 2.5, b = 0.625, \rho_1 = 0.25, \rho_2 = 0.2$. Statistical errors are smaller than symbol size.

straightforward. With the relabelling $\hat{S}_-(p,t) \equiv \hat{S}_1(p,t)$, $\hat{S}_+(p,t) \equiv \hat{S}_2(p,t)$ one arrives at

$$\hat{S}_\pm(p,t) = \frac{1}{\sqrt{2\pi}} \exp\left(-iv_\pm pt - C_\pm |p|^\varphi t \left[1 \pm i\mathrm{sgn}(p(v_- - v_+)) \tan\left(\frac{\pi\varphi}{2}\right)\right]\right) \tag{4.46}$$

with golden mean $\gamma = \varphi \equiv (1+\sqrt{5})/2$ and the scale factors

$$C_\pm = \frac{1}{2}|v_+ - v_-|^{1-\frac{2}{\varphi}} \left(\frac{2G^1_{22}G^2_{11}}{\varphi \sin\left(\frac{\pi\varphi}{2}\right)}\right)^{\varphi-1} \left(\frac{G^1_{22}}{G^2_{11}}\right)^{\pm(1+\varphi)}. \tag{4.47}$$

Notice that $\varphi - 1 = 1/\varphi$.

For numerical simulation of this new universality class we choose the parameter manifold (4.34) of the two-lane model where one has the characteristic velocities

$$v_\pm = (1+\gamma\rho_2)(1-2\rho_1) \pm \gamma\sqrt{\rho_1(1-\rho_1)\rho_2(1-\rho_2)}. \tag{4.48}$$

We have chosen $\gamma = 2.5$, $b = 0.625$ and $\rho_1 = 0.25$, $\rho_2 = 0.2$ corresponding to the mode coupling matrices

$$G^1 = \begin{pmatrix} 0 & -0.406416 \\ -0.406416 & -0.105726 \end{pmatrix}, \quad G^2 = \begin{pmatrix} -0.812833 & -0.052863 \\ -0.052863 & 0 \end{pmatrix} \tag{4.49}$$

and transformation matrix

$$R^{-1} = \begin{pmatrix} -0.734553 & 0.734553 \\ 0.678551 & 0.678551 \end{pmatrix}. \tag{4.50}$$

The columns of R are the eigenmodes with velocities $v_1 \equiv v_- = 0.3170$, $v_2 \equiv v_+ = 1.183$ respectively. In order to measure the dynamical exponent $\varphi \approx 1.618$, which is rather close to $z = 5/3 \approx 1.667$ appearing in the (5/3L,KPZ) scenario studied in [17], we focus on the large-time regime rather than looking into corrections to scaling for the asymmetry as done above. We use simulation parameters $n = 300$, $m = 3$, $\tau = 120$ and $n = 1000$, $m = 46$, $\tau = 120$.

Fig. 4.8 shows the measured dynamical structure function for both golden modes moving on lattice 1. The peaks are well separated already at the earliest time $t = 480$ shown in the figure. The center of mass velocities have no perceptible deviation from the theoretical predictions.

In Fig. 4.9 we plot the maximum of the dynamic structure function for mode 2 (which scale as $t^{-1/z}$) as a function of time. A least square fit with 95% confidence bounds gives a measured

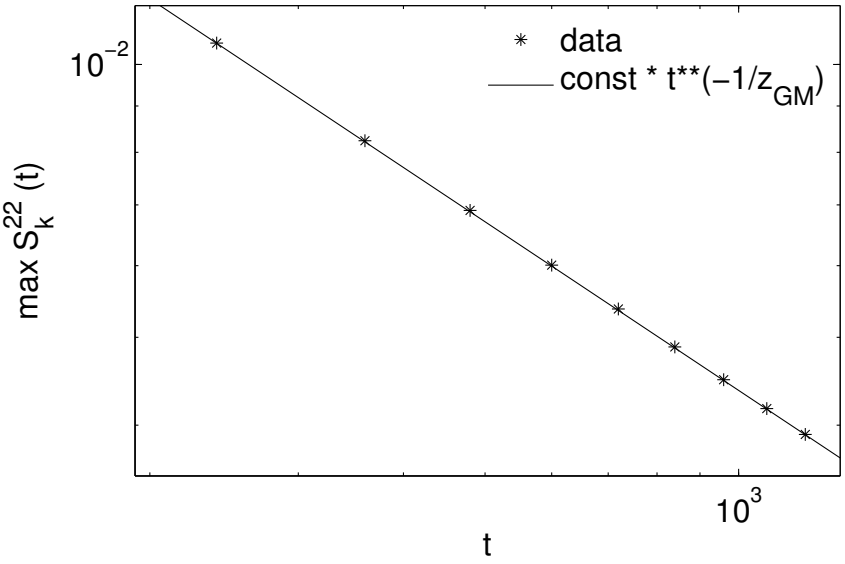

Figure 4.9.: (Color online) Maximum of the dynamical structure function for mode 2 versus time, plotted in double logarithmic scale. The line with the theoretically predicted slope (notice: $z_{GM} \equiv \varphi$) is a guide to the eye. Model parameters are as in Fig. 4.8.

dynamical exponent $z = 1.619$, with error bars $1.613 < z < 1.624$. This agrees well with the theoretically predicted golden mean value $z = \varphi \approx 1.618$.

To investigate the convergence of the scaling function, we plot both the measured structure function and the theoretically predicted φ-stable distribution for a fixed time, see Fig. 4.10. The theoretical prediction is well borne out by the simulation. Small deviations are visible in the right (fast decaying) tail, see also the closeup view shown in the inset of Fig. 4.10. A fit with a maximally asymmetric 5/3-stable Lévy distribution shows a markedly poorer agreement.

Finally, we remark that the left peak in Figure 4.8 corresponding to mode 1 is considerably less asymmetric than the peak of mode 2 shown in more detail in Figure 4.10. To get some intuition for this observation we point out to the numerical values G^1_{22} and G^2_{11} (4.49). The ratio of their square is $(G^1_{22}/G^2_{11})^2 \approx 0.017$, so the coupling strengths differ by almost two orders of magnitude. If G^1_{22} was zero, we would be back to the (D,$\frac{3}{2}$L) scenario discussed in the previous subsection and mode 1 would be a symmetric Gaussian peak. Therefore one indeed expects for mode 1 at finite times a more symmetric function than predicted for the asymptotic regime.

4.4.3. KPZ mode and 5/3 - Lévy mode

In [17] we reported the occurrence of the ($\frac{5}{3}$L,KPZ) universality class for the totally asymmetric version of the two-lane exclusion process. The measured dynamical exponents were shown to agree well with the theoretical prediction. Here we expand on these result by briefly discussing the scaling function. In Figure 4.11 one can see that a reasonable fit of the numerical data can be obtained with a 5/3-stable Lévy distribution predicted by mode coupling theory [16].

The measured dynamical structure function, however, exhibits an asymmetry much less than the predicted maximal value. Indeed, for small times its amplitude is rather small. We attribute this discrepancy to finite-time effects, cf. the argument for the left GM mode of the previous subsection. In order to substantiate this claim we show in Table 4.2 numerically determined asymmetries. They grow in time, thus supporting the argument. We do not have a theoretical

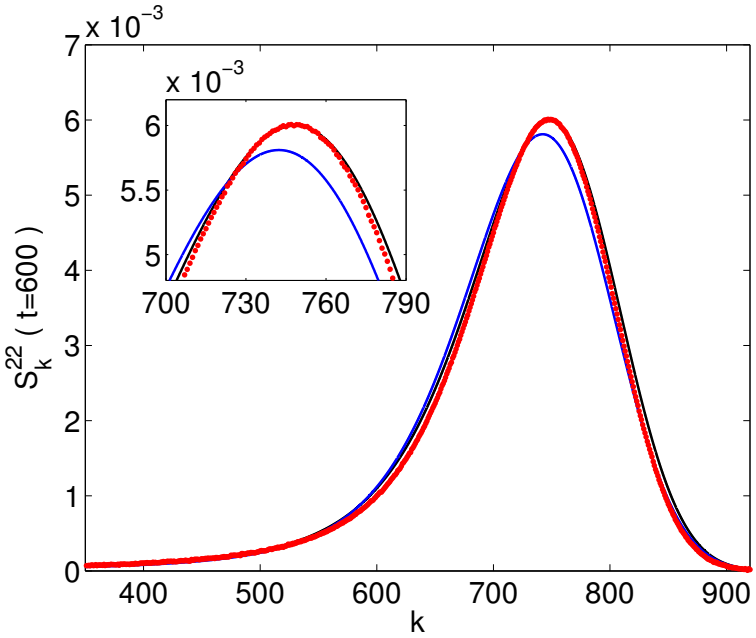

Figure 4.10.: (Color online) Measured dynamic structure function for mode 2 at time $t = 600$. Monte Carlo data correspond to red dots, and black (blue) curves correspond to the best least square fits of the Monte Carlo data with the $z = \varphi$ ($z = 5/3$) stable Lévy distribution with maximal asymmetry, and theoretically predicted center of mass position. The inset shows a close-up view of the peak region. Model parameters are as in Fig. 4.8.

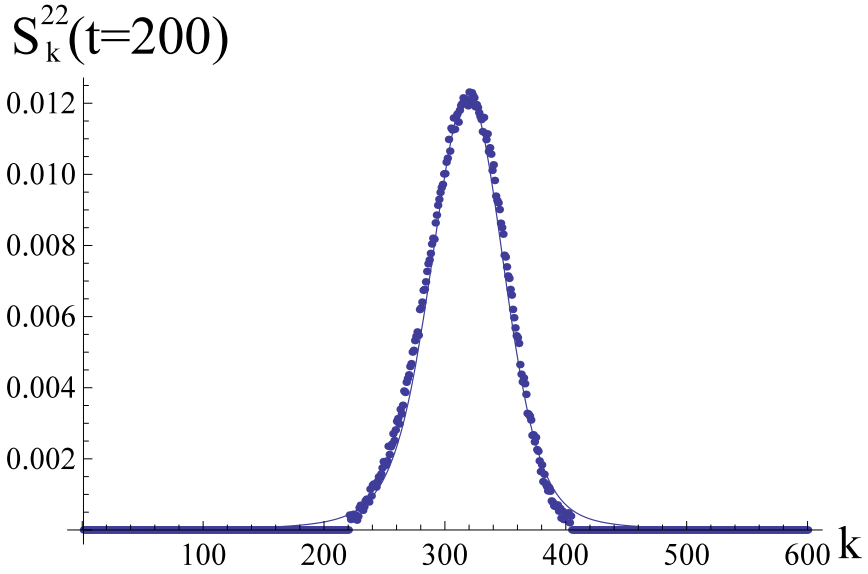

Figure 4.11.: (Color online) Measured dynamic structure function for mode 2 at time $t = 200$. The curve is a fit with the 5/3-stable Lévy distribution with non-maximal asymmetry..

prediction of how they should grow.

t	20	40	60	80	100
β	-0.0229	-0.0504	-0.0685	-0.0797	-0.0825
t	120	140	160	200	
β	-0.0872	-0.0918	-0.0916	-0.1000	

Table 4.2.: Asymmetry β of a 5/3-Lévy distribution obtained from a fit to the numerical data for the 5/3-Lévy mode of [17] for different early times $t \leq 200$. The predicted asymptotic value is -1.

4.5. Conclusions

We have studied time-dependent density fluctuations in driven diffusive system with two conservation laws. For one conservation law it is well-established that the appropriate tool to describe the universal properties of these fluctuations is non-linear fluctuating hydrodynamics (4.9). Recent work, reviewed in [16], shows that the approach can be extended to anharmonic chains with more than one conservation law and also to Hamiltonian dynamics with three conservation laws [13]. From the present work and our preliminary results reported in [17] we conclude that the predictions of the theory apply also to driven diffusive systems with stochastic lattice gas dynamics with two conservation laws. Specifically, for a two-lane asymmetric simple exclusion process we argue that all theoretically possible universality classes for two-component systems, discussed also in [39], can be realized (see Table 4.1). Among these, our Monte-Carlo simulations of a two-lane asymmetric exclusion process confirm two superdiffusive universality classes which have gone unnoticed so far in the literature on driven diffusive systems.

Mode coupling theory not only predicts the dynamical exponents z for these universality classes, but also the scaling forms of the dynamical structure functions for these novel superdiffusive modes. In most cases these scaling functions are z-stable Lévy distributions with maximal asymmetry. The numerical simulation confirms these predictions with great accuracy both for the 3/2-mode and a golden mean mode with $z = (1 + \sqrt{5})/2$ shown to occur also in anharmonic chains [39]. For some modes the z-stable Lévy distributions provide excellent fits, but with an effective asymmetry that is not maximal. However, our data show that the numerically fitted asymmetry increases with time in the cases we considered, thus supporting the notion that asymptotically the maximal value will be reached.

Which universality classes actually occur in a system at given values of the physical parameters of the model is completely encoded in the stationary current-density relation $\vec{j}(\rho_1, \rho_2)$, no other knowledge about a given model is required. The stationary compressibility matrix $K(\rho_1, \rho_2)$, related to the current-density relation through a time-reversal symmetry proved in [36], allows for the prediction also of the scale factors that enter the scaling functions, unless diffusive modes are relevant. Thus generically the scaling functions are completely determined by two simple stationary properties: The current-density relation $\vec{j}(\rho_1, \rho_2)$ and the compressibility matrix $K(\rho_1, \rho_2)$. Going beyond specific lattice gas models, we have computed the mode coupling matrices in general form for arbitrary input data, i.e., arbitrary current-density relation and compressibility matrix. From the diagonal matrix elements of these one can then directly read off the scaling functions for arbitrary two-component systems, except in the presence of the diffusive universality class where the scale factors contain a phenomenological diffusion coefficient not predicted by the theory and which may modify the KPZ mode.

It is interesting to notice that all possible scenarios of universality classes (see Table 4.1) can be realized with the simple current-density relation (4.2). This relation is minimal in the sense that the non-linearity of the conserved current j_λ is only quadratic and the coupling of this non-linearity to the other conserved quantity is only linear, i.e., $\rho_\lambda^2 \rho_\mu$ for $\lambda \neq \mu$. Thus it is not necessary to have a more complicated current-density relation in order to observe all allowed universality classes. Moreover, this minimal current-density relation has the nice property that one does not expect logarithmic corrections to diffusive modes [38]. Our two-lane exclusion process, which is an extension of the model studied by us previously [17], provides a simple microscopic realization for this minimal current-density relation.

Throughout this discussion we have tacitly assumed that the current-density relation is strictly hyperbolic, i.e., the collective velocities v_α of the two modes are different. This assumption is crucial for the decoupling argument for the modes that underlies the mode-coupling computations. Indeed, the nonequilibrium time reversal symmetry (4.58) [36] rules out umbilic points (where $v_1 = v_2$) in any model which has minimal current-density relation and at the same time a diagonal compressibility matrix. Therefore in the model presented here the issue does not actually arise. However, umbilic points are a generic feature of more complicated models, either with the same minimal current-density relation, but a non-diagonal compressibility matrix [29], or for non-minimal current-density relations [40]. From numerical observations [40] one expects the dynamical exponent $z = 3/2$ as for KPZ, but non-KPZ scaling functions. How mode coupling theory can predict the behaviour at umbilic points is an open problem. It would also be interesting to extend mode coupling theory to predict the convergence of the finite-time asymmetry in the Lévy distribution to the asymptotic maximal value.

Acknowledgements

The authors are indebted to H. Spohn for pointing out the possibility of the golden mean universality class prior to publication of [39]. Indeed, this hint motivated us to systematically explore the structure of the mode-coupling matrices. We also thank him and G. Stoltz for useful comments on a preliminary version of the manuscript and M. Barma, R. Livi, H. Posch, A. Schadschneider and H. van Beijeren for enlightening discussions. Financial support by Deutsche Forschungsgemeinschaft (DFG) is gratefully acknowledged. We thank the INFN and the Galileo Galilei Institute for Theoretical Physics, where part of this work was done, for hospitality and for partial support.

Appendix

4.A. Mode coupling matrices for strictly hyperbolic two-component systems

4.A.1. Notation

We consider a general system with two conservation laws. For definiteness we choose the language of driven diffusive systems with currents $j_\lambda(\rho_1, \rho_2)$, $\lambda = 1, 2$ for the conserved densities ρ_λ. We define the general flux Jacobian

$$J = \begin{pmatrix} J_{11} & J_{12} \\ J_{21} & J_{22} \end{pmatrix} \tag{4.51}$$

with matrix elements

$$J_{\lambda\mu} = \frac{\partial j_\lambda}{\partial \rho_\mu} \tag{4.52}$$

The transposed matrix is denoted J^T.

We define

$$\delta := (J_{11} - J_{22})\sqrt{1 + \frac{4J_{12}J_{21}}{(J_{11} - J_{22})^2}} \tag{4.53}$$

which is the signed square root of the discriminant of the characteristic polynomial of J with the sign given by $J_{11} - J_{22}$. The two eigenvalues of J are

$$v_\pm = \frac{1}{2}\left(J_{11} + J_{22} \pm \delta\right). \tag{4.54}$$

We associate velocity v_- with eigenmode 1 and v_+ with eigenmode 2, irrespective of the sign of $v_- - v_+$ which is equal to the sign of $J_{22} - J_{11}$.

The matrix elements of the Hessians are denoted

$$H^\lambda = \begin{pmatrix} h_1^\lambda & \bar{h}^\lambda \\ \bar{h}^\lambda & h_2^\lambda \end{pmatrix} \tag{4.55}$$

with

$$h_1^\lambda = (\partial_1)^2 j_\lambda, \quad h_2^\lambda = (\partial_2)^2 j_\lambda, \quad \bar{h}^\lambda = \partial_1\partial_2 j_\lambda. \tag{4.56}$$

They are symmetric by definition.

The compressibility matrix is denoted

$$K = \begin{pmatrix} \kappa_1 & \bar{\kappa} \\ \bar{\kappa} & \kappa_2 \end{pmatrix} \tag{4.57}$$

It is symmetric by definition. Without loss of generality we can assume $\kappa_1\kappa_2 \neq 0$ since a vanishing self-compressibility corresponds to a "frozen" lane without fluctuations which would reduce the dynamics of the two-lane system to a dynamics with a single conservation law. Time-reversal yields the Onsager-type symmetry [36]

$$JK = KJ^T \tag{4.58}$$

which implies

$$J_{21}\kappa_1 - J_{12}\kappa_2 = (J_{11} - J_{22})\bar{\kappa}. \tag{4.59}$$

Relation (4.58) also guarantees that the eigenvalues $v_\pm$ of a physical flux Jacobian J are generally real. A related symmetry relation was noted earlier in the context of classical fluids [34].

We point out the somewhat surprising fact that for *any* model with $\bar{\kappa} = 0$, i.e., whenever the stationary distribution factorizes in the conserved quantities, the compressibilities satisfy $J_{21}\kappa_1 = J_{12}\kappa_2$. Thus a vanishing cross derivative $J_{\lambda\mu}$ for one of the currents implies a vanishing cross derivative $J_{\mu\lambda}$ also of the other, without any *a priori* assumption on the stochastic dynamics. The same is true also on parameter manifolds where $J_{11} = J_{22}$.

4.A.2. Normal modes

We focus on the strictly hyperbolic case $v_+ \neq v_-$ corresponding to $\delta \neq 0$. Since J is not assumed to be symmetric we have to distinguish right (column) and left (row) eigenvectors, denoted by $\vec{c}^{\pm}$ and $\vec{r}^{\pm}$, respectively. Here

$$\vec{c}^{\pm} = \begin{pmatrix} c_1^{\pm} \\ c_2^{\pm} \end{pmatrix}, \quad \vec{r}^{\pm} = \left(r_1^{\pm}, r_2^{\pm}\right). \tag{4.60}$$

We normalize them to obtain a biorthogonal basis with scalar product

$$\vec{r}^{\sigma} \cdot \vec{c}^{\sigma'} := r_1^{\sigma} c_1^{\sigma'} + r_2^{\sigma} c_2^{\sigma'} = \delta_{\sigma,\sigma'} \tag{4.61}$$

with $\sigma, \sigma' \in \{\pm\}$. Using

$$\frac{J_{22} - J_{11} - \delta}{2\sqrt{J_{12}J_{21}}} = \frac{2\sqrt{J_{12}J_{21}}}{J_{11} - J_{22} - \delta} \tag{4.62}$$

this yields

$$\vec{c}^{\pm} = \frac{1}{2\delta y_\pm} \begin{pmatrix} 2J_{12} \\ J_{22} - J_{11} \pm \delta \end{pmatrix}, \tag{4.63}$$

$$\vec{r}^{\pm} = \frac{y_\pm}{\delta \pm (J_{22} - J_{11})} \left(2J_{21},\, J_{22} - J_{11} \pm \delta\right) \tag{4.64}$$

with arbitrary normalization constants $y_\pm$.

Next we introduce (bearing in mind that $\delta \neq 0$)

$$R = \begin{pmatrix} r_1^- & r_2^- \\ r_1^+ & r_2^+ \end{pmatrix}, \quad R^{-1} = \begin{pmatrix} c_1^- & c_1^+ \\ c_2^- & c_2^+ \end{pmatrix}. \tag{4.65}$$

Biorthogonality and normalization give $RR^{-1} = 1$. The fact that R contains the left eigenvectors as its rows implies $RJ = \Lambda R$ where $\Lambda = diag(v_-, v_+)$. Therefore

$$RJR^{-1} = \Lambda. \tag{4.66}$$

Then the linearized Eulerian hydrodynamic equations (4.7) read

$$\frac{\partial}{\partial t}\vec{\phi} + \Lambda \frac{\partial}{\partial x}\vec{\phi} = 0 \tag{4.67}$$

with $\vec{\phi} = R\vec{u}$.

The diagonalizer R is uniquely defined up to multiplication by an invertible diagonal matrix which is reflected in the arbitrariness of the normalization factors $y_\pm$. In order to fix these constants we first observe that from (4.58) it follows that $R(JK)R^T = \Lambda(RKR^T) = R(KJ^T)R^T = (RKR^T)\Lambda$. Hence RKR^T must be diagonal since Λ is diagonal. This allows us to fix the normalization constants $y_\pm$ by demanding

$$RKR^T = \mathbb{1}. \tag{4.68}$$

This normalization condition has its origin in the fact that the structure matrix $\bar{S}(k,t)$ (whose components are the dynamical structure functions (4.11)) is by definition normalized such that $\sum_k \bar{S}(k,t) = K$, see next subsection. For computing the normalization factors we first consider $J_{12}J_{21} \neq 0$.

It is convenient to parametrize R by diagonal matrices $Z = diag(z_-, z_+)$, $U = diag(1, u)$ and an orthogonal matrix O such that

$$R = ZOU = \begin{pmatrix} z_- \cos\vartheta & -uz_- \sin\vartheta \\ z_+ \sin\vartheta & uz_+ \cos\vartheta \end{pmatrix} \tag{4.69}$$

with

$$\tan\vartheta = \frac{J_{11} - J_{22} + \delta}{2\sqrt{J_{12}J_{21}}}, \quad u = \sqrt{\frac{J_{12}}{J_{21}}}. \tag{4.70}$$

Notice that $J_{12}J_{21} \neq 0$ implies $u \neq 0$, $\sin\vartheta \neq 0$ and $\cos\vartheta \neq 0$. There are several useful identities involving the rotation angle ϑ, viz. $\tan(2\vartheta) = 2\sqrt{J_{12}J_{21}}/(J_{22} - J_{11})$, $\sqrt{J_{12}J_{21}}(\cos^2\vartheta - \sin^2\vartheta) = (J_{22} - J_{11})\cos\vartheta\sin\vartheta$ and $\delta = (J_{22} - J_{11})(\cos^2\vartheta - \sin^2\vartheta) + 4\sqrt{J_{12}J_{21}}\cos\vartheta\sin\vartheta = (J_{22} - J_{11})\cos(2\vartheta) + 2\sqrt{J_{12}J_{21}}\sin 2\vartheta = (J_{22} - J_{11})/\cos(2\vartheta) = 2\sqrt{J_{12}J_{21}}/\sin(2\vartheta)$.

Now we use that for $\bar{\kappa} \neq 0$ one can write

$$UJU^{-1} = \mu UKU + \nu\mathbb{1} \tag{4.71}$$

with

$$\mu = \frac{J_{21}}{\bar{\kappa}}, \quad \nu = \frac{1}{2}\left(J_{11} + J_{22} - \frac{J_{21}\kappa_1 + J_{12}\kappa_2}{\bar{\kappa}}\right). \tag{4.72}$$

Therefore

$$\begin{aligned} RKR^T &= ZOUKUO^TZ = \frac{1}{\mu}\left(ZOUJU^{-1}O^TZ - \nu Z^2\right) \\ &= \frac{1}{\mu}\begin{pmatrix} v_- - z_-^2\nu & 0 \\ 0 & v_+ - z_+^2\nu \end{pmatrix} \end{aligned} \tag{4.73}$$

which yields

$$z_\pm^2 = \frac{v_\pm - \mu}{\nu}. \tag{4.74}$$

By comparing with (4.65) one finds that the normalization factors for the eigenvectors are given by $y_- = uz_-\sin\vartheta$, $y_+ = uz_+\cos\vartheta$. For $\bar{\kappa} = 0$ one obtains directly from (4.59) and (4.69) that

$$y_-^2 = \frac{\sin^2\vartheta}{\kappa_2}, \quad y_+^2 = \frac{\cos^2\vartheta}{\kappa_2}. \tag{4.75}$$

Even though not relevant for the two-lane model of this paper we mention for completeness that some care with limits has to be taken when $J_{12}J_{21} = 0$. First notice that in this case the physical requirement $\kappa_1\kappa_2 \neq 0$ implies $\bar{\kappa} \neq 0$. Specifically for $J_{12} = 0$, $J_{21} \neq 0$ one has $\delta = J_{11} - J_{22}$, $v_- = J_{11}$, $v_+ = J_{22}$, $J_{21}\kappa_1 = (J_{11} - J_{22})\bar{\kappa}$ and

$$R = \begin{pmatrix} \tilde{z}_- & 0 \\ \frac{\tilde{z}_+ J_{21}}{J_{22} - J_{11}} & \tilde{z}_+ \end{pmatrix} \tag{4.76}$$

with

$$\tilde{z}_-^{-2} = \kappa_1, \quad \tilde{z}_+^{-2} = \kappa_2 - \frac{\bar{\kappa}^2}{\kappa_1}. \tag{4.77}$$

Notice that here strict hyperbolicity implies $J_{11} \neq J_{22}$ so that R is well-defined.

Similarly one obtains for $J_{21} = 0$, $J_{12} \neq 0$ with $v_- = J_{11} \neq v_+ = J_{22}$ the relation $J_{12}\kappa_2 = (J_{22} - J_{11})\bar{\kappa}$ and

$$R = \begin{pmatrix} \hat{z}_- & \frac{\hat{z}_- J_{12}}{J_{11} - J_{22}} \\ 0 & \hat{z}_+ \end{pmatrix} \tag{4.78}$$

with

$$\hat{z}_-^{-2} = \kappa_1 - \frac{\bar{\kappa}^2}{\kappa_2}, \quad \hat{z}_+^{-2} = \kappa_2. \tag{4.79}$$

If $J_{12} = J_{21} = 0$ then J is diagonal. For the strictly hyperbolic case $J_{11} \neq J_{22}$ one necessarily has $\bar{\kappa} = 0$ and the normalization condition (4.68) yields $R = diag(\kappa_1^{-1}, \kappa_2^{-1})$.

4.A.3. Normal modes and the microscopic dynamical structure function

In order to explain the origin of the normalization condition and to apply it to the two-lane model. We define the random variables $f_k^\lambda(t) := n_k^{(\lambda)}(t) - \rho_\lambda$ and $f_0^\lambda := f_0^\lambda(0)$ where the random variable $n_k^{(\lambda)}(t)$ is the particle number on site k of lane λ with particle density ρ_λ at time t. We also define the two-component column vector $\vec{f}_k(t)$ with components $f_k^\lambda(t)$ and the two-component row vector $\vec{f}_0^T := (f_0^1, f_0^2)$. Expectation w.r.t. the stationary distribution is denoted by $\langle \cdot \rangle$. By translation invariance and stationarity one has $\langle f_k^\lambda(t) \rangle = 0$. The expectation of a matrix is understood as the matrix of the expectations of its components. Defining the 2×2-matrix $\bar{\mathcal{S}}_k(t) = \vec{f}_k(t) \otimes \vec{f}_0^T$ (the components of which are random variables) the dynamical structure matrix with components (4.11) can be written $\bar{S}_k(t) = \langle \bar{\mathcal{S}}_k(t) \rangle$.

The normalization of the dynamical structure matrix, defined by the sum over the whole lattice, is given by

$$\sum_k \bar{S}_k(t) = K. \tag{4.80}$$

It is independent of time because of translation invariance and particle number conservation. Now we consider the lattice normal modes

$$\vec{\phi}_k(t) = R\vec{f}_k(t) \tag{4.81}$$

with components $\phi_k^\alpha(t)$ where R is the diagonalizer (4.65). In components

$$\phi_k^1(t) = r_{11} f_k^1(t) + r_{12} f_k^2(t), \quad \phi_k^2(t) = r_{21} f_k^1(t) + r_{22} f_k^2(t) \tag{4.82}$$

and similarly $\phi_0^\alpha := \phi_0^\alpha(0)$. In terms of the lattice normal modes the structure matrix has the form $S_k(t) := \langle \mathcal{S}_k(t) \rangle$ with $\mathcal{S}_k(t) := \vec{\phi}_k(t) \otimes \vec{\phi}_0^T$. This yields

$$S_k(t) = R\bar{S}_k(t)R^T \tag{4.83}$$

with matrix elements $S_{\alpha\beta}(k,t) = \langle \phi_k^\alpha(t)\phi_0^\beta \rangle$. The desired normalization

$$\sum_k S_k(t) = RKR^T = \mathbb{1} \tag{4.84}$$

leads to the requirement (4.68).

4.A.4. Computation of the mode-coupling matrices

The mode-coupling coefficients are given by

$$G^{\gamma}_{\alpha\beta} := \frac{1}{2}\sum_{\lambda} R_{\gamma\lambda}\left[(R^{-1})^T H^{\lambda} R^{-1}\right]_{\alpha\beta}. \tag{4.85}$$

where $G^{\gamma}_{\alpha\beta} = G^{\gamma}_{\beta\alpha}$. Using the previous results one finds for G^1 the matrix elements

$$\begin{aligned}
G^1_{11} &= \frac{1}{2z_-}\left[\cos^2\vartheta\left(h^1_1\cos\vartheta - uh^2_1\sin\vartheta\right) + u^{-2}\sin^2\vartheta\left(h^1_2\cos\vartheta - uh^2_2\sin\vartheta\right)\right. \\
&\quad \left. -2u^{-1}\cos\vartheta\sin\vartheta\left(\bar{h}^1\cos\vartheta - u\bar{h}^2\sin\vartheta\right)\right] && (4.86)\\
G^1_{22} &= \frac{z_-}{2z_+^2}\left[\sin^2\vartheta\left(h^1_1\cos\vartheta - uh^2_1\sin\vartheta\right) + u^{-2}\cos^2\vartheta\left(h^1_2\cos\vartheta - uh^2_2\sin\vartheta\right)\right. \\
&\quad \left. +2u^{-1}\cos\vartheta\sin\vartheta\left(\bar{h}^1\cos\vartheta - u\bar{h}^2\sin\vartheta\right)\right] && (4.87)\\
G^1_{12} &= \frac{1}{2z_+}\left[\cos\vartheta\sin\vartheta\left(h^1_1\cos\vartheta - uh^2_1\sin\vartheta - u^{-2}h^1_2\cos\vartheta + u^{-1}h^2_2\sin\vartheta\right)\right. \\
&\quad \left. u^{-1}(\cos^2\vartheta - \sin^2\vartheta)\left(\bar{h}^1\cos\vartheta - u\bar{h}^2\sin\vartheta\right)\right], && (4.88)
\end{aligned}$$

and for G^2 one has

$$\begin{aligned}
G^2_{22} &= \frac{1}{2z_+}\left[\sin^2\vartheta\left(h^1_1\sin\vartheta + uh^2_1\cos\vartheta\right) + u^{-2}\cos^2\vartheta(h^1_2\sin\vartheta + uh^2_2\cos\vartheta)\right. \\
&\quad \left. +2u^{-1}\cos\vartheta\sin\vartheta\left(\bar{h}^1\sin\vartheta + u\bar{h}^2\cos\vartheta\right)\right] && (4.89)\\
G^2_{11} &= \frac{z_+}{2z_-^2}\left[\cos^2\vartheta\left(h^1_1\sin\vartheta + uh^2_1\cos\vartheta\right) + u^{-2}\sin^2\vartheta\left(h^1_2\sin\vartheta + h^2_2 u\cos\vartheta\right)\right. \\
&\quad \left. -2u^{-1}\cos\vartheta\sin\vartheta\left(\bar{h}^1\sin\vartheta + u\bar{h}^2\cos\vartheta\right)\right] && (4.90)\\
G^2_{12} &= \frac{1}{2z_-}\left[\cos\vartheta\sin\vartheta\left(h^1_1\sin\vartheta + uh^2_1\cos\vartheta - u^{-2}h^1_2\sin\vartheta - u^{-1}h^2_2\cos\vartheta\right)\right. \\
&\quad \left. u^{-1}(\cos^2\vartheta - \sin^2\vartheta)\left(\bar{h}^1\sin\vartheta + u\bar{h}^2\cos\vartheta\right)\right]. && (4.91)
\end{aligned}$$

In terms of the model parameters $a, b, c, d, \kappa_{1,2}, \bar{\kappa}$ The quantities ϑ and u are given in (4.70) and the quantities $z_\pm$ are given in (4.74). The parameter δ appearing in (4.70) is given in (4.53).

In order to analyze the manifolds where diagonal elements of the mode coupling matrices vanish it is convenient to introduce

$$g^1_1 := h^1_1,\ g^1_2 := u^{-2}h^1_2,\ \bar{g}^1 := u^{-1}\bar{h}^1 \tag{4.92}$$

$$g^2_1 := uh^2_1,\ g^2_2 := u^{-1}h^2_2,\ \bar{g}^2 := \bar{h}^2. \tag{4.93}$$

and define the polynomials

$$\begin{aligned}
D^1_1(\omega) &:= g^1_1 - \left(g^2_1 + 2\bar{g}^1\right)\omega + \left(g^1_2 + 2\bar{g}^2\right)\omega^2 - g^2_2\omega^3 && (4.94)\\
D^1_2(\omega) &:= g^1_2 - \left(g^2_2 - 2\bar{g}^1\right)\omega + \left(g^1_1 - 2\bar{g}^2\right)\omega^2 - g^2_1\omega^3 && (4.95)\\
D^2_1(\omega) &:= g^2_1 + \left(g^1_1 - 2\bar{g}^2\right)\omega + \left(g^2_2 - 2\bar{g}^1\right)\omega^2 + g^1_2\omega^3 && (4.96)\\
D^2_2(\omega) &:= g^2_2 + \left(g^1_2 + 2\bar{g}^2\right)\omega + \left(g^2_1 + 2\bar{g}^1\right)\omega^2 + g^1_1\omega^3. && (4.97)
\end{aligned}$$

with $\omega := \tan\vartheta$. Only the Hessian and the parameters u and $\tan\vartheta$ given in (4.70) enter these functions. They do not depend on the compressibilities. Then one has

$$G_{11}^1 = \frac{\cos^3\vartheta}{2z_-} D_1^1(\omega), \quad G_{22}^1 = \frac{z_-\cos^3\vartheta}{2z_+^2} D_2^1(\omega) \tag{4.98}$$

$$G_{11}^2 = \frac{z_+\cos^3\vartheta}{2z_-^2} D_1^2(\omega), \quad G_{22}^2 = \frac{\cos^3\vartheta}{2z_+} D_2^2(\omega). \tag{4.99}$$

Notice the symmetry properties $D_1^1(\omega) = -\omega^3 D_2^2(-\omega^{-1})$ and $D_2^1(\omega) = -\omega^3 D_1^2(-\omega^{-1})$.

Bibliography

[1] S. Lepri, R. Livi, A. Politi, Thermal conduction in in classical low-dimensional lattices. Phys. Rep. **377**, 1–80 (2003).

[2] M. Kardar, G. Parisi, and Y.-C. Zhang, Dynamic scaling of growing interfaces. Phys. Rev. Lett. **56**, 889–892 (1986).

[3] M. Prähofer and H. Spohn, Exact scaling functions for one-dimensional stationary KPZ growth. J. Stat. Phys. **115**, 255–279 (2004).

[4] M. Prähofer and H. Spohn, in: *In and Out of Equilibrium*, edited by V. Sidoravicius, Vol. 51 of Progress in Probability (Birkhauser, Boston, 2002).

[5] L. Miettinen, M. Myllys, J. Merikoski, and J. Timonen, Experimental determination of KPZ height-fluctuation distributions. Eur. Phys. J. B **46**, 55–60 (2005).

[6] K.A. Takeuchi and M. Sano, Universal fluctuations of growing interfaces: evidence in turbulent liquid crystals. Phys. Rev. Lett. **104**, 230601 (2010).

[7] P.F. Arndt, T. Heinzel, and V. Rittenberg, Spontaneous breaking of translational invariance in one-dimensional stationary states on a ring. J. Phys. A: Math. Gen. **31** L45–L51 (1998)

[8] P.L. Ferrari, T. Sasamoto and H. Spohn, Coupled Kardar-Parisi-Zhang equations in one dimension. J. Stat. Phys. **153**, 377–399 (2013).

[9] D. Huse, B. Kaufmann and G.M. Schütz, work in progress.

[10] A. Rákos and G.M. Schütz, Exact shock measures and steady state selection in a driven diffusive system with two conserved densities. J. Stat. Phys. **117**, 55–76 (2004).

[11] D. Das, A. Basu, M. Barma, and S. Ramaswamy, Weak and strong dynamic scaling in a one-dimensional driven coupled-field model: Effects of kinematic waves. Phys. Rev. E **64**, 021402 (2001).

[12] A. Nagar, M. Barma, and S. N. Majumdar, Passive Sliders on Fluctuating Surfaces: Strong-Clustering States. Phys. Rev. Lett. **94**, 240601 (2005).

[13] H. van Beijeren, Exact results for anomalous transport in one-dimensional Hamiltonian systems. Phys. Rev. Lett. **108**, 108601 (2012).

[14] C.B. Mendl and H. Spohn, Dynamic correlators of FPU chains and nonlinear fluctuating hydrodynamics. Phys. Rev. Lett. **111**, 230601 (2013).

[15] S. G. Das, A. Dhar, K. Saito, Ch. B. Mendl, and H. Spohn, Numerical test of hydrodynamic fluctuation theory in the Fermi-Pasta-Ulam chain. Phys. Rev. E **90**, 012124 (2014)

[16] H. Spohn, Nonlinear Fluctuating hydrodynamics for anharmonic chains. J. Stat. Phys. **154**, 1191–1227 (2014).

[17] V. Popkov, J. Schmidt, and G.M. Schütz, Superdiffusive modes in two-species driven diffusive systems. Phys. Rev. Lett. **112**, 200602 (2014).

[18] C. Bernardin and P. Gonçalves, Anomalous fluctuations for a perturbed Hamiltonian system with exponential interactions. Commun. Math. Phys. **325**, 291–332 (2014).

[19] M. R. Evans, D. P. Foster, C. Godrèche, and D. Mukamel, Symmetric Exclusion Model with Two Species: Spontaneous Symmetry Breaking. Phys. Rev. Lett. **74**, 208–211 (1995).

[20] V. Popkov and I. Peschel, Symmetry breaking and phase coexistence in a driven diffusive two-channel system. Phys. Rev. E **64** 026126 (2001).

[21] R.D. Willmann, G.M. Schütz, and S. Großkinsky, Dynamical origin of spontaneous symmetry breaking in a field-driven nonequilibrium system. Europhys. Lett. **71** 542–547 (2005).

[22] V. Popkov, M. R. Evans, and D. Mukamel, Spontaneous symmetry breaking in a bridge model fed by junctions. J. Phys. A **41**, 432002 (2008).

[23] S. Gupta, D. Mukamel, and G.M. Schütz, Robustness of spontaneous symmetry breaking in a bridge model. J. Phys. A: Math. Theor. **42**, 485002 (2009)

[24] M.R. Evans, Y. Kafri, H.M. Koduvely, and D. Mukamel, Phase separation and coarsening in one-dimensional driven diffusive systems: Local dynamics leading to long-range Hamiltonians. Phys. Rev. E **58** 2764–2778 (1998).

[25] R. Lahiri, M. Barma, and S. Ramaswamy, Strong phase separation in a model of sedimenting lattices. Phys. Rev. E **61**, 1648–1658 (2000).

[26] J.T. Mettetal, B. Schmittmann, and R.K.P. Zia , Coarsening dynamics of a quasi-one-dimensional driven lattice gas. Europhys. Lett. **58**, 653–658 (2002).

[27] M. Clincy and M.R. Evans, Phase transition in the ABC model. Phys. Rev. E **67** 066115 (2003).

[28] G.M. Schütz, Critical phenomena and universal dynamics in one-dimensional driven diffusive systems with two species of particles. J. Phys. A: Math. Gen. **36**, R339–R379 (2003).

[29] V. Popkov and G.M. Schütz, Unusual shock wave in two-species driven systems with an umbilic point. Phys. Rev. E **67** 031139 (2012).

[30] V. Popkov, *Eur. Phys. J. Special Topics* **216**, 139–151 (2013)

[31] G.M. Schütz, R. Ramaswamy and M. Barma, Pairwise balance and invariant measures for generalized exclusion processes, J. Phys. A: Math. Gen. **29**, 837–845 (1996).

[32] V. Popkov and G.M. Schütz, Shocks and excitation dynamics in a driven diffusive two-channel system, J. Stat. Phys. **112**, 523–540 (2003).

[33] V. Popkov and M. Salerno, Hydrodynamic limit of multichain driven diffusive models. Phys. Rev. E **69**, 046103 (2004).

[34] H. Spohn, *Large Scale Dynamics of Interacting Particles.* (Springer, Berlin, 1991)

[35] C. Kipnis and C. Landim, *Scaling limits of interacting particle systems* (Springer, Berlin, 1999)

[36] R. Grisi and G.M. Schütz, Current symmetries for particle systems with several conservation laws. J. Stat. Phys. **145**, 1499–1512 (2011).

[37] B. Tóth and B. Valkó, J. Stat. Phys. **112**, 497–521 (2003).

[38] P. Devillard and H. Spohn, Universality class of interface growth with reflection symmetry. J. Stat. Phys. **66**, 1089–1099 (1992).

[39] H. Spohn and G. Stoltz, Nonlinear fluctuating hydrodynamics in one dimension: The case of two conserved fields. to appear in J. Stat. Phys., same volume (2015).

[40] D. Ertaş and M. Kardar, Dynamic roughening of directed lines. Phys. Rev. Lett. **69**, 929–932 (1992).

[41] E. Lieb, D. Robinson, The finite group velocity of quantum spin systems. Commun. Math. Phys. 28, 251—257, (1972)

5. The Fibonacci family of dynamical universality classes

Vladislav Popkov[1], Andreas Schadschneider[1], Johannes Schmidt[1] and Gunter M. Schütz[2]

[1] *Institut für Theoretische Physik, Universität zu Köln, Zülpicher Str. 77, 50937 Cologne, Germany*
[2] *Institute of Complex Systems II, Theoretical Soft Matter and Biophysics, Forschungszentrum Jülich, 52425 Jülich, Germany*

Published in: Proceedings of the National Academy of Sciences (PNAS)
Oct. 2015, vol. 112, no. 41, pp. 12645-12650
doi: 10.1073/pnas.1512261112

Abstract: Universality is a well-established central concept of equilibrium physics. However, in systems far away from equilibrium a deeper understanding of its underlying principles is still lacking. Up to now, a few classes have been identified. Besides the diffusive universality class with dynamical exponent $z = 2$ another prominent example is the superdiffusive Kardar-Parisi-Zhang (KPZ) class with $z = 3/2$. It appears e.g. in low-dimensional dynamical phenomena far from thermal equilibrium which exhibit some conservation law. Here we show that both classes are only part of an infinite discrete family of non-equilibrium universality classes. Remarkably their dynamical exponents z_α are given by ratios of neighbouring Fibonacci numbers, starting with either $z_1 = 3/2$ (if a KPZ mode exist) or $z_1 = 2$ (if a diffusive mode is present). If neither a diffusive nor a KPZ mode are present, all dynamical modes have the Golden Mean $z = (1+\sqrt{5})/2$ as dynamical exponent. The universal scaling functions of these Fibonacci modes are asymmetric Lévy distributions which are completely fixed by the macroscopic current-density relation and compressibility matrix of the system and hence accessible to experimental measurement.

Keywords: nonequilibrium physics | universality | dynamical exponent | driven diffusion

Significance

Universality is a well-established central concept of equilibrium physics. It asserts that, especially near phase transitions, the properties of a physical system do not depend on its details such as the precise form of interactions. Far from equilibrium such universality has also been observed, but in contrast to equilibrium a deeper understanding of its underlying principles is still lacking. We show that the two best-known examples of non-equilibrium universality classes, the diffusive and KPZ-classes, are only part of an infinite discrete family. The members of this family can be identified by their dynamical exponent which surprisingly can be expressed by a Kepler ratio of Fibonacci numbers. This strongly indicates the existence of a simpler underlying mechanism that determines the different classes.

The Golden Mean $\varphi = 1/2 + \sqrt{5}/2 \approx 1.61803..$, also called Divine Proportion, has been an inspiring number for many centuries. It is widespread in nature, i.e. arrangements of petals of the flowers and seeds in the sunflower follow the golden rule [1]. Being considered an ideal proportion, the Golden Mean appears in famous architectural ensembles such as Parthenon in Greece, Giza Great Pyramids in Egypt, or Notre Dame de Paris in France. Ideal proportions of the human body follow the Golden Rule.

Mathematically, the beauty of the Golden Mean number is expressed in its continued fraction representation: All the coefficients in the representation are equal to unity,

$$\varphi = 1 + \cfrac{1}{1 + \cfrac{1}{1 + \cfrac{1}{1 + \ddots}}} \tag{5.1}$$

Systematic truncation of the above continued fraction gives the so-called Kepler ratios, $1/1, 2/1, 3/2, 5/3, 8/5, ...$, which approximate the Golden Mean. Subsets of denominators (or numerators) of the Kepler ratios form the celebrated Fibonacci numbers, $F_i = 1, 1, 2, 3, 5, 8, ..$, such that Kepler ratios are ratios of two neighbouring Fibonacci numbers. As well as the Golden Mean, Fibonacci ratios and Fibonacci numbers are widespread in nature [1].

The occurrence of the Golden Mean is not only interesting for aesthetic reasons, but often indicates the existence of some fundamental underlying structure or symmetry. Here we demonstrate that the Divine Proportion, as well as all the truncations (Kepler ratios) of the continued fraction (5.1), appear as universal numbers, viz., the dynamical exponents, in low-dimensional dynamical phenomena far from thermal equilibrium. The two well-known paradigmatic universality classes, Gaussian diffusion with dynamical exponent $z = 2$ [2, 3] and the Kardar-Parisi-Zhang (KPZ) universality class with $z = 3/2$ [4] enter the Kepler ratios hierarchy as the first two members of the family.

The universal dynamical exponents in the present context characterize the self-similar space-time fluctuations of locally conserved quantities, characterizing e.g. mass, momentum or thermal transport in one-dimensional systems far from thermal equilibrium [5]. The theory of nonlinear fluctuating hydrodynamics (NLFH), has recently emerged as a powerful and versatile tool to study space-time fluctuations, and specifically the dynamical structure function which describes the behaviour of the slow relaxation modes, and from which the dynamical exponents can be extracted [6].

The KPZ universality class [1] has been shown to explain the dynamical exponent observed in interface growth processes as diverse as the propagation of flame fronts [10, 11], the growth of bacterial colonies [12], or the time evolution of droplet shapes such as coffee stains [13] where the Gaussian theory fails. The dynamical structure function originating from the one-dimensional KPZ equation has a non-trivial scaling function obtained exactly by Prähofer and Spohn from the totally asymmetric simple exclusion process (TASEP) and the polynuclear growth model [14, 15] and was beautifully observed in experiments on turbulent liquid crystals [16, 17]. Also the theoretical treatment, both numerical and analytical, of generic model systems with Hamiltonian dynamics [18], anharmonic chains [19, 20] and lattice models for driven diffusive systems [21, 22], have demonstrated an extraordinary robust universality of fluctuations of the conserved slow modes in one-dimensional systems.

Despite this apparent ubiquity, frequently dynamical exponents different from $z = 2$ or $z = 3/2$ were observed. Usually it is not clear whether this corresponds to genuinely different dynamical critical behaviour or is just a consequence of imperfections in the experimental setting. Moreover,

[1] For a nice introduction into the KPZ class and its relevance we refer to [7]. Recent reviews [8, 9] provide a more detailed account of theoretical and experimental work on the KPZ class.

recently a new universality class with dynamical exponent $z = 5/3$ for the heat mode in Hamiltonian dynamics [18] was discovered, followed by the discovery of some more universality classes in anharmonic chains [19, 20] and lattice models for driven diffusive systems [21, 22]. What is lacking, even in the conceptually simplest case of the effectively one-dimensional systems that we are considering, is the understanding of the plethora of dynamical non-equilibrium universality classes within a larger framework. Such a framework exists e.g. for two-dimensional critical phenomena in equilibrium systems where the spatial symmetry of conformal invariance together with internal symmetries give rise to discrete families of universality classes in which all critical exponents are simple rational numbers.

It is the aim of this article to demonstrate that also far from thermal equilibrium discrete families of universality classes with fractional critical exponents appear. This turns out to be a hidden feature of the NLFH equations which we extract using mode-coupling theory. It is remarkable that one finds dynamical exponents z_α which are ratios of neighbouring Fibonacci numbers $\{1, 1, 2, 3, 5, 8, \dots\}$ defined recursively as $F_n = F_{n-1} + F_{n-2}$. The first two members of this family are diffusion ($z = 2 = F_3/F_2$) and KPZ ($z = 3/2 = F_4/F_3$). The corresponding universal scaling functions are computed and shown to be (in general asymmetric) z_α-stable Lévy distributions with parameters that can be computed from the macroscopic current-density relation and compressibility matrix of the corresponding physical system and which thus can be obtained from experiments without detailed knowledge of the microscopic properties of the system. The theoretical predictions, obtained by mode coupling theory, are confirmed by Monte-Carlo simulations of a three-lane asymmetric simple exclusion process which is a model of driven diffusive transport of three conserved particle species.

5.1. Nonlinear fluctuating hydrodynamics

We consider a rather general interacting non-equilibrium system of length L described macroscopically by n conserved order parameters $\rho_\lambda(x,t)$ with stationary values ρ_λ and associated macroscopic stationary currents $j_\lambda(\rho_1, \dots, \rho_n)$ and compressibility matrix K with matrix elements $K_{\lambda\mu} = \frac{1}{L}\langle (N_\lambda - \rho_\lambda L)(N_\mu - \rho_\mu L)\rangle$ where $N_\lambda = \int_0^L \mathrm{d}x \rho_\lambda(x,t)$ are the time-independent conserved quantities.

The starting point for investigating density fluctuations $u_\lambda(x,t) := \rho_\lambda(x,t) - \rho_\lambda$ in the non-equilibrium steady state are the NLFH equations [5]

$$\partial_t \vec{u} = -\partial_x \left(J\vec{u} + \frac{1}{2}\langle u|\vec{H}|u\rangle - \partial_x D\vec{u} + B\vec{\xi} \right) \tag{5.2}$$

where J is the current Jacobian with matrix elements $J_{\lambda\mu} = \partial j_\lambda/\partial\rho_\mu$, $\vec{H}$ is a column vector whose entries $\left(\vec{H}\right)_\lambda = H^\lambda$ are the Hessians with matrix elements $H^\lambda_{\mu\nu} = \partial^2 j_\lambda/(\partial\rho_\mu\partial\rho_\nu)$ and the bra-ket notation represents the inner product in component space $\langle\, u\,|(\vec{H})_\lambda|\, u\,\rangle = \vec{u}^T H^\lambda \vec{u} = \sum_{\mu\nu} u_\mu u_\gamma H^\lambda_{\mu\nu}$ with $\langle\, u\,| = \vec{u}^T$, $|\, u\,\rangle = \vec{u}$. The diffusion matrix D is a phenomenological quantity. The noise term $B\vec{\xi}$ does not appear explicitly below, but plays an indirect role in the mode-coupling analysis. The product JK of the Jacobian with the compressibility matrix $K_{\lambda\mu}$ is symmetric [23] which guarantees a hyperbolic system of conservation laws [24]. We ignore possible logarithmic corrections arising from cubic contributions [25].

This system of coupled noisy Burgers equations is conveniently treated in terms of normal modes $\vec{\phi} = R\vec{u}$ where $RJR^{-1} = \mathrm{diag}(v_\alpha)$ and the transformation matrix R is normalized such that $RKR^T = 1$. The eigenvalues v_α of J are the characteristic velocities of the system. From (5.2) one thus arrives at
$\partial_t\phi_\alpha = -\partial_x\left(v_\alpha\phi_\alpha + \langle\phi|G^\alpha|\phi\rangle - \partial_x(\tilde{D}\vec{\phi})_\alpha + (\tilde{B}\vec{\xi})_\alpha\right)$ with $\tilde{D} = RDR^{-1}$, $\tilde{B} = RB$ and the mode

coupling matrices

$$G^\alpha = \frac{1}{2}\sum_\beta R_{\alpha\beta}(R^{-1})^T H^\beta R^{-1} \tag{5.3}$$

whose matrix elements we denote by $G^\alpha_{\beta\gamma}$.

5.2. Computation of the dynamical structure function

For $\alpha > 1$, the dynamical structure function describes the stationary fluctuations of the conserved slow modes and is thus a key ingredient for understanding the interplay of noise and non-linearity and their role for transport far from equilibrium. We focus on the case of strict hyperbolicity where all v_α are pairwise different and study the large scale behaviour of the dynamical structure function $S^{\alpha\beta}(x,t) = \langle\, \phi_\alpha(x,t)\phi_\beta(0,0)\,\rangle$. Since all modes have different velocities only the diagonal elements $S_\alpha(x,t) := S^{\alpha\alpha}(x,t)$ are non-zero for large times. Mode coupling theory yields [5]

$$\begin{aligned}\partial_t S_\alpha(x,t) &= (-v_\alpha\partial_x + D_\alpha\partial_x^2)S_\alpha(x,t) \\ &+ \int_0^t \mathrm{d}s \int_{\mathbb{R}} \mathrm{d}y S_\alpha(x-y,t-s)\partial_y^2 M_{\alpha\alpha}(y,s)\end{aligned} \tag{5.4}$$

with the diagonal element $D_\alpha := \tilde{D}_{\alpha\alpha}$ of the phenomenological diffusion matrix for the eigenmodes and the memory kernel $M_{\alpha\alpha}(y,s) = 2\sum_{\beta,\gamma}(G^\alpha_{\beta\gamma})^2 S_\beta(y,s)S_\gamma(y,s)$. The task therefore is to extract for arbitrary n the large-time and large-distance behaviour from this non-linear integro-differential equation.

Remarkably, these equations can be solved exactly in the long-wavelength limit and for $t \to \infty$ by Fourier and Laplace transformation (see "Materials and Methods" and Supplementary Material). Using a suitable scaling ansatz for the transformed structure function then allows to analyze the small-p behaviour from which the dynamical exponents can be determined. We find that different conditions arise depending on which diagonal elements of the mode-coupling matrices vanish.

5.3. The Fibonacci family of dynamical universality classes

5.3.1. Fibonacci case

First, we consider the case where the self-coupling $G^\alpha_{\alpha\alpha}$ is nonzero for one mode only, e.g. $G^1_{11} \neq 0$. For all other modes $\alpha \neq 1$ we assume a single nonzero coupling to the previous mode, so $G^\alpha_{\alpha-1,\alpha-1} \neq 0$, and $G^\alpha_{\beta,\beta} = 0$ for $\beta \neq \alpha - 1$. Then, as follows from our analysis (see "Materials and Methods"), we find the following recursion for the dynamical exponents:

$$z_\alpha = 1 + \frac{1}{z_{\alpha-1}} \tag{5.5}$$

with $z_1 = 3/2$.

The dynamical structure function in momentum space is proportional to the z_α-stable Lévy distribution with maximal asymmetry $\sigma^\alpha = \pm 1$, see [26] and eq. (5.13) below. The sign of the asymmetry depends whether the mode $(\alpha - 1)$ has bigger or smaller velocity than the mode α, $\sigma^\alpha = -\mathrm{sgn}(v_\alpha - v_{\alpha-1})$. The dynamical exponents (5.5) form a sequence of rational numbers

$$z_\alpha = \frac{F_{\alpha+3}}{F_{\alpha+2}} \tag{5.6}$$

which are consecutive ratios of neighbouring Fibonacci numbers F_α, defined by $F_\alpha = F_{\alpha-1}+F_{\alpha-2}$ with initial values $F_0 = 0, \quad F_1 = 1$, which converge exponentially to the Golden Mean $\varphi := \frac{1}{2}(1+\sqrt{5}) \approx 1.618$, as first observed by Kepler in 1611 in a treatise on snow flakes. In a model with n conservation laws, one has the Fibonacci modes with dynamical exponents $\{3/2,\ 5/3,\ 8/5, ...,\ z_n\}$.

Finally, we remark that if mode 1 is diffusive rather than KPZ, then we find the same sequence (5.6) of exponents except that it starts with $z_1 = F_2 = 2$.

In Fig. 5.1 we show some representative examples of the scaling functions which are quite different in shape. Furthermore the relation between the exponents z_α , determined by eq. (5.11) in "Materials and Methods", and the mode coupling matrices G^α is illustrated for the case $n = 2$.

5.3.2. Golden Mean case

As second representative example we consider the case where all self-coupling coefficients vanish, $G^\alpha_{\alpha\alpha} \equiv 0$ for all α, while each mode has at least one nonzero coupling to other mode, $G^\alpha_{\beta\beta} \neq 0$ for some $\beta \neq \alpha$. Then, (5.5) reduces to $z_\alpha = 1 + 1/z_\beta$ for all modes $\alpha,\ \beta$. The unique solution of this equation is the Golden Mean $z_\alpha = \varphi = (1+\sqrt{5})/2$ for all α. The scaling functions (see Suppl. Material) are proportional to φ-stable Lévy distributions with parameters fixed by the collective velocities and the mode-coupling coefficients. The asymmetry of the fastest right-moving (left-moving) mode is predicted to be $\beta = -1$ ($\beta = 1$).

5.4. Simulation results

In order to check the theoretical predictions in the two cases we simulate mass transport with three conservation laws, i.e., three distinct species of particles. To maintain a far-from-equilibrium situation a driving force is applied that leads to a constant drift superimposed on undirected diffusive motion. This is a natural setting for transport of charged particles in nanotubes, where a direct measurement of the stationary particle currents is experimentally possible [27]. However, due to the universal applicability of NLFH the actual details of the interaction of the particles with their environment and the driving field are irrelevant for the theoretical description of the large-scale dynamics. Hence for good statistics we simulate a lattice model for transport which represents a minimal realization of the essential ingredients, namely a non-linear current-density relation for all three conserved masses.

Our model is the three-species version of the multi-lane totally asymmetric simple exclusion process [28]. Particles hop randomly in field direction on three lanes to their neighbouring sites on a periodic lattice of $3 \times L$ sites with rates that depend on the nearest-neighbour sites. Lane changes are not allowed so that the total number of particles on each lane is conserved. Due to excluded-volume interaction each lattice site can be occupied by at most one particle. Thus the occupation numbers $n_k^{(\lambda)}$ of site k on lane λ take only values 0 or 1. The hopping rate $r_k^{(\lambda)}$ from site k on lane λ to site $k+1$ on the same lane is given by

$$r_k^{(\lambda)} = b_\lambda + \frac{1}{2} \sum_{\{\mu:\, \mu\neq\lambda\}} \gamma_{\lambda\mu} \left(n_k^{(\mu)} + n_{k+1}^{(\mu)} \right) \tag{5.7}$$

with a species dependent drift parameter b_λ and symmetric interaction constants $\gamma_{\lambda\mu} = \gamma_{\mu\lambda}$. Hopping attempts onto occupied sites are rejected. The conserved quantities are the three total numbers of particles N_λ on each lane with corresponding densities $\rho_\lambda = N_\lambda/L$.

The stationary distribution of this model factorizes [28] and thus allows for the exact computation of the macroscopic current-density relations $j_\lambda(\rho_1, \rho_2, \rho_3)$ and the compressibility matrix $K(\rho_1, \rho_2, \rho_3)$. Since there is no particle exchange between lanes the compressibility matrix is

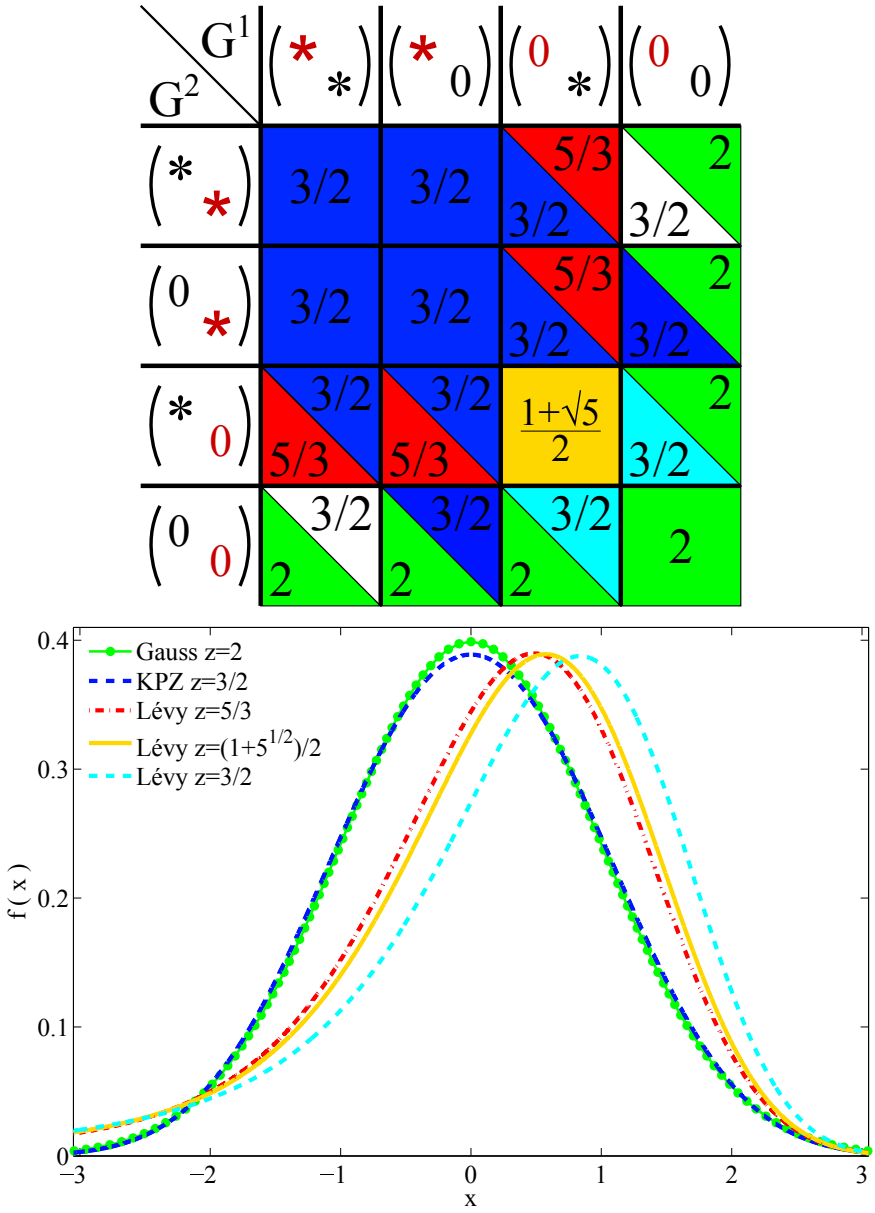

Figure 5.1.: The scaling functions (bottom) and dynamical exponents are related to the structure of the mode coupling matrices G^α (top). The table shows the dynamical exponents z_α in the case $n = 2$, see eq. (5.11). The symbols $*$ and $\star$ denote non-zero elements. Red symbols correspond to self-coupling, black symbols to couplings to other modes. Matrix elements not indicated can take any value. The colors in the table correspond to the colors of the graphs of the scaling functions.

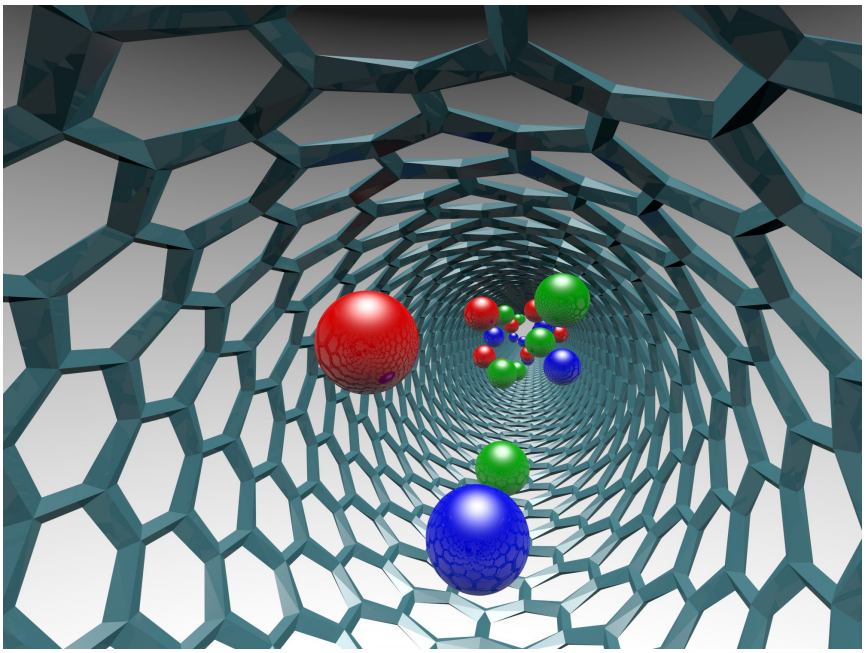

Figure 5.2.: Schematic drawing of three particle species drifting inside a nanotube. Due to the interaction between the particles and with the walls one expects a non-linear current density relation.

diagonal with elements denoted by κ_λ. One has

$$j_\lambda = \rho_\lambda(1-\rho_\lambda)\left(b_\lambda + \sum_{\{\mu:\,\mu\neq\lambda\}} \gamma_{\lambda\mu}\rho_\mu\right) \tag{5.8}$$

$$\kappa_\lambda = \rho_\lambda(1-\rho_\lambda). \tag{5.9}$$

The diagonalization matrix R and the mode-coupling matrices G^α are fully determined by these quantities.

According to mode-coupling theory three different Fibonacci-modes with $z_1 = 3/2, z_2 = 5/3, z_3 = 8/5$ occur e.g. when $G^1_{11} \neq 0$, $G^2_{11} \neq 0$, $G^3_{22} \neq 0$, and $G^2_{22} = G^2_{33} = G^3_{33} = 0$. For our simulation we compute numerically densities, bare hopping rates and interaction parameters to satisfy these properties as described in "Materials and Methods". For this choice the velocities of the normal modes are $v_1 = 0.592315$, $v_2 = 0.0281578$, $v_3 = 1.58226$ which ensures a good spatial separation after quite small times. The propagation of the three normal modes (Fig. 5.3) with the predicted velocities is observed with an error of less than 10^{-3}. Moreover, the numerically obtained dynamical structure function for mode 3 shows a startling agreement with the theoretically predicted Lévy scaling function with $z = 8/5$ and maximal asymmetry, see Fig. 5.4. It takes longer for the other two modes (KPZ mode and Lévy stable 5/3 mode) to reach their asymptotic form, which we argue is due to the much smaller respective couplings, $(G^1_{11}/G^3_{22})^2 \ll 1$, $(G^2_{11}/G^3_{22})^2 \ll 1$.

In order to observe three Golden Mean modes it is sufficient to require that each mode has zero self-coupling and at least one nonzero coupling to other modes. This can be achieved with the set of parameters given in "Materials and Methods" which lead to the velocities $v_1 = 1.83149$, $v_2 = 0.762688$, $v_3 = 0.326778$ of the normal modes. The propagation of the three normal modes with the predicted velocities is observed, approaching for large times a very small relative error of

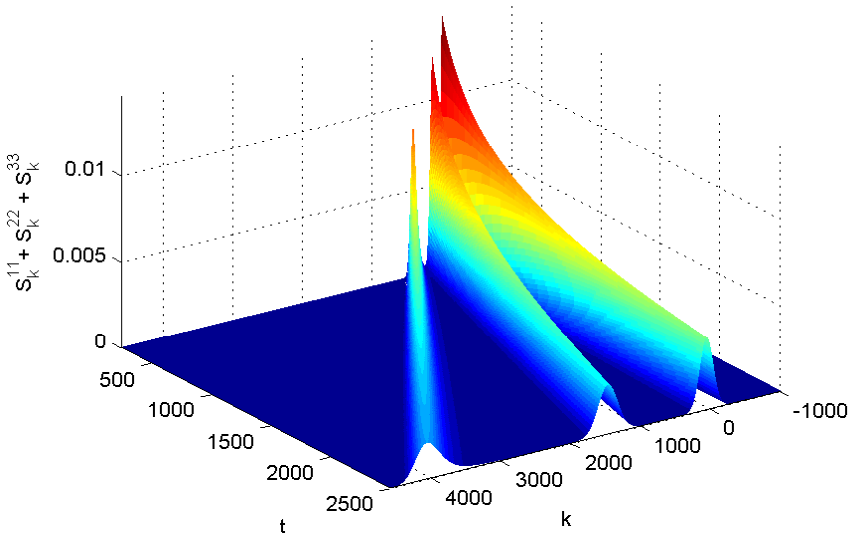

Figure 5.3.: Space-time propagation of three normal modes in the three-lane model. The modes (from left to right) are the Fibonacci mode with $z = 8/5$ (mode 3), the KPZ mode with $z = 3/2$ (mode 1), and the Fibonacci mode with $z = 5/3$ (mode 2). The physical and simulation parameters are given in the Appendices.

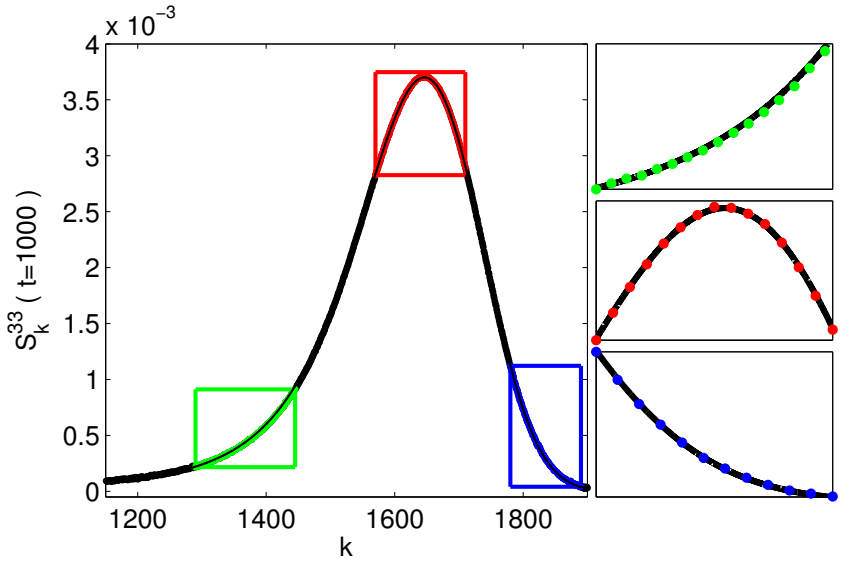

Figure 5.4.: Left Panel: Vertical least squares fit of the numerically obtained dynamical structure function for the Fibonacci 8/5-mode (points), at time $t = 1000$ with a 8/5-stable Lévy distribution, maximal asymmetry -1 and theoretical center of mass (line), predicted by the mode coupling theory. The only fit parameter is the scale parameter of the Lévy stable distribution. The simulation results agree very well with the asymptotic theoretical result already for moderate times. Right Panel: Insets show closeups of the peak region and tail regions, according to a colour code. Every 10-th datapoint is plotted to improve the visibility of the data. The statistical error $\epsilon_{99\%}$ with 99% confidence bound is for every data point smaller than $1.6299 \cdot 10^{-5}$.

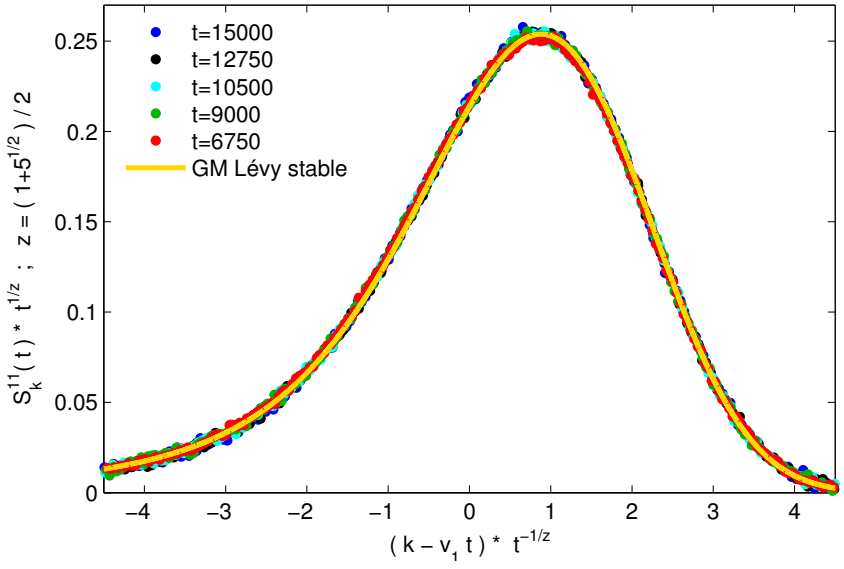

Figure 5.5.: Scaling plot of the measured structure function of mode 1 with dynamical exponent $z \equiv \varphi = \left(1+\sqrt{5}\right)/2$ for the Golden Mean case, fitted to a φ-stable Lévy distribution with maximal asymmetry -1 (see Eq. (5.13)). The scale parameter E_1 for the Lévy-stable distribution and the center of mass velocity v_1 are obtained by a vertical least square fit. Fitted parameters are $v_{1,\mathrm{fit}} = 1.83107 \pm 0.00009$ and $E_{1,\mathrm{fit}} = 1.1 \pm 0.01$. The fitted velocity $v_{1,\mathrm{fit}}$ differs by 0.02% from the theoretical velocity.

about 10^{-4}. The structure function for the fastest mode 1 converges to its asymptotic shape faster than for the other modes, due to the large coupling coefficient G_{33}^1. In Fig. 5.5 we show a scaling plot of the measured structure function for mode 1 with dynamical exponent $z \equiv \varphi = \left(1+\sqrt{5}\right)/2$ together with a fitted to a φ-stable Lévy function (5.13) with maximal asymmetry $\beta = -1$ as predicted by the theory. The data collapse shows a striking agreement between the measured and theoretical scaling function. Alternatively, the dynamical exponent z_α can be derived from the maximum of the structure function, which scales as $\max(S_1(x,t)) = \mathrm{const} \cdot t^{-1/z}$. We obtain $z \approx 1.63$ which differs from the predicted value $z \equiv \varphi = (1+\sqrt{5})/2$ by less than 0.8%.

5.5. Discussion

Our work demonstrates that non-equilibrium phenomena are much richer than just the diffusive and KPZ universality suggest. We have established that in non-equilibrium phenomena governed by non-linear fluctuating hydrodynamics with n conservation laws mode coupling theory predicts a family of dynamical universality classes with dynamical exponents given by the sequence of consecutive Kepler ratios (5.6) of Fibonacci numbers. With slightly modified initial conditions on G_1^{11} this result is easily generalized for the case when the first mode $\alpha = 1$ is diffusive. Then the sequence of dynamical exponents becomes shifted by one unit with respect to (5.6). On the other hand, if all self-couplings vanish, one has as unique solution for all modes α the fixed point value $z_\alpha = z_\infty = \varphi$ which is the Golden Mean.

For general mode coupling matrices all critical exponents can be computed (from (5.11) in "Materials and Methods"). The scaling functions of the non-diffusive and non-KPZ modes are asymmetric Lévy distributions whose parameters are completely determined by the macroscopic current-density relation and compressibility matrix of the system.

For 1+1 dimensional systems out of equilibrium this is the first time an infinite family of discrete universality classes is found. Recalling that 1+1 dimensional non-equilibrium systems with short-range interactions can be mapped onto two-dimensional equilibrium systems (with the time evolution operator playing the role of the transfer matrix) one is reminded of the discrete families of conformally invariant critical equilibrium systems in two space dimensions [29, 30]. We do not know whether there is any mathematical link, but the analogy is suggestive in so far as conformal invariance is a local symmetry of spatially isotropic systems with $z = 1$ (which happens to be the lowest order Kepler ratio) while $z > 1$ corresponds to strongly anisotropic systems for which also local symmetry groups are known to exist [31].

Since an infinite number of lanes of coupled one-dimensional systems corresponds to a two-dimensional system, it is intriguing to observe that the Golden Mean is close to the numerical value $z = 1.612 - 1.618$ of the dynamical exponent of the $2+1$-dimensional KPZ-equation [32, 33]. The scaling function of the $2 + 1$-dimensional KPZ-equation, however, is not Lévy [34].

In order to observe and distinguish between the different new classes highly precise experimental data will be required. E.g. in the Fibonacci case the dynamical exponents converge quickly to the Golden Mean. A feature which might be easier to observe experimentally is the scaling function itself, which for higher Fibonacci ratios $5/3, 8/5, ...$ usually has a strong asymmetry (see Figs. 5.1, 5.4 and 5.5) while KPZ and Gauss scaling functions are symmetric. Growth processes which can be mapped on exclusion processes with several conservation laws, might be potentially suitable candidates for an experimental verification, see e.g. [16, 17] for an example of a system with one conservation law.

5.6. Materials and Methods

5.6.1. Computation of the dynamical structure function

The mode coupling equations (5.4) can be solved in the scaling limit by applying a Fourier transform (FT) $f(x) \to \tilde{f}(p)$ and a Laplace transform (LT) $f(t) \to \tilde{f}(\omega)$. For more details we refer to [22] where the case $n = 2$ of two conservation laws has been treated. After making the scaling ansatz

$$\tilde{S}_\alpha(p, \tilde{\omega}_\alpha) = p^{-z_\alpha} g_\alpha(\zeta_\alpha) \tag{5.10}$$

for the transformed dynamical structure function where $\hat{S}_\alpha(p, 0) = 1/\sqrt{2\pi}$ and $\zeta_\alpha = \tilde{\omega}_\alpha |p|^{-z_\alpha}$ we are in a position to analyze the small-p behaviour. One has to search for dynamical exponents for which the limit $p \to 0$ is non-trivial, which requires a self-consistent treatment of all modes. We find that different conditions arise depending on which diagonal elements of the mode-coupling matrices vanish. In order to characterize the possible scenarios we define the set $\mathbb{I}_\alpha := \{\beta : G^\alpha_{\beta\beta} \neq 0\}$ of non-zero diagonal mode coupling coefficients. Through power counting one obtains

$$z_\alpha = \begin{cases} 2 & \text{if} \quad \mathbb{I}_\alpha = \emptyset \\ 3/2 & \text{if} \quad \alpha \in \mathbb{I}_\alpha \\ \min_{\beta \in \mathbb{I}_\alpha} \left[\left(1 + \frac{1}{z_\beta} \right) \right] & \text{else} \end{cases} \tag{5.11}$$

and the domain

$$1 < z_\alpha \leq 2 \quad \forall \alpha. \tag{5.12}$$

for the possible dynamical exponents.

In the Fibonacci case, the dynamical structure function of mode α in momentum space has the scaling form

$$\hat{S}_\alpha(p, t) = \frac{1}{\sqrt{2\pi}} \mathrm{e}^{-iv_\alpha pt - E_\alpha |p|^{z_\alpha} t \left(1 - i\sigma_p^{\alpha\beta} \tan\left(\frac{\pi z_\alpha}{2} \right) \right)} \tag{5.13}$$

with inverse time scales E_α. The dynamical exponents then satisfy the recursion (5.5). Up to the normalization $1/\sqrt{2\pi}$ the scaling form (5.13) is a α-stable Lévy distribution [26].

5.6.2. Simulation algorithm

For the Monte-Carlo simulation of the model we choose a large system size $L = 5 \cdot 10^5$ which avoids finite-size effects. At time $t = 0$, N_λ particles are placed on each lane according to the desired initial state. One Monte-Carlo time unit consists of $3 \cdot L \cdot r^*$ random sequential update steps where $r^* = \max\left\{ {r_k}^{(\lambda)} \right\}$: In each update step a bond $(k^{(\lambda)}, k^{(\lambda)} + 1)$ is chosen randomly with uniform distribution. If $n_k^{(\lambda)} \left(1 - n_{k+1}^{(\lambda)} \right) = 1$ then the particle at site k is moved to $k + 1$ with probability $r_k^{(\lambda)}/r^*$ where r^* is the maximal value that the $r_k^{(\lambda)}$ can take among all possible particle configurations on the neighbouring lanes. If $n_k^{(\lambda)}(1 - n_{k+1}^{(\lambda)}) = 0$ the particle configuration remains unchanged.

5.6.3. Simulation of the dynamical structure function

In order to determine the dynamical structure function we initialize the system by placing N_λ particles uniformly on each lane λ. This yields a random initial distribution drawn from the stationary distribution of the process. No relaxation is required.

Then we use translation invariance and compute the space- and time average

$$\sigma_{L,k}^{\lambda\mu}(M,\tau,t) = \frac{1}{M}\sum_{j=1}^{M}\frac{1}{L}\sum_{l=1}^{L} n_{l+k}^{(\lambda)}(j\tau+t)n_l^{(\mu)}(j\tau) - \rho_\lambda\rho_\mu. \tag{5.14}$$

To avoid noisy data of $\sigma_{L,k}^{\lambda\mu}$ in (5.14) we take the system size L and the time average parameter M sufficiently large. In order to obtain $S_k^{\lambda\mu}(t)$ we average over P independently generated and propagated initial configurations of $\sigma_{L,k}^{\lambda\mu}$. The error estimates for $S_k^{\lambda\mu}(t)$ are calculated from the P independent measurements. From $S_k^{\lambda\mu}(t)$ we compute the structure function of the normal modes by transformation with the diagonalizing matrix R determined by (5.8) and (5.9).

In order to obtain model parameters for three different Fibonacci-modes with $z_1 = 3/2, z_2 = 5/3, z_3 = 8/5$ we solve the equations given in the text after Eq. (5.9) numerically with a C-program performing direct minimization of the absolute values of the targeted G-elements until the given tolerance value (10^{-6}) is reached. The data shown here for the three mode case have been obtained from simulations with densities $\rho_1 = 0.2$, $\rho_2 = 0.25$, $\rho_1 = 0.3$, bare hopping rates $b_1 = 0.613185$, $b_2 = 0.425714$, $b_3 = 0.799831$ and interaction parameters $\gamma_{12} = 1.36145$, $\gamma_{23} = 3.69786$, $\gamma_{13} = 0.143082$ for which the needed relations are satisfied. This choice of parameters yields $G_{11}^1 = 0.322507$, $G_{11}^2 = -0.15$, $G_{22}^3 = 1.04547$, while the the absolute values of G_{22}^2, G_{33}^2, G_{33}^3 are smaller than 10^{-6}. Besides these physical parameters, the simulation parameters for the Fibonacci modes (Fig. 5.3, 5.4) are $L = 500.000$, $\tau = 250$, $M = 1400$, $P = 98$.

For the Golden Mean case (Fig. 5.5) the set of parameters $\rho_1 = 0.2$, $\rho_2 = \rho_3 = 0.25$, $\gamma_{12} = 0.0082334758646$, $\gamma_{23} = 1.68447706968$, $\gamma_{13} = 3.72140740146$, and $b_1 = 0.905073261248$, $b_2 = 0.86$, and $b_3 = 1.18875738638$. This leads to $G_{22}^1 = 0.405702$, $G_{33}^1 = 0.929315$, $G_{11}^2 = -0.104141$, $G_{33}^2 = -0.208477$, $G_{11}^3 = -0.182467$, $G_{22}^3 = 0.271246$, while the absolute value of $G_{11}^1, G_{22}^2, G_{33}^3$ is smaller than 10^{-6}. The simulation parameters for the Golden Mean case are $L = 5.000.000$, $\tau = 750$, $M = 30$ and $P = 303$.

5.7. Supporting Information

Remarkably, the mode coupling equations eq. (5.4) can be solved exactly in the scaling limit by Fourier and Laplace transformation. To this end we define the Fourier transform (FT) as

$$\hat{f}(p) := \frac{1}{\sqrt{2\pi}}\int_{-\infty}^{\infty} \mathrm{d}x\, \mathrm{e}^{-ipx} f(x), \tag{5.15}$$

and the Laplace transform (LT) as

$$\tilde{f}(\omega) := \int_0^{\infty} \mathrm{d}t\, \mathrm{e}^{-\omega t} f(t). \tag{5.16}$$

With $\widehat{D}_\alpha(p) = iv_\alpha p + D_\alpha p^2$ we obtain from eq. (4) of the paper in momentum-frequency space

$$\tilde{S}_\alpha(p,\omega) = \frac{\hat{S}_\alpha(p,0)}{\omega + \widehat{D}_\alpha(p) + \tilde{C}_{\alpha\alpha}(p,\omega)} \tag{5.17}$$

with memory kernel

$$\tilde{C}_{\alpha\alpha}(p,\omega) = 2\sum_{\beta,\gamma}(G_{\beta\gamma}^\alpha)^2 p^2 \int_0^{\infty} \mathrm{d}s\, \mathrm{e}^{-\omega s}\int_{\mathbb{R}} \mathrm{d}q \hat{S}_\beta(q,s)\hat{S}_\gamma(p-q,s). \tag{5.18}$$

and $\hat{S}_\alpha(p,0) = 1/\sqrt{2\pi}$.

Next we introduce $\tilde{\omega}_\alpha := \omega + iv_\alpha p$ and make the scaling ansatz

$$\tilde{S}_\alpha(p, \tilde{\omega}_\alpha) = p^{-z_\alpha} g_\alpha(\zeta_\alpha) \tag{5.19}$$

with $\zeta_\alpha = \tilde{\omega}_\alpha |p|^{-z_\alpha}$. Having in mind systems with short-range interactions we anticipate that all modes spread subballistically, i.e., $z_\alpha > 1$ for all α. Using strict hyperbolicity one obtains after some substitutions of variables

$$\begin{aligned} g_\alpha(\zeta_\alpha) &= \lim_{p\to 0} \Bigg[\zeta_\alpha + D_\alpha |p|^{2-z_\alpha} + Q_{\alpha\alpha} \zeta_\alpha^{2-z_\alpha-\frac{1}{z_\alpha}} |p|^{3-2z_\alpha} \\ &+ \sum_{\beta\neq\alpha} Q_{\alpha\beta} \left(-iv_p^{\alpha\beta}\right)^{\frac{1}{z_\beta}-1} |p|^{1+\frac{1}{z_\beta}-z_\alpha} \Bigg]^{-1} . \end{aligned} \tag{5.20}$$

with $v_p^{\alpha\beta} := |v_\alpha - v_\beta| \mathrm{sgn}[p(v_\alpha - v_\beta)]$ and

$$Q_{\alpha\beta} = 2(G^\alpha_{\beta\beta})^2 \Gamma \left(1 - \frac{1}{z_\beta}\right) \Omega[\hat{S}_\beta] \geq 0. \tag{5.21}$$

where

$$\Omega[\hat{f}] = \int_{-\infty}^{\infty} \mathrm{d}p\, \hat{f}(p)\hat{f}(-p). \tag{5.22}$$

With $\sigma_p^{\alpha\beta} = \mathrm{sgn}[p(v_\alpha - v_\beta)]$ one has

$$\begin{aligned} &\left(-iv_p^{\alpha\beta}\right)^{\frac{1}{z_\beta}-1} = \sin\left(\frac{\pi}{2z_\beta}\right) |v_\alpha - v_\beta|^{\frac{1}{z_\beta}-1} \times \\ &\left[1 - i\sigma_p^{\alpha\beta} \tan\left(\left(1+\frac{1}{z_\beta}\right)\frac{\pi}{2}\right)\right]. \end{aligned} \tag{5.23}$$

Now we are in a position to analyze the small-p behaviour. One has to search for dynamical exponents for which the limit $p \to 0$ is non-trivial, which is determined by the smallest power of p in (5.20). This has to be done self-consistently for all modes. We find that different conditions arise depending on which diagonal elements of the mode-coupling matrices vanish. In order to characterize the possible scenarios we define the set $\mathbb{I}_\alpha := \{\beta : G^\alpha_{\beta\beta} \neq 0\}$ of non-zero diagonal mode coupling coefficients. One obtains from (5.20) through power counting the system of equations

$$z_\alpha = \begin{cases} 2 & \text{if} \quad \mathbb{I}_\alpha = \emptyset \\ 3/2 & \text{if} \quad \alpha \in \mathbb{I}_\alpha \\ \min_{\beta\in\mathbb{I}_\alpha}\left[\left(1+\frac{1}{z_\beta}\right)\right] & \text{else} \end{cases} \tag{5.24}$$

and the domain

$$1 < z_\alpha \leq 2 \quad \forall\alpha. \tag{5.25}$$

for the possible dynamical exponents.

Acknowledgements

We thank Herbert Spohn for helpful comments on a preliminary version of the manuscript. This work was supported by Deutsche Forschungsgemeinschaft (DFG) under grant SCHA 636/8-1.

Bibliography

[1] Livio M (2003) The Golden Ratio: The Story of PHI, the World's Most Astonishing Number, Broadway Books (ISBN 978076790815).

[2] Landi GT, de Oliveira MJ (2014) Fourier's law from a chain of coupled planar harmonic oscillators under energy-conserving noise. Phys. Rev. E 89(2): 022105.

[3] Gendelman OV, Savin AV (2014) Normal heat conductivity in chains capable of dissociation. EPL 106: 34004.

[4] Kardar M, Parisi G, Zhang Y-C (1986) Dynamic scaling of growing interfaces. Phys. Rev. Lett. 56: 889–892.

[5] Spohn H (2014) Nonlinear Fluctuating hydrodynamics for anharmonic chains. J. Stat. Phys. 154: 1191–1227.

[6] Spohn H (2015) Fluctuating hydrodynamics approach to equilibrium time correlations for anharmonic chains. arXiv:1505.05987.

[7] Buchanan M (2014) Equivalence principle. Nature Physics 10: 543.

[8] Halpin-Healy T, Takeuchi K.A. (2015) A KPZ cocktail - shaken, not stirred: toasting 30 years of kinetically roughened surfaces. J. Stat. Phys. 160: 794.

[9] Quastel J, Spohn H (2015) The one-dimensional KPZ equation and its universality class. J. Stat. Phys. 160: 965.

[10] Maunuksela J, Myllys M, Kähkönen O-P, Timonen J, Provatas N, Alava MJ, Ala-Nissila T (1997) Kinetic roughening in slow combustion of paper. Phys. Rev. Lett. 79: 1515.

[11] Miettinen L, Myllys M, Merikoski J, Timonen J (2005) Experimental determination of KPZ height-fluctuation distributions. Eur. Phys. J. B 46: 55–60.

[12] Wakita J, Itoh H, Matsuyama T, Matsushita M (1997) *Self-affinity for the growing interface of bacterial colonies*, J. Phys. Soc. Jpn. 66: 6772.

[13] Yunker PJ, Lohr MA, Still T, Borodin A, Durian DJ, Yodh AG (2013) Effects of particle shape on growth dynamics at edges of evaporating drops of colloidal suspensions. Phys. Rev. Lett. 110: 035501.

[14] Prähofer M, Spohn H (2004) Exact scaling functions for one-dimensional stationary KPZ growth. J. Stat. Phys. 115: 255–279.

[15] Prähofer M, Spohn H (2002) Current fluctuations in the totally asymmetric simple exclusion process. *In and Out of Equilibrium*, Vol. 51 of Progress in Probability, ed. Sidoravicius V (Birkhauser, Boston).

[16] Takeuchi KA, Sano M (2010) Universal fluctuations of growing interfaces: evidence in turbulent liquid crystals. Phys. Rev. Lett. 104: 230601.

[17] Takeuchi KA, Sano M, Sasamoto T, Spohn H (2011) Growing interfaces uncover universal fluctuations behind scale invariance. Sci. Rep. 1: 34.

[18] Van Beijeren H (2012) Exact results for anomalous transport in one-dimensional Hamiltonian systems. Phys. Rev. Lett. 108: 108601.

[19] Mendl CB, Spohn H (2013) Dynamic correlators of FPU chains and nonlinear fluctuating hydrodynamics. Phys. Rev. Lett. 111: 230601.

[20] Spohn H, Stoltz G (2015) Nonlinear fluctuating hydrodynamics in one dimension: The case of two conserved fields. J. Stat. Phys. 160: 861.

[21] Popkov V, Schmidt J, Schütz GM (2014) Superdiffusive modes in two-species driven diffusive systems. Phys. Rev. Lett. 112: 200602.

[22] Popkov V, Schmidt J, Schütz GM (2015) Universality classes in two-component driven diffusive systems. J. Stat. Phys. 160: 835–860.

[23] Grisi R, Schütz GM (2011) Current symmetries for particle systems with several conservation laws. J. Stat. Phys. 145: 1499–1512.

[24] Tóth B, Valkó B (2003) Onsager relations and Eulerian hydrodynamic limit for systems with several conservation laws. J. Stat. Phys. 112: 497–521.

[25] Devillard P, Spohn H (1992) Universality class of interface growth with reflection symmetry. J. Stat. Phys. 66: 1089–1099.

[26] Durrett R (2010) Probability: Theory and Examples (4th Edition), Cambridge University Press, Cambridge, p. 141.

[27] Lee CH, Choi W, Han J-H, Strano MS (2010) Coherence resonance in a single-walled carbon nanotube ion channel. Science 329: 1320–1324.

[28] Popkov V, Salerno M (2004) Hydrodynamic limit of multichain driven diffusive models. Phys. Rev. E 69: 046103.

[29] Cardy J (1996) *Scaling and Renormalization in Statistical Physics* (Cambridge University Press, Cambridge)

[30] Henkel M (1999) *Conformal Invariance and Critical Phenomena* (Springer, Berlin).

[31] Henkel M (2002) Phenomenology of local scale invariance: From conformal invariance to dynamical scaling. Nucl. Phys. B 641: 405–486.

[32] Pagnani A, Parisi G (2015) Numerical estimate of the Kardar-Parisi-Zhang universality class in (2+1) dimensions. Phys. Rev. E 92, 010101

[33] Halpin-Healy, T (2012) (2+1)-dimensional directed Polymer in a random medium: scaling phenomena and universal distributions. Phys. Rev. Lett. 109, 170602

[34] Kloss T, Canet L, Wschebor N (2012) Nonperturbative renormalization group for the stationary Kardar-Parisi-Zhang equation: Scaling functions and amplitude ratios in 1+1, 2+1, and 3+1 dimensions. Phys. Rev. E86, 051124

6. Exact scaling solution of the mode coupling equations for non-linear fluctuating hydrodynamics in one dimension

Vladislav Popkov[1], Andreas Schadschneider[2], Johannes Schmidt[2] and Gunter M. Schütz[3]

[1] *Helmholtz-Institut für Strahlen-und Kernphysik, Universität Bonn, Nussallee 14-16, 53119 Bonn, Germany*
[2] *Institut für Theoretische Physik, Universität zu Köln, Zülpicher Str. 77, 50937 Cologne, Germany*
[3] *Institute of Complex Systems II, Theoretical Soft Matter and Biophysics, Forschungszentrum Jülich, 52425 Jülich, Germany*

PACS numbers: 05.60.Cd, 05.20.Jj, 05.70.Ln, 47.10.-g

Published in: Journal of Statistical Mechanics (JSTAT)
Published in: 093211 (2016)
doi: 10.1088/1742-5468/2016/09/093211

Abstract: We obtain the exact solution of the one-loop mode-coupling equations for the dynamical structure function in the framework of non-linear fluctuating hydrodynamics in one space dimension for the strictly hyperbolic case where all characteristic velocities are different. All solutions are characterized by dynamical exponents which are Kepler ratios of consecutive Fibonacci numbers, which includes the golden mean as a limiting case. The scaling form of all higher Fibonacci modes are asymmetric Lévy-distributions. Thus a hierarchy of new dynamical universality classes is established. We also compute the precise numerical value of the Prähofer-Spohn scaling constant to which scaling functions obtained from mode coupling theory are sensitive.

6.1. Introduction

Recently new insights into the dynamical universality classes of nonequilibrium systems have been gained. In the presence of slow modes due to locally conserved currents (such as energy, momentum, density etc.) not only the well-established diffusive and the Kardar-Parisi-Zhang (KPZ) universality classes arise in one space dimension, but also a heat mode and other long-lived modes with unexpected scaling properties were discovered [1, 2, 3]. Going further we have demonstrated in [4] that in the presence of several conserved quantities there is an infinite family of dynamical universality classes that is characterized by dynamical exponents which take the form of Kepler ratios $z_\alpha = F_{\alpha+2}/F_{\alpha+1}$ where $F_\alpha = 1, 1, 2, 3, 5, \ldots$ are the Fibonacci numbers defined recursively by $F_\alpha = F_{\alpha-1} + F_{\alpha-2}$ with starting values $F_1 = F_2 = 1$. This conclusion was based on a scaling analysis of the mode coupling equations for non-linear fluctuating hydrodynamics (NLFH) [5] and supported by extensive Monte-Carlo simulations of multi-lane asymmetric exclusion processes. The first level of the hierarchy (apart from the usual diffusion with $z = 2 = z_1$) includes the Kardar-Parisi-Zhang (KPZ) universality class with $z = 3/2 = z_2$ which continues to inspire both due to its links to intriguing mathematical problems and beautiful experimental results, see e.g. the special issue J. Stat. Phys. 160, (2015) dedicated to it, and in particular the review by Halpin-Healey and Takeuchi [6]. Also the golden mean, which is the limiting Kepler ratio $z_\infty = \varphi \approx 1.618...$, occurs in systems with at least two conservation laws [2, 3].

NLFH has emerged as a universal tool to analyze general one-dimensional systems such Hamiltonian dynamics [1, 7], anharmonic chains [5, 3, 8, 9, 10, 11] or driven diffusive systems [4, 2, 12, 13, 14, 15, 16]. The theory is robust. The essential ingredients appear to be only the above-mentioned locally conserved currents and long-time dynamics dominated by the long wave length modes of the associated conserved quantities. Mathematically rigorous results for some specific models support the validity of the theory [17, 18]. It is the purpose of this work to provide a detailed analysis of the one-loop mode-coupling equations for the dynamical structure function for an arbitrary number of conservation laws in the strictly hyperbolic setting where all characteristic velocities are different.

6.2. Computation of the dynamical structure function

6.2.1. Basis of nonlinear fluctuating hydrodynamics

Consider an interacting system with n locally conserved currents j_λ associated to physical quantities such as energy, momentum, particle numbers etc. that are conserved under the microscopic dynamics of the system. The starting point for investigating the large-scale dynamics is the system of conservation laws

$$\frac{\partial}{\partial t}\vec{\rho}(x,t) + \frac{\partial}{\partial x}\vec{j}(x,t) = 0 \tag{6.1}$$

where component $\rho_\lambda(x,t)$ of the vector $\vec{\rho}(x,t)$ is a coarse-grained conserved quantity and the component $j_\lambda(x,t)$ of the current vector $\vec{j}(x,t)$ is the associated locally conserved current. We shall refer to the $\rho_\lambda(x,t)$ as densities. Notice that in our convention $\vec{\rho}$ and $\vec{j}$ are regarded as column vectors. Transposition is denoted by a superscript T.

This system of conservation laws can be obtained from the law of a large numbers and the postulate of local equilibrium [19, 20]. Thus the current is a function of x and t only through its dependence on the local conserved densities. Hence these equations can be rewritten as

$$\frac{\partial}{\partial t}\vec{\rho}(x,t) + \bar{\mathbf{J}}\frac{\partial}{\partial x}\vec{\rho}(x,t) = 0 \tag{6.2}$$

where $\bar{\mathbf{J}} \equiv \bar{\mathbf{J}}(\vec{\rho}(x,t))$ is the current Jacobian with matrix elements $\bar{J}_{\lambda\mu} = \partial j_\lambda/\partial\rho_\mu$.

To get some basic insight we first notice that constant densities ρ_λ are a (trivial) stationary solution of (6.2). Stationary fluctuations of the conserved quantities are captured in the covariance matrix $\mathbf{K}$ of the conserved quantities that we shall not describe explicitly. However, we have in mind the generic case where $\mathbf{K}$ is positive definite, i.e., we do not allow for vanishing fluctuations of a locally conserved quantity that can occur in systems with slowly decaying stationary correlations. We shall refer to $\mathbf{K}$ as compressibility matrix.

Expanding the local densities $\rho_\lambda(x,t) = \rho_\lambda + u_\lambda(x,t)$ around their long-time stationary values ρ_λ and taking a linear approximation (where $\bar{\mathbf{J}}$ is a constant matrix $\mathbf{J} \equiv \mathbf{J}(\vec{\rho})$ with matrix elements determined by the stationary densities $\vec{\rho}$) leads to a system of coupled linear PDE's which is solved by diagonalizing $\mathbf{J}$. One transforms to normal modes $\vec{\phi} = \mathbf{R}\vec{u}$ where $\mathbf{RJR}^{-1} = \mathrm{diag}(v_\alpha)$ and the transformation matrix R is normalized such that $\mathbf{RKR}^T = \mathbb{1}$. Thus one finds decoupled equations $\partial_t \phi_\alpha = v_\alpha \partial_x \phi_\alpha$ whose solutions are travelling waves $\phi_\alpha(x,t) = \phi^0_\alpha(x - v_\alpha t)$ with initial data $\phi_\alpha(x,0) = \phi^0_\alpha(x)$. This shows that the eigenvalues v_α of $\mathbf{J}$ play the role of characteristic speeds.

The product $\mathbf{JK}$ of the Jacobian with the compressibility matrix $\mathbf{K}$ is symmetric which can be proved already on microscopic level [21] for sufficiently fast decaying stationary correlations. This guarantees that on macroscopic scale the full non-linear system (6.2) is hyperbolic [22], i.e., all eigenvalues v_α of $\mathbf{J}$ are guaranteed to be real. If the eigenvalues v_α are non-degenerate the system is called strictly hyperbolic. The occurrence of complex eigenvalues signals macroscopic phase separation [16], consistent with the absence of fast decaying stationary correlations on microscopic level, and coarsening dynamics.

Notice that (6.2) is completely deterministic. In the NLFH approach [5] the effect of fluctuations is captured by adding a phenomenological diffusion matrix D and white noise terms ξ_λ. This turns (6.2) into a non-linear stochastic PDE. From renormalization group considerations it is known that polynomial non-linearities of order higher than 4 are irrelevant for the large-scale behaviour and order 3 leads at most to logarithmic corrections if the generic quadratic non-linearity is absent [23]. Thus one expands $\bar{\mathbf{J}}$ around the stationary densities $\vec{\rho}$ but keeps only quadratic non-linearities so that the fluctuation fields $u_\lambda(x,t)$ satisfy the system of coupled noisy Burgers equations

$$\partial_t \vec{u} = -\partial_x \left(J_0 \vec{u} + \frac{1}{2} \vec{u}^T \vec{H} \vec{u} - D \partial_x \vec{u} + B\vec{\xi} \right) \tag{6.3}$$

where $\vec{H}$ is a column vector whose entries $(\vec{H})_\lambda = \mathbf{H}^\lambda$ are the Hessians with matrix elements $H^\lambda_{\mu\nu} = \partial^2 j_\lambda / (\partial\rho_\mu \partial\rho_\nu)$. If the quadratic non-linearity is absent one has diffusive behaviour.

Using normal modes one thus arrives at

$$\partial_t \phi_\alpha = -\partial_x \left(v_\alpha \phi_\alpha + \vec{\phi}^T G^\alpha \vec{\phi} - \partial_x (\tilde{D}\vec{\phi})_\alpha + (\tilde{B}\vec{\xi})_\alpha \right) \tag{6.4}$$

with $\tilde{\mathbf{D}} = \mathbf{RDR}^{-1}$ and $\tilde{\mathbf{B}} = \mathbf{RB}$. The matrices

$$\mathbf{G}^\alpha = \frac{1}{2} \sum_\lambda R_{\alpha\lambda} (\mathbf{R}^{-1})^T \mathbf{H}^\lambda \mathbf{R}^{-1} \tag{6.5}$$

are the mode coupling matrices with the mode-coupling coefficients $G^\alpha_{\beta\gamma} = G^\alpha_{\gamma\beta}$ which are, by construction, symmetric. From the linear theory one concludes that the fluctuation fields are peaked around $x_\alpha(t) = x_\alpha(0) + v_\alpha t$. For short-range interactions fluctuations spread generally sub-ballistically and therefore the width of the peak grows in sublinearly time, as indeed will be seen explicitly below.

We stress that the macroscopic current-density relation given by the components of the current vector $\vec{j}$ arises from the microscopic model from the stationary current-density relation $\vec{j}(\vec{\rho})$. Similarly, the compressibility matrix $\mathbf{K}$ is computed from the stationary distribution of the microscopic model. Hence the mode coupling matrices (and with them the dynamical universality

classes as shown below) are completely determined by these two macroscopic stationary properties of the system. However, the *exact* stationary current-density relations and the *exact* stationary compressibilities are required.

The main quantity of interest are the dynamical structure functions

$$S^{\alpha\beta}(x,t) = \langle\, \phi^{\alpha}(x,t)\phi^{\beta}(0,0)\,\rangle \tag{6.6}$$

(where $\langle \dots \rangle$ denotes the stationary ensemble average) which describe the stationary space-time fluctuations. Since we work with normal modes we have the normalization

$$\int_{-\infty}^{\infty} \mathrm{d}x\, S^{\alpha\beta}(x,t) = \delta_{\alpha,\beta}. \tag{6.7}$$

For strictly hyperbolic systems the characteristic velocities are all different. As a result the off-diagonal elements of S decay quickly and for long times and large distances one is left with the diagonal elements which we denote by

$$S_{\alpha}(x,t) := S^{\alpha\alpha}(x,t). \tag{6.8}$$

The large scale behaviour of the diagonal elements is expected to have the scaling form

$$S_{\alpha}(x,t) \sim t^{-1/z_{\alpha}} f_{\alpha}(\xi_{\alpha}) \tag{6.9}$$

with the scaling variable

$$\xi_{\alpha} = (x - v_{\alpha}t)\, t^{-1/z_{\alpha}} \tag{6.10}$$

and dynamical exponent z_{α} which has to be determined and which indicates the dynamical universality class of the mode α. The exponent in the power law prefactor follows from the conservation law. In momentum space, with the Fourier transform convention

$$\hat{S}_{\alpha}(k,t) := \frac{1}{\sqrt{2\pi}} \int_{-\infty}^{\infty} \mathrm{d}x\, \mathrm{e}^{-ikx} S_{\alpha}(x,t) \tag{6.11}$$

one has the scaling form

$$\hat{S}_{\alpha}(k,t) \sim \mathrm{e}^{-iv_{\alpha}kt} \hat{f}_{\alpha}(kt^{1/z_{\alpha}}) \tag{6.12}$$

where $\hat{f}_{\alpha}$ is the Fourier transform of the scaling function (6.9).

6.2.2. Mode coupling equations

The starting point for computing the diagonal elements of the dynamical structure function are the mode coupling equations [5]

$$\partial_t S_{\alpha}(x,t) = D_{\alpha} S_{\alpha}(x,t) + \int_0^t \mathrm{d}s \int_{-\infty}^{\infty} \mathrm{d}y\, S_{\alpha}(x-y, t-s) M_{\alpha\alpha}(y,s) \tag{6.13}$$

with diffusion operator

$$D_{\alpha} = -v_{\alpha}\partial_x + D_{\alpha}\partial_x^2 \tag{6.14}$$

and memory term

$$M_{\alpha\alpha}(y,s) = 2\sum_{\beta,\gamma} (G^{\alpha}_{\beta\gamma})^2 \partial_y^2 S_{\beta}(y,s) S_{\gamma}(y,s). \tag{6.15}$$

Only the diagonal elements $D_{\alpha} := D_{\alpha\alpha}$ of the diffusion matrix and of the memory kernel are kept here.

In momentum space this reads

$$\partial_t \hat{S}_\alpha(k,t) = -\widehat{D}_\alpha(k)\hat{S}_\alpha(k,t) - \int_0^t \mathrm{d}s\, \hat{S}_\alpha(k,t-s)\widehat{M}_{\alpha\alpha}(k,s) \tag{6.16}$$

with

$$\widehat{D}_\alpha(k) = iv_\alpha k + D_\alpha k^2 \tag{6.17}$$

and

$$\widehat{M}_{\alpha\alpha}(k,s) = 2\sum_{\beta,\gamma}(G^\alpha_{\beta\gamma})^2 k^2 \int_{-\infty}^{\infty} \mathrm{d}q\, \hat{S}_\beta(q,s)\hat{S}_\gamma(k-q,s). \tag{6.18}$$

Finally we perform the Laplace transformation

$$\tilde{S}_\alpha(k,\omega) := \int_0^\infty \mathrm{d}t\, \mathrm{e}^{-\omega t}\hat{S}_\alpha(k,t) \tag{6.19}$$

by multiplying (6.16) on both sides by $\mathrm{e}^{-\omega t}$ and integrating over t. This yields

$$\tilde{S}_\alpha(k,\omega) = \frac{\hat{S}_\alpha(k,0)}{\omega + \widehat{D}_\alpha(k) + \tilde{C}_{\alpha\alpha}(k,\omega)} \tag{6.20}$$

with memory kernel

$$\tilde{C}_{\alpha\alpha}(k,\omega) = 2\sum_{\beta,\gamma}(G^\alpha_{\beta\gamma})^2 k^2 \int_0^\infty \mathrm{d}s\, \mathrm{e}^{-\omega s}\int_{-\infty}^{\infty} \mathrm{d}q\, \hat{S}_\beta(q,s)\hat{S}_\gamma(k-q,s). \tag{6.21}$$

and $\hat{S}_\alpha(k,0) = 1/\sqrt{2\pi}$.

Remark 6.2.1. *For $k = 0$ the solution is trivial, with the exact result $\hat{S}_\alpha(0,t) = 1/\sqrt{2\pi}$ given by the Fourier convention (6.11) and the normalization (6.7).*

So far this is an exact reformulation of the original mode coupling equations (6.13). In order to proceed we make impose successively various conditions (Conditions 1 - 3). We stress that conditions 1 and 2 do not lead to any loss of generality in the subsequent treatment.

Condition 1: Scaling ($k \neq 0$).

The mode coupling equation (6.16) can be further analyzed using the scaling form (6.12). To this end we first rewrite (6.20) in terms of $\tilde{\omega}_\alpha := \omega + iv_\alpha k$. This yields

$$\tilde{S}_\alpha(k,\tilde{\omega}_\alpha) = \hat{S}_\alpha(k,0)\left[\tilde{\omega}_\alpha + D_\alpha k^2 + 2\sum_{\beta,\gamma}(G^\alpha_{\beta\gamma})^2 I_{\beta\gamma}(k,\tilde{\omega}_\alpha)\right]^{-1} \tag{6.22}$$

with modified memory integral

$$I_{\beta\gamma}(k,\tilde{\omega}_\alpha) = k^2\int_0^\infty \mathrm{d}s\, \mathrm{e}^{-(\tilde{\omega}_\alpha - iv_\alpha k)s}\int_{-\infty}^{\infty}\mathrm{d}q\, \hat{S}_\beta(q,s)\hat{S}_\gamma(k-q,s). \tag{6.23}$$

Using the scaling ansatz (6.12) we arrive at

$$I_{\beta\gamma}(k,\tilde{\omega}_\alpha) \;=\; k^2\int_0^\infty \mathrm{d}s\, \mathrm{e}^{-(\tilde{\omega}_\alpha + i(v_\gamma - v_\alpha)k)s}A_{\beta\gamma}(k,s) \tag{6.24}$$

$$= k^2 \int_0^\infty \mathrm{d}s\, \mathrm{e}^{-(\tilde{\omega}_\alpha + i(v_\beta - v_\alpha)k)s} A_{\gamma\beta}(k,s) \tag{6.25}$$

with

$$A_{\beta\gamma}(k,s) = \int_{-\infty}^\infty \mathrm{d}q\, \mathrm{e}^{i(v_\gamma - v_\beta)qs} \hat{f}_\beta(qs^{\frac{1}{z_\beta}}) \hat{f}_\gamma((k-q)s^{\frac{1}{z_\gamma}}). \tag{6.26}$$

As pointed out above, in the static case $k = 0$ the constant solution to the mode coupling equations is exact. Therefore we can focus on the non-static case $k \neq 0$. With $k = |k|\mathrm{sgn}(k)$ and the substitution of integration variables $|k|s \to s$ we obtain

$$I_{\beta\gamma}(k,\tilde{\omega}_\alpha) = |k| \int_0^\infty \mathrm{d}s\, \mathrm{e}^{-(\tilde{\omega}_\alpha |k|^{-1} + i(v_\gamma - v_\alpha)\mathrm{sgn}(k))s} B_{\beta\gamma}(k,s) \tag{6.27}$$

$$= |k| \int_0^\infty \mathrm{d}s\, \mathrm{e}^{-(\tilde{\omega}_\alpha |k|^{-1} + i(v_\beta - v_\alpha)\mathrm{sgn}(k))s} B_{\gamma\beta}(k,s) \tag{6.28}$$

with

$$B_{\beta\gamma}(k,s) = \int_{-\infty}^\infty \mathrm{d}q\, \mathrm{e}^{i(v_\gamma - v_\beta)q|k|^{-1}s} \hat{f}_\beta(q|k|^{-\frac{1}{z_\beta}} s^{\frac{1}{z_\beta}}) \hat{f}_\gamma((k-q)|k|^{-\frac{1}{z_\gamma}} s^{\frac{1}{z_\gamma}}). \tag{6.29}$$

Condition 2: Local interactions ($z_\alpha > 1\ \forall\alpha$).

As discussed above, for sufficiently fast decaying interaction strength one expects that all modes spread sub-ballistically around their centers at $x_\alpha(t)$, i.e., $z_\alpha > 1\ \forall\alpha$. Then the small-$k$ behaviour of the integral (6.29) simplifies since the term $k|k|^{-\frac{1}{z}\gamma}$ in the second argument vanishes. One is left with

$$B_{\beta\gamma}(k,s) = \int_{-\infty}^\infty \mathrm{d}q\, \mathrm{e}^{i(v_\gamma - v_\beta)q|k|^{-1}s} \hat{f}_\beta(q|k|^{-\frac{1}{z_\beta}} s^{\frac{1}{z_\beta}}) \hat{f}_\gamma(-q|k|^{-\frac{1}{z}\gamma} s^{\frac{1}{z}\gamma}). \tag{6.30}$$

For $v_\gamma = v_\beta$ this expression reduces to

$$B_{\beta\gamma}(k,s) = \int_{-\infty}^\infty \mathrm{d}q\, \hat{f}_\beta(q|k|^{-\frac{1}{z_\beta}} s^{\frac{1}{z_\beta}}) \hat{f}_\gamma(-q|k|^{-\frac{1}{z}\gamma} s^{\frac{1}{z}\gamma}). \tag{6.31}$$

Taking $\beta = \gamma$ this yields the diagonal elements

$$B_{\beta\beta}(k,s) = \int_{-\infty}^\infty \mathrm{d}q\, \hat{f}_\beta(q|k|^{-\frac{1}{z_\beta}} s^{\frac{1}{z_\beta}}) \hat{f}_\beta(-q|k|^{-\frac{1}{z}\beta} s^{\frac{1}{z_\beta}})$$

$$= |k|^{\frac{1}{z_\beta}} s^{-\frac{1}{z_\beta}} \Omega[\hat{f}_\beta] \tag{6.32}$$

with the functional

$$\Omega[f] = \int_{-\infty}^\infty \mathrm{d}k\, \hat{f}(k)\hat{f}(-k) = \int_{-\infty}^\infty \mathrm{d}x\, (f(x))^2. \tag{6.33}$$

Thus we find from (6.27)

$$I_{\beta\beta}(k,\tilde{\omega}_\alpha) = |k|^{1+\frac{1}{z_\beta}} \Omega[\hat{f}_\beta] \int_0^\infty \mathrm{d}s\, s^{-\frac{1}{z_\beta}} \mathrm{e}^{-(\tilde{\omega}_\alpha |k|^{-1} + i(v_\beta - v_\alpha)\mathrm{sgn}(k))s}. \tag{6.34}$$

With the scaling variable

$$\zeta_\alpha = \tilde{\omega}_\alpha |k|^{-z_\alpha} \tag{6.35}$$

and the shorthand notation

$$v_k^{\alpha\beta} = (v_\alpha - v_\beta)\,\mathrm{sgn}(k) \tag{6.36}$$

this reads

$$I_{\beta\beta}(k,\zeta_\alpha) = |k|^{1+\frac{1}{z_\beta}}\Omega[\hat{f}_\beta]\int_0^\infty \mathrm{d}s\,\mathrm{e}^{-(\zeta_\alpha|k|^{z_\alpha-1}-iv_k^{\alpha\beta})s}s^{-\frac{1}{z_\beta}} \tag{6.37}$$

$$= |k|^{1+\frac{1}{z_\beta}}\Omega[\hat{f}_\beta]\Gamma\left(1-\frac{1}{z_\beta}\right)\left(\zeta_\alpha|k|^{z_\alpha-1}-iv_k^{\alpha\beta}\right)^{\frac{1}{z_\beta}-1} \tag{6.38}$$

which also holds for $\beta=\alpha$. Here we have used the integral representation

$$\Gamma(x) = p^x\int_0^\infty \mathrm{d}u\,u^{x-1}\mathrm{e}^{-pu} = p^x/x\int_0^\infty \mathrm{d}u\,\mathrm{e}^{-pu^{1/x}} \tag{6.39}$$

for $\Re(x)>0$, $\Re(p)>0$ of the Gamma-function.

Condition 3: Strict hyperbolicity ($v_\beta \neq v_\gamma\ \forall \beta\neq\gamma$).

Up to this point the assumption of strict hyperbolicity has only led us to consider the mode-coupling equations in the form (6.13), but it has not yet entered their analysis. Strict hyperbolicity plays a role only in (6.30). We make the substitution of integration variables $q(s/|k|)^x \to q$ where $x=\max[\frac{1}{z_\beta},\frac{1}{z}{}_\gamma]<1$. Then (6.30) becomes

$$B_{\beta\gamma}(k,s) = |k/s|^x\int_{-\infty}^\infty \mathrm{d}q\,\mathrm{e}^{i(v_\gamma-v_\beta)q|k/s|^{x-1}}\hat{f}_\beta(q|k/s|^{x-\frac{1}{z_\beta}})\hat{f}_\gamma(-q|k/s|^{x-\frac{1}{z}\gamma}). \tag{6.40}$$

This leads to a term $|k|^{x-1}\to\infty$ in the exponential. Thus for $v_\gamma\neq v_\beta$ we have a rapidly oscillating term and the integral vanishes exponentially fast.

This proves that the leading contributions to the dynamical structure function come from the diagonal elements $\beta=\gamma$ of the mode coupling matrix. Therefore (6.22) reads

$$\tilde{S}_\alpha(k,\zeta_\alpha) = \frac{1}{\sqrt{2\pi}}|k|^{-z_\alpha}h_\alpha(\zeta_\alpha) \tag{6.41}$$

where from (6.38) we have

$$h_\alpha(\zeta_\alpha) = \lim_{k\to0}\Bigg[\zeta_\alpha + D_\alpha|k|^{2-z_\alpha} + Q_{\alpha\alpha}\zeta_\alpha^{\frac{1}{z_\alpha}-1}|k|^{3-2z_\alpha} + \sum_{\beta\neq\alpha}Q_{\alpha\beta}\left(\zeta_\alpha|k|^{z_\alpha-1}-iv_k^{\alpha\beta}\right)^{\frac{1}{z_\beta}-1}|k|^{1+\frac{1}{z_\beta}-z_\alpha}\Bigg]^{-1}. \tag{6.42}$$

with the generally positive constants

$$Q_{\alpha\beta} = 2(G^\alpha_{\beta\beta})^2\Gamma\left(1-\frac{1}{z_\beta}\right)\Omega[\hat{f}_\beta]\geq 0. \tag{6.43}$$

We invoke again strict hyperbolicity and subballistic scaling to deduce that the term $\zeta_\alpha|k|^{z_\alpha-1}$ in (6.42) can be neglected for the long wave length behaviour. This yields for the diagonal terms

$$h_\alpha(\zeta_\alpha) = \lim_{k\to0}\Bigg[\zeta_\alpha + D_\alpha|k|^{2-z_\alpha} + Q_{\alpha\alpha}\zeta_\alpha^{\frac{1}{z_\alpha}-1}|k|^{3-2z_\alpha} + \sum_{\beta\neq\alpha}Q_{\alpha\beta}\left(-iv_k^{\alpha\beta}\right)^{\frac{1}{z_\beta}-1}|k|^{1+\frac{1}{z_\beta}-z_\alpha}\Bigg]^{-1}. \tag{6.44}$$

This is the starting point for the subsequent analysis of the small-k behaviour. We remark that with the shorthand notation

$$\sigma_k^{\alpha\beta} = \mathrm{sgn}[k(v_\alpha - v_\beta)] \tag{6.45}$$

we have

$$\begin{aligned}
\left(-iv_k^{\alpha\beta}\right)^{\frac{1}{z_\beta}-1} &= |v_\alpha - v_\beta|^{\frac{1}{z_\beta}-1} \exp\left(i\sigma_k^{\alpha\beta}\left(1-\frac{1}{z_\beta}\right)\frac{\pi}{2}\right) && (6.46)\\
&= \frac{\cos\left(\left(1-\frac{1}{z_\beta}\right)\frac{\pi}{2}\right)}{|v_\alpha - v_\beta|^{1-\frac{1}{z_\beta}}}\left[1 + i\sigma_k^{\alpha\beta}\tan\left(\left(1-\frac{1}{z_\beta}\right)\frac{\pi}{2}\right)\right] && (6.47)\\
&= \frac{\sin\left(\frac{\pi}{2z_\beta}\right)}{|v_\alpha - v_\beta|^{1-\frac{1}{z_\beta}}}\left[1 - i\sigma_k^{\alpha\beta}\tan\left(\left(1+\frac{1}{z_\beta}\right)\frac{\pi}{2}\right)\right] && (6.48)
\end{aligned}$$

In the last line we made use of $\tan(-x) = -\tan(x)$ and $\tan(x) = \tan(x-\pi)$.

6.2.3. Asymptotic analysis

Now one has to search for the dynamical exponents for which the limit $k \to 0$ is non-trivial, i.e., $h_\alpha(\zeta_\alpha)$ finite and $h_\alpha(\zeta_\alpha) \neq \zeta_\alpha$ (which would correspond to the δ-peak of the linear theory which does not exhibit the fluctuations). This has to be done self-consistently for all modes. Different self-consistency conditions arise depending on which diagonal elements of the mode-coupling matrices vanish. In the following we consider some fixed mode α and study all possible scenarios which depend on which is the smallest power in k in (6.44) that yields a non-trivial scaling form. To this end we define the set

$$\mathbb{I}_\alpha := \{\beta : G^\alpha_{\beta\beta} \neq 0\} \tag{6.49}$$

of non-zero diagonal mode coupling coefficients. Thus $\mathbb{I}_\alpha$ is the set of modes β that give rise to a non-linear term in the time-evolution of the mode α that one considers.

Case A: $\mathbb{I}_\alpha = \emptyset$

If mode α decouples, i.e., if *all* diagonal terms $G^\alpha_{\beta\beta} = 0$ then one has $h_\alpha(\zeta_\alpha) = \left[\zeta_\alpha + D_\alpha|k|^{2-z_\alpha}\right]^{-1}$ and therefore

$$z_\alpha = 2 \tag{6.50}$$

and

$$\hat{S}_\alpha(k,t) = \frac{1}{\sqrt{2\pi}}\mathrm{e}^{-iv_\alpha kt - D_\alpha k^2 t} \tag{6.51}$$

which is pure diffusion. (We remind the reader that we ignore possible logarithmic corrections from cubic contributions to the NLFH equations.)

From (6.51) we read off the scaling function

$$\hat{f}_\alpha(\kappa_\alpha) = \frac{1}{\sqrt{2\pi}}\mathrm{e}^{-D_\alpha\kappa_\alpha^2} \tag{6.52}$$

with scaling variable $\kappa_\alpha = kt^{1/2}$. This yields

$$\Omega[\hat{f}_\alpha] = \frac{1}{2\sqrt{2\pi D_\alpha}} \quad \text{for diffusive modes } \alpha \tag{6.53}$$

and

$$Q_{\beta\alpha} = \frac{(G^{\beta}_{\alpha\alpha})^2}{\sqrt{2D_\alpha}} \quad \text{for non-diffusive modes } \beta \neq \alpha. \tag{6.54}$$

Case B: $\alpha \notin \mathbb{I}_\alpha$, $\mathbb{I}_\alpha \neq \emptyset$

If $G^{\alpha}_{\alpha\alpha} = 0$, but some $G^{\alpha}_{\beta\beta} \neq 0$, then mode α has quadratic contributions from one or more other modes β. One has

$$h_\alpha(\zeta_\alpha) = \lim_{k\to 0}\left[\zeta_\alpha + D_\alpha|k|^{2-z_\alpha} + \sum_{\beta\neq\alpha} Q_{\alpha\beta}\left(-iv_k^{\alpha\beta}\right)^{\frac{1}{z_\beta}-1}|k|^{1+\frac{1}{z_\beta}-z_\alpha}\right]^{-1}. \tag{6.55}$$

corresponding to

$$\hat{S}_\alpha(k,t) = \frac{1}{\sqrt{2\pi}}\exp\left(-iv_\alpha kt - \left[D_\alpha k^2 + \sum_\beta Q_{\alpha\beta}\left(-iv_k^{\alpha\beta}\right)^{\frac{1}{z_\beta}-1}|k|^{1+\frac{1}{z_\beta}}\right]t\right) \tag{6.56}$$

Since by Condition 2 one has $1+\frac{1}{z_\beta} < 2$ it follows that $2 - z_\alpha > 1 + \frac{1}{z_\beta} - z_\alpha$. Hence the diffusive term in (6.56) is subleading and the dominant terms in (6.56) are those terms proportional to $(G^{\alpha}_{\beta\beta})^2$ which have the largest z_β. We shall denote this value by z_β^{max} and the define the set $\mathbb{I}^*_\alpha = \{\beta \in \mathbb{I}_\alpha : z_\beta = z_\beta^{max}\}$. This leads to

$$z_\alpha = \min_{\beta\in\mathbb{I}_\alpha}\left[\left(1+\frac{1}{z_\beta}\right)\right] = 1 + \frac{1}{z_\beta^{max}} > 1. \tag{6.57}$$

Hence the assumption of subballistic scaling that arises from Condition 2 is self-consistent. The dynamical structure (6.56) reduces to

$$\hat{S}_\alpha(k,t) = \frac{1}{\sqrt{2\pi}}\exp\left(-iv_\alpha kt - \sum_{\beta\in\mathbb{I}^*_\alpha} Q_{\alpha\beta}\left(-iv_k^{\alpha\beta}\right)^{z_\alpha-2}|k|^{z_\alpha}t\right) \tag{6.58}$$

where from (6.48) and (6.57) we have

$$\left(-iv_k^{\alpha\beta}\right)^{z_\alpha-2} = \frac{\sin\left((z_\alpha-1)\frac{\pi}{2}\right)}{|v_\alpha - v_\beta|^{2-z_\alpha}}\left(1 - i\sigma_k^{\alpha\beta}\tan\left(\frac{\pi z_\alpha}{2}\right)\right). \tag{6.59}$$

Defining

$$E_\alpha = \sum_{\beta\in\mathbb{I}^*_\alpha} Q_{\alpha\beta}\frac{\sin\left((z_\alpha-1)\frac{\pi}{2}\right)}{|v_\alpha - v_\beta|^{2-z_\alpha}} \tag{6.60}$$

$$F_\alpha = \sum_{\beta\in\mathbb{I}^*_\alpha} Q_{\alpha\beta}\frac{\sin\left((z_\alpha-1)\frac{\pi}{2}\right)}{|v_\alpha - v_\beta|^{2-z_\alpha}}\mathrm{sgn}(v_\alpha - v_\beta) \tag{6.61}$$

$$A_\alpha = \frac{F_\alpha}{E_\alpha} \tag{6.62}$$

allows us to write

$$\hat{S}_\alpha(k,t) = \frac{1}{\sqrt{2\pi}}\exp\left(-iv_\alpha kt - E_\alpha|k|^{z_\alpha}t\left[1 - iA_\alpha\tan\left(\frac{\pi z_\alpha}{2}\right)\mathrm{sgn}(k)\right]\right). \tag{6.63}$$

One recognizes in (6.63) an asymmetric α-stable Lévy-distribution with asymmetry $A_\alpha \in [-1,1]$ which generically has two algebraic tails. If mode α is to the left or right of *all* modes with z_β^{max} that control it i.e. if $v_\alpha < v_\beta \forall \beta \in \mathbb{I}_\alpha^*$ or if $v_\alpha > v_\beta \forall \beta \in \mathbb{I}_\alpha^*$ (meaning that it is a spatially extremal mode), then $\sigma_k^{\alpha\beta}$ has the same sign for all $\beta \in \mathbb{I}_\alpha^*$ and as a consequence $A_\alpha = \pm 1$. This means that then the asymmetry is maximal and as a consequence one has a stretched exponential decay towards the exterior of the extremal mode, while only towards the interior there is a power law. This stretched exponential decay is a classical analogue of the Lieb-Robinson bound which is a theoretical upper limit on the speed at which information can propagate in non-relativistic quantum systems [24].

From (6.63) we obtain the scaling function

$$\hat{f}_\alpha(\kappa) = \frac{1}{\sqrt{2\pi}} \exp\left(-E_\alpha |\kappa|^{z_\alpha} \left[1 - iA_\alpha \mathrm{sgn}(\kappa) \tan\left(\frac{\pi z_\alpha}{2}\right)\right]\right) \tag{6.64}$$

which gives (see (6.33) and (6.39))

$$\Omega[\hat{f}_\alpha] = \frac{1}{\pi z_\alpha} (2E_\alpha)^{-\frac{1}{z_\alpha}} \Gamma\left(\frac{1}{z_\alpha}\right) \quad \text{for Fibonacci modes } \alpha. \tag{6.65}$$

Using the identity

$$\Gamma\left(1 - \frac{1}{x}\right) = \frac{\pi}{\Gamma\left(\frac{1}{x}\right) \sin\left(\frac{\pi}{x}\right)} \tag{6.66}$$

one finds

$$Q_{\alpha\beta} = \frac{2(G^\alpha_{\beta\beta})^2 \left(2E_\beta\right)^{-\frac{1}{z_\beta}}}{z_\beta \sin\left(\frac{\pi}{z_\beta}\right)} \quad \text{for Fibonacci modes } \beta \neq \alpha \tag{6.67}$$

for the constant (6.43). We recall that E_α is not a simple constant depending only on mode α, but a functional that depends on all modes $\beta \in \mathbb{I}_\alpha^*$.

The upshot of cases A and B is that if $G^\alpha_{\alpha\alpha} = 0$ one has the bounds

$$1 < z_\alpha \leq 2 \tag{6.68}$$

for the dynamical exponents of modes whose self-coupling constant vanishes. The equality $z = 2$ is attained if and only if all diagonal coupling constants of that mode vanish. The relation (6.57) determines the dynamical exponents. The scaling functions are asymmetric Lévy functions.

Case C: $\alpha \in \mathbb{I}_\alpha$

For $G^\alpha_{\alpha\alpha} \neq 0$, i.e., non-vanishing quadratic self-coupling, imagine first that $z_{\beta^\star} > 2$ for some mode $\beta^\star$. Then according to (6.44) a non-trivial scaling form is obtained for the following values of the dynamical exponent: $z_\alpha = 1 + 1/z_{\beta^\star} < 3/2$ (from the term proportional to $G^\alpha_{\beta^\star\beta^\star}$), $z_\alpha = 3/2$ (from the self-coupling term $G^\alpha_{\alpha\alpha}$), or $z_\alpha = 2$ (from the diffusive term). This excludes the possibility $z_\alpha > 2$ for $G^\alpha_{\alpha\alpha} \neq 0$. Above it was established that $z_\alpha \leq 2$ for $G^\alpha_{\alpha\alpha} = 0$. Thus we conclude that for *all* modes the bounds (6.68) are valid self-consistently. Therefore below we can assume without loss of generality $1 < z_\beta \leq 2$.

Next we observe the leading small-k behaviour of (6.44) with non-trivial scaling form is obtained for $z_\alpha = \min\{2, 3/2, 1 + 1/z_\beta\}$. Thus

$$z_\alpha = 3/2 \tag{6.69}$$

because of (6.68).

Even though the dynamical exponent is uniquely given by $z_\alpha = 3/2$ if $G^\alpha_{\alpha\alpha} \neq 0$, there are two different families of scaling functions. If $z_\beta < 2$ for all modes, i.e., if all modes have at least one non-zero diagonal element, then

$$h_\alpha(\zeta_\alpha) = \left[\zeta_\alpha + Q_{\alpha\alpha}\zeta_\alpha^{-\frac{1}{3}}\right]^{-1}. \tag{6.70}$$

This corresponds to the usual KPZ-mode where mode-coupling theory is known to be quantitative quite good but not exact [25, 26]. On the other hand, if $z_\beta = 2$ for some diffusive modes from a set B^{diff}, then

$$h_\alpha(\zeta_\alpha) = \left[\zeta_\alpha + Q_{\alpha\alpha}\zeta_\alpha^{-\frac{1}{3}} + \sum_{\beta\in B^{diff}} Q_{\alpha\beta}\left(-iv_k^{\alpha\beta}\right)^{-\frac{1}{2}}\right]^{-1}. \tag{6.71}$$

This corresponds to a modified KPZ-mode [3] which has not been studied yet in detail.

The constants defined in (6.43) are

$$Q_{\alpha\beta} = 2(G^\alpha_{\beta\beta})^2\Gamma\left(1/3\right)\Omega[\hat{f}_\beta] \text{ for } \beta = \text{KPZ, KPZ'} \tag{6.72}$$

for a KPZ or modified KPZ mode β. In order to compute $\Omega_{\text{KPZ}} \equiv \Omega[\hat{f}_{\text{KPZ}}]$ for $\beta = \text{KPZ}$ we use the exact scaling form $S_{\text{KPZ}}(x,t) = (\lambda t)^{-2/3} f_{\text{KPZ}}((x - v_\beta t)/(\lambda t)^{2/3})$ with $\lambda = 2\sqrt{2}|G^\beta_{\beta\beta}|$ [5]. With the scaling variable $\xi = (x - v_\beta t)/t^{2/3}$ as defined in (6.10) we obtain the real-space scaling function $f_\beta(\xi) = \lambda^{-2/3} f_{\text{KPZ}}(\lambda^{-2/3}\xi)$. Therefore, by definition we have

$$\Omega_{\text{KPZ}} = \int_{-\infty}^{\infty} \mathrm{d}\xi (f_\beta(\xi))^2 = \lambda^{-2/3}\int_{-\infty}^{\infty} \mathrm{d}x (f_{\text{KPZ}}(x))^2 = \frac{1}{2}(G^\beta_{\beta\beta})^{-2/3} c_{PS}. \tag{6.73}$$

For the universal constant

$$c_{PS} := \int_{-\infty}^{\infty} \mathrm{d}x (f_{\text{KPZ}}(x))^2 = 0.3898135914137278 \tag{6.74}$$

we do not have an expression in closed form but its value can be computed numerically with high precision from the Prähofer-Spohn scaling function $f_{\text{KPZ}}(x)$ tabulated in [29]. The double precision result (sixteen significant digits) shown in (6.74) is numerically exact and was obtained from the data in [29] by trapezoidal integration.[1] The scale factors E_α (6.60) that enter the scaling functions of Fibonacci modes with non-zero coupling to a KPZ mode are sensitive to c_{PS} and therefore a precise value is important for numerical fits. For the modified KPZ mode $\beta = \text{KPZ}'$ the functional $\Omega_{\text{KPZ}'}$ has the same form as (6.73), but the numerical value of the integral is not known since the scaling function $f_{\text{KPZ}'}(x)$ for the modified KPZ mode is not known.

6.2.4. Classification of universality classes

We set out to classify the possible universality classes. We summarize the equations that determine the dynamical exponents for a system with n modes:

$$z_\alpha = \begin{cases} 2 & \text{if} \quad \mathbb{I}_\alpha = \emptyset \\ 3/2 & \text{if} \quad \alpha \in \mathbb{I}_\alpha \\ \min_{\beta\in\mathbb{I}_\alpha}\left[\left(1 + \frac{1}{z_\beta}\right)\right] & \text{else} \end{cases} \tag{6.75}$$

[1] Using the data tabulated in [29] one can calculate $f_{\text{KPZ}}(x)$ with at least 90 digits accuracy in the interval $x \in [-8.5, 8.5]$. From this one can achieve with trapezoidal integration a much higher accuracy of c_{PS} than given here. Notice a small but significant numerical error of just over 10% in the value of c_{PS} given below Eq. (10) in Ref. [11].

and

$$1 < z_\alpha \leq 2 \quad \forall \alpha \tag{6.76}$$

In order to solve the non-linear recursion (6.75) in case B we iterate the recursion to find e.g. for a five-fold iteration the continued fraction

$$z_5 = 1 + \cfrac{1}{1 + \cfrac{1}{1 + \cfrac{1}{1 + \frac{1}{z_1}}}} \,. \tag{6.77}$$

Here the modes are ordered in such a fashion that the mode that minimizes the exponent of mode 2 is mode 1 and so on. The continued fraction terminates when a set $\mathbb{I}_\beta$ in this iteration of (6.75) is empty. Remarkably, for $z_1 = 1$ this is the well-known continued-fraction representation of the Kepler ratios which implies that if z_1 is any Kepler ratio $F_\alpha/F_{\alpha+1}$ then $z_n = F_{n+\alpha-1}/F_{n+\alpha}$ is also a Kepler ratio. Thus for each parent critical exponent 2 or 3/2 from case A or case C (which are both Kepler ratios) one generates descendant dynamical exponents which are Kepler ratios as long as the sets $\mathbb{I}_\beta$ are non-empty. If there is no coupling from any mode in case B to a mode from case A or C then the unique solution to the recursion is the golden mean $z_\alpha = \varphi$ for all modes from case B. The golden mean is defined by

$$\varphi := \frac{1}{2}(\sqrt{5} + 1)\,. \tag{6.78}$$

Useful relations are

$$\varphi^{-1} = \frac{1}{2}(\sqrt{5} - 1), \quad \varphi = 1 + \varphi^{-1}, \quad \varphi^2 = 1 + \varphi, \quad \varphi^{-2} = 2 - \varphi. \tag{6.79}$$

The numerical value is $\varphi \approx 1.618$.

6.3. Examples

Given as input parameters the diagonal mode-coupling constants $G^\alpha_{\beta\beta}$, the diffusion coefficients D_α and the KPZ-functionals $\Omega[\hat{f}_{KPZ}]$, $\Omega[\hat{f}_{KPZ'}]$, the explicit scaling solutions of the mode-coupling equations are (6.51), (6.63), (6.70) and (6.71). The dynamical exponents z_α have to be determined self-consistently from the sets $\mathbb{I}_\alpha$ defined in (6.49), using (6.50), (6.57), (6.68) and (6.69). The prefactors of the scaling variable E_α for the Fibonacci modes are then given by (6.54), (6.60), (6.67), (6.72). The asymmetry for the Fibonacci modes is determined by (6.62). We stress that no assumptions other than strict hyperbolicity and subballistic scaling have been made to arrive at these results.

6.3.1. Example 1: $G^1_{11} = G^1_{22} = G^2_{22} = 0$, $G^2_{11} \neq 0$

Mode 1:

For mode 1 we have case A. Eq. (6.50) gives

$$z_1 = 2 \tag{6.80}$$

and (6.51) gives

$$\hat{S}_1(k,t) = \frac{1}{\sqrt{2\pi}} \mathrm{e}^{-iv_1kt - D_1k^2t} \tag{6.81}$$

which is diffusion.

Mode 2:

For mode 2 we have case B. Since there is only one other mode, which has $z_1 = 2$, (6.57) gives

$$z_2 = 3/2. \tag{6.82}$$

From (6.54) we obtain

$$Q_{21} = \frac{(G^2_{11})^2}{\sqrt{2D_1}}, \tag{6.83}$$

from (6.60)

$$E_2 = Q_{21}\frac{\cos\left((2-z_2)\,\frac{\pi}{2}\right)}{|v_2 - v_1|^{2-z_2}} = \frac{(G^2_{11})^2}{2\sqrt{D_1|v_2 - v_1|}} \tag{6.84}$$

and from (6.62)

$$A_2 = \mathrm{sgn}(v_2 - v_1)\,. \tag{6.85}$$

Since $\tan(z_2\pi/2) = -1$ we arrive at

$$\hat{S}_2(k,t) = \frac{1}{\sqrt{2\pi}}\exp\Big(-iv_2kt - E_2|k|^{3/2}t\,(1 + i\mathrm{sgn}(k(v_2 - v_1)))\Big) \tag{6.86}$$

which is in agreement with [2].

6.3.2. Example 2: $G^1_{11} = G^2_{22} = 0$, G^1_{22}, $G^2_{11} \neq 0$

For both modes we have case B. It is expedient to define

$$H_\alpha := 2E_\alpha \tag{6.87}$$
$$g_1 := (G^1_{22})^2 \tag{6.88}$$
$$g_2 := (G^2_{11})^2 \tag{6.89}$$
$$\theta := \frac{4\sin\left((1-\varphi)\frac{\pi}{2}\right)}{\varphi\sin\left(\frac{\pi}{\varphi}\right)|v_1 - v_2|^{2-\varphi}} \tag{6.90}$$

For modes 1 and 2 we have from (6.57)

$$z_1 = 1 + \frac{1}{z_2}, \quad z_2 = 1 + \frac{1}{z_1} \tag{6.91}$$

The solution of these two equations is

$$z_1 = z_2 = \frac{1}{2}(1 + \sqrt{5}) = \varphi \tag{6.92}$$

(see also the relations (6.79)).

From (6.60) and (6.67) we obtain

$$H_1 = Q_{12}\frac{2\sin\left((1-\varphi)\frac{\pi}{2}\right)}{|v_1 - v_2|^{2-\varphi}}, \qquad H_2 = Q_{21}\frac{2\sin\left((1-\varphi)\frac{\pi}{2}\right)}{|v_2 - v_1|^{2-\varphi}} \tag{6.93}$$

$$Q_{12} = \frac{2g_1H_2^{-1/\varphi}}{\varphi\sin\left(\frac{\pi}{\varphi}\right)} \qquad Q_{21} = \frac{2g_2H_1^{-1/\varphi}}{\varphi\sin\left(\frac{\pi}{\varphi}\right)}. \tag{6.94}$$

This yields

$$H_1 = \theta g_1 H_2^{-1/\varphi}, \quad H_2 = \theta g_2 H_1^{-1/\varphi}. \tag{6.95}$$

Solving for H_1 gives

$$H_1^{\varphi-\frac{1}{\varphi}} = \frac{(\theta g_1)^\varphi}{\theta g_2}. \tag{6.96}$$

Using the property $\varphi - 1/\varphi = 1$ of the golden mean we find

$$E_1 = \frac{1}{2}\left(\theta^2 g_1 g_2\right)^{\frac{\varphi-1}{2}} \left(\frac{g_1}{g_2}\right)^{\frac{\varphi+1}{2}} \tag{6.97}$$

Next we use the property of the golden mean to obtain

$$\frac{2\sin\left((1-\varphi)\frac{\pi}{2}\right)}{\sin\left(\frac{\pi}{\varphi}\right)} = \frac{\sin\left((1-\varphi)\frac{\pi}{2}\right)}{\sin\left(\frac{\pi}{2\varphi}\right)\cos\left(\frac{\pi}{2\varphi}\right)} = \frac{1}{\sin\left(\frac{\pi\varphi}{2}\right)}. \tag{6.98}$$

Thus

$$E_1 = \frac{1}{2}\left(\frac{2G_{22}^1 G_{11}^2}{\varphi\sin\left(\frac{\pi\varphi}{2}\right)|v_1-v_2|^{2-\varphi}}\right)^{\varphi-1}\left(\frac{G_{22}^1}{G_{11}^2}\right)^{\varphi+1}. \tag{6.99}$$

With a similar calculation one obtains

$$E_2 = \frac{1}{2}\left(\frac{2G_{22}^1 G_{11}^2}{\varphi\sin\left(\frac{\pi\varphi}{2}\right)|v_1-v_2|^{2-\varphi}}\right)^{\varphi-1}\left(\frac{G_{11}^2}{G_{22}^1}\right)^{\varphi+1}. \tag{6.100}$$

in agreement with [2] since $(2-\varphi)(1-\varphi) = 1 - 2/\varphi$.

Excursion: For $\lambda := G_{22}^1 = G_{11}^2$ and $c = -v_1 = v_2$ this case was treated in [3] in a different way. We demonstrate how the amplitude $E := E_1 = E_2$ arises from Eqs. (6.11), (6.12) and (6.14) in [3]. The point to prove is

$$E = C \tag{6.101}$$

where C is the amplitude of the scaling variable defined in the first line of (6.14).

Proof: We have to compute C from (6.11) and (6.12). To this end we define

$$\mu := 2(4\pi\lambda)^2 a, \quad \nu := \frac{1}{\gamma}\Gamma\left(\frac{1}{\gamma}\right) \tag{6.102}$$

with

$$a = (4\pi c)^{-1+1/\gamma}\frac{\pi}{2\Gamma\left(\frac{1}{\gamma}\right)\cos\left(\frac{\pi}{2\gamma}\right)} = (4\pi c)^{\gamma-2}\frac{\pi}{2\gamma\nu\sin\left(\frac{\pi\gamma}{2}\right)} \tag{6.103}$$

given in (6.11). In the second equality we used $\cos\left(\frac{\pi}{2\gamma}\right) = \sin\left(\frac{\pi\gamma}{2}\right)$ which follows from $1/\gamma = \gamma - 1$.

Now observe that (6.12) yields

$$A = (\mu A)^{-1/\gamma}\nu. \tag{6.104}$$

Taking this to the power γ and using $\gamma - 1 = 1/\gamma$ yields $A^\gamma = (\mu A)^{-1}\nu^\gamma = \mu^{-1+1/\gamma}\nu^{\gamma-1}A^{1/\gamma}$. Since $\gamma - 1/\gamma = 1$ we arrive at

$$A = \mu^{-1}(\mu\nu)^{1/\gamma} \tag{6.105}$$

where according to (6.103)

$$\mu\nu = 2(4\pi\lambda)^2(4\pi c)^{\gamma-2}\frac{\pi}{2\gamma\sin\left(\frac{\pi\gamma}{2}\right)} = \frac{4^\gamma\pi^{1+\gamma}\lambda^2}{\gamma\sin\left(\frac{\pi\gamma}{2}\right)}c^{\gamma-2}. \tag{6.106}$$

This yields

$$(\mu\nu)^{1/\gamma} = 4\pi^\gamma \left(\frac{\lambda^2}{\gamma \sin\left(\frac{\pi\gamma}{2}\right)} \right)^{1/\gamma} c^{1-2/\gamma}. \tag{6.107}$$

Now we note that by definition ((6.12) and first line of (6.14))

$$C = \frac{1}{2}\mu(2\pi)^{-\gamma} A \tag{6.108}$$

which gives

$$C = \frac{1}{4}2^{1-\gamma}\pi^{-\gamma}(\mu\nu)^{1/\gamma} = \frac{1}{2^{1/\gamma}} \left(\frac{\lambda^2}{\gamma \sin\left(\frac{\pi\gamma}{2}\right)} \right)^{1/\gamma} c^{1-2/\gamma} \tag{6.109}$$

Finally we rewrite E in terms of these parameters and $\varphi = \gamma$:

$$E = \frac{1}{2} \left(\frac{2\lambda^2}{\gamma \sin\left(\frac{\pi\gamma}{2}\right)} \right)^{1/\gamma} (2c)^{1-2/\gamma} = \frac{1}{2^{1/\gamma}} \left(\frac{\lambda^2}{\gamma \sin\left(\frac{\pi\gamma}{2}\right)} \right)^{1/\gamma} c^{1-2/\gamma} \tag{6.110}$$

which proves $C = E$. □

6.3.3. Example 3: Two KPZ-modes and the heat mode

Consider three conservation laws and label the modes by 0 and $\sigma = \pm 1$. We consider $G^\sigma_{\sigma\sigma} = \gamma_s$, $G^0_{00} = 0$ and $G^0_{11} = -G^0_{-1-1} = \gamma_h$. Furthermore we assume $v_\sigma = \sigma v$, $v_0 = 0$.

In this case $\mathbb{I}^*_\sigma = \{\sigma\}$ which means that the two modes $\sigma = \pm 1$ are KPZ. Following [1] they can be interpreted as sound modes and mode 0 is the heat mode. For the two sound modes one has [5]

$$\phi_\sigma(x,t) = (\lambda_s t)^{-2/3} f_{KPZ}((x - \sigma v t)/(\lambda_s t)^{2/3}) \tag{6.111}$$

with

$$\lambda_s = 2\sqrt{2}|\gamma_s| = 2^{3/2}|\gamma_s|. \tag{6.112}$$

Notice that $\lambda_s^{-2/3} = 1/2|\gamma_s|^{-2/3}$.

For the heat mode we find from (6.72) the constants $Q_{01} = Q_{0-1} = 2\gamma_h^2 \Gamma(1/3)\,\Omega_{KPZ}$. The structure of the mode-coupling matrices yields $\mathbb{I}^*_0 = \{1, -1\}$. Therefore $z_0 = 5/3$ and from (6.60) one has $E_0 = 2Q_{01}\sin(\pi/3)v^{-1/3}$, $F_0 = 0$. Thus (6.62) gives $A_0 = 0$ and

$$\hat{S}_0(k,t) = \frac{1}{\sqrt{2\pi}} \exp\left(-E_0|k|^{5/3}t\right) \tag{6.113}$$

with

$$E_0 = 2\Gamma\left(\frac{1}{3}\right) \sin\left(\frac{\pi}{3}\right) \gamma_h^2 v^{-1/3} \gamma_s^{-2/3} c_{PS}. \tag{6.114}$$

In order to see that this agrees with Eq. (4.12) of Ref. [5] one has to show that $E_0 = \lambda_h(2\pi)^{-5/3}$ with

$$\lambda_h = \lambda_s^{-2/3}(G^0_{\sigma\sigma})^2(4\pi)^2(2\pi c)^{-1/3} \frac{\pi}{2\Gamma(2/3)\cos(\pi/3)} c_{PS} \tag{6.115}$$

and $v = c$. Indeed, one has, using (6.66) with $x = 3/2$,

$$\begin{aligned} \lambda_h(2\pi)^{-5/3} &= 4\lambda_s^{-2/3}(G^0_{\sigma\sigma})^2 v^{-1/3} \frac{\pi}{2\Gamma(2/3)\cos(\pi/3)} c_{PS} \\ &= 4\gamma_h^2 v^{-1/3} \lambda_s^{-2/3} \frac{\Gamma(1/3)\sin(2\pi/3)}{2\cos(\pi/3)} c_{PS} \end{aligned}$$

$$
\begin{aligned}
&= 4\gamma_h^2 v^{-1/3}\lambda_s^{-2/3}\Gamma(1/3)\sin(\pi/3)c_{PS} \\
&= 2\gamma_h^2 v^{-1/3}\gamma_s^{-2/3}\Gamma(1/3)\sin(\pi/3)c_{PS} \\
&= E_0
\end{aligned}
\tag{6.116}
$$

which is what needed to be shown.

6.4. Conclusions

We have shown that in the scaling limit the one-loop mode-coupling equations for the dynamical structure function for an arbitrary number of conservation laws in the strictly hyperbolic setting can be solved exactly. The solution yields a discrete family of dynamical universality classes with dynamical exponents that are the Kepler ratios $z_\alpha = F_{\alpha+2}/F_{\alpha+1}$ which are in the range $3/2 \leq z_\alpha \leq 2$. The largest exponent $z_1 = 2$ corresponds to a Gaussian diffusive mode, possibly with logarithmic corrections (that we did not consider). The smallest exponent $z_2 = 3/2$ represents three distinct universality classes with different scaling forms of the dynamical structure function: One has the KPZ universality class with the Prähofer-Spohn scaling function [27, 28], a modified KPZ universality class with unknown scaling function [3], and a Fibonacci mode where the scaling function is given by the 3/2-Lévy stable distribution [15, 2, 3]. All higher modes $\alpha \geq 3$ are Fibonacci modes with z_α-Lévy stable distributions as scaling functions, including the golden mean $z_\infty = \varphi$. In order to have a mode α with dynamical exponent z_α one needs at least $\alpha - 1$ conservation laws, with the exception of the golden mean which requires only two conservation laws and always appears at least twice.

Which combinations of universality classes are actually realized in a given physical system depends on which diagonal elements of the mode coupling matrices vanish. This information is fully contained in the macroscopic stationary current-density relation alone. Symmetries of the microscopic equations of motion may also encode relevant information about the diagonal elements of the mode coupling matrices. E.g. for Hamiltonian dynamics as considered in [1] (with three modes denoted by $0, \pm$) only the four diagonal elements $G^{\pm}_{\pm\pm}$, $G^{\mp}_{\pm\pm}$ $G^{\pm}_{00}$ and $G^{0}_{\pm\pm}$ may be non-vanishing by symmetry which generically leads two KPZ modes and a Fibonacci heat mode with $z = 5/3$. In anharmonic chains with three conservation laws only three cases of the classification are realised, viz. (a) 2 KPZ-modes and a Fibonacci 5/3-mode, or 2 diffusive modes and Fibonacci 3/2-mode, or three golden mean Fibonacci modes [30].

The upshot is that diffusion, KPZ, modified KPZ and the Fibonacci family provide a *complete* classification of the dynamical universality classes which we expect to be generic for one-dimensional conservative systems where the long-time dynamics are dominated by the long-wave length behaviour of the modes associated with the conservation laws.

Acknowledgements

This work was supported by Deutsche Forschungsgemeinschaft (DFG) under grant SCHA 636/8-2.

Bibliography

[1] H. van Beijeren, Exact results for anomalous transport in one-dimensional Hamiltonian systems. Phys. Rev. Lett. **108**, 108601 (2012).

[2] Popkov V, Schmidt J, Schütz GM (2015) Universality classes in two-component driven diffusive systems. J. Stat. Phys. **160**(4) 835–860.

[3] Spohn H, Stoltz G (2015) Nonlinear fluctuating hydrodynamics in one dimension: The case of two conserved fields. J. Stat. Phys. **160**(4) 861–884 (2015).

[4] V. Popkov, A. Schadschneider, J. Schmidt, G.M. Schütz, Fibonacci family of dynamical universality classes, Proc. Natl. Acad. Science (USA) **112**(41) 12645-12650 (2015).

[5] H. Spohn, Nonlinear Fluctuating hydrodynamics for anharmonic chains. J. Stat. Phys. **154**, 1191–1227 (2014).

[6] T. Halpin-Healy, K.A. Takeuchi, A KPZ Cocktail-Shaken, not Stirred..., J. Stat. Phys. **160**(4), 794–814 (2015).

[7] A. Roy, A. Dhar, O. Narayan, and S. Sabhapandit, Tagged Particle Diffusion in One-Dimensional Systems with Hamiltonian Dynamics-II, J. Stat. Phys. **160**(1), 73–88 (2015).

[8] L. Delfini, S. Denisov, S. Lepri, R.Livi, P.K. Mohanty and A. Politi, Energy diffusion in hard-point systems. Eur. Phys. J. Special Topics **146**, 21–35 (2007).

[9] A. Politi, Heat conduction of the hard point chain at zero pressure, J. Stat. Mech., P03028 (2011)

[10] C.B. Mendl and H. Spohn, Dynamic correlators of FPU chains and nonlinear fluctuating hydrodynamics. Phys. Rev. Lett. **111**, 230601 (2013).

[11] S. G. Das, A. Dhar, K. Saito, Ch. B. Mendl, and H. Spohn, Numerical test of hydrodynamic fluctuation theory in the Fermi-Pasta-Ulam chain. Phys. Rev. E **90**, 012124 (2014)

[12] D. Das, A. Basu, M. Barma, and S. Ramaswamy, Weak and strong dynamic scaling in a one-dimensional driven coupled-field model: Effects of kinematic waves. Phys. Rev. E **64**, 021402 (2001).

[13] A. Nagar, M. Barma, and S. N. Majumdar, Passive Sliders on Fluctuating Surfaces: Strong-Clustering States. Phys. Rev. Lett. **94**, 240601 (2005).

[14] P.L. Ferrari, T. Sasamoto and H. Spohn, Coupled Kardar-Parisi-Zhang equations in one dimension. J. Stat. Phys. **153**, 377–399 (2013).

[15] V. Popkov, J. Schmidt, and G.M. Schütz, Superdiffusive modes in two-species driven diffusive systems. Phys. Rev. Lett. **112**, 200602 (2014).

[16] S. Chakraborty, S. Pal, S. Chatterjee, and M. Barma, Large compact clusters and fast dynamics in coupled nonequilibrium systems, Phys. Rev. E **93**, 050102(R) (2016).

[17] C. Bernardin and P. Gonçalves, Anomalous fluctuations for a perturbed Hamiltonian system with exponential interactions. Commun. Math. Phys. **325**, 291–332 (2014).

[18] T. Komorowski1 and S. Olla, Ballistic and superdiffusive scales in the macroscopic evolution of a chain of oscillators, Nonlinearity **29**, 962–999 (2016)

[19] H. Spohn, *Large Scale Dynamics of Interacting Particles.* (Springer, Berlin, 1991)

[20] C. Kipnis and C. Landim, *Scaling limits of interacting particle systems* (Springer, Berlin, 1999)

[21] Grisi R, Schütz GM (2011) Current symmetries for particle systems with several conservation laws. J. Stat. Phys. **145** 1499–1512.

[22] Tóth B, Valkó B (2003) Onsager relations and Eulerian hydrodynamic limit for systems with several conservation laws. J. Stat. Phys. **112** 497–521.

[23] Devillard P, Spohn H (1992) Universality class of interface growth with reflection symmetry. J. Stat. Phys. **66** 1089–1099.

[24] E. Lieb, D. Robinson, The finite group velocity of quantum spin systems. Commun. Math. Phys. **28**, 251–257, (1972)

[25] E. Frey, U.C. Täuber, T. Hwa, Mode-coupling and renormalization group results for the noisy Burgers equation. Phys. Rev. E **53**, 4424–4438 (1996).

[26] F. Colaiori and M.A. Moore, Numerical Solution of the Mode-Coupling Equations for the Kardar-Parisi-Zhang Equation in One Dimension Phys. Rev. E **65**, 017105 (2001).

[27] M. Prähofer and H. Spohn, in: *In and Out of Equilibrium*, edited by V. Sidoravicius, Vol. 51 of Progress in Probability (Birkhauser, Boston, 2002).

[28] M. Prähofer and H. Spohn, Exact scaling functions for one-dimensional stationary KPZ growth. J. Stat. Phys. **115**, 255–279 (2004).

[29] M. Prähofer and H. Spohn, http://www-m5.ma.tum.de/KPZ

[30] H. Spohn, The Kardar-Parisi-Zhang equation - a statistical physics perspective. arXiv:1601.00499, (2016).

Part III.

Published Contributions: Defect-Induced Phase Transitions In Driven Diffusive Systems

7. When is a bottleneck a bottleneck?

Andreas Schadschneider, Johannes Schmidt and Vladislav Popkov

Institut für Theoretische Physik, Universität zu Köln, Zülpicher Str. 77, 50937 Cologne, Germany

Published in: Traffic and Granular Flow '15
ISBN 978-3-319-33482-0
doi: 10.1007/978-3-319-33482-0

Abstract: Bottlenecks, i.e. local reductions of capacity, are one of the most relevant scenarios of traffic systems. The asymmetric simple exclusion process (ASEP) with a defect is a minimal model for such a bottleneck scenario. One crucial question is "What is the critical strength of the defect that is required to create global effects, i.e. traffic jams localized at the defect position". Intuitively one would expect that already an arbitrarily small bottleneck strength leads to global effects in the system, e.g. a reduction of the maximal current. Therefore it came as a surprise when, based on computer simulations, it was claimed that the reaction of the system depends in non-continuous way on the defect strength and weak defects do not have a global influence on the system. Here we reconcile intuition and simulations by showing that indeed the critical defect strength is zero. We discuss the implications for the analysis of empirical and numerical data.

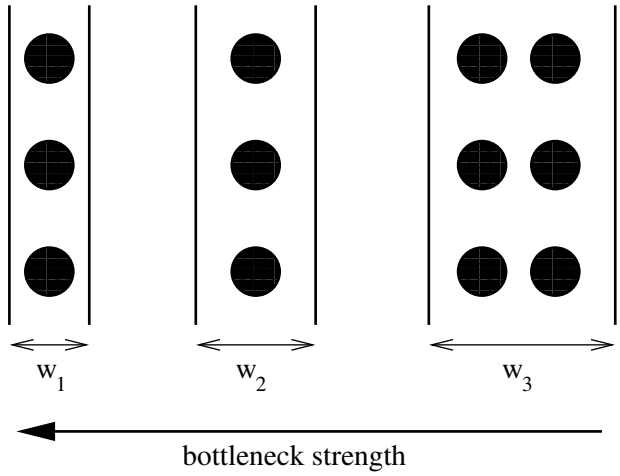

Figure 7.1.: Three corridors of different widths w_j. The bottleneck strength is inversely proportional to w_j. Lane formation leads to a non-continuous dependence of the current on the bottleneck strength.

7.1. Introduction

One of the most important scenarios in any traffic system are bottlenecks, i.e. (local) flow limitations. Typical examples are a reduction in the number of lanes on a highway, local speed limits or narrowing corridors or exits in pedestrian dynamics. The identification of bottlenecks gives important information about the performance of the system. E.g. in evacuations, egress times are usually strongly determined by the relevant bottlenecks. Therefore a proper understanding of bottlenecks and their influence on properties like the flow is highly relevant.

One of the most natural questions is "When does a bottleneck lead to a traffic jam?" Does any bottleneck immediately lead to jam formation or is there a minimal bottleneck strength required? Intuitively one would say that even a small bottleneck strength leads to macroscropically observable effects, like a reduction of the maximal current or jams. However, other scenarios have been considered as well and have even been part of legal guidelines. One prime example in pedestrian dynamics is the dependence of the current on the width of a corridor [1, 2]. Originally it was believed that the current increases stepwise, i.e. non-continuously, with increasing bottleneck width. This increase was assumed to happen when the corridor width allows an additional lane of pedestrians to be formed (Fig. 7.1). Taking the corridor width as measure for the bottleneck strength (rather its inverse) this implies that an increasing bottleneck strength not necessarily leads to smaller current values or jam formation. In the meantime we know that this scenario is not correct and the current increases linearly with the width [1]. However it is still possible that there are situations where lane formation is relevant and this scenario is more adequate, e.g. in colloidal systems [3].

In the following we will take a theoretical physics point of view by considering a minimal model for bottlenecks. Experience shows that the results capture the generic nature of bottleneck transitions.

7.2. Bottlenecks in the ASEP

The Asymmetric Simple Exclusion Process (ASEP) is a paradigmatic model of of nonequilibrium physics (for reviews, see e.g. [4, 5, 6, 7, 8]) and arguably the simplest model that captures essential

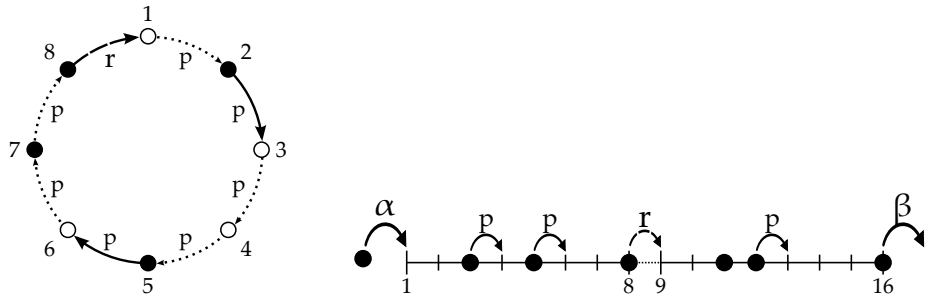

Figure 7.2.: ASEP with a defect (slow bond) where the hopping probability is $r < p$. $r = p$ corresponds to the homogeneous case. Left: Periodic boundary conditions with $N = 8$ sites, the slow bond is between sites 8 and 1. Right: Open boundary conditions with $N = 16$ sites, the slow bond is between sites 8 and 9.

features of traffic systems, i.e. directed motion, volume exclusion and stochastic dynamics. It describes interacting (biased) random walks on a discrete lattice of N sites, where an exclusion rule forbids occupation of a site by more than one particle. A particle at site j moves to site $j + 1$ with rate p if site $j + 1$ is not occupied by another particle (Fig. 7.2). In the following we will mainly use a random-sequential update. If sites are updated synchronously (parallel update) the model is the $v_{\max} = 1$ limit of the Nagel-Schreckenberg model [8, 9]. Many exact results are known for the homogeneous case of the ASEP, e.g. the fundamental diagram and the phase diagram in case of open boundary conditions [4, 5, 6, 7, 8].

A simple but generic model for a bottleneck is obtained by replacing one of the hopping probabilities p by a defect, or slow bond, with hopping probability $r < p$ (Fig. 7.2). Many properties of this defect system have been obtained in a seminal paper by Janowsky and Lebowitz [10]. They have shown that the shape of the fundamental diagram can be understood by a simple mean-field theory. In the stationary state the current can be obtained by matching the current J_{hom} in the homogeneous system with the current J_{def} at the defect. Neglecting correlations at the defect site one finds that the defect has no influence on the system for low densities $\rho < \rho_1$ and large densities $\rho > \rho_2$ [1]. The density remains uniform throughout the whole system and the current is identical to that of the homogeneous system (Fig. 7.3).

For densities $\rho_1 < \rho < \rho_2$, on the other hand, the fundamental diagram exhibits a plateau where the current is independent of the density (Fig. 7.3). The plateau value J_{plat} corresponds to the maximal current that is supported by the defect. In this density regime the stationary state is no longer characterized by a uniform density. Instead phase separation into a high and a low density region is observed. The high density region corresponds to a jam that is formed at the defect position (Fig. 7.4). For periodic boundary conditions the length of jam shows characteristic fluctuations (Fig. 7.4, left) [10].

For the ASEP with periodic boundary conditions, random-sequential update and a defect r mean-field theory makes quantitative predictions for the phase separated regime [10]. The value of the current in the plateau region is given by

$$J_{\text{plat}} = \frac{pr}{(p+r)^2} \tag{7.1}$$

and the densities in the low and high density region by

$$\rho_\ell = \frac{r}{p+r}\,. \qquad \text{and} \qquad \rho_h = \frac{p}{p+r} \tag{7.2}$$

[1] For the ASEP, due to particle-hole symmetry, $\rho_1 = 1 - \rho_2$.

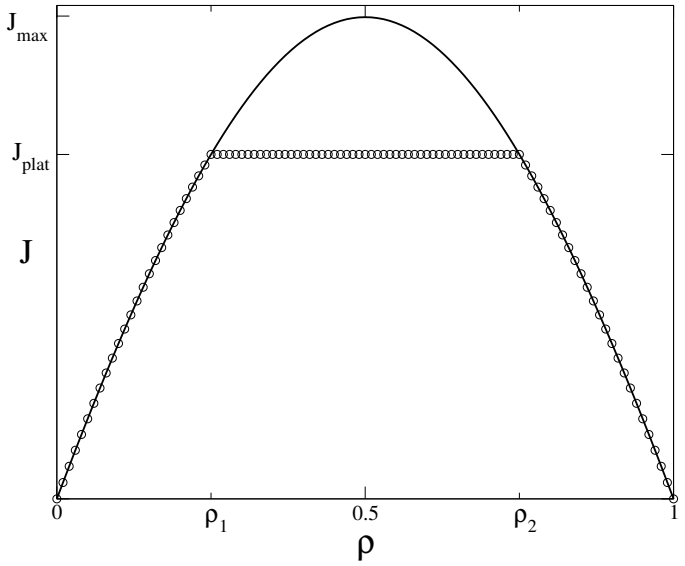

Figure 7.3.: Fundamental diagram of the ASEP with a defect r (circles). The full line is the fundamental diagram of the homogeneous system without defect. The current $J(r)$ is independent of the global density ρ for $\rho_1 < \rho < \rho_2$. The plateau value J_{plat} in this region is smaller than the maximal flow J_{max} in the homogeneous system.

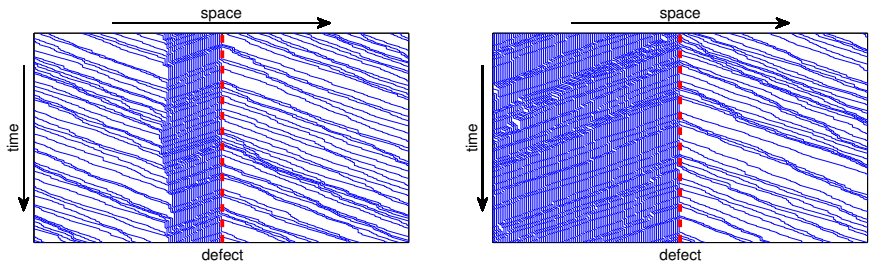

Figure 7.4.: Phase separation in the plateau regime. Left: Periodic boundary conditions. Right: Open boundary conditions.

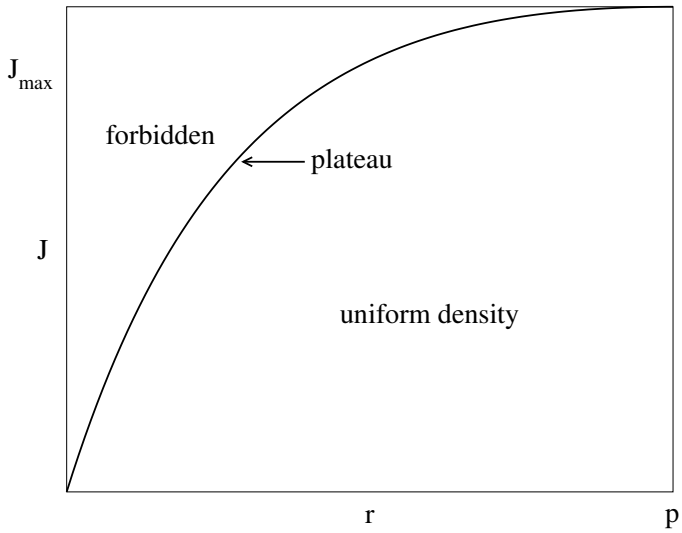

Figure 7.5.: Phase diagram of the ASEP with defect according to [10]. The full line shows the current at the plateau as function of the defect hopping rate r. Any $r < p$ leads to a reduction of the maximal current compared to that of the homogeneous system $J_{\max}$. In the phase of uniform density the defect has only local effects.

The critical densities ρ_1, ρ_2 which determine the plateau regime $\rho_1 < \rho < \rho_2$ are simply

$$\rho_1 = \rho_\ell \qquad \text{and} \qquad \rho_2 = \rho_h \,. \tag{7.3}$$

The mean-field results are supported by systematic series expansions [11].

Fig. 7.5 shows the resulting phase diagram. For any defect $r < p$ only currents up to the plateau value J_{plat} can be realized in the system which then phase separates into a high density region pinned at the defect and a low density regime. For currents $J < J_{\text{plat}}$ the density is uniform. The important point is that $J_{\text{plat}} < J_{\max}$ for any $r < p$ where $J_{\max}$ is the maximal current in the homogeneous system. In other words: any bottleneck leads to a reduction of the current and a phase separated state (at intermediate densities).

7.3. What is the critical bottleneck strength?

Mean-field theory predicts that any bottleneck $r < p$ leads to the formation of a plateau in the fundamental diagram and the associated phase-separated state [10]. Defining the bottleneck strength by

$$\Delta p = \frac{p - r}{p} \tag{7.4}$$

this implies that the critical bottleneck strength $(\Delta p)_c$ at which the defect has global influence on the system (e.g. its current or the density) is predicted to be

$$(\Delta p)_c = 0 \,, \qquad \text{i.e.} \quad r_c = p \,. \tag{7.5}$$

As mentioned in the Introduction this is what is intuitively expected. Therefore it came as quite a surprise when it was claimed [12], based on extensive computer simulations, that $r_c \approx 0.8$, i.e.

$$(\Delta p)_c^{(\text{Ha})} \approx 0.2 \,. \tag{7.6}$$

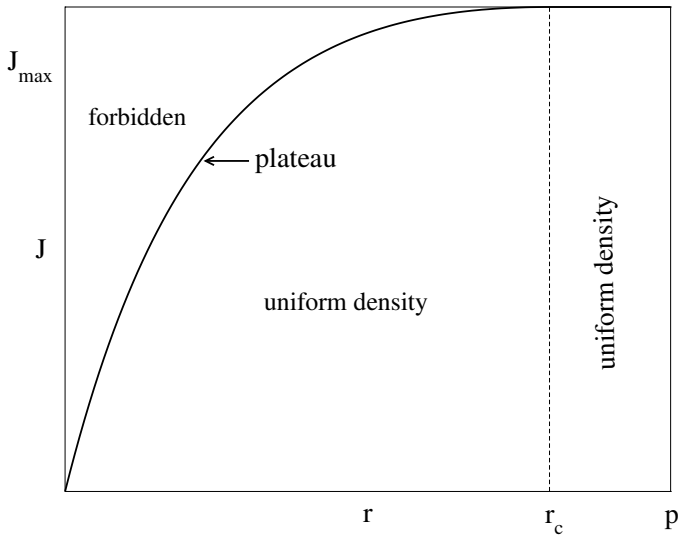

Figure 7.6.: Phase diagram of ASEP with defect according to [12]. Defects with $r_c < r \leq p$ have no influence on the current J.

The corresponding phase diagram is shown in Fig. 7.6. In contrast to Fig. 7.5, for defects $r > r_c$ all currents up to $J_{\max}$ can be realized and there is no phase separation at any density for weak defects! In this case the bottleneck has only *local* effects which can be observed near the defect, but not in the whole system.

Due to this apparent contradiction with expectations we have revisited the ASEP defect problem in [13] based on highly accurate Monte Carlo simulations. Similar to [12] we have simulated the ASEP with open boundary conditions, random-sequential dynamics (with $p = 1$) and a defect in the middle of the system (Fig. 7.2). However, choosing $\alpha = \beta = \frac{1}{2}$ as in [12], corresponds exactly to the phase boundary of the high, low and maximal current phase [5, 6, 8]. Fluctuations in finite-size systems will systematically underestimate the defect current $J(r)$ [13]. We have therefore choosen $\alpha = \beta = 1$ well inside the maximal current phase which allows to obtain a much better statistics.

To determine rather subtle bottleneck effects, very good statistics and advanced Monte Carlo techniques are required. To minimizes errors induced by pseudo-random number generators we have used the Mersenne Twister [13].

Measurements of bottleneck effects for small defect strengths are easily hidden by fluctuations. Instead of using independent measurements for each defect strength r the systems are evolved in parallel, i.e. with the same protocol and the same set of random numbers, which leads to a strong suppression of fluctuations [13].

In order to minimize finite-size corrections, system lengths of up to $N = 200.000$ were considered (Fig. 7.7) which is two orders of magnitude larger than the systems considered in [12].

To estimate the global effects of the defect we first considered the finite-size current $J(N, r)$ through a system of length N and with a defect r. Due to the fact that finite size corrections lead to an enhanced current, i.e. $J(r, N) > J(r, N = \infty)$, one finds a lower bound for the critical hopping rate by satisfying $J(N, r_c) - J(N = \infty, r = 1) < 0$. However, in this way we only could derive a lower bound $r_c \geq 0.86$ for the critical hopping rate (Fig. 7.7). Assuming the existence of an essential singularity at $r_c = 1$, *i.e.* $j(1) - j(r) \sim \exp(-a/(1-r))$ [11], further improvement of the lower bound for the critical defect r_c by increasing the system length is a hopeless enterprise: e.g. a numerical proof of $r_c > 0.9$, $r_c > 0.95$, $r_c > 0.99$ would require $N > 10^{10}$, $N > 10^{22}$,

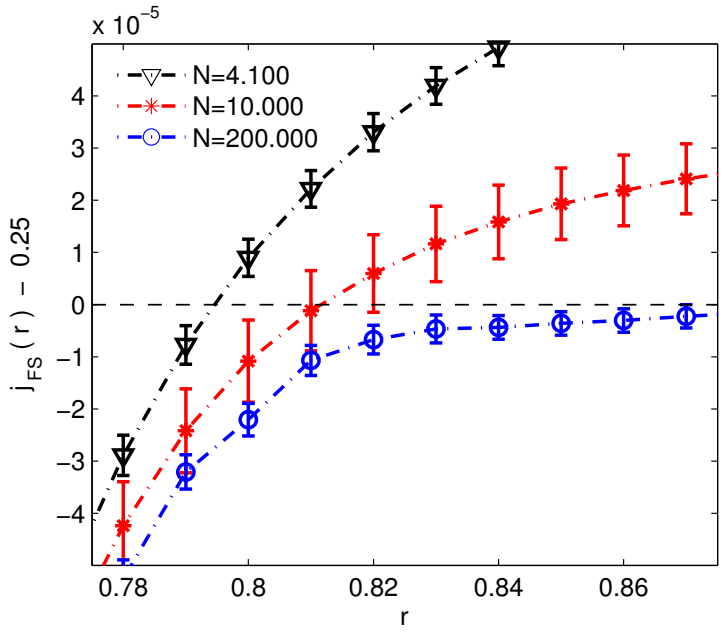

Figure 7.7.: Finite-size corrections to the current. The exactly known current in the infinite homogeneous system is $J(N = \infty, r = 1) = 1/4$.

$N > 10^{147}$, respectively.

A much better quantity to determine the global influence of the defect (see e.g. Fig. 7.4, right) is the density profile or rather the difference between the density profile of the defect system with a corresponding homogeneous system (Fig. 7.8). Using the approach of parallel evolving systems we could clearly show a nonlocal influence on the density profile for defect strengths up to $r = 0.99$ (Fig. 7.8). This strongly supports the mean-field prediction $r_c = 1$.

7.4. Discussion and relevance for empirical results

Despite its relevance for applications some fundamental aspects of bottlenecks are not fully understood. Even for a minimal model like the ASEP with a defect the influence of weak bottlenecks is rather subtle and can be easily lost in fluctuations.

We have shown how to reconcile computer simulations with the intuition that even small defects have a global influence on the system. These effects are not easily seen in a reduction of the current which presumably shows a non-analytic dependence on the bottleneck strength. Bottlenecks are better identified by their effects on the density profile which spreads throughout the whole system..

Based on a careful statistical analysis of Monte Carlo simulations we have found strong evidence that an arbitrarily weak defect $\Delta p \to 0$ in the ASEP has a global influence on the system. Meanwhile a mathematical proof of $(\Delta p)_c = 0$ has been announced in [14].

These results are believed to be generic for bottleneck systems. As a consequence the identification of weak bottlenecks in noisy empirical data is extremely difficult. Even for computer simulations very good statistics is required. Since the effect on the current is rather small, the density profile might be a better indicator for the presence of weak bottlenecks.

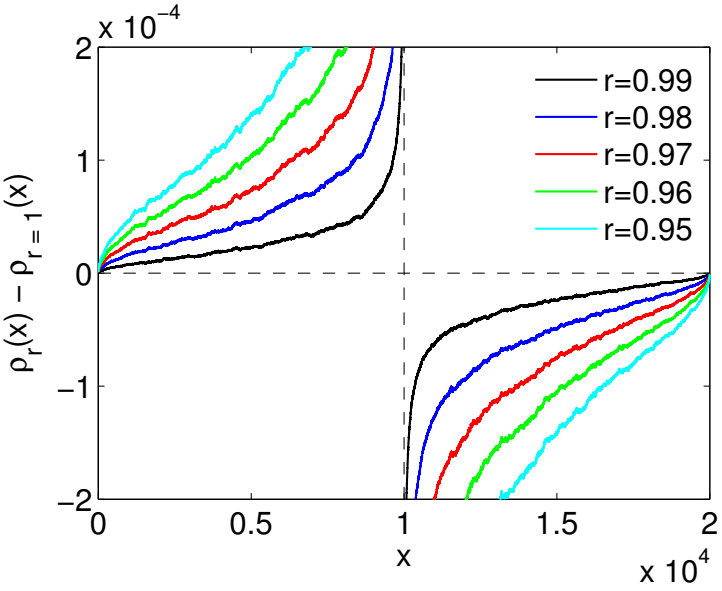

Figure 7.8.: Arbitrary defects r have a non-local effect on the density profile. The figure shows the difference between the density profile $\rho_r(x)$ with and that without defect $\rho_{r=1}(x)$ where $x = j/N$ is the rescaled position.

Acknowledgements

We dedicate this contribution to the memory of our friend and colleague Matthias Craesmeyer. Financial support by the DFG under grant SCHA 636/8-1 is gratefully acknowledged.

Bibliography

[1] Seyfried, A., Passon, O., Steffen, B., Boltes, M., Rupprecht, T., Klingsch, W.: New insights into pedestrian flow through bottlenecks. Transp. Science **43**, 395 (2009)

[2] Schadschneider, A., Seyfried, A.: Empirical results for pedestrian dynamics and their implications for modeling. Netw. Heterog. Media **6**, 545 (2011)

[3] Vissers, T., Wysocki, A., Rex, M., Löwen, H., Royall, C., Imhof, P.A., van Blaaderen, A.: Lane formation in driven mixtures of oppositely charged colloids. Soft Matter **7**, 2352 (2011)

[4] Liggett, T.M.: Stochastic Interacting Systems: Contact, Voter and Exclusion Processes, Springer, New York (1999)

[5] Derrida, B.: An exactly soluble non-equilibrium system: The asymmetric simple exclusion process. Phys. Rep. **301**, 65 (1998)

[6] Schütz, G.M.: Exactly Solvable Models for Many-Body Systems Far from Equilibrium. in: Phase Transitions and Critical Phenomena, Vol. 19, C. Domb and J. L. Lebowitz Ed., Academic Press, San Diego (2001)

[7] Blythe, R.A., Evans, M.R.: Nonequilibrium steady states of matrix product form: a solver's guide. J. Phys. A: Math. Gen. **40**, R333 (2007)

[8] Schadschneider, A., Chowdhury, D., Nishinari, K.: Stochastic Transport in Complex Systems: From Molecules to Vehicles, Elsevier Science, Amsterdam (2010)

[9] Nagel, K., Schreckenberg, M.: A cellular automaton model for freeway traffic. J. Phys. I (France) **2**, 2221 (1992)

[10] Janowsky, S.A., Lebowitz, J.L.: Finite-size effects and shock fluctuations in the asymmetric simple-exclusion process. Phys. Rev. A **45**, 618 (1992)

[11] Costin, O., Lebowitz, J.L., Speer, E.R., Troiani, A.: The blockage problem. Bull. Inst. Math. Acad. Sin. **8**, 49 (2013)

[12] Ha, M., Timonen, J., den Nijs, M.: Queuing transitions in the asymmetric simple exclusion process. Phys. Rev. E **58**, 056122 (2003)

[13] Schmidt, J., Popkov, V., Schadschneider, A.: Defect-induced phase transition in the asymmetric simple exclusion process. EPL **110**, 20008 (2015)

[14] Basu, R., Sidoravicius, V., Sly, A.: Last passage percolation with a defect line and the solution of the slow bond problem. arXiv:1408.3464

8. Defect-induced phase transition in the asymmetric simple exclusion process

Johannes Schmidt[1], **Vladislav Popkov**[1,2] **and Andreas Schadschneider**[1]

[1] *Institut für Theoretische Physik, Universität zu Köln, Zülpicher Str. 77, 50937 Cologne, Germany*
[2] *CSDC Università di Firenze, via G.Sansone 1, 50019 Sesto Fiorentino, Italy*

PACS numbers: 02.50.Ey, 05.70.Fh, 05.60.-k

Published in: Europhysics Letters (EPL)
May 2015, vol. 110, no. 2, p. 20008
doi: 10.1209/0295-5075/110/20008

Abstract: We reconsider the long-standing question of the critical defect hopping rate r_c in the one-dimensional totally asymmetric exclusion process (TASEP) with a slow bond (defect). For $r < r_c$ a phase separated state is observed due to queuing at the defect site whereas for $r \geq r_c$ the defect site has only local effects on the stationary state of the homogeneous system. Mean-field theory predicts $r_c = 1$ (when hopping rates outside the defect bond are equal to 1) but numerical investigations seem to indicate $r_c \approx 0.80(2)$. Here we improve the numerics to show that $r_c > 0.99$ and give strong evidence that indeed $r_c = 1$ as predicted by mean-field theory, and anticipated by recent theoretical findings.

8.1. Introduction

Despite much progress in recent years, our understanding of nonequilibrium stationary states is far from complete. This especially concerns the effects of disorder and defects in driven diffusive systems. Although it is well established that in driven systems already a localized defect can have a global influence on the behavior, many open questions remain. Since e.g. no analogue of the Harris criterion [1] is known for nonequilibrium situations no general statements on the influence of weak disorder on the critical behavior can be made [2].

Surprisingly even for the simplest model of driven diffusion, the totally asymmetric exclusion process (TASEP), the precise influence of a single defect has not been fully clarified for a long time. It is well-known since the seminal work of Janowsky and Lebowitz [3, 4] that such a defect has not just a local effect, but changes the nature of the stationary state dramatically (for reviews, see e.g. [5, 6]). What is not clear up to now is whether a finite critical strength of the defect is required to create global effects. Mean-field theory predicts a global influence already for arbitrarily small defect strengths whereas the most accurate numerical investigations up to date [7] show strong indications that a finite defect strength is required.

Recently the problem has been newly addressed in the mathematical literature, in a series of works [8, 9, 10, 11]. In [8], based on analytical arguments from series expansions and results for related systems (e.g. directed polymers) it was argued that an arbitrarily small defect in a TASEP with open boundaries will have global effects, e.g. on the current and on the density profile. In [9], the authors claim to have proved rigorously, that the steady current in TASEP with a slow bond is always affected for any nonzero defect strength.

In view of these new findings, the numerical studies predicting finite critical blockage strength, appear even more paradoxical, with the $r_c = 1$ problem finally settled. It remains to understand if the effects of the slow bond are so weak that they cannot be observed in numerics, which would make the beautiful theoretical result a pure theoretical construction without any practical content.

It is the purpose of this letter to show that this is not the case, and to provide detailed results from highly accurate Monte Carlo simulations which strongly support the theory. Moreover, we also resolve the apparent numerical paradox, revisiting previous numerical studies and pointing out exactly where the error of the previous numerical studies was.

8.2. Model

The totally asymmetric simple exclusion process (TASEP) is a paradigmatic model of nonequilibrium physics (for reviews, see e.g. [12, 13, 14, 15, 16, 17, 18]) describes interacting (biased) random walks on a discrete lattice of N sites, where an exclusion rule forbids occupation of a site by more than one particle. A particle at site k moves to site $k+1$ at rate p if site $k+1$ is not occupied by another particle. The boundary sites $k = 1$ and $k = N$ are coupled to particle reservoirs. If site 1 is empty, a particle is inserted at rate α. A particle on site N is removed from the system at rate β. Sites are updated using random-sequential dynamics. Throughout the paper, we will set $p = 1$.

Here we consider a system of two TASEPs of length $N/2$ coupled by a slow bond between sites $N/2$ and $N/2+1$ with reduced hopping rate $r \leq p$ (Fig. 8.1). This is equivalent to a TASEP of N sites with a defect site in the middle and defect strength $p - r$.

For periodic boundary conditions this problem has been analyzed by Janowsky and Lebowitz [3, 4]. Below a critical rate r_c they found a phase separation into high and low density regions due to queuing at the defect site. The two phases are separated by a shock (domain wall). The phase separation is also reflected in the current-density relation (fundamental diagram) which

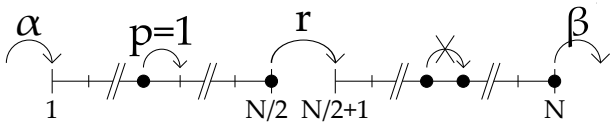

Figure 8.1.: Open TASEP with a slow bond ($r < 1$) in the middle.

shows a density-independent current at intermediate densities due to the current-limiting effect of the slow bond. A mean-field theory that neglects correlations at the defect site predicts that $r_c = 1$ [3], i.e. an arbitrarily small defect leads to a phase separated stationary state. This is supported by series expansions obtained from exact results for small systems [4]. Exact results have been obtained for the case of sublattice-parallel update with deterministic bulk hopping by Bethe Ansatz [19] and matrix-product Ansatz [20]. Also in this case $r_c = 1$.

For open boundary conditions, a mean-field treatment of the TASEP with a defect in the middle of the system yields $r_c = 1$ [21]. Later Ha et al. [7] studied the problem numerically (with rates $p = 1$, $\alpha = \beta = 1/2$). They suggested that $r_c = 0.80\,(2)$, see next section for details.

Due to its relevance e.g. for intracellular transport, recently the open TASEP with several defects has attracted some attention, see e.g. [22, 23, 24, 25, 26, 27, 28, 29, 30, 31, 32, 33].

8.3. Simulations

In order to analyze the system with a defect we perform Monte Carlo (MC) simulations for an open TASEP on a chain of large size ($N \leq 200.000$), to minimize finite-size effects as much as possible. Both bulk hopping rates and boundary hopping rates are chosen equal to 1. This corresponds to a point in the maximal current phase which is characterized by a spatially homogeneous steady state with bulk density of particles $\rho_{\text{bulk}} = 1/2$ and the current $j(\infty) = \rho_{\text{bulk}}(1 - \rho_{\text{bulk}}) = 1/4$ in the limit of an infinite system size [13].

Initially $N/2$ particles are distributed randomly within a homogeneous chain without a defect. Then, the relaxation of the system is performed for $100N^2$ single Monte Carlo updates [34], according to the dynamical rules for $\alpha = \beta = 1$.

After the initial relaxation, the weak bond is introduced in the middle of the system, meaning that a particle hop from site $k = N/2$ to $N/2 + 1$ occurs with reduced rate $r < 1$, see Fig. 8.1. Then the system is relaxed further for $100N^2$ single Monte Carlo updates and the average current is recorded. It can be written as

$$j_{\text{FS}}(r, N, \alpha, \beta) = j(r, \infty) + \delta_{\text{FS}}(r, N, \alpha, \beta) \tag{8.1}$$

where δ_{FS} are finite-size corrections. The relaxation to steady state is controlled by a comparison of the finite-size corrections of the current measured numerically with the theoretically-predicted value, see Fig. 8.2.

We aim at determining a lower bound for the critical r_c at which the phase separation starts. It is well-known [35] that the leading finite-size corrections to the current of the homogeneous TASEP for $\alpha = \beta = 1$ are positive,

$$\begin{aligned} j_{\text{FS}}(r = 1, N, \alpha = 1, \beta = 1) &= j(r = 1, \infty) + \frac{3}{8N} + O(N^2) \\ &> j(r = 1, \infty)\,. \end{aligned} \tag{8.2}$$

Therefore, if for some defect hopping rate r_0 the steady current within the error bars is *smaller* than its limiting value, $j(r_0, N) < 1/4$, this would definitely mean that $r_c > r_0$. The lower bound

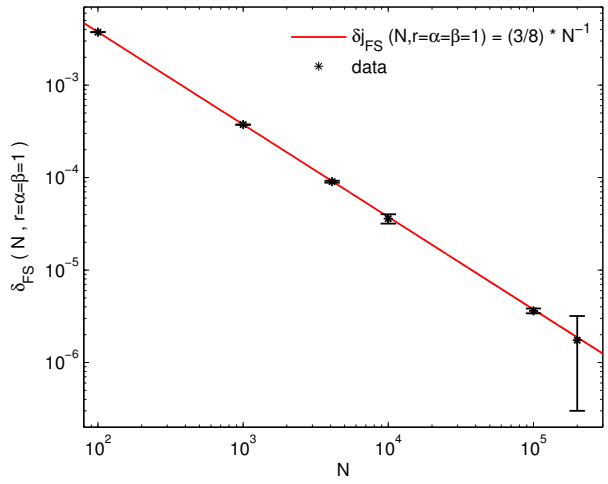

Figure 8.2.: Finite-size corrections of the steady current for a homogeneous model without slow bond. Error bars show the 99% confidence bound, the red line marks the exact leading finite-size correction in $1/N$.

r^* for r_c is then calculated as the point where $j(r^*, N) = 1/4$, accounting also for error bars, see Fig. 8.3. Note that our reasoning does not involve any a priori assumptions except from the positiveness of finite-size corrections to the current. In this way, we obtain a lower bound for r_c which depends on the system size. For larger system size, finite-size corrections are smaller and better estimates for the lower bound can be made, see Fig. 8.3. For system size $N = 2 \cdot 10^5$ we obtain the following lower bound estimate,

$$r_c > 0.86\,. \tag{8.3}$$

It is difficult to improve the lower bound (8.3) by a further increase of the system size N, because much larger system sizes are not numerically accessible. However, already the lower bound value 0.86 definitely contradicts the result of Ha et al. [7], where $r_c = 0.80\,(2)$ was found. Their estimate was based on a different argument. In order to understand the reason for the contradiction, we repeated Monte Carlo simulations with the same parameters as in [7], and in particular using the much smaller system size of $N = 4100$.

The key quantity analyzed by Ha et al., is defined as

$$\Delta_b \propto \left| \rho_{\text{bulk,segment}} - \frac{1}{2} \right| \tag{8.4}$$

or

$$\Delta_b = 2\sqrt{j(r=1,N) - j(r,N)}\,. \tag{8.5}$$

It is assumed to obey the scaling form

$$\Delta_b \sim (r_c - r)^{-\beta} \tag{8.6}$$

near the phase boundary. Then, the best straight line fit on the double logarithmic plot of Δ_b versus $r_c - r$, has lead to the conclusion $r_c = 0.80\,(2)$. We repeated the relevant Monte Carlo simulations for the parameters chosen in [7]. Fig. 8.4 shows the double logarithmic plot of Δ_b versus $r_c - r$. The square window corresponds to the area shown in the original paper, see Fig. 4a of [7]. We can see that what might look as a straight line inside the window, certainly fails to

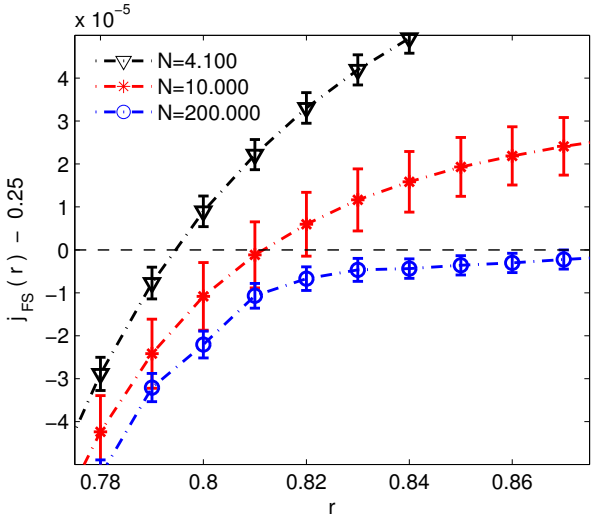

Figure 8.3.: Finite-size current j_{FS} (see eq. (8.1)) versus defect rate r for $\alpha = \beta = 1$. With $j(r) \leq j_{FS}(r)$ the plot shows $r_c > 0.86$ which is significantly larger than $r_c = 0.80\,(2)$ suggested in [7]. Currents are averaged over all sites with $7.5 \cdot 10^7 - 5 \cdot 10^8$ histories. Error bars show the 99% confidence interval.

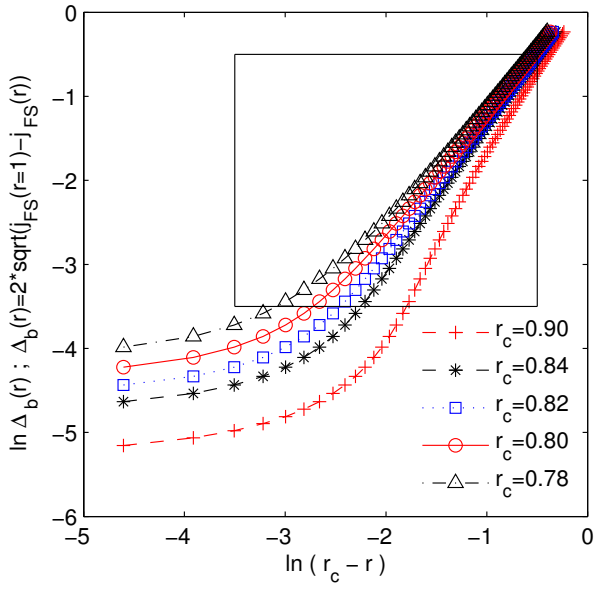

Figure 8.4.: Double logarithmic plot of Δ_b versus $(r_c - r)$. Parameters are $N = 4100, \alpha = \beta = 0.5$. The box indicates the regime plotted in Fig. 4a of [7]. Averaging over all sites of the system and over $3 \cdot 10^8$ histories is performed. Statistical errors are smaller than the symbol size.

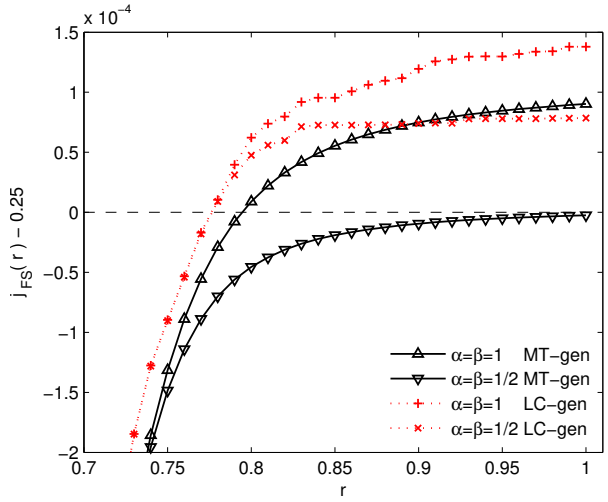

Figure 8.5.: Finite-size corrections of the current eq. (8.1), for a different choices of a random number generators. Parameters: $N = 4100$. Triangles correspond to Mersenne Twister random number generator and crosses correspond to a standard Park and Miller new minimal standard (LC-gen, linear congruential) random number generator [37]. Averaging of the current over all bonds and over $3 \cdot 10^8 - 5 \cdot 10^8$ histories is performed. Statistical errors are smaller than the symbol size.

straighten outside the window. Thus the conclusion of [7] of a phase transition at $r_c = 0.80\,(2)$ is not justified.

It is instructive at this point to stress the importance of a choice of an adequate random generator to perform the Monte Carlo update. This choice is crucial for producing high quality Monte Carlo data [36]. In Fig. 8.5, Monte Carlo data for the current, produced by different random number generators, are compared and show systematic differences. For our simulations throughout this paper we are using Mersenne-Twister-generator which is known for producing high quality pseudo-random numbers. In Fig. 8.5 it is seen that using the most common Park and Miller new minimal standard linear congruential generator [37] leads to a systematic overestimation of the current, and might consequently lead to wrong conclusions in the subtle TASEP blockage problem.

We also note, that the point $\alpha = \beta = 1/2$ as chosen for studying the blockage problem in [7] lies exactly at the phase boundary between the maximal current, low density and high density phases [12, 13, 14, 15, 16, 17, 18]. This may lead to further complications and an additional reduction of the steady current due to fluctuations. We stress that for our study we choose $\alpha = \beta = 1$, i.e. a point well inside the maximal current phase far from the boundaries with the low density TASEP phase ($\alpha = 1/2$) and the high density TASEP phase ($\beta = 1/2$).

8.4. Effects of a defect in finite systems: parallel evolution

As is already mentioned, both mean-field theory and series expansions arguments hint at $r_c = 1$. Assuming the existence of an essential singularity at $r_c = 1$, $j(1) - j(r) \sim \exp(-a/(1-r))$ [8], further improvement of the lower bound for the weak bond problem by an increase of the system size is a hopeless enterprise: e.g. a numerical proof $r_c > 0.9, r_c > 0.95, r_c > 0.99$) with the direct method (see Fig. 8.3) would require $N > 10^{10}$, $N > 10^{22}$, $N > 10^{147}$ respectively.

Instead of increasing the system size, we address the problem of a critical blockage strength in

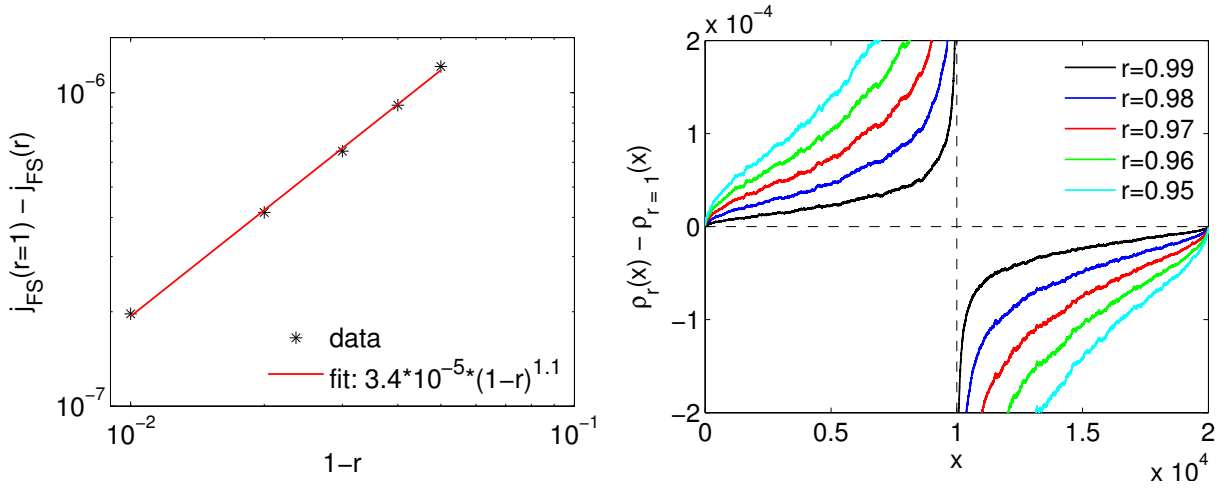

Figure 8.6.: Steady current differences (top) and density differences (bottom) between the parallel evolving copies of the same system (with and without defect). Averaging over 10^9 histories is performed for systems with $N = 2 \cdot 10^4$ sites. For the currents (top) error bars (not shown) are of the order of the symbol size. For the density differences (bottom), statistical errors are in the range from 10^{-8} close to the reservoirs up to $4.6 \cdot 10^{-6}$ in the vicinity of the defect.

different way by measuring how a TASEP responds to a slow bond, as discussed below.

After the pre-relaxation performed on the homogeneous system as described above, we make two copies of the system configuration. Then a slow bond is introduced in one copy whereas the other remains homogeneous. Both copies evolve in time according to the same protocol, i.e. using the same set of random numbers for both systems. The averaged density profiles of both copies are compared after sufficiently large relaxation time. Due to the defect site, one expects a density gradient forming locally in the vicinity of the blockage for any $r < 1$. If the disturbance remains local, the state of the system far from the blockage will not change, with respect to a homogeneous system. In contrast, a non-local disturbance spreading to the whole system would lead to a reduction of the global current and to phase separation. Thus the current and the density profile are sensitive probes for the effects of the slow bond and for the possible occurrence of a phase separated state.

Performing extensive MC simulations we are able to see a non-local effect of the blockage up to $r = 0.99$, both in steady current and in local particle density far away from the blockage, see Fig. 8.6. Consequently, a presence of the weak bond has a small but systematic effect on both the current and the local density n_k far away from the blockage site. This shows that the blockage produces perturbations which do not remain local, but spread over the bulk.

8.5. Conclusion

We have revisited a long-standing problem of a TASEP with a weak bond. Since the effects are small for small defect strength, this is a subtle problem that requires high numerical accuracy in simulations. We have shown that here even the choice of the random number generator is crucial. By Monte Carlo simulations performed on large systems (up to 200.000 sites), we have established a new lower bound for the critical defect strength leading to phase separation. For the current, we could clearly show a reduction compared to the value $j(r = 1) = 1/4$ of the homogeneous

system for defect hopping rates up to $r = 0.86$. Therefore we conclude that $r_c > 0.86$. Studying a parallel evolution of two initially identical systems, with and without a weak bond, we find systematic *global* effects induced by the weak bond for defect hopping rate up to $r \leq 0.99$. Our study supports the hypothesis that the critical blockage hopping rate is $r_c = 1$, and definitely rules out a previously obtained critical value $r_c = 0.80(2)$. This indicates that the mean-field theory prediction is indeed correct which is important since it is used quite frequently also in more complex situations, like flows on networks [38, 39, 40, 41, 42] or as effective models for highway traffic near ramps [43].

Acknowledgements

We thank Herbert Spohn for helpful comments on a preliminary version of the manuscript. This work was supported by Deutsche Forschungsgemeinschaft (DFG) under grant SCHA 636/8-1.

Bibliography

[1] A.B. Harris: J. Phys. C 7, 1671 (1974)

[2] R. Stinchcombe: J. Phys.: Condens. Matter 14, 1473 (2002)

[3] S.A. Janowsky, J.L. Lebowitz: Phys. Rev. A 45, 618 (1992)

[4] S.A. Janowsky, J.L. Lebowitz: J. Stat. Phys. 77, 35 (1994)

[5] J. Krug: Braz. J. Phys. 30, 97 (2000)

[6] M. Barma: Physica A 372, 22 (2006)

[7] M. Ha, J. Timonen, M. den Nijs: Phys. Rev. E 58, 056122 (2003)

[8] O. Costin, J. L. Lebowitz, E. R. Speer, A. Troiani: Bulletin of the Institute of Mathematics Academia Sinica 8, 49 (2013)

[9] R. Basu, V. Sidoravicius and A. Sly, arXiv:1408.3464

[10] J.Calder, J. Stat. Phys. **158**, 903 (2015)

[11] B. Scoppola, C. Lancia e R. Mariani, arXiv:1409.0268

[12] T.M. Liggett: *Stochastic Interacting Systems: Contact, Voter and Exclusion Processes*, Springer, New York (1999)

[13] G.M. Schütz, in *Phase Transitions and Critical Phenomena vol 19.*, C. Domb and J. L. Lebowitz Ed., Academic Press, San Diego (2001)

[14] R. K. P. Zia and B. Schmittmann, J. Stat. Mech. (2007) P07012

[15] A. Schadschneider, D. Chowdhury, K. Nishinari: *Stochastic Transport in Complex Systems: From Molecules to Vehicles*, Elsevier Science, Amsterdam (2010)

[16] P.L. Krapivsky, S. Redner, E. Ben-Naim: *A Kinetic View of Statistical Physics*, Cambridge University Press, Cambridge (2010)

[17] R.A. Blythe, M.R. Evans: J. Phys. A: Math. Gen. 40, R333 (2007)

[18] B. Derrida: J. Stat. Mech. (2007) P07023

[19] G. Schütz: J. Stat. Phys. 71, 471 (1993)

[20] H. Hinrichsen, S. Sandow: J. Phys. A 30, 2745 (1997)

[21] A.B. Kolomeisky: J. Phys. A 31, 1153 (1998)

[22] G. Tripathy, M. Barma: Phys. Rev. E **58**, 1911 (1997)

[23] T. Chou, G.W. Lakatos: Phys. Rev. Lett. 93, 198101 (2004)

[24] G.W. Lakatos, J. O'Brien, T. Chou: J. Phys. A 39, 2253 (2006)

[25] R.J. Harris, R.B. Stinchcombe: Phys. Rev. E **70**, 016108 (2004)

[26] C. Enaud, B. Derrida: Europhys. Lett. **66**, 83 (2004)

[27] R. Juhasz, L. Santen, F. Igloi: Phys. Rev. E **74**, 061101 (2006)

[28] P. Pierobon, M. Mobilia, R. Kouyos, E. Frey: Phys. Rev. E 74, 031906 (2006)

[29] J.J. Dong, B. Schmittmann, R.K.P. Zia: J. Stat. Phys. 128, 21 (2007)

[30] M.E. Foulaadvand, S. Chaaboki, M. Saalehi: Phys. Rev. E **75**, 011127 (2007)

[31] P. Greulich, A. Schadschneider: Physica A387, 1972 (2008)

[32] P. Greulich, A. Schadschneider: J. Stat. Mech. (2008) P04009

[33] P. Greulich, A. Schadschneider: Phys. Rev. E 79, 031107 (2009)

[34] A single Monte Carlo update consists in choosing a bond at random, and updating its configuration according to dynamical rules.

[35] B. Derrida, M. Evans: J. Physique I 3, 311 (1993)

[36] P. L'Ecuyer, R. Simard: ACM Trans. Math. Softw. 33, 22 (2007)

[37] S. K. Park, K. W. Miller: Commun. ACM 31, 1192 (1988)

[38] B. Embley, A. Parmeggiani, N. Kern: Phys. Rev. E 80, 041128 (2009)

[39] T. Ezaki, K. Nishinari: J. Stat. Mech. (2012) P11002

[40] A. Raguin, A. Parmeggiani, N. Kern: Phys. Rev. E 88, 042104 (2013)

[41] I. Neri, N. Kern, A. Parmeggiani: New J. Phys. 15, 085005 (2013)

[42] Y. Baek, M. Ha, J. Jeong: Phys. Rev. E 90, 062111 (2014)

[43] G. Diedrich, L. Santen, A. Schadschneider, J. Zittartz: Int. J. Mod. Phys. C 11, 335 (2000)

Part IV.

Conclusions

Conclusions of Part II - Dynamical Universality Classes

This project started initially with the identifications of new dynamical universality classes, known from anharmonic chains, in driven diffusive systems. Crucial hints by Herbert Spohn pointing out the possibility of the golden mean universality class prior to publication [90] and the richness of supported universality classes in multi-component driven diffusive systems already for minimal settings motivated us to explore mode coupling equations for nonlinear fluctuating hydrodynamics more carefully.

We generalized the one-loop mode coupling equations to arbitrary many conservation laws and solved them exactly in the asymptotic limit for a strictly hyperbolic setting.

The solution reveals an infinite discrete family of dynamical universality classes. Remarkably, their exponents z_α are given by quotients of neighboring Fibonacci numbers, starting with either $z_1 = 2$ (if a diffusion mode exists) or $z_1 = 3/2$ (if a KPZ mode is present and no diffusion mode exists). If neither a diffusion nor a KPZ mode are present, all modes have the golden mean $\varphi = (1 + \sqrt{5})/2$ as their dynamical exponent $z_\alpha = \varphi$. In order to have a mode $\alpha \geq 3$ with dynamical exponent $z_\alpha = F_{\alpha+2}/F_{\alpha+1}$ and Fibonacci numbers $F_{\alpha+2} = F_{\alpha+1} + F_{\alpha+2}$ starting at $F_1 = F_2 = 1$ one needs at least $\alpha - 1$ conservation laws. The minimum setting for a golden mean modes requires at least two conserved fields. All possible exponents are in the range of $3/2 \leq z_\alpha \leq 2$. The largest exponent $z = 2$ represents the diffusion class with Gaussian scaling belonging to the family of stable-distributions. In contrast, the smallest superdiffusive exponent $z = 3/2$ represents three different universality classes showing distinct scaling functions. The KPZ universality class with the Prähofer-Spohn scaling function [74, 75], a modified KPZ universality class with unknown scaling function [90], and a Fibonacci mode with a scaling function described by the 3/2-Lévy stable distribution [70, 90]. The universal scaling functions of all higher ($\alpha \geq 3$) Fibonacci modes, including the golden mean case, are asymmetric z_α-Lévy stable distributions.

Notably, the one-loop mode coupling solution reveals that all fastest left or right moving modes will have maximal asymmetry for Fibonacci modes. Additionally, numerical results reveal a cutoff of the heavy tails of Fibonacci modes by the fastest right or left moving mode. This observation is consistent with the fact that information will propagate within the light cone. In summary, the diffusion, KPZ, modified KPZ, and the Fibonacci family provide a *complete* classification of the dynamical universality classes in strictly hyperbolic systems with locally conserved fluctuation fields. The universality classes realized by the system are encoded in the zeros of the diagonal mode coupling matrix elements which are *completely* fixed by the macroscopic stationary current-density relation alone. In case of nonexistent diffusive modes the stationary compressibility matrix $K(\vec{\rho})$ allows also the prediction of the scale factors and asymmetry of the scaling functions.

Moreover, one should note that symmetries of the current-density relations may encode some information about supported universality classes. Taking, for instance, the two-lane model with indistinguishable lanes, one mode is fixed to the diffusive mode while the other might belong to any of the three $z = 3/2$ classes (Eq. (4.33)). Symmetries also play a major role for other systems. In anharmonic chains symmetries of the three conservation laws restrict the system to only three possible cases for the classification: (1) two KPZ-modes and a 5/3-Fibonacci mode, (2) two diffusion modes and 3/2-Fibonacci mode, and (3) all

golden mean Fibonacci modes [91]. Short-ranged Hamiltonian systems as considered in [5] are even more restricted and support generically only two KPZ sound modes and one 5/3-Fibonacci heat mode.

Already minimal models of driven diffusive lattice gases support all possible classification cases for two and three components. Therefore, we believe the appearance of Fibonacci universality classes to be generic for driven diffusive systems. We have not checked this statement for more components in our model, since we are no longer able to diagonalize the current-density Jacobian analytically and a numerical analysis involves the risk of errors. However, an identification of the role of symmetries would be of great interest and might allow the construction of driven diffusive lattice gases supporting certain universality classes by symmetry. Furthermore, we stress that current-density relations have to be known *exactly*. Approximations obtained from, e.g., stationary mean-field theory will, in general, only accidentally provide the correct dynamical universality classes. Using the role of symmetries it might be possible to predict the universality classes even for models with unknown exact current-density relations.

All results achieved so far with respect to dynamical universality classes, both theoretically and in computer simulations, refer to strongly hyperbolic systems. In other words, all mode velocities are distinct which allows to neglect, in the asymptotic limit, contributions from nondiagonal elements of the mode coupling matrices $\{G^\alpha\}$. Nondiagonal elements of $\{G^\alpha\}$ might play an important role for early time behavior, but their coupling breaks down when the modes are well separated. Simulation results show a sensitive shape of the early time structure functions to strong nondiagonal mode couplings. This modified shape might persist for some time. To access asymptotic behavior of the structure function in computer simulations it is advisable to choose models with large diagonal and relatively small nondiagonal terms of the mode coupling matrices $\{G^\alpha\}$. Doing so, we were able to provide numerical evidence for the appearance of the Fibonacci classes with $z = 3/2$, $z = 5/3$, $z = 8/5$, and $z = (1 + \sqrt{5})/2$. In case of strong diagonal and negligible nondiagonal couplings we found additionally an astonishing agreement with the scaling function predicted by mode coupling theory. Our asymptotic solutions are obtained within the one-loop approximation. It is not clear how to formulate the memory kernel in general, but the one-loop kernel provides a good approximation and might even reveal exact results. Comparing fitted nonuniversal scaling factors to the mode coupling scaling factors we find the same order of magnitude while their differences seem to depend on nondiagonal elements of the mode coupling matrices. However, the predicted scaling functions could still be exact except for some corrections to the nonuniversal scaling factors arising from correction to the one-loop approximation.

Although we learned a lot about dynamical universality classes in driven diffusive systems some questions are left open.

In order to explore the nonuniversal scaling factors and their sensitivity to nondiagonal mode coupling-matrix elements, we aim to compare numerical results of our driven diffusive lattice gas models to numerical results for short range Hamiltonian systems and anharmonic chains. The idea is to fix the diagonal and allow for different nondiagonal elements of the mode coupling matrices $\{G^\alpha\}$. The comparison of data for different models might additionally shed some light on the role of symmetries for constructions of corrections to the one-loop memory kernel. Anyway, the improved mode coupling memory kernel is likely to become messy and hard to evaluate. The simple structure of the one-loop solution and the appearance of its predicted dynamical exponents and scaling functions in different kinds of systems strongly indicates the existence of a simpler underlying mechanism that

determines different universality classes. Knowing the role of symmetries will provide a first step for a more general description. The identification of fundamental mechanisms leading to universality is promising to allow a rigorously proof of the Fibonacci dynamical exponents and their associated Lévy stable scaling functions.

Furthermore, we plan to investigate systems with the so-called *umbilic point* , characterized by equal characteristic velocities. For umbilic modes the peaks will not separate and therefore nondiagonal elements of the mode coupling matrices $\{G^{\alpha}\}$ play an important role. As a result a qualitatively new universality class is expected.

Our numerical results are obtained for coupled single-lane TASEPs with random-sequential update. The Nagel-Schreckenberg (NaSch) model of traffic flow [59] with a parallel update[1] rule contains the TASEP with parallel update as a special case for maximal vehicle velocity $v_{\max} = 1$. For $v_{\max} > 1$, vehicles have an internal degree of freedom and NaSch dynamics become more complicated. Numerical studies of the dynamics for $v_{\max} > 1$ revealed a density dependent dynamical exponent [78]. Using our developed Monte Carlo techniques, we study the dynamical exponents and scaling factors further inside the asymptotic regime. These results allow to construct lower boundaries for a proper relaxation time which is crucial for a trustworthy data analysis since no steady state is known.

[1] All particles (vehicles) attempt to jump at the same time.

Conclusions of Part III - Critical Defect Strength

We have revisited the long standing problem of the critical defect hopping rate r_c in the TASEP with open boundary conditions. For $r < r_c$ the current of the system is reduced and consequently the system reacts globally to the defect. Previously, a purely numerical analysis [29] predicted $r_c = 0.80(2)$. This result came without a theoretical framework and disagrees with the analytical prediction $r_c = 1$ made by mean-field theory and supported by series expansion results [13, 38]. To dissolve the contradiction between previous numerical results and analytic prediction we have addressed r_c numerically from different perspectives. We have shown that the defect current measured in Monte Carlo simulations strongly depends on the choice of the pseudo random number generator. For the used Mersenne Twister pseudo random generator we could not find deviations from available analytical results[2] within Monte Carlo errors and therefore the presented data are assumed to be significant within their errors.

Furthermore, we point out that the choice of boundary conditions is crucial for finite systems. The choice of $\alpha = \beta = 1/2$, as used in [29], seems to be beneficial since the steady state of the pure system factorizes and therefore supports for all finite systems a flat steady state density profile and the infinite system maximum current $j_\infty(r) = 1/4$. One should note that the choice $\alpha = \beta = 1/2$ lies exactly at the boundaries to the low- and high-density phase. Fluctuations around the phase boundaries become very important if we add inhomogeneities in finite systems and significant influences of the boundaries are to be expected. Measuring the defect current we find a significant reduction already for $r = 0.99$ which disagrees with $r_c = 0.80(2)$ suggested by [29]. Indeed, $r_c = 0.80(2)$ turned out to be a result of insufficient analyzed data.

To ensure that the measured defect phenomena arise from bulk dynamics and are not controlled by fluctuations of the boundaries we investigated r_c for systems well inside the maximum current phase with boundary rates $\alpha = \beta = 1$. Different to $\alpha = \beta = 1/2$, the steady state current of the pure system is enhanced by finite-size effects [16], i.e.,

$$j_{\alpha=\beta=1,L} = \frac{1}{4}\left(1 + \frac{3}{1+4L}\right). \tag{8.7}$$

We defined a lower bound for r_c by satisfying $j_{\alpha=\beta=1,L}(r_c) - j_{\alpha=\beta=1,\infty}(r=1) < 0$. However, in this way, using systems of length $L = 200,000$, we could only derive a lower bound $r_c \geq 0.86$ for the critical hopping rate. Assuming the existence of an essential singularity at $r_c = 1$, i.e., $j(1) - j(r) \sim \exp(-a/(1-r))$ [13], further improvement of the lower bound for the critical defect r_c by increasing the system length is a hopeless enterprise: e.g., a numerical proof of $r_c > 0.9$, $r_c > 0.95$, $r_c > 0.99$ would require $L > 10^{10}$, $L > 10^{22}$, $L > 10^{147}$, respectively. Measuring a defect current $j_{\alpha=\beta=1,L}(r) > j_{\alpha=\beta=1,\infty}(r=1) = 1/4$ might raise the question if the system recovers from defects and therefore reacts only locally. Consequently, a much better quantity to determine r_c, is the density profile or rather the difference between the density profiles of the defect system with a corresponding pure system. The critical r_c defect strength is then identified by the defect leading to a global adjustment of the system to the defect. To achieve a significantly improved bound for

[2] E.g., steady state currents for the pure system.

r_c we studied the density profiles of two parallel evolving systems with and without the defect. The established covariance between both systems allows to efficiently distinguish between fluctuation and defect phenomena. Studying differences for systems with $r = 1$ and $r = 0.99$ we improved the computation time by a factor of $10,000$ compared to the naive approach and allows to generate very precise data. We have shown a significant global adjustment to the defect for $r = 0.99$ and therefore established $r_c > 0.99$ which supports the mean-field prediction. We could not find any anomaly in our data which supports the existence of $r_c < 1$.

As discussed in Section 1.3.2, parallel evolving systems can be mapped to a system of first- and second-class particles. These first-class particles may only separate at the defect site into a pair of nonconserved up and down second-class particles. A pair of different second-class particles recovers into a first-class particle when meeting each other (see. Fig. 1.7). Second-class particles are generated only at the defect site in case a first-class particle cannot jump due to the defect. Taking any steady state configuration of the pure system we can split any first-class particle, when passing the "slow bond", into a pair of second-class particle. This is done only once and we evolve the system containing the pair of second-class particles according to the pure rules for all sites. This setting corresponds to an infinitesimal defect rate starting at the extremely rare event where a pair of second-class particles is generated. Whenever this pair of second-class particles recovers to a first-class particle, the global current will be unchanged by the defect-event. But in case one second-class particle leaves at the left and the other at the right boundary, then the current of the "defect" system will never recover from this introduced defect event. Furthermore, the steady state density profile for $\alpha = \beta = 1$ decays monotonically algebraic and therefore supports a separation drift of both second-class particles.

This argument is similarly constructed for periodic systems. We assume again an infinitesimal small defect rate and artificially introduce a single pair of second-class particles when a first-class particle tries to pass the "defect" site. Depending on the direction of the recovery into a first-class particle the current of the "defect" system might never recover from the defect event.

A more detailed study of second-class particle dynamics in the context of small defects is very promising to achieve very accurate numerical results allowing to shed some light on the essential singularity suggested for the defect current [38, 13].

Furthermore, we suggest an alternative way to measure currents in the future. Using parallel evolving systems we achieved an extremely large covariance in the vicinity of the boundaries. Instead of measuring the current by averaging over the whole steady state system, one should use the density difference of both systems at the first (last) site. Since we know the exact current of the pure system, the defect current is given by

$$j_{\alpha=\beta=1,L}(r) = \frac{1}{4}\left(1 + \frac{3}{1+4L}\right) + \langle\, n_1 \,\rangle_p - \langle\, n_1 \,\rangle_d \tag{8.8}$$

where $\langle\, n_1 \,\rangle_d$ ($\langle\, n_1 \,\rangle_p$) denotes the density at the first site in the defect (pure) system. Finally, we stress that our developed technique might be easily extended for the study of multiple inhomogeneities or even bottlenecks.

Bibliography for Part I and IV

[1] D. ben Avraham, J. Köhler, Mean-field (n, m)-cluster approximation for lattice models, Phys. Rev. A, 45:8358, 1992.

[2] M.T. Bachelor, The Bethe Ansatz after 75 years, Physics Today, 1:36, 2007.

[3] A.-L. Barabási H.E. Stanley, Fractal Concepts in Surface Growth, Cambridge University Press 1995

[4] M. Barma, Driven diffusive systems with disorder, Physica A 372, 22 (2006)

[5] H. van Beijeren, Exact results for anomalous transport in one-dimensional Hamiltonian systems. Phys. Rev. Lett. 108, 108601 (2012).

[6] H. Bethe, Zur Theorie der Metalle, I. Eigenwerte und Eigenfunktionen der linearen Atomkette, Z. Phys., 71:205, 1931.

[7] R. Blythe, M.R. Evans, Nonequilibrium steady states of matrix product form: a solver's guide. J. Phys. A, 40:R333, 2007.

[8] N. Boccara, Modeling Complex Systems, Springer (2004).

[9] J. M. Burgers, The Nonlinear Diffusion Equation. Riedel, Boston, (1974).

[10] D. Chandler, Introduction to Modern Statistical Mechanics, Oxford University Press (1987)

[11] G. De Chiara, M. Rizzi, D. Rossini, S. Montangero. Density matrix renormalization group for dummies. J. Comput. Theor. Nanosci., 5:1277, 2008.

[12] I. Corwin, Kardar-Parisi-Zhang Universality, Notices of the AMS vol. 63 no. 3 230-239 (2016)

[13] Costin, O., Lebowitz, J.L., Speer, E.R., Troiani, A.: The blockage problem. Bull. Inst. Math. Acad. Sin. 8, 49 (2013)

[14] A. Crisanti, G. Paladin, and A. Vulpiani, Products of Random Matrices in Statistical Physics. Springer (1993).

[15] L. Delfini, S. Lepri, R. Livi, and A. Politi, Anomalous kinetics and transport from 1D self-consistent mode-coupling theory J. Stat. Mech. P02007 (2007).

[16] B. Derrida, E. Domany, D. Mukamel, An exact solution of a one dimensional asymmetric exclusion model with open boundaries, J. Stat. Phys. 69:667-687 (1992).

[17] B. Derrida, M. R. Evans, V. Hakim, V. Pasquier, Exact solution of a 1D asymmetric exclusion model using a matrix formulation, J. Phys. A: Math. Gen. 26 1493–517 (1993)

[18] B. Derrida, S. A. Janowsky, J. L. Lebowitz, E. R. Speer Exact solution of the totally asymmetric simple exclusion process: Shock profiles JSP, vol. 73, iss. 5, pp 813-842 (1993)

[19] M. Doi, Second quantization representation for classical many-particle system, J. Phys. A, 9:1465, 1976.

[20] M. Doi, Stochastic theory of diffusion-controlled reaction, J. Phys. A, 9:1479, 1976.

[21] S.N. Dorogovtsev, J.F.F. Mendes, Evolution of Networks, Oxford University Press (2003)

[22] P. L'Ecuyer, R. Simard, Testu01: A c library for empirical testing of random number generators ACM Trans. Math. Softw. 33(4) (2007).

[23] J.W. Gibbs. Elementary principles in statistical mechanics. Yale University Press 1902, reprint Ox Bow Press 1981

[24] M.B. Giles, Multilevel Monte Carlo Path Simulation Oper. Res. 56, 607 (2008)

[25] M.B. Giles, Multilevel Monte Carlo methods, Acta Numerica, Vol. 24, 2015, pp. 259-328.

[26] W. R. Gilks, Markov Chain Monte Carlo (2005), Encyclopedia of Biostatistics. 4.

[27] R. Glauber, Time-dependent statistics of the Ising model, J. Math. Phys. 4:294 (1963).

[28] H.A. Gutowitz, J.D. Victor, and B.W. Knight, Local structure theory for cellular automata, Physica, 28D:18, 1987.

[29] M. Ha, J. Timonen, M. den Nijs: Queuing transitions in the asymmetric simple exclusion process. Phys. Rev. E 58, 056122 (2003)

[30] A.-L. Haji-Alim, F. Nobile, R. Tempone, Multi-index Monte Carlo: when sparsity meets sampling Numerische Mathematik 132-4 767-806 (2016)

[31] K. Hallberg, New trends in density matrix renormalization. Adv. Phys., 55:477, 2006.

[32] T. Halpin-Healy, Y.-C. Zhang, Kinetic roughening phenomena, stochastic growth, directed polymers and all that. Aspects of multidisciplinary statistical mechanics. Phys. Rep., 254:215, 1995.

[33] S. Haykin, Neural Networks, Prentice-Hall (1999)

[34] S. Heinrich, Multilevel Monte Carlo Methods, Lect. Notes Comp. Sci. 2179, 58 (2008)

[35] M. Henkel, Conformal Invariance and Critical Phenomena, Springer (1999)

[36] M. Henkel, Reaction-diffusion processes and their connection with integrable quantum spin chains In A. Kundu, editor, Classical and Quantum Nonlinear Integrable Systems: Theory and Applications, page 256. IOP Publishing, 2003.

[37] H. Hinrichsen, Non-equilibrium critical phenomena and phase transitions into absorbing states, Advances in Physics, Vol 49 Iss 7 815-958 (2000)

[38] S. A. Janowski, J. L. Lebowitz, Exact Results for the Asymmetric Simple Exclusion Process with a Blockage J. Stat. Phys. 77:35-51 (1993)

[39] M. Kardar, G. Parisi, and Y.-C. Zhang, Dynamic scaling of growing interfaces Phys. Rev. Lett. 56, 889 (1986).

[40] C. Kipnis and C. Landim, Scaling limits of interacting particle systems (Springer, Berlin, 1999).

[41] A. Kirman, J.-B. Zimmermann, Economics with Heterogeneous Interacting Agents, Springer (2001)

[42] A. Kleidon, R. D. Lorenz, Non-equilibrium Thermodynamics and the Production of Entropy, Springer (2015)

[43] J. Krug, H. Spohn. Universality classes for deterministic surface growth. Phys. Rev. A, 38:4271, 1988.

[44] J. Krug, Boundary-induced phase transitions in driven diffusive systems, Physical Review Letters 67, 1882-1885 (1991).

[45] J. Krug, H. Spohn. Kinetic roughening of growing surfaces. In C. Godr'eche, editor, Solids far from Equilibrium: Growth, Morphology and Defects. Cambridge University Press, 1991.

[46] J. Krug, Origins of scale invariance in growth processes, Adv. Phys. 46, 139 (1997).

[47] J. Krug, Phase separation in disordered exclusion models, Brazilian Journal of Physics 30, 97-104 (2000).

[48] J. Krug Nonequilibrium stationary states as products of matrices, J. Phys. A, 49:421002 (2016)

[49] M. Le Bellac, F. Martessagne, G.G. Batrouni, Equilibrium and Non-Equilibrium Statistical Thermodynamics, Cambridge (2001)

[50] T.D. Lee and C.N. Yang. Statistical theory of equations of state and phase transitions. II. Lattice gas and Ising model. Phys. Rev., 87:410, 1952.

[51] I. N. Levine, Physical Chemistry, McGRAW-HILLL (2008)

[52] E. Lieb, D. Robinson, The finite group velocity of quantum spin systems. Commun. Math. Phys. 28, 251–257, (1972)

[53] MacDonald C T, Gibbs J H and Pipkin A C 1968 Kinetics of biopolymerization on nucleic acid templates, Biopolymers vol. 6 p.1–25

[54] B. B. Mandelbrot, Fractals and Scaling in Finance, Springer (1997)

[55] C.B. Mendl, H. Spohn, Dynamic correlators of FPU chains and nonlinear fluctuating hydrodynamics. Phys. Rev. Lett. 111, 230601 (2013).

[56] C.B. Mendl,H. Spohn Searching for the Tracy-Widom distribution in nonequilibrium processes PHYSICAL REVIEW E 93, 060101(R) (2016)

[57] T. Michely, J. Krug, Islands, Mounds and Atoms. Patterns and Processes in Crystal Growth Far from Equilibrium, Springer (2004)

[58] G. Mussardo, Statistical Field Theory, Oxford Graduate Texts (2009)

[59] K. Nagel, M. Schreckenberg. A cellular automaton model for freeway traffic. J. Physique I, 2:2221, 1992.

[60] M. E. J. Newman, Networks, Oxford University Press (2010)

[61] M.E.J. Newman, G.T. Barkema, Monte Carlo Methods in Statistical Physics (1999), Oxford University Press

[62] M. A. Nowak, Evolutionary Dynamics, Belknap/Harvard (2006)

[63] I. Peschel, X. Wang, M. Kaulke, and K. Hallberg, editors. Density-Matrix Renormalization, volume 528 of Lecture Notes in Physics. Springer, 1999.

[64] Phillips, Kondev, Theriot, Garcia, Orme, Physical Biology of the Cell, Garland Science (2013)

[65] M. Plischke, Z. Rácz, D. Liu, Time-reversal invariance and universality of two-dimensional growth models. Phys. Rev. B 35, 3485 (1987)

[66] V. Popkov and G.M. Schütz, Shocks and excitation dynamics in a driven diffusive two-channel system, J. Stat. Phys. 112, 523-540 (2003).

[67] Popkov V, Salerno M (2004) Hydrodynamic limit of multichain driven diffusive models. Phys. Rev. E 69: 046103.

[68] V. Popkov, M. R. Evans, D. Mukamel, Spontaneous symmetry breaking in a bridge model fed by junctions, J. Phys. A 41, 432002 (2008).

[69] Popkov V, Schmidt J, Schütz GM (2014) Superdiffusive modes in two-species driven diffusive systems. Phys. Rev. Lett. 112: 200602.

[70] Popkov V, Schmidt J, Schütz GM (2015) Universality classes in two-component driven diffusive systems. J. Stat. Phys. 160: 835–860.

[71] V. Popkov, A. Schadschneider, J. Schmidt, G. M. Schütz, The Fibonacci family of dynamical universality classes, PNAS, Oct. 2015, vol. 112, no. 41, pp. 12645-12650

[72] M. Prähofer, H. Spohn, Universal distributions for growth processes in 1+1 dimensions and random matrices, Physical Review Letters 84, 4882-4886 (2000).

[73] M. Prähofer, H. Spohn, Current Fluctuations for the Totally Asymmetric Simple Exclusion Process, in: In and Out of equilibrium, edited by V. Sidoravicius, Progress in Probability Vol. 51 pp. 185-204 (Birkhauser, Boston, 2002)

[74] M. Prähofer and H. Spohn, Exact scaling functions for one-dimensional stationary KPZ growth. J. Stat. Phys. 115, 255–279 (2004).

[75] M. Prähofer and H. Spohn, http://www-m5.ma.tum.de/KPZ

[76] N. Pttier, Nonequilibrium Statistical Physics, Oxford Graduate Texts (2011)

[77] A. Rá kos, M. Paessens, G.M. Schütz. Hysteresis in one-dimensional reaction-diffusion systems. Phys. Rev. Lett., 91:238302, 2003.

[78] M. Sasvári, J. Kertész, Cellular automata models of single-lane traffic, Phys. Rev. E. 56:4, 4104-4110 (1997)

[79] A. Schadschneider, D. Chowdhury, K, Nishinari, Stochastic Transport in Complex Systems, Elsevier (2011)

[80] B. Schmittmann, R.K.P. Zia, Statistical mechanics of driven-diffusive systems, In C. Domb and J. L. Lebowitz, editors, Phase Transitions and Critical Phenomena, Vol. 17. Academic Press, 1995.

[81] B. Schmittmann, R.K.P. Zia, Driven diffusive systems: An introduction and recent developments, Phys. Rep., 301:45, 1998.

[82] U. Schollwöck. The density-matrix renormalization group. Rev. Mod. Phys., 77:259, 2005.

[83] M. Schreckenberg, A. Schadschneider, K. Nagel, N. Ito, Discrete stochastic models for traffic flow, Phys. Rev. E, 51:2939, 1995.

[84] G. M. Schütz, E. Domany, Phase transitions in an exactly soluble one-dimensional exclusion process, J. Stat. Phys. 72 277–96 (1993)

[85] G.M. Schütz, Exactly solvable models for many-body systems far from equilibrium, In C. Domb and J. L. Lebowitz, editors, Phase Transitions and Critical Phenomena, Vol. 19. Academic Press, 2001.

[86] R. Soto, Kinetic Theory and Transport Phenomena, Oxford University Press (2016)

[87] F. Spitzer, Interaction of Markov processes, Adv. Math. 5 246–90 (1970)

[88] H. Spohn, Large Scale Dynamics of Interacting Particles, Springer (1991)

[89] H. Spohn, Nonlinear Fluctuating hydrodynamics for anharmonic chains. J. Stat. Phys. 154, 1191–1227 (2014).

[90] H. Spohn, G. Stoltz, Nonlinear fluctuating hydrodynamics in one dimension: The case of two conserved fields. J. Stat. Phys., Volume 160, Issue 4, pp 861–884, (2015)

[91] H. Spohn, The Kardar-Parisi-Zhang equation - a statistical physics perspective. arXiv:1601.00499, (2016).

[92] M. Treiber, A. Kesting, Traffic Flow Dynamics, Springer (2012)

[93] Universality classes in nonequilibrium lattice systems G. Ódor, Rev. Mod. Phys. 76, 663 (2004)

[94] D. Wodarz, N. L. Komarova, Dynamics of Cancer, World Scientific (2014)

[95] L. V. Yakushevich, Nonlinear Physics of DNA, WILEY-VCH

Acknowledgments

At this point, I would like to thank Andreas Schadschneider and Petra Neubauer-Guenther for their support. They were the one who stood in for my doctoral scholarship of the BCGS as well as financial support by the DFG and primarily made my doctoral degree possible.

Besides, I would like to thank my supervisors Vladislav Popkov, Andreas Schadschneider and Gunter Schütz. They continuously came up with new and highly relevant questions which gave me the chance to work on various exciting projects. Their dedication to our research projects and their constant availability for discussions contributed to my motivation and productivity for this thesis. Moreover, they have always had a keen sense of which ideas to follow upon without getting on the wrong track. If we found ourselves stuck somewhere with our ideas and needed a break, Vladislav Popkov and I put on our running shoes and went for a long run in the forest or ended up climbing the Dolomites.

Moreover, I am very grateful for the fact that Andreas Schadschneider and Jan de Gier provided me the opportunity to go to Melbourne for a research trip. During my stay in Australia, Jan de Gier cared for my well-being and allowed me to visit scientific conferences where I had the chance to exchange interesting insights with other scientists.

I would like to thank Alexandr Garbaly who is currently postdoc in Jan de Gier's group for our coffee breaks in his office and exciting trips during holidays. I keep my fingers crossed that he will find the Q operator for the A_2^2 model.

Furthermore, I would like to thank Angela Kunoth for providing me the chance to visit the summer school in Austin, Texas. It was due to her that I could participate in the seminar even though it had been fully booked. She additionally arranged a contact person for me who helped me with finding accommodation so that I had the chance of meeting other PhD students and sharing revealing discussions with them. I also benefited from the summer school in so far that I learned new strategies of improving Monte Carlo Simulations from leading people of this area.

I would like to thank Andreas Schadschneider, Christian Mollet and Robert Neiss for proofreading my thesis even at the very last weekend before my hand-in. They helped me to rephrase paragraphs so that people who are not an expert in my thesis' focus can understand my reasoning. Besides this, they reviewed each formula to ensure that these do not have any mistakes. I also would like to thank Stefan Bittihn and Christos Christou for proofreading the final version of my thesis.

Christoph Peters, my former classmate and close friend, provided me with lots of advice on efficiently programming c++ which I am very grateful for.

I would like to thank my colleagues Christos Christou, Stefan Bittihn, Charles Guggenheim, Jochen Peschutter, Dominik Ostermayr and Robert Neiss for positively contributing to any interposed question. But in particular, I am not only thankful for their technical support, but also for the fact that we privately get along very well so that we ended up climbing, snowboarding and skiing, wakeboarding, surfing, cycling or just having a nice chat once in a while.

Last but not least, I would like to thank my girlfriend Isabel Hackstein. Although she has a business background, she has always been sharing my enthusiasm for my research during my Master and my PhD phase. In particular, I am grateful for her patience when usually the one last hour of work at a day turned out to be two or three.

Financial support by the Deutsche Forschungsgemeinschaft (DFG) under grant SCHA 636/8-2 and Bonn-Cologne Graduate School (BCGS) is greatfully acknowledged.

Beteiligung an den in Teil II und III aufgefürten Veröffentlichungen

- Kapitel 3: V. Popkov, J. Schmidt, G. M. Schütz
  Non-KPZ modes in two-species driven diffusive systems
  PRL, May 2014, vol. 112, iss. 20, p. 200602

  In dieses Projekt wurde ich im Rahmen meiner Masterarbeit eingebunden. Die Entwicklung der Monte-Carlo Algorithmen und die numerische Datenauswertung wurden von mir durchgeführt.

- Kapitel 4: V. Popkov, J. Schmidt, G. M. Schütz
  Universality classes in two-component driven diffusive systems
  J Stat Phys, Aug. 2015, vol. 160, iss. 4, pp. 835-860

  Die Idee zu diesem Artikel ergab sich aus der Kommunikation mit Herbert Spohn (Professor an der TU München) und den Ergebnissen aus meiner Masterarbeit. Mir ist es gelungen nachzuweisen, dass in diffusiven Mehrteilchensystemen alle von der Mode-Coupling Theorie bislang vorhergesagten Universalitätsklassen realisiert werden können. Die Entwicklung der Messmethoden und Monte-Carlo Algorithmen sowie die Auswertung der numerischen Daten wurden von mir durchgeführt. Der Artikel wurde zusammen mit Gunter Schütz und Slava Popkov verfasst.

- Kapitel 5: V. Popkov, A. Schadschneider, J. Schmidt, G. M. Schütz
  The Fibonacci family of dynamical universality classes
  PNAS, Oct. 2015, vol. 112, no. 41, pp. 12645-12650

  Die Idee zu dieser Arbeit wurde von allen Autoren aus den Ergebnissen der Publikation in Kapitel 4 abgeleitet. Die Entwicklung von Messmethoden und Monte-Carlo Algorithmen sowie die Auswertung der numerischen Daten wurden von mir durchgeführt. Der Artikel wurde im Wesentlichen von Andreas Schadschneider und Gunter Schütz verfasst. An dessen konzeptioneller Darstellung war ich beteiligt.

- Kapitel 6: V. Popkov, A. Schadschneider, J. Schmidt, G. M. Schütz
  Exact scaling solution of the mode coupling equations for non-linear fluctuating hydrodynamics in one dimension
  J. Stat. Mech. (2016) 093211

  Dieser Artikel enstand ergänzend zur Publikation Kapitel 5. Der Artikel wurde im wesentlichen von Gunter Schütz verfasst. Alle Authoren haben zur analytischen Rechnung und ihrer Darstellung beigetragen.

- Kapitel 7: A. Schadschneider, J. Schmidt, V. Popkov
  When is a bottleneck a bottleneck?
  Traffic and Granular Flow '15, ISBN 978-3-319-33482-0

  Dieser Artikel entstand als Beitrag zur Konferenz "Traffic and Granular Flow '15". Die Idee zu diesem Artikel stammt von Andreas Schadschneider und beabsichtigt die Problematiken eines Defekt Systems einer breiteren Kommunity aus dem angewandten/experimentellen Bereich zugänglich zu machen. Der Artikel wurde von Andreas Schadschneider und mir verfasst.

- Kapitel 8: J. Schmidt, V. Popkov, A. Schadschneider
  Defect-induced phase transition in the asymmetric simple exclusion process
  Europhysics Letters (EPL) May 2015, vol. 110, no. 2, p. 20008

  Die Idee zu diesem Artikel wurde von Andreas Schadschneider und mir aus den Ergebnissen meiner Masterarbeit (AG Schadschneider) abgeleitet. Die Ausarbeitung der bisherigen Problematiken, Entwicklung von besseren Messmethoden und Monte-Carlo Algorithmen sowie die Auswertung aller Daten wurden von mir durchgeführt. Der Artikel wurde von mir konzipiert und zusammen mit Andreas Schadschneider und Slava Popkov verfasst.

Köln, den 12. Januar 2017 Johannes Schmidt

Erklärung

Ich versichere, dass ich die von mir vorgelegte Dissertation selbständig angefertigt, die benutzten Quellen und Hilfsmittel vollständig angegeben und die Stellen der Arbeit – einschließlich Tabellen, Karten und Abbildungen –, die anderen Werken im Wortlaut oder dem Sinn nach entnommen sind, in jedem Einzelfall als Entlehnung kenntlich gemacht habe; dass diese Dissertation noch keiner anderen Fakultät oder Universität zur Prüfung vorgelegen hat; dass sie – abgesehen von Teilpublikationen Kapitel 3 bis 8– noch nicht veröffentlicht worden ist sowie, dass ich eine solche Veröffentlichung vor Abschluss des Promotionsverfahrens nicht vornehmen werde. Die Bestimmungen der Promotionsordnung sind mir bekannt. Die von mir vorgelegte Dissertation ist von Prof. Dr. Andreas Schadschneider und Prof. Dr. Gunter M. Schütz betreut worden.

Köln, den 26. Dezember 2016 Johannes Schmidt